UNIVERSITÉ DE GENÈVE

Archive ouverte UNIGE
https://archive-ouverte.unige.ch

Thèse 2018

Open Access

This version of the publication is provided by the author(s) and made available in accordance with the copyright holder(s).

Development of sensing principles for electrochemical detection of nutrients and species relevant to the carbon cycle

Pankratova, Nadezda

How to cite

PANKRATOVA, Nadezda. Development of sensing principles for electrochemical detection of nutrients and species relevant to the carbon cycle. Doctoral Thesis, 2018. doi: 10.13097/archive-ouverte/unige:102939

This publication URL: https://archive-ouverte.unige.ch/unige:102939
Publication DOI: 10.13097/archive-ouverte/unige:102939

© This document is protected by copyright. Please refer to copyright holder(s) for terms of use.

UNIVERSITÉ DE GENÈVE FACULTÉ DES SCIENCES

Section de chimie et biochimie
Département de chimie minérale et analytique Professeur E. Bakker

Development of Sensing Principles for Electrochemical Detection of Nutrients and Species Relevant to the Carbon Cycle

THÈSE

présentée à la Faculté des sciences de l'Université de Genève
pour obtenir le grade de Docteur ès sciences, mention chimie

par

Nadezda PANKRATOVA

de

St. Pétersbourg (la Fédération Russie)

Thèse N^{o} 5169

GENÈVE

Atelier d'impression ReproMail

2018

UNIVERSITÉ DE GENÈVE

FACULTÉ DES SCIENCES

DOCTORAT ÈS SCIENCES, MENTION CHIMIE

Thèse de Madame Nadezda PANKRATOVA

intitulée :

«Development of Sensing Principles for Electrochemical Detection of Nutrients and Species Relevant to the Carbon Cycle»

La Faculté des sciences, sur le préavis de Monsieur E. BAKKER, professeur ordinaire et directeur de thèse (Département de chimie minérale et analytique), Madame K. SUGIHARA, professeure assistante (Département de chimie physique) et Monsieur B. WEHRLY, professeur (Eidgenössische Technische Hochschule Zurich, Luzern, Schweiz) autorise l'impression de la présente thèse, sans exprimer d'opinion sur les propositions qui y sont énoncées.

Genève, le 17 janvier 2018

Thèse - 5169 -

Le Doyen

N.B. - La thèse doit porter la déclaration précédente et remplir les conditions énumérées dans les "Informations relatives aux thèses de doctorat à l'Université de Genève".

DEVELOPMENT OF SENSING PRINCIPLES FOR ELECTROCHEMICAL DETECTION OF NUTRIENTS AND SPECIES RELEVANT TO THE CARBON CYCLE

Doctoral Thesis

Submitted by

Nadezda Pankratova

Under the supervision of Prof. Eric Bakker

University of Geneva

Department of inorganic and analytical chemistry

I certify that the work presented here is, to the best of my knowledge and belief, original and the result of my own investigations, except as acknowledged, and has not been submitted, either in part or whole, for a degree at this or any other University.

Date 30.01.2018

Signature / Nadezda Pankratova /

DÉVELOPPEMENT DE PRINCIPES POUR LA DÉTECTION ÉLECTROCHIMIQUE DE NUTRIMENTS ET ESPÈCES IMPLIQUÉES DANS LE CYCLE DU CARBONE

Thèse de Doctorat

Soumis par

Nadezda Pankratova

Sous la supervision de Prof. Eric Bakker

Université de Genève

Département de chimie minérale et analytique

L'auteur de ce projet est le seul responsable de son contenu, qui n'engage en rien la responsabilité de l'Université ou celle du professeur chargé de sa supervision. Par ailleurs, l'auteur atteste que le contenu est de sa propre rédaction, en dehors des citations parfaitement identifiées, empruntées à d'autres sources.

Date 30.01.2018

Signature / Nadezda Pankratova /

To my best friend and the dearest person in the world

To a great mind, a kind soul and a free spirit

To the beautiful mother of amazing kids

To the one so far away but always so close to my heart

To the best present my parents have ever given to me

To my beloved sister Katja

SUMMARY

The main goal of this doctoral thesis has been the development of sensors, new tools, in-line setups and approaches for on-site and *in-situ* monitoring of nutrients and species relevant to the carbon cycle and as well as their subsequent integration for field analysis in freshwater and/or seawater.

Monitoring of nutrients and species related to the carbon cycle as well as relevant biogeochemical processes in aquatic ecosystems is of vital importance since aquatic systems are very sensitive to environmental changes. Many undesirable effects resulting from nutrient enrichment have been documented, ranging from localized high concentrations of suspended algae to marked dissolved oxygen depletion and death of biota. At the same time, the ocean surface pH has decreased significantly in the last few decades, resulting in notable changes in structure and biodiversity of aquatic ecosystems. Detection and quantification of relevant ionic species is of great importance in order to predict and to be able to deal with the consequences of anthropogenic influences. Thus, high quality monitoring data are in this context crucial for tracing and understanding the mechanisms that drive aquatic ecosystem dynamics.

Significant progress has been made in developing flow analysis techniques for *in-situ* monitoring of aquatic environments, yet most of the commonly used techniques are still based on traditional sampling procedures which require manipulation of the sample during sampling, sample transport and storage. The latter often leads to significant changes in the sample integrity due to re-equilibration of the aquatic sample with atmospheric CO_2, oxidation/reduction processes and change of conditions such as light, depth/pressure, saturation state etc. Therefore, further development of robust analytical techniques is required to provide accurate *in-situ* species determination in aquatic environments, with suitable temporal and spatial resolution.

This work has been started in 2014 as a part of an interdisciplinary project “Sensing Aquatic Microscale Heterogeneity” and aimed at providing new tools to scale up and predict the effect of microenvironmental dynamics on the ecology of aquatic ecosystems. The project proposed a close cooperation between sensor development teams and scientists directly involved in field monitoring studies. It includes development of new electrochemical sensors and sensing approaches, their integration for the field measurements, field monitoring in freshwater and seawater, as well as validation of proposed arrangement consistency by comparing the field and laboratory measurements.

The thesis is divided into 3 main chapters (1. Introduction, 2. Results and Discussions, 3. Conclusions), supplemented by Appendices (Chapter 4). Chapter 2 ("Results and Discussion") presents the main achievements of the research and has been structured in different sections, each one describing a particular newly-proposed sensor, sensing array, approach, setup or a combination thereof.

Section 2.1 reports on the potentiometric sensing array for on-site measurements of ionic species, such as hydrogen ion, calcium, nitrate, nitrite and carbonate, and its integration for field measurements on the lake Greifensee (Switzerland). The described array operates autonomously, with measurement, calibration, fluidic control and acquisition triggers all integrated into a self-contained instrument. The adequate performance of the proposed setup was validated *ex situ*.

Section 2.2 reports on the development of submersible potentiometric probes for *in-situ* determination of species relevant to the carbon cycle and their deployment in seawater, namely in Arcachon Bay (France) and Genoa Harbor (Italy). The developed deployable prototype has been shown to be promising for obtaining rapid and trustable information about ion concentrations in marine systems and allows for simple integration of other ion sensors that may require sample pretreatment.

Section 2.3 describes three different concepts for local acidification of the membrane of anion-selective electrode in order to overcome the pH interference, as well as their integration for nitrite and phosphate determination in freshwater matrix. All three concepts are based on proton release in the thin layer adjacent to the electrode membrane, require nor flow neither sample pretreatment and suggest direct contact of the sensor with the environmental sample to be analysed.

Section 2.4 provides the detailed description of a newly-proposed module for in-line acidification of environmental samples and its integration for nitrite detection in aquarium water and dechloridized seawater. The acidification principle is based on the ion-exchange process between cations present in the sample and protons released through the preconditioned cation-exchange membrane. The proposed concept is robust and easy to integrate for detections methods in the flow requiring decrease and adjusting of sample pH.

Section 2.5 is dedicated to potentiometric properties of fluorinated tripodal receptors discovered in view of searching for appropriate phosphate receptor. No adequate sensitivity and selectivity towards phosphate was found within this search but another practically significant application of one of the receptors has been reported, namely for

chloride detection in biological samples. The discovered receptor was shown to possess sufficient sensitivity and selectivity for chloride detection in undiluted human serum, along with good long-term stability.

Section 2.6 describes the in-line configuration for electrochemical detection of phosphate using square wave voltammetry (SWV). The formation of the electroactive phosphomolybdate complex for SWV detection is achieved *via* preceding in-line delivery of molybdate and hydrogen ions into a thin layer sample through anion- and cation-exchange membranes (respectively), coupled together. The proposed configuration with SWV detection allows for resolving phosphate concentrations as low as 0.1 μM and is easy to integrate into the previously developed submersible sensing module (Section 2.2).

RÉSUMÉ

L'objectif principal de cette thèse de doctorat est le développement de capteurs et de nouveaux outils analytiques et leur intégration pour des nouvelles approches de la surveillance sur site et *in situ* des nutriments et des espèces impliquées dans le cycle du carbone en eau douce ou eau de mer.

La surveillance des nutriments et des espèces liés au cycle du carbone, ainsi que des processus biogéochimiques spécifiques aux écosystèmes aquatiques, est d'une importance vitale, puisque les systèmes aquatiques sont très sensibles aux changements environnementaux et aux pressions anthropiques. De nombreux effets indésirables résultant de l'enrichissement en éléments nutritifs ont été documentés, allant de fortes concentrations localisées d'algues en suspension à un appauvrissement important de l'oxygène dissous conduisant à la mort du biota. Dans le même temps, le pH de la surface des océans a considérablement diminué pendant les dernières décennies. Ceci a entraîné des changements significatifs dans la structure et la biodiversité des écosystèmes aquatiques. La détection et la quantification d'espèces ioniques caractéristiques sont d'une grande importance pour suivre leur évolution, prédire leurs impacts, et de y remédier. Dans un tel contexte, il est crucial d'obtenir des données de contrôle de haute qualité pour étudier et comprendre les mécanismes qui animent la dynamique des écosystèmes aquatiques.

Des progrès considérables ont été réalisés dans l'élaboration de techniques d'analyse en flux pour l'observation *in-situ* des milieux aquatiques. La plupart des techniques communément utilisées sont encore basées sur des procédures d'échantillonnage, transport et stockage d'échantillons. La rééquilibration du CO_2 entre échantillon et l'atmosphère, des processus d'oxydation/réduction, et des changements de conditions telles que la lumière, pression, état de saturation etc. entrainent des changements importants de l'intégrité des échantillons. Par conséquent, la poursuite du développement de techniques d'analyse robustes est primordiale pour permettre la détection *in-situ* de composés spécifiques dans les milieux aquatiques, avec une résolution temporelle et spatiale adéquate.

Ce travail a été commencé en 2014. Il fait partie d'un projet interdisciplinaire aquatique 'Sensing Aquatic Microscale Heterogeneity' visant à fournir de nouveaux outils pour mieux comprendre et prédire l'effet de la dynamique micro-environnementales sur l'écologie des écosystèmes aquatiques. Le projet a impliqué une coopération étroite entre les équipes de développement des capteurs et les scientifiques impliqués directement dans

des études de monitoring sur le terrain. Il comprend le développement de nouveaux capteurs électrochimiques et d'approches de détection, leur intégration pour les mesures sur le terrain, la surveillance en eau douce et en eau de mer, ainsi que la validation l'arrangement proposé en comparant des mesures effectuées *in situ* et en laboratoire.

La thèse est divisée en 3 chapitres principaux (1. Introduction, 2. Résultats et discussions, 3. Conclusions), complétés par des Annexes (Chapitre 4). Le chapitre 2 («Résultats et discussions») présente les réalisations principales de la recherche. Il est structuré en différentes sections, chacune d'elle décrivant un nouveau capteur, un réseau de détection, une approche, une configuration ou une combinaison de ceux-ci.

La section 2.1 rend compte d'une suite réseau de capteurs développés pour la détection potentiométrique sur site d'espèces ioniques, telles que les ions hydrogène, calcium, nitrate, nitrite et carbonate ; et de leur intégration en réseau pour des mesures sur le lac Greifensee (Suisse). Le système décrit fonctionne de manière autonome, avec des déclencheurs de mesure, d'étalonnage, de contrôle fluidique et d'acquisition des données. Les performances adéquates de la configuration proposée ont été validées en laboratoire.

La section 2.2 rend compte de la mise au point de sondes potentiométriques submersibles pour la détermination *in-situ* des espèces pertinentes au cycle du carbone et leur déploiement dans l'eau de mer, notamment dans le bassin d'Arcachon (France) et le port de Gênes (Italie). Ces prototypes mis au point se sont avérés prometteurs pour obtenir des informations rapides et fiables sur les concentrations d'ions dans les systèmes marins. Une intégration d'autres capteurs d'ions et/ou dispositifs analytiques est envisageable pour étendre les capacités de ces systèmes à d'autres composés.

La section 2.3 décrit trois concepts différents pour (i) l'acidification locale de l'échantillon à la surface de la membrane de l'électrode sélective aux anions afin de surmonter l'interférence de pH, et (ii) leur intégration pour la détermination de nitrite et de phosphate dans la matrice d'eau douce. Les trois concepts sont basés sur l'apport de protons dans la couche mince adjacente à la membrane de l'électrode, ne nécessitant ni pompe pour l'ajout d'un réactif et ainsi ni dilution des échantillons environnementaux à analyser.

La section 2.4 fournit la description détaillée d'un nouveau module proposé pour l'acidification en ligne des échantillons environnementaux et son intégration pour la détection des nitrites dans l'eau douce et l'eau de mer après élimination de chlorure. Le principe d'acidification est basé sur le processus d'échange d'ions entre les cations présents dans l'échantillon et les protons libérés à travers une membrane échangeuse de cations

preconditionné. Le concept proposé est robuste et facile à intégrer pour des méthodes de détection en flux nécessitant une diminution et un ajustement du pH de l'échantillon.

La section 2.5 est consacrée aux propriétés potentiométriques des récepteurs tripodaux fluorés étudiés en vue de la recherche d'un récepteur phosphate approprié. Aucune sensibilité adéquate et aucune sélectivité vis-à-vis du phosphate n'ont été trouvées dans cette recherche, mais une autre application pratique de l'un des récepteurs a été découverte, à savoir pour la détection de chlorure dans des échantillons biologiques. Le récepteur découvert s'est avéré posséder une sensibilité et une sélectivité suffisantes pour la détection du chlorure dans le sérum humain non dilué, ainsi qu'une bonne stabilité à long terme.

La section 2.6 décrit un dispositif analytique en ligne pour la détection électrochimique du phosphate à l'aide de la voltampérométrie à onde carrée (SWV). La formation du complexe de phosphomolybdate électroactif pour la détection au moyen de SWV est réalisée *via* le transport, à travers des membranes échangeuses d'anions et de cations respectivement couplées ensemble, d'ions molybdate et d'hydrogène dans un échantillon en couche mince. La configuration proposée avec détection SWV permet de détecter des concentrations de phosphate aussi faibles que 0,1 µM et est facile à coupler à la matrice de détection submersible développée précédemment (la section 2.2).

LIST OF PUBLICATIONS

1. Cuartero M., Pankratova N., Cherubini T., Crespo G. A., Massa F., Confalonieri F., Bakker E. In Situ Detection of Species Relevant to the Carbon Cycle in Seawater with Submersible Potentiometric Probes. *Environ. Sci. Technol. Lett.* **2017**, *4,* 410-415.

2. Pankratova N., Cuartero M., Jowett L. A., Howeb E. N. W., Gale P. A., Bakker E., Crespo G. A. Fluorinated tripodal receptors for potentiometric chloride detection in biological fluids. *Biosens. Bioelectron.* **2018**, *99*, 70-76.

3. Pankratova N., Cuartero M., Crespo G. A., Bakker E. In-line acidification for potentiometric sensing of nitrite in natural waters. *Anal. Chem.* **2017**, *89*, 571-575.

4. Pankratova N., Ghahraman Afshar M. Yuan, D., Crespo G. A., Bakker E. Local acidification of membrane surfaces for potentiometric sensing of anions in environmental samples. *ACS Sens.* **2016**, *1*, 48-54.

5. Pankratova N., Crespo G. A., Afshar M. G., Crespi M. C., Jeanneret S., Cherubini T., Tercier-Waeber M.-L., Pomati F., Bakker E. Potentiometric sensing array for monitoring aquatic systems. *Environ. Sci. Process. Impacts* **2015**, *17*, 906-914.

6. Yuan D., Anthis A. H. C., Ghahraman Afshar M., Pankratova N., Cuartero M., Crespo G. A., Bakker E. All-solid-state potentiometric sensors with a multiwalled carbon nanotube inner transducing layer for anion detection in environmental samples. *Anal. Chem.* **2015**, *87*, 8640-8645.

7. Kiprianov A., Pankratova N. Modeling the synthesis of oxyhalide glass of the Li2O-LiCl-SiO2 system. *Glass Phys. Chem.* **2015**, *41* (4), 359-366.

8. Kiprianov A., Pankratova N. Electrode properties of lithium-barium and lithium-cesium-silicate glass with fluorine and chlorine additives. *Glass Phys. Chem.* **2015**, *41* (3), 284-289.

9. Bakker, E., Tercier-Waeber M.-L., Cherubini T., Crespi M. C., Crespo G. A., Cuartero M., Afshar M. G., Jarolimova Z., Jeanneret S., Mongin S., Neel B., Pankratova N., Touilloux R., Xie X., Zhai J. Environmental sensing of aquatic systems at the University of Geneva. *Chimia* **2014**, *68*, 772-777.

10. Kiprianov A., Pankratova N. Investigation of fluorine binding by lithium barium alkali silicate glass. *Glass Phys. Chem.* **2014**, *40* (2), 133-137.

11. Kiprianov A., Pankratova N., Ponomarev I. Potentiometric pH sensors for measurements in fluoride-containing solutions. *Russian J. Appl. Chem.* **2011**, *84* (11), 1883-1889.

ACKNOWLEDGEMENTS

Foremost I would like to thank Prof. Eric Bakker for offering me this great opportunity to join his group at Geneva University, for his guidance, patience and belief in me.

I would like to thank my ex-supervisor at St. Petersburg State University, Dr. Andrey Alekseevich Kiprianov, without whom I would have never reached this point, for the time he has invested in my scientific education, for his care and understanding.

Many thanks to Prof. Kaori Sugihara and Prof. Bernhard Wehrli for having accepted the request to review my thesis and to join the jury for my defense.

I am very grateful to late Prof. Anatolii Aleksandrovich Belyustin and his wonderful wife Dr. Irina Sergeevna Ivanovskaya for supporting me in choosing my path and their cordiality at all stages of my personal and professional development.

I am thankful to Thomas Cherubini, Guy Lecoultre, Stéphane Jeanneret and Serge Rodak for their technical assistance and their constant support.

Thank you so much to Magali Cissokho for the administrative support, patience and encouraging.

I wish to thank Dr. Maria Cuartero and Prof. Gaston Crespo for our successful collaboration and numerous fruitful discussions.

My gratitude to Mary-Lou Tercier-Waeber for the organization of numerous field campaigns, valuable advices and help in the field and in the lab.

Special thanks to my current and former colleagues who have become my dearest friends during this adventurous time: Zdenka Jarolimova, Elena Zdrachek, Abra Penezic, Bastien Neel and Jingying Zhai, for their support, engagement and accepting me as I am.

I am grateful to my dear colleagues I have had pleasure to work with during my stay at the University of Geneva: Romain Touilloux, Sandrine Mongin, Miquel Coll Crespi, Majid Affshar, Agustín Gutiérrez, Sutida Jansod, Suphasinee Sateanchok, Lu Wang, Tao Yuan and especially Dajing Yuan and Xiaojiang Xie.

All my love and thanks to you my dear friends: Olga Kurapova, Tarun Garg, Anna Faustova, Igor Boev, Alesya Mikhailovskaya, Ksenia Lebedeva and Manuel Fernandes.

I am eternally grateful to my parents Marina and Maxim for everything I am and everything they have taught me, as well as my late grandmother Ada for encouraging me to strive for better.

My sincere gratitude to my beloved sister and best friend Katja who has been there for me at all times.

Nadezda Pankratova January 2018

CONTENTS

LIST OF ABBREVIATIONS AND ACRONYMS

AAS: atomic absorption spectroscopy
AES: atomic emission spectroscopy
AUX: auxiliary electrode
CE: counter electrode *or* capillary electrophoresis
GC: glassy carbon
CNTs: carbon nanotubes
CV: cyclic voltammetry
DEHP: bis(2-ethylhexyl) phthalate
DIC: (total) dissolved inorganic carbon
DMSO: dimethyl sulfoxide
DOA: bis(2-ethylhexyl) adipate
DOS: bis(2-ethylhexyl) sebacate
EMF: electromotive force
FIA: flow-injection analysis
IC: ion chromatography
ICP-AES: inductively couple plasma atomic emission spectroscopy
ICP-MS: inductively couple plasma mass spectrometry
ID: inner diameter
IE: indicator electrode
ISE: ion-selective electrode
KTFPB: potassium tetrakis[3,5-bis-(trifluoromethyl)phenyl]borate
KTClPB: potassium tetrakis (4-chlorophenyl) borate
MB: molybdenum blue
MES: 2-morpholinoethanesulfonic acid
MWCNTs: multi-walled carbon nanotubes (here often shortened to CNTs)
NDIR: non-dispersive infrared analysis
NTA: nitrilotriacetic acid
OCP: open circuit potential
OD: outer diameter
o-NPOE: 2-nitrophenyl octyl ether
PEEK: polyether-ether-ketone
PTFE: polytetrafluoroethylene
PVC: poly(vinyl chloride)
RE: reference electrode
SFA: segmented flow analysis
SIA: sequential injection analysis
SWV: square wave voltammetry
TBA: tetrabutylammonium
TDDA: tetradodecylammonium chloride
TDMACl: tridodecylmethylammonium chloride
TDMAN: tridodecylmethylammonium nitrate
THF: tetrahydrofuran
Tris: tris(hydroxymethyl)aminomethane
WE: working electrode

LIST OF APPENDICES

1 INTRODUCTION

1.1 State of the Art

1.1.1 Nutrient detection

Nutrients, such as phosphorus, nitrate and nitrite, are essential for living cells, however, excess of nutrients in surface water can lead to excessive algal growth and thus to decomposition, depletion in dissolved oxygen, eutrophication, as well as reduction of water quality. Cultural eutrophication, stimulated by the anthropogenic nutrients accumulation, has become the major problem for most surface waters and one of the most visible examples of biosphere changes resulting from human activity.[1-3] Essentially eutrophication is the excessive plant growth due to nutrient enrichment leading to many harmful effects, such as formation of toxic bloom-forming algal species, reduced population of fish and shellfish, reduction in transparency, diebacks of sea grasses and corals, and loss of biodiversity.[1,3-6] Managing phosphorus, as well as nitrogen inputs, has been widely considered as a critical and necessary approach to maintain the integrity of the ecosystem and the desirable water quality.[4,5,7] Yet very little understanding has been achieved so far in the interactions between nutrients, their producers and consumers in most aquatic ecosystems.[4]

Therefore, the characterization of nutrient distribution and biogeochemical processes in aquatic ecosystems is of vital importance. Traditional techniques based on sampling, transport and storage of collected samples followed by lab bench analysis are inadequate to provide for high temporal and special resolution. The main challenges in the development

of sensors for *in-situ* monitoring are sensitivity, accuracy, response time, long term drift, size/weight, power consumption, ease of installation and maintenance.[8] Therefore, lots of efforts have been made in the last few decades for the development of *in-situ* techniques that would meet the needs of ecological monitoring. Numerous flow analysis techniques have been developed for *in-situ* species determination of nutrients in aquatic environments providing high quality analytical data.[9,10]

1.1.1.1 Determination of nitrate and nitrite

The mismanagement of natural resources along with active use of inorganic fertilizers in the last few decades has resulted in a significant perturbation of both local and global nitrogen cycles.[11,12] Input of nitrate and nitrite in the environment occurs mainly from agricultural sources, though some amount is being released by industrial and domestic combustion processes resulting in photochemical conversion of gaseous NO_x to NO_3^- within the atmosphere.[11] Elevated nitrate and nitrite concentrations lead to eutrophication of the lakes and algal blooms of coastal waters, contamination of groundwater and drinking water and other harmful effects mentioned above in respect to cultural eutrophication. Therefore, since excessive concentrations of nitrogen species present a significant danger for the state of ecosystems as well as human health, there is a high demand in analytical methods for the determination of nitrate and nitrite species in various environmental matrices. Numerous methods have been reported for the detection of nitrite and nitrate species, including spectrophotometric, chemiluminescent, electrochemical, chromatographic, capillary electrophoresis, spectrofluorometric and electrochemiluminescent methods.[13] However, most of the developed methods are very difficult to implement for *in-situ* measurements.

Most methods reported for *in-situ* determination of nitrate and nitrite species are based on flow analysis with spectrophotometric detection. The latter involves reduction of nitrate to nitrite, followed by the Griess reaction resulting in diazotization with sulfanilimide with subsequent coupling with N-(1-maphthyl)-ethylenediemine dihydrochloride (NED) to form a pink azo dye that is detected at 520-540 nm.[9] The reduction of nitrate to nitrite can be performed by several methods comprising as a main step either the use of copperized cadmium granules or hydrazine-reduction or photoreduction. Multiple modifications of Griess methods were proposed in order to improve the detection limits and eliminate the matrix effect in complex mixtures and samples. One of the peculiar examples of the modified methods is the HPLC-Griess system which has recently become commercially

available and allows for post-column derivatization of chromatographically separated nitrate and nitrite. However, these types of techniques are very expensive and their implementation for *in-situ* detection is hardly achievable.[13] Moreover, all methods based on the Griess reaction suffer in many cases from insufficient sensitivity and interferences (e.g. from silicate or high chloride concentrations) and are time-consuming.[11,13,14]

Hybrid methods comprising chromatography or electrophoresis as a separation step possess the highest sensitivity (down to 10^{-8} M) but require additional steps, such as derivatization procedures, as well as expensive equipment and cannot currently be applied outside a laboratory environment.

Electrochemical methods of detection provide potential low-cost and portability and present one of the most attractive options for the realization of *in-situ* nitrate/nitrite sensors. There are a number of electrochemical approaches for nitrate and nitrite detection which could be used for *in-situ* implementation. The various electrochemical approaches can be classified into two main categories: voltammetric and potentiometric methodologies. Voltammetric techniques have been involved from the very beginning of the 20th century, starting with electrochemical reduction of nitrate at copper electrodes. Various different electrode substrates have been developed since that time, such as nickel, copper-nickel alloys, cadmium, platinum, gold, lead, glassy carbon and other materials.[11,13,15-17] Due to slow kinetics of charge transfer of nitrite and especially nitrate reduction reaction, detection at bare electrode leads to poor sensitivity and often irreproducibility. Various surface modifications have been suggested in order to achieve required sensitivity and stability, e.g. immobilization of the electrocatalysts or enzymes, modification with carbon nanotubes (CNTs), electrolytic plating of fresh layer of metal ions (Cu/Cd) prior to each analysis in order to maintain large active electrode surface area, sol-gel and other modifications[13,18] as well as numerous often quite sophisticated voltammetric or amperometric approaches.[11]

Potentiometric measurements using ion-selective electrodes (ISEs) offer another possibility for nitrate and nitrite detection. Potentiometric sensors present a very attractive tool for *in-situ* monitoring owing to their fast response, possibility of miniaturization, low cost and energy consumption and easy operation.[19,20] Recently developed protocols involving the integration of potentiometric nutrient sensors based on polymeric liquid membranes, are promising for the *in-situ* detection of a wide range of ionic species.[21] Significant progress has been made in developing new membrane materials for lowering detection limits and improving stability of the sensors. Nitrate is normally present in natural samples in

micromolar concentrations, thus simple ion-exchanger-based membranes (typically with tetradodecylammonium nitrate) containing no ionophore can provide a sufficient detection limit, without the need for any special pretreatment of the sample. Nitrite concentration being significantly lower compared to nitrate, direct potentiometric nitrite sensing with currently available ionophores is not feasible. Most of the nitrite-selective electrodes exhibit a large potentiometric pH response due to the favourable hydroxide legation of the ionophore metallic centre.[22] Thus, preliminary removal of hydroxide interference is required prior to potentiometric detection. Moreover, chloride elimination/partial removal is necessary to overcome chloride interference for the analysis of seawater samples (dechloridization approaches have been employed but not developed within the framework of this doctoral thesis).

Due to aforementioned reasons, a large part of the described research aimed at the integration of the most promising ion-selective membranes for *in-situ* potentiometric determination of nutrients (nitrate and nitrite) in environmental samples. Approaches were suggested to improve the detection limits of the potentiometric sensors for the detection of nitrate and nitrite in freshwater by suppressing hydroxide interference.

1.1.1.2 Determination of phosphate

Phosphorus is one of the most vital elements for all living organisms as it is needed for almost all essential biomolecules (nucleic acids, phospholipids) as well most metabolic processes such as photosynthesis, respiration and energy delivery.[1] However, excessive concentrations of phosphate, resulting mainly from human activity, have a very harmful effect on environmental aquatic systems as they promote eutrophication.[4] Monitoring and control of this element is needed in order to avoid its excessive levels.

The standard method for the determination of soluble phosphate is colorimetry using molybdenum blue reaction (MB). The latter is quite difficult and expensive to adapt for *in-situ* or on-line measurements since it requires safe disposal of large amount of corresponding reagents, rigorous observation of temperature conditions and time intervals between detection and reagent addition, in order to control the reduction process (degree of product formation) and product stability.[10,23] The method has been widely accepted in 1960s even though the reaction itself was mentioned by Scheele already in 1783 and re-discovered later by Berzelius in 1826.[24] Over few decades the method has been differently optimized for real analytical applications and various modifications of the method exist

today. The common features of MB methods are the following: all of them require strong acidic media (pH~0-1), a source of Mo (VI) and the reducing agent/protocol.[23]

The stages of the reaction can be simplistically described by two following equations:

$$PO_4^{3-} + 12MoO_4^{2-} + 27H^+ \rightarrow H_3PO_4(MoO_3)_{12} + 12H_2O \qquad \text{(eq. 1.1)}$$

$$H_3PMo(VI)_{12}O_{40} + \text{Reductant} \rightarrow [H_4PMo(VI)_8Mo(V)_4O_{40}]^{3-} \qquad \text{(eq. 1.2)}$$

The ratio between acid and molybdate is essential both for the formation of the heteropoly acid (equation 1.1) and for controlling its reduction (equation 1.2).

By far the most widely-used reduction method for batch and automated analyses is based on the approach described by Murphy and Riley, suggesting using ascorbic acid for the reduction of phosphomolybdate complex in the presence of antimony potassium tartrate as the catalyst.[23,25,26] In the last two-three decades increased attention has been payed to the implementation of MB reaction in flow analysis for phosphate determination and further development of *in-situ* phosphate sensing.[26] In order to achieve reliable performance of MB reaction-based approaches, one must take special care of the sample presentation and reagent stability. One must as well take into account that it is only in polluted/eutrophic water or wastewater, containing highly elevated phosphate levels (ranges of mg L^{-1} of P), where direct colorimetric phosphate determination is possible. The detection limit of colorimetry-based analytical methods is often insufficient for the determination of phosphate in natural water and especially in pristine waters with very low phosphate levels (<1 µg L^{-1} P).[27,28] In this extreme case sample preconcentration is necessary to enable phosphate detection, using for example anion-exchange resins (in low ionic strength waters), magnesium hydroxide-induced co-precipitation, precipitation with lanthanum nitrate, reverse osmosis and other methods.[28]

Except for water with very low phosphate concentrations, currently available flow methods (flow injection analysis [FIA], segmented flow analysis [SFA], sequential injection analysis [SIA] etc.) often provide sufficiently low detection limits for the analysis of natural samples. Among the latter are FIA-methods based on aforementioned UV-VIS spectrophotometry (there are numerous FIA and SIA variations for the spectrophotometric phosphate determination), as well as on ICP-AES detection, fluorometric or chemiluminescent detection.[9,27] Despite of wide acceptance of MB-based spectrophotometric methods, the latter meet few main challenges in view of *in-situ* application in environmental samples, such as turbidity interference and operational

complexity.[9] Moreover, significant interfering effect of other species other than phosphate can be observed, the major interfering ion being silicate.[9,29]

Electrochemical methods of detection have as well found their application for phosphate species determination in real samples. The most common flow methods using electrochemical detection are based on potentiometric and amperometric approaches[27]. Recently a few promising FIA-based voltammetric approaches have been proposed for phosphate determination real samples.[1,30,31] Potentiometric detection would have been the most cost-effective and the simplest approach do adapt for *in-situ* analysis. However, as of today, potentiometric determination of submicromolar anion concentrations using polymeric membrane-based ion-selective electrodes is accessible only for a very small number of ions, such as iodide or perchlorate.[32] For such hydrophilic anions as phosphate the natural levels even in moderately polluted/eutrophic waters are not accessible by potentiometry. Owing to the absence of sufficiently sensitive phosphate receptors for potentiometric detection, the current work integrates the voltammetric approach for phosphate detection, allowing for considerably lower detection limits compared to potentiometry.

1.1.2 Determination of species relevant to the carbon cycle

1.1.2.1 Determination of CO_2

The oceanic carbon cycle is a complex process influenced by various chemical, physical as well as biological parameters.[8] It has been widely accepted that oceans are the global sink for anthropogenic atmospheric CO_2, yet it remains unclear how big the size of this sink is and what exactly are the processes regulating the CO_2 fluxes into the ocean.[2,33] Quantification of the uptake of anthropogenic CO_2 by the oceans is crucial in order to be able to predict and to deal with the consequences of anthropogenic influences as well as to understand and to predict the net community metabolism, air-sea gas exchange, carbon export from the surface to depth and the causes of carbon cycle variability from seasonal to interannual timescales.[8,34]

In fact the CO_2 uptake by the ocean helps to moderate the climate changes; however the hydrolysis of CO_2 in seawater results in gradual decrease of seawater pH according to the following reaction:[35]

$$CO_2 + CO_3^{2-} + H_2O \leftrightarrow 2HCO_3^- \qquad \text{(eq. 1.3)}$$

It has been shown that ocean surface pH has decreased by approximately 0.1 pH unit since the beginning of the industrial period while the estimated pH drop by the end of the 21st century is about 0.4 pH units.[35,36] The latter is a drastic change for the typically slowly evolving marine environments and may lead to significant changes in structure and biodiversity of aquatic ecosystems.[35-37] Thus the development of accurate systems with high spatial and temporary resolution for CO_2 monitoring is of high importance.

The aquatic carbon dioxide system is excessively described by two CO_2 system parameters, including pH, total dissolved inorganic carbon (DIC), total alkalinity (A_T), CO_2 fugacity (fCO_2) and carbonate ion (CO_3^{2-}) concentration.[8,38] Shipboard methods for fCO_2, A_T, DIC, and pH are well established, most commonly used parameter pairs being pH–A_T, pH–DIC, fCO_2–A_T, or fCO_2–DIC.[38] pH is commonly measured using potentiometry with pH glass electrode or spectrophotometry, with indicator dyes; DIC determination in seawater is typically achieved by coulometry or non-dispersive infrared (NDIR) analysis; total alkalinity is most often determined by potentiometric titration and less often using spectrophotometric methods.[8,39] fCO_2 determination in seawater is commonly achieved using gas chromatography, NDIR measurements or fiber-optic pCO_2 sensors based on gas transfer across permeable membrane into pH-sensitive dye solution.[8,33,40]

Exceptional precision and accuracy are required for environmental monitoring, hence the shipboard techniques that have achieved this are of a very complex fluidic design and require frequent calibrations. The use of different equilibration designs based either on bubble-type equilibrator or membranes in different form limit the response time of the systems. The *in-situ* systems with adequate performance for full CO_2 system characterization are very complex since they require numerous pumps and valves, considerable power and frequent operational interactions.[8,40] Moreover, some of the analysers, e.g. NDIR analysers can be affected by vibration on ships which leads to increased instability of the readings.[8] In fact NDIR analysers, with the measurement principle based on the absorption of radiation at a specific wavelength by the gas molecules, are most commonly used in automated CO_2 instruments.[8,41] Along with infrared source, measuring chamber, wavelength filter and infrared detector, these systems require rigorous temperature control, automatic zero-correction in order to correct for the drift and either moisture correction or drying the air prior to the analysis owing to the absorption of infra-red radiation by the moisture.[8,41] The complexity of the developed systems determines their high costs and expensive maintenance. Thus, the development of a new

generation of reliable arrays for carbonate system characterization is required, with reduced complexity and cost, to displace the traditional lab bench methodologies in order to collect high quality CO_2 data with high temporal resolution, enabling monitoring of both long and short-term CO_2 changes.

Potentiometric sensors are promising tools for the realization of *in-situ* monitoring systems for aquatic environments owing to their low cost, simple fabrication, easy miniaturization and low energy consumption.[42-45] However, the lower detection limit of the well-established Severinghaus electrode[46] for potentiometric CO_2 determination is often not sufficient for the determination of low pCO_2 levels. Moreover, additional difficulties for *in-situ* integration are caused by the poor stability of the signal and long response time, as well as possible interferences from other gaseous species.[47,48] Within the framework of this research we aimed to integrate a more robust concept, based on all-solid-state hydrogen and carbonate-selective electrodes. To the best of our knowledge, it is the first time here that the *in-situ* monitoring of species related to the carbonate cycle in the sea has been accomplished by potentiometric measurements of pH-CO_3^{2-} variables couple.[49] The developed approach can be easily adapted to the one proposed recently by Xie et al.[48] for the determination of dissolved CO_2, comprising a pH glass electrode measured against a carbonate-selective electrode. However, no direct coupling between the two electrodes has been implemented within this research owing to the configuration of the submersible probe requiring a common reference electrode for multi-ion detection.[49]

1.1.2.2 Determination of calcium

Dissolved calcium is a prime participant in calcium carbonate formation by shell-forming marine organisms and by inorganic precipitation and its concentration is in control of precipitation and solution processes in the aquatic environments.[50] Moreover, calcium concentration is a parameter related to changes in total alkalinity and DIC and has to be taken into consideration for a thorough description of processes relevant to the carbon cycle, such as in particular the dissolution of marine carbonates, resulting in the neutralization of anthropogenic CO_2.[36] Therefore, determination of calcium concentration is of particular interest for aquatic scientists.

The marine carbonates include biogenic magnesian calcites (from coralline algae), aragonite (from corals and pteropods) and calcite (from coccolithophorids and foraminifera).[36] Calcium is affecting the total alkalinity via the following dissolution reaction:[36]

$$CO_2 + CaCO_3 + H_2O \leftrightarrow 2HCO_3^- + Ca^{2+} \qquad \text{(eq. 1.4)}$$

The reaction mentioned (equation 1.4) is mainly governed by the carbonate shells of the marine plankton produced in euphotic (sunlight) zone which are dissolved or deposited in the sea sediments upon their death.[36] The increase of anthropogenic CO_2 levels in the ocean results in the increase of dissolution and the decrease of calcium carbonate saturation state. The resulting reduced export of calcium carbonate from the high latitudes would in its turn lead to increased surface concentration of carbonate, thereby promoting the CO_2 uptake from the atmosphere.[35] At the same time, the occurring calcium carbonate undersaturation may have significant impact on the structure and biodiversity of ecosystems.

Thus, dissolved calcium concentration is one of the parameters closely related to CO_2 uptake by seawater and must be taken into account in order to understand and quantify the carbonate cycle. Traditionally used methods for calcium determination are typically lab bench approaches based on spectrometric methods (e.g. atomic absorption spectrometry [AAS], inductively coupled plasma-atomic emission spectrometry [ICP-AES], inductively coupled plasma-mass spectrometry [ICP-MS]), separation methods (ion chromatography [IC], capillary electrophoresis [CE]), wet chemical methods (titration, gravimetry) or electroanalytical methods (potentiometry, voltammetry).[51,52] Electroanalytical methods, in particular potentiometry, are simplest and most cost-effective ones in order to integrate into *in-situ* analysis. Therefore, the potentiometric approach to calcium determination has been chosen within the framework of this work, provided that calcium-selective receptors with adequate selectivity and sensitivity are today available. [20]

1.2 Objectives

This work is intended to provide new tools, approaches and experimental arrangements for the detection of nutrients and species relevant to the carbon cycle, in order to predict and scale up the effect of micro-environmental dynamics on the ecology of aquatic ecosystems.

The general objectives of the project were as follows:

1. Development of protocols for the determination of nitrate, nitrite, inorganic phosphate, dissolved calcium, pH and carbonate species in environmental samples (freshwater and/or seawater), in view of their subsequent integration for *in-situ* or on-site measurements.
2. Testing of the proposed approaches in real world sample matrices in the laboratory.
3. Optimization of the effectively developed protocols and their implementation for field monitoring with subsequent execution *in situ* or/and on-site.
4. Evaluation of performance. Validation of the results obtained in real sample matrices by other analytical techniques.

This project proposes a close collaboration between sensor development teams and scientists directly involved in field monitoring studies carried out at the Lake Greifensee (Switzerland), in Genoa Harbor (Italy) and Arcachon Bay (France).

1.3 Electrochemical Techniques

The electrochemical techniques used within the framework of this research are discussed in the following section.

1.3.1 Zero-Current Potentiometry

Potentiometry is a zero-current technique in which the information about the sample composition is obtained by measuring the potential established across the membrane of the indicator electrode.[53] The choice of the membrane composition depends on the analyte as well as the type of application (concentration range, interferences, sample matrix etc.).

A potentiometric sensor generally consists of two parts: the selector element and the transduction element. The selector element must provide the selectivity towards the analyte ion and the conversion of chemical information about the ionic species in the sample into a domain which is measurable by the nonselective transduction element.[45] It is the potential difference between the indicator electrode (IE) and the reference electrode (RE) that is being measured in potentiometry (see Figure 1.3.1a). The device used to measure the open circuit potential (OCP, or potential at zero current) should not cause any current flow in a galvanic cell to avoid the ohmic voltage drop, thus electronic voltmeters with digital readout and very low current drain (ca. 10^{-14} A) are used for such measurements.[54]

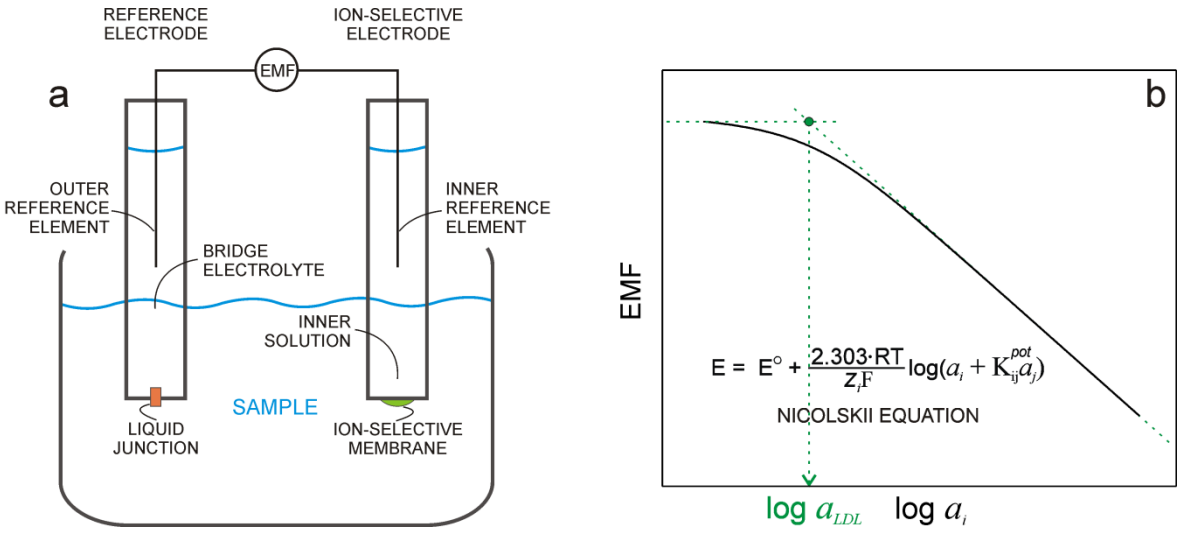

Figure 1.3.1. Potentiometric protocol: (a) a cell for potentiometric determinations; (b) typical potentiometric response in mixed solution of ions of the same valency, described by the Nicolskii equation. Vertical line indicates the lower detection limit.

The reference electrode must have a defined stable potential, independent of the sample composition.[55] Typical reference electrode example is a silver chloride-coated silver electrode immersed into solution of highly concentrated potassium chloride (e.g., Ag|AgCl|KCl, 3M). In this case the potential of the electrochemical cell (see Figure 1.3.1a) is defined by the activity of the analyte ions.

The indicator electrode membrane may be composited of a pure metal (e.g. copper electrode, selective for Cu^{2+}) or metal compound (e.g. Ag/AgCl electrode, selective for chloride), glass (e.g. pH glass electrode), crystalline materials (single crystal membranes, e.g. lanthanum fluoride crystal doped with europium (II), selective for fluoride; or polycrystalline membranes, e.g. Ag_2S-based membrane for sulphide; or mixtures of salts, e.g. mixture of PbS, CdS and CuS with Ag_2S selective for Pb^{2+}, Cd^{2+} and Cu^{2+}), liquid polymer membrane materials doped with ionophore and/or ion-exchanger (e.g. polyvinylchloride or polyurethane-based membranes, selectivity available for various number of inorganic anions and cations).[55]

Under the conditions that the activity of the analyte ions in the membrane remains constant, the composition of the membrane-sample interface is constant and the liquid-junction potential of the cell is negligible, the potential at the indicator electrode membrane measured against the reference electrode is described by the well-known Nernst equation[56]:

$$E = E^0 + \frac{RT}{z_i F} \ln a_i \qquad \text{(eq. 1.5)}$$

where a_i is the activity of the primary (analyte) ion and E^0 is a constant including all sample-independent potential contributions defined by the design of a particular galvanic cell (reference and indicator electrode configuration)[53]. In the presence of interfering ions the potential of the galvanic cell can be described by Nicolskii equation[56]:

$$E = E^0 + \frac{RT}{z_i F} \ln\left(a_i + \sum_{j \neq i} K_{ij}^{pot} a_j \right) \qquad \text{(eq. 1.6)}$$

where a_i and a_j are the activities of the primary (i) and interfering (j) ions in a mixed sample, z_i is the charge of ions i, K_{ij}^{pot} is the potentiometric selectivity coefficient.

The selectivity coefficient K_{ij}^{pot} characterizes the selectivity of the electrode for ion i over ion j present in the sample. The smaller the K_{ij}^{pot} value is, the more selective the electrode is for i-ions.[56] The selectivity coefficient is an important characteristic defining the lower

detection limit of a given ion-selective electrode. A typical illustartion of Nicolskii-Eisenman formalism is given in Figure 1.3.1.b, where the thermodynamic lower detection limit (defined as $a_{i,LDL} = K_{ij}^{pot} a_j$ by equation 1.6) correponds to the activity of ion *i* at the intersection of the two extrapolated linear segments of the $E - \log a_i$ plot (see Figure 1.3.1.b).[57] The application of the Nicolskii formalism is limited to the mixtures of ions of the same valency. More complex theories have been developed to describe the potential response in mixed solutions of ions with different charge.[56,58,59]

The field of ion-selective potentiometric sensor has matured a lot in the last few decades.[60] Potentiometry is probably the most widely used method in chemical instrumental analysis.[55] It has been especially broadly accepted in clinical analysis for the routine determination of pH, pCO_2 and concentrations of Li^+, K^+, Ca^{2+}, Mg^{2+}, Na^+, Cl^-, CO_3^{2-} /HCO_3^- and other ionic species.[44,55,61-63] As of today, due to the development of new molecular receptors and considerable improvement of the detection limits of ion-selective electrodes, the interest to the application of potentiometric methodologies has increased in other areas, in particular in environmental analysis.[64-66] However, further studies and development are needed in order to integrate this simple, fast-responding and cost-effective methodology for environmental monitoring requiring very high accuracy, precision and sensitivity, as well as very high stability, the latter being very critical for long-term measurements.[66,67]

1.3.2 Dynamic Electrochemistry

Dynamic electrochemistry generally refers to a group of various electrochemical techniques involving the imposition of a current or potential program which results in the response of the system that can be measured or recorded.[68] Two general experimental arrangements are possible, that is using either a two-electrode or a three-electrode cell (see Figure 1.3.2a).[69]

A two-electrode cell consists of a working (indicator) electrode coupled with the reference electrode (see Figure 1.3.2a). The reference electrode should be an electrode with the behaviour close to nonpolarizable (the passage of current does not affect its potential), with a known constant potential. The use of a two-electrode cell is reasonable in systems with a small ohmic potential drop (iR_s value of few mV), as for example in classic polarography.[69] In non-aqueous solutions with low conductivity or in large-scale galvanic/electrolytic cells the use of a three-electrode systems is preferable (see

Figure 1.3.2b).[69] In this case no current flows in the circuit of the reference electrode, which therefore is not polarized.[54]

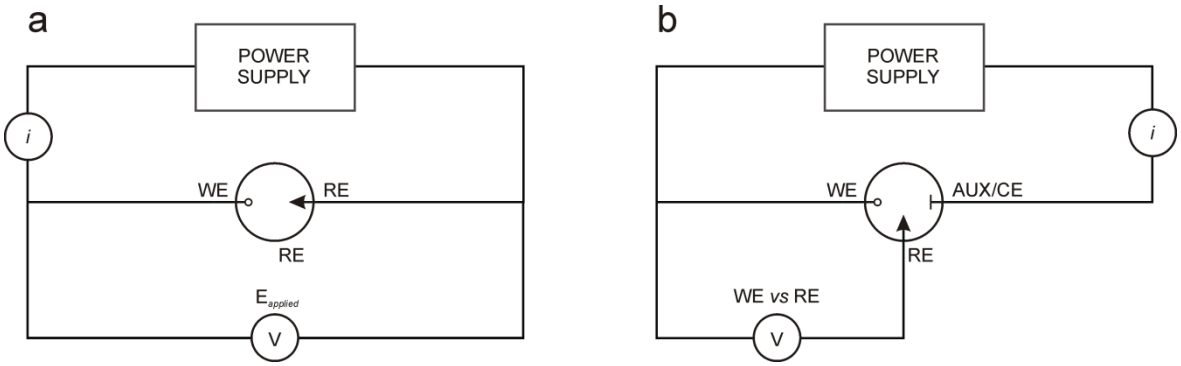

Figure 1.3.2. Schematic diagram of cells for dynamic electrochemistry: (a) two-electrode cell, (b) three-electrode cell.[69]

Most frequently one is interested in the reaction occurring at only one electrode (working, or indicator electrode).[69] When an electric potential is applied and current passes through the system, charge is transported across the solution-electrode surface interface. When the redox reaction does not happen spontaneously, it may still occur in a certain range of potentials: a cathodic reaction at electrode potentials more negative and the anodic reaction at electrode potentials more positive than the equilibrium potential.[54] By imposing more negative potentials the energy of the electrons can be raised to a level high enough to favour the transfer into vacant electronic states on species in the electrolyte. Or, vice versa, upon applying a more positive potential, electrons on solutes in the electrolyte may find a more favourable energy on the electrode and will transfer there.[69]

However, in general case the reaction occurring at the working electrode is governed not exclusively by the electron transfer. There are two types of processes that occur at the electrode surface. The fist type refers to faradaic processes which comprise the electron transfer between the solution and the electrode surface, resulting in the oxidation or reduction. The second type corresponds to such processes as adsorption and desorption and the change of the electrode surface-solution interface owing to the changes in potential, electrode area and/or solution composition, resulting in external current flow (at least transiently).[69] The main steps of a general reduction reaction are as follows (see Figure 1.3.3): (1) mass transfer from the bulk of the solution to the electrode surface, (2) electron transfer at the electrode surface, (3) chemical reactions proceeding or following the electron transfer, (4) surface reactions (adsorption, desorption, crystallization).[69] The reaction is governed by all these processes, one of them typically being the rate-limiting. For example, if the electrode reaction kinetics is sufficiently fast, the process at the

electrode surface would be controlled by the mass transport (in the absence of chemical reactions).[70]

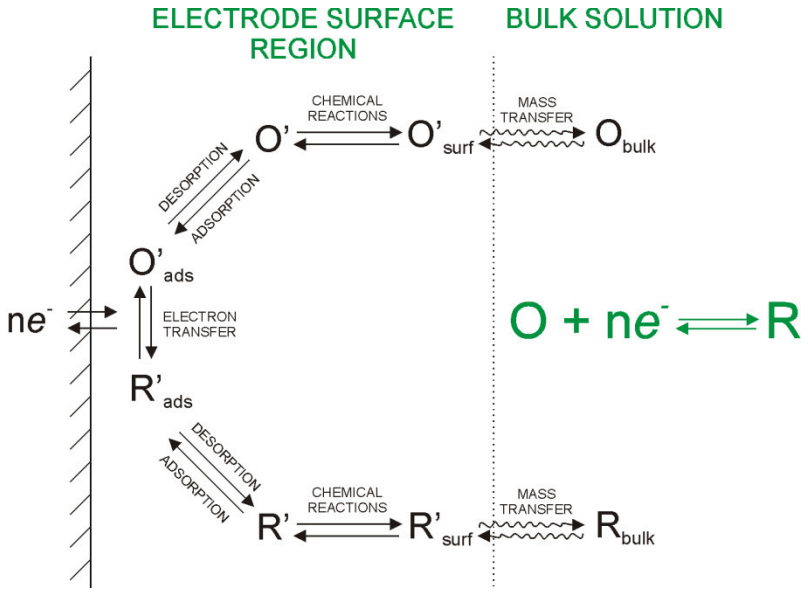

Figure 1.3.3. Pathway of a general electrode reaction (Figure from [69])

Unlike in zero-current potentiometry, no strict equilibrium is established in dynamic electrochemical techniques and thus the resulting response relates to the transient or/and steady state of the system.[68] The currents measured in the steady state are purely faradaic while in the transient measurements (relaxation measurements) the current consists of both faradaic and non-faradaic components. The transient approaches are relevant for studying electrode surfaces and the kinetics of fast electrochemical reactions.[54] They are performed rapidly, essentially by applying the perturbation and measuring the system response as a function of time.[54]

The transient measurements can be classified according to the controlled parameter: potentiostatic or potentiodynamic (controlled potential), galvanostatic or galvanodynamic (controlled current), coulonostatic (controlled charge). The latter can be in their turn grouped (see Figure 1.3.4) according to the shape of perturbation (step (1) or continuous (2) variation of the perturbation parameter), and according to the number of perturbation: single (2), pulses (square or rectangular (3), triangular (4)), cyclic perturbations (repetitive excursions, (5), (6)) as well as more complex pulses composed of a combination of perturbation protocols, such as (7) and (8).

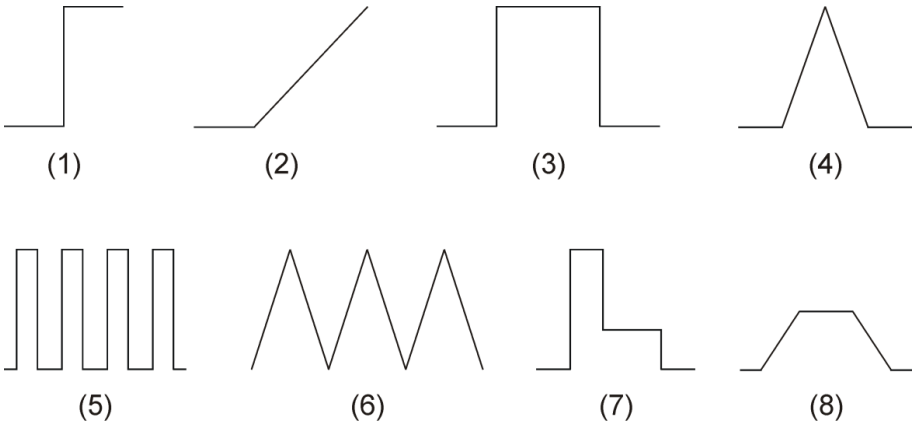

Figure 1.3.4. Various types of perturbations for transient measurements.[54] See the text above for the details.

Here below we will only discuss two dynamic techniques relevant to the current work: cyclic voltammetry and square wave voltammetry.

1.3.2.1 Cyclic Voltammetry (CV)

Cyclic voltammetry is one of the most common techniques for electrode testing and qualitative characterization of electrode reactions (coupled to homogeneous chemical reactions in the solution).[53,71,72] Cyclic voltammetry is a very useful method for the identification of different electrochemically active species and different phases occurring during oxidation or reduction of the electrode material.[71] It is often used as the first step of the electroanalytical study as it allows for the rapid determination of the redox potential of electroactive species and quick evaluation of media influence.[53]

In CV technique the potential of the working electrode is linearly scanned in an unstirred solution using a triangular potential waveform (see Figure 1.3.5a). Singular or multiple potential scans may be used, depending on the application. The resulting current is measured while cycling the potential of the working electrode; the obtained current-potential plot is called cyclic voltammogram.[53,55,72]

A typical cyclic voltammogram is shown in Figure 1.3.5b. In the first potential sweep (forward scan, here we consider oxidized form as a starting point) the potential is scanned towards more negative values. When the potential is reduced to a sufficiently low value in order to reduce the species O, the cathodic current starts increasing fast, until the concentration of species O at the electrode surface substantially decreases resulting in the peak on the cyclic voltammogram. As concentration of oxidized species O at the electrode surface is depleted, the current decay is observed after the peak. Thereafter the potential scan direction is switched to the reverse scan causing rapid anodic current increase owing

to oxidation of species R, then a peak current and subsequent current decay are observed again, resulting from the depletion of reduced form R at the electrode surface.[72]

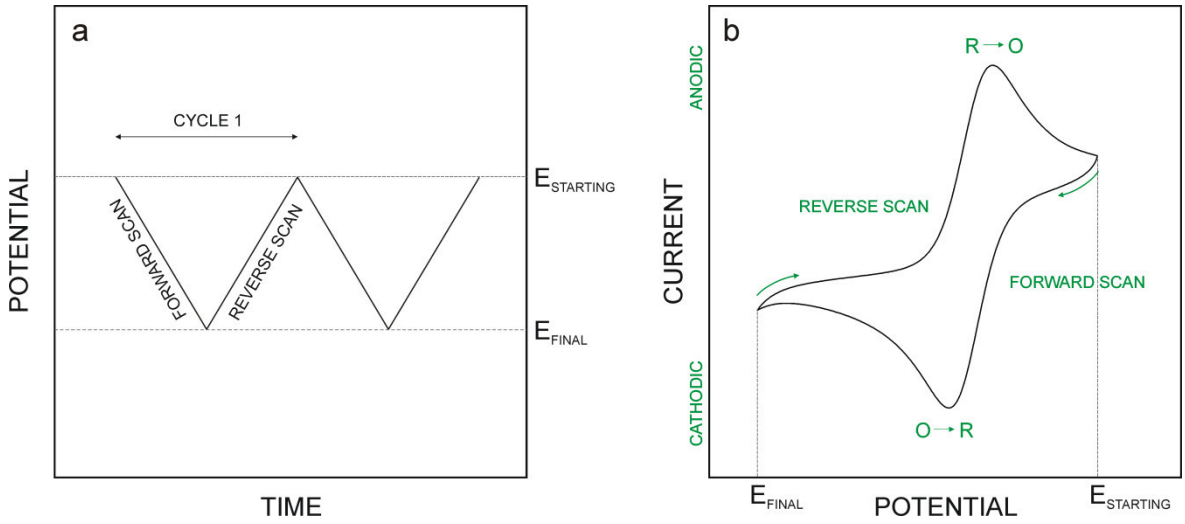

Figure 1.3.5. Cyclic voltammetry (CV) protocol: (a) CV excitation signal, (b) typical cyclic voltammogram for one of the consecutive cycles for a reversible redox reaction: $O + ne^- \leftrightarrow R$.

Cyclic voltammetry is commonly applied to study the kinetics of electrochemical reaction, for example to estimate its reversibility. For a reversible electrochemical reaction the anodic and cathodic peak currents should be identical. At the same time the ratio between the two peak currents is significantly affected by chemical reactions coupled to the electrode process.[72] The difference between peak potentials of the forward and reverse current peaks may give important information about electron transfer kinetics. Furthermore, it allows predicting the limiting step of the electrode reaction in given conditions: if the electrochemical reaction is controlled by diffusion, the peak height is proportional to the square root of the sweep rate.[71]

At sufficiently low sweep rates, when electrochemical process are sufficiently fast, the integration of the current versus time in thin layer samples gives an accurate value of the capacity of the active mass (in coulomb), a characteristic independent of time. Running linear potential scan and then reversing the sweep rate, resulting in the reverse redox reaction, allows evaluation of reversibility and coulombic efficiency of the occurring reaction by integrating the current *vs* time.[71,73]

1.3.2.2 Square Wave Voltammetry (SWV)

While cyclic voltammetry is one of the most commonly used electroanalytical techniques for qualitative studies of electrode reactions, pulse techniques are generally advantageous for quantitative measurements.[72] Square wave voltammetry is one of the most widely used

pulse techniques for electroanalytical analysis as it offers the advantage of good speed and high sensitivity.[55]

The excitation waveform for SWV (shown in Figure 1.3.6a) consists of a square wave superimposed on a staircase. The current is being sampled both at the end of the forward and backward pulses (see circles in Figure 1.3.6a) and corresponding oxidation and reduction waves are obtained (see Figure 1.3.6b). The resulting signal (δi) is taken by subtracting the reduction scan from the oxidation scan (or vice versa) and the voltammogram is obtained by plotting δi *vs* the base staircase potential.[53,70] The peak current of the obtained peak-shaped voltammogram for a rapid reversible redox system is proportional to the concentration of electrochemically active species.

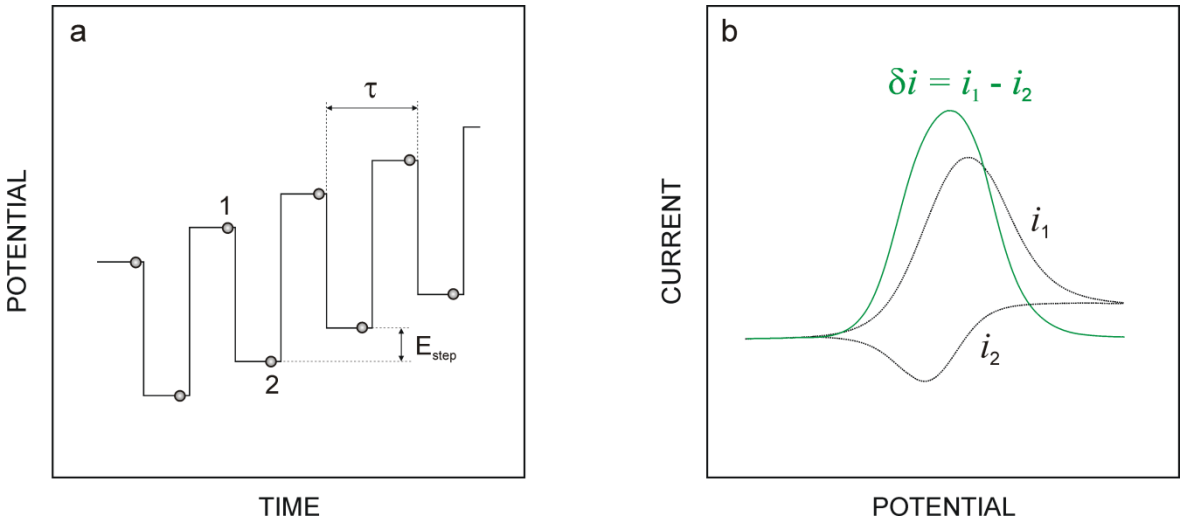

Figure 1.3.6. Square wave voltammetry (SWV) protocol: (a) SWV excitation signal; (b) typical square wave voltammogram for a reversible redox reaction: $O + ne^- \leftrightarrow R$. In this example i_1 is the forward current, i_2 is the reverse current. The resulting signal (δi) is obtained by extracting the current at potential 2 from the current at potential 1 (see Figure 1.3.6a).

Owing to the fact the net signal is the difference between anodic and cathodic currents and thus is larger than forward or backward component taken separately, square wave voltammetry provides better sensitivity than cyclic voltammetry or simple step techniques, resulting in the detection limits as low as 10^{-8} M.[53] Another major advantage of SWV technique is its speed. The effective scan rate is defined by the potential step height (E_{step}) and the frequency (f). Frequencies up to hundreds of Hz can be used, allowing for very high effective scan rates (for example, typical frequency 100 Hz and step potential 5 mV provide for effective scan rate of 500 mV/s) and very rapid recording of the complete voltammogram.[53]

1.4 References

(1) Talarico, D.; Cinti, S.; Arduini, F.; Amine, A.; Moscone, D.; Palleschi, G. *Environ. Sci. Technol.* **2015**, *49*, 7934-7939.

(2) DeGrandpre, M. D.; Hammar, T. R.; Smith, S. P.; Sayles, F. L. *Limnol. Oceanogr.* **1995**, *40*, 969-75.

(3) McDowell, R. W.; Hamilton, D. P. *Mar. Freshwater Res.* **2013**, *64*, iii-vi.

(4) Smith, V. H.; Schindler, D. W. *Trends Ecol. Evol.* **2009**, *24*, 201-7.

(5) Schindler, D. W. *Limnol. Oceanogr.* **2006**, *51*, 356-363.

(6) Smith, V. H. *Limnol. Oceanogr.* **2006**, *51*, 377-384.

(7) Smith, V. H.; Joye, S. B.; Howarth, R. W. *Limnol. Oceanogr.* **2006**, *51*, 351-355.

(8) Schuster, U.; Hannides, A.; Mintrop, L.; Körtzinger, A. *Ocean Science* **2009**, *5*, 547-558.

(9) Gray, S.; Hanrahan, G.; McKelvie, I.; Tappin, A.; Tse, F.; Worsfold, P. *Environ. Chem.* **2006**, *3*, 3-18.

(10) Warwick, C.; Guerreiro, A.; Soares, A. *Biosens. Bioelectron.* **2013**, *41*, 1-11.

(11) Moorcroft, M. J.; Davis, J.; Compton, R. G. *Talanta* **2001**, *54*, 785-803.

(12) Brimblecombe, P.; Stedman, D. H. *Nature* **1982**, *298*, 460-2.

(13) Wang, Q.-H.; Yu, L.-J.; Liu, Y.; Lin, L.; Lu, R.-g.; Zhu, J.-p.; He, L.; Lu, Z.-L. *Talanta* **2017**, *165*, 709-720.

(14) Crompton, T. R. *Determination of anions in natural and treated waters*; CRC Press: London, 2002, p 880.

(15) Da Silva, S. M.; Mazo, L. H. *Electroanalysis* **1998**, *10*, 1200-1203.

(16) Armijo, F.; Goya, M. C.; Reina, M.; Canales, M. J.; Arevalo, M. C.; Aguirre, M. J. *J. Mol. Catal. A: Chem.* **2007**, *268*, 148-154.

(17) Milhano, C.; Pletcher, D. *J. Electroanal. Chem.* **2008**, *614*, 24-30.

(18) Doherty, A. P.; Forster, R. J.; Smyth, M. R.; Vos, J. G. *Anal. Chim. Acta* **1991**, *255*, 45-52.

(19) Bobacka, J.; Ivaska, A.; Lewenstam, A. *Chem. Rev.* **2008**, *108*, 329-351.

(20) Bakker, E.; Pretsch, E. *Angew. Chem.* **2007**, *46*, 5660-5668.

(21) Crespo, G. A.; Bakker, E. *RSC Adv.* **2013**, *3*, 25461-25474.

(22) Hassan, S. S. M.; Marei, S. A.; Badr, I. H.; Arida, H. A. *Electroanalysis* **2000**, *12*, 1312-1317.

(23) Nagul, E. A.; McKelvie, I. D.; Worsfold, P.; Kolev, S. D. *Anal. Chim. Acta* **2015**, *890*, 60-82.

(24) Mueller, A.; Serain, C. *Acc. Chem. Res.* **2000**, *33*, 2-10.

(25) Murphy, J.; Riley, J. P. *Anal. Chim. Acta* **1962**, *27*, 31-6.

(26) McKelvie, I. D.; Peat, D. M. W.; Worsfold, P. J. *Anal. Proc.* **1995**, *32*, 437-45.

(27) Estela, J. M.; Cerda, V. *Talanta* **2005**, *66*, 307-331.

(28) Nollet, L. M. L. *Handbook of Water Analysis, Second Edition*; CRC Press: Boca Raton, 2007, p 769.

(29) Udnan, Y.; McKelvie, I. D.; Grace, M. R.; Jakmunee, J.; Grudpan, K. *Talanta* **2005**, *66*, 461-466.

(30) Barus, C.; Romanytsia, I.; Striebig, N.; Garçon, V. *Talanta* **2016**, *160*, 417-424.

(31) Cheng, W.-L.; Sue, J.-W.; Chen, W.-C.; Chang, J.-L.; Zen, J.-M. *Anal. Chem.* **2010**, *82*, 1157-1161.

(32) Malon, A.; Radu, A.; Qin, W.; Qin, Y.; Ceresa, A.; Maj-Zurawska, M.; Bakker, E.; Pretsch, E. *Anal. Chem.* **2003**, *75*, 3865-3871.

(33) Lefevre, N.; Ciabrini, J. P.; Michard, G.; Brient, B.; DuChaffaut, M.; Merlivat, L. *Mar. Chem.* **1993**, *42*, 189-98.

(34) Seidel, M. P.; DeGrandpre, M. D.; Dickson, A. G. *Mar. Chem.* **2008**, *109*, 18-28.

(35) Orr, J. C.; Fabry, V. J.; Aumont, O.; Bopp, L.; Doney, S. C.; Feely, R. A.; Gnanadesikan, A.; Gruber, N.; Ishida, A.; Joos, F.; Key, R. M.; Lindsay, K.; Maier-Reimer, E.; Matear, R.; Monfray, P.; Mouchet, A.; Najjar, R. G.; Plattner, G.-K.; Rodgers, K. B.; Sabine, C. L.; Sarmiento, J. L.; Schlitzer, R.; Slater, R. D.; Totterdell, I. J.; Weirig, M.-F.; Yamanaka, Y.; Yool, A. *Nature* **2005**, *437*, 681-686.

(36) Feely, R. A.; Sabine, C. L.; Lee, K.; Berelson, W.; Kleypas, J.; Fabry, V. J.; Millero, F. J. *Science* **2004**, *305*, 362-367.

(37) Sabine, C. L.; Feely, R. A.; Gruber, N.; Key, R. M.; Lee, K.; Bullister, J. L.; Wanninkhof, R.; Wong, C. S.; Wallace, D. W. R.; Tilbrook, B.; Millero, F. J.; Peng, T.-H.; Kozyr, A.; Ono, T.; Rios, A. F. *Science* **2004**, *305*, 367-371.

(38) Robert H. Byrne; Michael D. DeGrandpre; R. Timothy Short; Todd R. Martz; Liliane Merlivat; Craig McNeil; Fred L. Sayles; Ryan Bell; Fietzek, P. *Proceedings of OceanObs'09: Sustained Ocean Observations and Information for Society. ESA Publication, WPP-306. OceanObs'09, Venice* **2010**, 8.

(39) Liu, X.; Byrne, R. H.; Adornato, L.; Yates, K. K.; Kaltenbacher, E.; Ding, X.; Yang, B. *Environ. Sci. Technol.* **2013**, *47*, 11106-11114.

(40) Friederich, G. E.; Brewer, P. G.; Herlien, R.; Chavez, F. P. *Deep Sea Res.* **1995**, *42*, 1175-86.

(41) Mendes, L. B.; Ogink, N. W.; Edouard, N.; Van Dooren, H. J. C.; Tinôco, I. d. F. F.; Mosquera, J. *Sensors* **2015**, *15*, 11239-11257.

(42) Bakker, E.; Telting-Diaz, M. *Anal. Chem.* **2002**, *74*, 2781-2800.

(43) Bakker, E.; Pretsch, E. *Angew. Chem., Int. Ed.* **2007**, *46*, 5660-5668.

(44) Oesch, U.; Ammann, D.; Simon, W. *Clin. Chem.* **1986**, *32*, 1448-59.

(45) Antonisse, M. M. G.; Reinhoudt, D. N. *Electroanalysis* **1999**, *11*, 1035-1048.

(46) Severinghaus, J. W.; Bradley, A. F. *J. Appl. Physiol.* **1958**, *13*, 515-20.

(47) Choi, Y. S.; Lvova, L.; Shin, J. H.; Oh, S. H.; Lee, C. S.; Kim, B. H.; Cha, G. S.; Nam, H. *Anal. Chem.* **2002**, *74*, 2435-2440.

(48) Xie, X.; Bakker, E. *Anal. Chem.* **2013**, *85*, 1332-1336.

(49) Cuartero, M.; Pankratova, N.; Cherubini, T.; Crespo, G. A.; Massa, F.; Confalonieri, F.; Bakker, E. *Environ. Sci. Technol. Lett.* **2017**, *4*, 410-415.

(50) Corless, J. T. *J. Chem. Educ.* **1965**, *42*, 421-3.

(51) Wang, T.; Kee Lee, H.; Yau Li, S. F. *J. Liq. Chromatogr. Relat. Technol.* **1998**, *21*, 2485-2496.

(52) Sauvage, J.; Spivack, A. J.; Murray, R. W.; D'Hondt, S. *Chem. Geol.* **2014**, *387*, 66-73.

(53) Wang, J. *Analytical electrochemistry, Third Edition*; John Wiley & Sons: Hoboken, 2006, p 250.

(54) Bagotsky, V. S. *Fundamentals of electrochemistry, Second Edition*; John Wiley & Sons: Hoboken, 2005, p 722.

(55) Skoog, D. A.; West, D. M.; Holler, F. J.; Crouch, S. *Fundamentals of analytical chemistry, Ninth Edition*; Mary Finch: Belmont, 2013, p 1090.

(56) Bakker, E.; Bühlmann, P.; Pretsch, E. *Chem. Rev.* **1997**, *97*, 3083-3132.

(57) Buck, R. P.; Lindner, E. *Pure Appl. Chem.* **1994**, *66*, 2527-36.

(58) Morf, W. E. The Principles of Ion-Selective Electrodes and of Membrane Transport; Elsevier: New York, 1981; Vol. 2, p 432.

(59) Bakker, E.; Buhlmann, P.; Pretsch, E. *Talanta* **2004**, *63*, 3-20.

(60) Pretsch, E. *Chimia* **2001**, *55*, 875-878.

(61) Oesch, U.; Ammann, D.; Pham, H. V.; Wuthier, U.; Zuend, R.; Simon, W. *J. Chem. Soc., Faraday Trans. 1* **1986**, *82*, 1179-86.

(62) Frost, M. C.; Meyerhoff, M. E. *Annu. Rev. Anal. Chem.* **2015**, *8*, 171-192.

(63) Dimeski, G.; Badrick, T.; St. John, A. *Clin. Chim. Acta* **2010**, *411*, 309-317.

(64) Ceresa, A.; Bakker, E.; Hattendorf, B.; Guenther, D.; Pretsch, E. *Anal. Chem.* **2001**, *73*, 343-351.

(65) Bakker, E.; Tercier-Waeber, M.-L.; Cherubini, T.; Crespo, G.; Cuartero, M.; Crespi, M. C.; Afshar, M. G.; Jarolimova, Z.; Jeanneret, S.; Mongin, S.; Néel, B.; Pankratova, N.; Touilloux, R.; Xie, X.; Zhai, J. *Chimia* **2014**, *68*, 772-777.

(66) Campbell, M. *Sensor systems for environmental monitoring*: Chapman & Hall: Glasgow, 1996; Vol. 1, p 310.

(67) Jacobsen, H. S.; Jensen, A. L. In *Monitoring of Water Quality: The Contribution of Advanced Technologies*; Elsevier: Aarhus, The Netherlands, 1998, pp 89-102.

(68) Anderson, J. L.; Coury, L. A.; Leddy, J. *Analytical Chemistry* **2000**, *72*, 4497-4520.

(69) Bard, A. J.; Faulkner, L. R. *Electrochemical Methods, 2nd Edition*: John Wiley & Sons: New York 2001, p 669.

(70) Brett, C. M. A.; Brett, A. M. O. *Electrochemistry: principles, methods, and applications*; Oxford University Press: Oxford, 1993, p 427.

(71) Fauvarque, J.-F.; Simon, P. In *Carbons for Electrochemical Energy Storage and Conversion Systems* CRC Press: Boca Raton, 2010, pp 1-36.

(72) Kissinger, P. T.; Heineman, W. R. *J. Chem. Educ.* **1983**, *60*, 702.

(73) Grygolowicz-Pawlak, E.; Sohail, M.; Pawlak, M.; Neel, B.; Shvarev, A.; de Marco, R.; Bakker, E. *Anal. Chem.* **2012**, *84*, 6158-6165.

2 RESULTS AND DISCUSSION

2.1 Potentiometric Sensing Array for Monitoring Aquatic Systems

The work described below has been published in: Pankratova, N.; Crespo, G. A.; Afshar, M. G.; Crespi, M. C.; Jeanneret, S.; Cherubini, T.; Tercier-Waeber, M.-L.; Pomati, F.; Bakker, E. Potentiometric Sensing Array for Monitoring Aquatic Systems. *Environ. Sci.: Processes Impacts* **2015**, *17*, 906-914.

The aim of this project has been the development of a potentiometric sensing array for monitoring concentrations of pH, calcium, nitrate, nitrite, carbonate and other ionic species in freshwater and its subsequent implementation for on-site measurements at the monitoring platform on lake Greifensee (Switzerland), followed by validation of performed measurements.

2.1.1 Abstract

Since aquatic environments are highly heterogeneous and dynamic, there is the need in aquatic ecosystem monitoring to replace traditional approaches based on periodical sampling followed by laboratory analysis with new automated techniques that allow one to obtain monitoring data with high spatial and temporal resolution. We report here on a potentiometric sensing array based on polymeric membrane materials for the continuous monitoring of nutrients and chemical species relevant for the carbon cycle in freshwater ecosystems. The proposed setup operates autonomously, with measurement, calibration,

fluidic control and acquisition triggers all integrated into a self-contained instrument. Experimental validation was performed on an automated monitoring platform on lake Greifensee (Switzerland) using potentiometric sensors selective for hydrogen ions, carbonate, calcium, nitrate and ammonium. Results from the field tests were compared with those obtained by traditional laboratory analysis. A linear correlation between calcium and nitrate activities measured with ion-selective electrodes and relevant concentrations measured in the laboratory was found, with the slopes corresponding to apparent single ion activity coefficients $\gamma^*_{Ca^{2+}} = 0.55$ ($SD = 0.1$ mM) and $\gamma^*_{NO_3^-} = 0.75$ ($SD = 4.7$ μM). Good correlation between pH values measured with ion-selective electrodes and CTD probes ($SD = 0.2$ pH) suggests adequate reliability of the methodology.

2.1.2 Introduction

Freshwater ecosystems, and in particular lakes, are threatened worldwide by an interaction of anthropogenic environmental changes, including eutrophication and climate change which strongly affect the physics and chemistry of the aquatic habitats.[1] Within aquatic ecosystems, phytoplankton communities are common indicators of environmental changes since they have fast generation times and respond rapidly to variations in both physical and chemical parameters of water.[2] Phytoplankton growth relies on macro-nutrients (nitrate, phosphate, salicylic acid), sunlight and other crucial substances such as Vitamin B and trace metals. While sunlight is attenuated as a function of depth, most of the nutrients are supplied from either deeper water or the sediments. As a result, light and concentration gradients in a water column are changing in opposed directions.[3] The effect of these natural processes on the growth of phytoplankton is still an open question to the scientific community. Indeed, recent theoretical studies have elucidated the understanding of the dynamic interactions between phytoplankton growth and the resources in a water column.[3] However, theoretical models need to be experimentally validated to more fully understand such complex systems, which have implications to questions of climate change, eutrophication and pollution [2].

High quality monitoring data are in this context crucial for tracing and understanding the mechanisms that drive phytoplankton and lake ecosystem dynamics. The latter requires a coupling of biological data obtained *in situ* with automated physical and chemical profiling. So far, most monitoring programs only poorly integrate biological data with direct sensing of standard physico-chemical parameters (e.g. temperature, conductivity,

pH, oxygen), nutrients (nitrate, ammonium, phosphate) and rarely pigment data like chlorophyll-*a*.[4-6] Current developments include the integration of existing methods into automated, complex and operational sensing systems for a comprehensive and long-term monitoring of both the biology and chemistry of water environments. The combination of a diverse set of sensor techniques will be most valuable for achieving a large chemical, spatial and temporal coverage.[7]

Over the past decades, potentiometric sensors based on liquid polymer membrane materials have become a promising tool for the realization of *in-situ* sensing devices. In the past years a considerable improvement of the detection limits, discrimination of interfering ions and the development of new molecular receptors along with appropriate theoretical treatments have been achieved. This has resulted in a strong foundation for application of potentiometric sensors in fields such as environmental trace analysis and potentiometric biosensing.[8] For example, this has allowed one to develop potentiometric sensors for the monitoring of microprofiles in sediments.[9,10]

We aim here to establish an integrated platform based on a flow potentiometric sensing array for measuring nitrogen and carbon cycle-related ionic species involved in phytoplankton growth in freshwaters. The sensing platform was initially validated and automated in house. A self-contained data acquisition instrument, GalvaPot v2 (see Appendix 1 for working modes of the device), was developed specifically for field applications. The device allows one to read out up to 12 electrodes and offers simultaneous control of a number of peripherals that include pumps, valves and other actuators. GalvaPot v2 can be programmed by a touch screen interface, without the need for a PC, and the recorded data are stored in internal memory. The potentiometric platform was validated in the field (lake Greifensee) during four days using an automated Eawag monitoring system, allowing for water sampling at different depths and subsequent potentiometric analysis after a delay of a few minutes. The analytical characterization of the proposed system is reported on in detail. The development of this sensing tool builds on a synergy between analytical chemists and limnologists to help stimulate this field and understand yet unresolved environmental processes.

2.1.3 Experimental

2.1.3.1 Materials and Chemicals

Potassium tetrakis[3,5-bis-(trifluoromethyl)phenyl]borate (KTFPB), bis(2-ethylhexyl) phthalate (DEHP), tridodecylmethylammonium nitrate (TDMAN), tetrakis(4-chlorophenyl)borate tetradodecylammonium salt (ETH 500), ammonium ionophore I (nonactin), potassium tetrakis (4-chlorophenyl)borate (KTClPB), hydrogen ionophore I (tridodecylamine), N,N-Dioctyl-3α,12α-bis(4-trifluoroacetylbenzoyloxy)-5β-cholan-24-amide (carbonate ionophore VII), N,N-Dicyclohexyl-N′,N′-dioctadecyl-3-oxapentanediamide (calcium ionophore IV, ETH 5234), bis(2-ethylhexyl) adipate (DOA), tridodecylmethylammonium chloride (TDMACl), high molecular weight poly(vinyl chloride) (PVC), tetradodecylammonium chloride (TDDA), 2-nitrophenyl octyl ether (o-NPOE), high molecular weight poly(vinyl chloride) (PVC), tetrahydrofuran (THF), calcium chloride dihydrate, sodium nitrate, sodium bicarbonate, ammonium chloride, potassium chloride, sodium hydroxide standard solution (2 mol L^{-1}), tris(hydroxymethyl)aminomethane (Tris), nitrilotriacetic acid (NTA) and sulfuric acid 96 % were purchased from Sigma−Aldrich and Fluka. Nitric and hydrochloric acids suprapur grade were purchased from Merck. Aqueous solutions were prepared by dissolving the appropriate salts in Milli-Q water (18.2 MΩ·cm).

2.1.3.2 Electrodes and Membrane Preparation

The commercial pH glass electrode (InLab Mono Pro) was purchased from Mettler Toledo. The cocktail for carbonate-selective membranes was prepared by dissolving 8.3 mg of carbonate ionophore VII, 60 mg of PVC, 2 mg of TDMACl, and 100 µL of DOA in 2 mL of THF. The cocktail for calcium-selective membranes contained 15 mmol kg^{-1} of calcium ionophore IV, 5 mmol kg^{-1} of ion-exchanger KTFPB, 66 mg of PVC and 131 mg of o-NPOE, dissolved in 2 mL of THF. The nitrate ISE-cocktail was composed of 10 mmol kg^{-1} ion-exchanger salt TDMAN, 15 mmol kg^{-1} inert lipophilic salt ETH 500, 65 mg of PVC and 130 mg of plasticizer DEHP. The cocktail for pH-sensitive PVC-based electrodes consisted of 20 mmol kg^{-1} TDDA, 5 mmol kg^{-1} KTClPB, 66 mg of PVC and 132 mg of plasticizer o-NPOE. Ammonium PVC-based membranes were prepared using 3 mmol kg^{-1} of nonactin, 62 mg PVC and 138 mg of plasticizer o-NPOE, without additional ion-exchanger.

Each individual cocktail was poured into glass rings (22 mm in diameter) placed on a glass slide and dried overnight at room temperature under a dust-free environment. After THF evaporation a membrane of 200 µm approximate thickness was obtained. Small disks (diameter ca. 8 mm) were punched from the cast films and subsequently conditioned in 1 mM solution of the corresponding salt $NaHCO_3$, $CaCl_2$, $NaNO_3$, NH_4Cl or HCl. The membranes were then mounted in Ostec electrode bodies with inner silver-silver chloride elements (Oesch Sensor Technology, Sargans, Switzerland). The inner solution was composed of 1 mM solution of the corresponding salt. In the case chloride ion was not present in the salt, 1 mM NaCl was added to the inner electrolyte to ensure a defined potential at the inner silver-silver chloride element.

2.1.3.3 Automated analysis setup

2.1.3.3.1 Potentiometric Cell Assembly

A commercial reference electrode (6.0726.100, Metrohm) with double junction (Ag | AgCl | KCl, 3 M | LiOAc, 1 M) was used for potentiometric measurements. Each indicator electrode was placed into an individual flow cell fabricated of acrylic glass (see Figure 2.1.1) with the sample flow passing over the outer surface of the membrane in a wall-jet configuration.[11] Six concentric channels (diameter ca. 1 mm, length ca. 4 mm) were drilled in the acrylic cell to connect the sample with the outer solution in the beaker containing constantly renewed 3M KCl. Eight flow cells were placed in the beaker surrounding the reference electrode at equal distance. Electrochemical measurements were performed using the custom-made potentiometer GalvaPot v2.

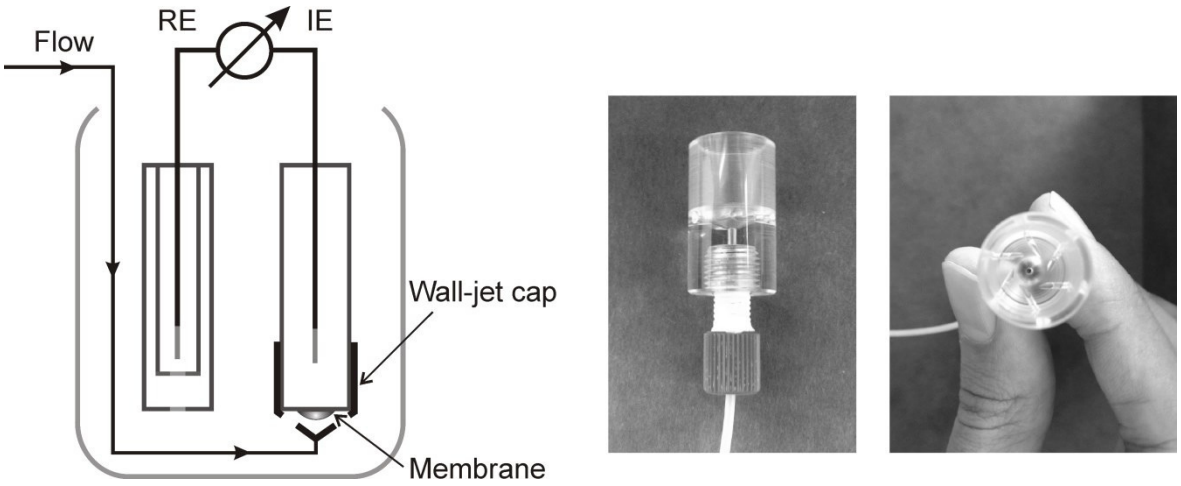

Figure 2.1.1. Flow cell design.[11]

2.1.3.3.2 Custom-made Instrument

We recently reported on a portable custom-made instrument, GalvaPot, for decentralized measurements with ionophore based electrodes[12] that served as the basis for the GalvaPot v2 adapted for field experiments and used for potentiometric measurements on lake Greifensee (Switzerland) within a framework of the project in question. The new design enables one to modify different parameters (changing the state of pumps, introducing a delay, starting or stopping the measurement) by the user in the field and to program commands for autonomous experiments.

2.1.3.3.3 Automated analysis arrangement

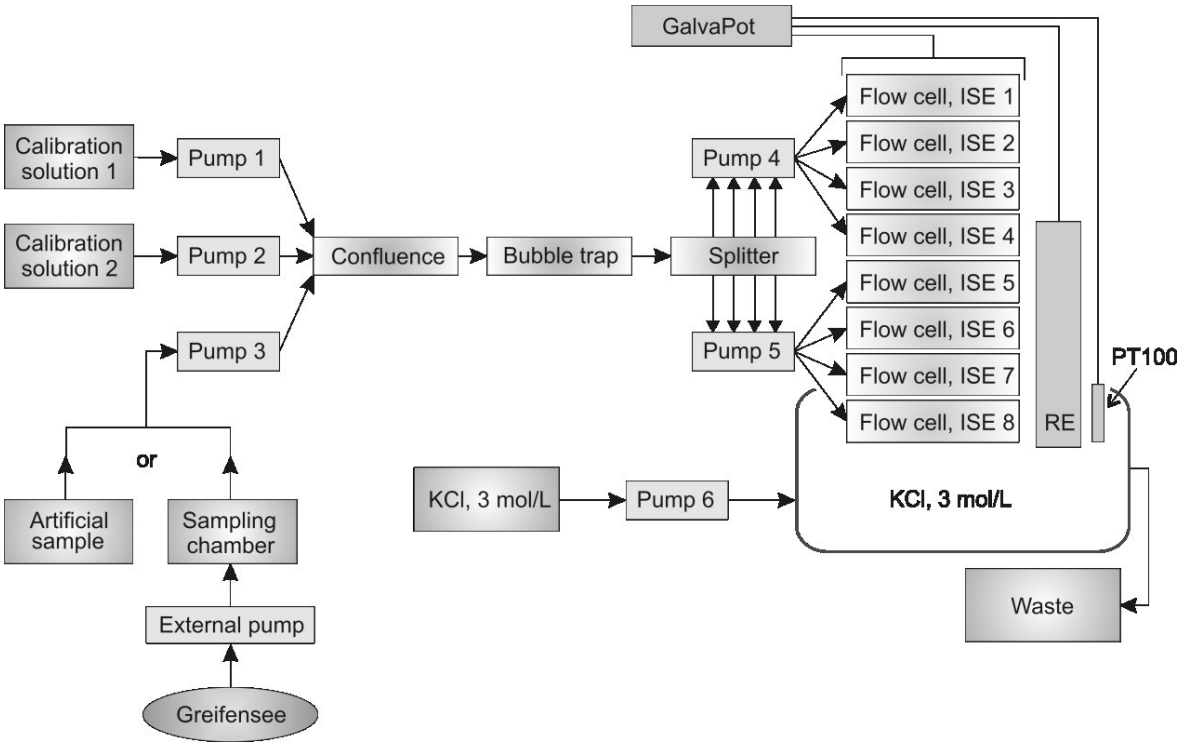

Figure 2.1.2. Schematic diagram of automated potentiometric detection arrangement reported.

The schematic diagram of the flow setup used for potentiometric measurements is presented in Figure 2.1.2. The water sample was delivered to the cell using peristaltic pumps equipped with ISMATEC tygon tubings (inner diameter 1.42 mm, wall 0.86 mm). The tygon tubings installed on the pumps were connected to the flow path composed of PTFE tubings (ID 0.8 mm, BOLA). Starting peristaltic Pump 3 supplying the sample (artificial or natural) was followed by immediate disconnection of the Pumps 1 and/or 2 supplying calibration solutions (Calibration and Experiments method descriptions are given in Appendix 1). The flow rate of the main Pumps 1-3 was set to 2.27 mL min^{-1} (corresponding to 202 rpm in the current setup). A bubble trap (purchased from Kinesis

GmbH) was installed between Pumps 1-3 and the splitter to avoid spontaneously occurring bubbles from penetrating to the surface of PVC membrane. The bubble trap was followed by the splitter, allowing one to divide the flow into 8 channels. To provide an equivalent flow rate in all 8 channels two more peristaltic pumps (Pumps 4 and 5), each with 4 heads, were installed after the splitter. The flow rate on each channel was set to 0.28 mL min^{-1} (24 rpm). The total flow rate on all eight channels was therefore 2.24 mL min^{-1}, slightly less than the flow rate on the main Pumps 1-3. The latter is important to avoid formation of bubbles in the channels. No filtration system was needed for the experiments described here, however the integration of on-line filtration configuration may need to be considered for longer-term experiments and in more eutrophic ecosystems. The flow from each channel was passed over the outer surfaces of eight ISEs, subsequently guided to the beaker containing 3 M KCl and containing the reference electrode. The dead time, i.e. time needed for a new solution to reach the flow cell, was around 2.5 min. The potassium chloride solution in the beaker was constantly renewed using the additional Pump 6, with the flow rate equal to Pumps 1-3. GalvaPot v2 was equipped with a temperature sensor (platinum resistance thermometer PT100), placed in the beaker together with the ISEs and reference electrode and calibrated daily using standard resistances: 100 Ω (corresponding to 0 °C) and 134.7 Ω (90 °C). When processing the data temperature correction was carried out based on Nernst equation.

The calibration of the sensors was performed using two solutions, the compositions of which are given in Table 2.1.1. Solutions were prepared in 5 L polyethylene bottles by dissolving corresponding chemicals in Milli-Q-purified distilled water. The setup of the experiment provides for a continuous flow through the cell since stop flow conditions would lead to the penetration of concentrated outer KCl solution from the beaker into the cell containing the ISE. To avoid this, calibration solutions were continuously flushing the membranes whenever measurements of water samples were stopped. For the same reason, another pump was started just before turning off one of main Pumps 1-3, keeping one of the main Pumps 1, 2 or 3 on at all times. Pumps 4 and 5 as well as Pump 6, were turned on throughout the experiment. Calibration solutions were delivered to the flow cell in the same way as the sample after starting corresponding Pumps 1 or 2 and immediate disconnection of Pump 3.

Table 2.1.1. Composition of calibration solutions 1 and 2 (in total concentrations)

CHEMICAL	*Calibration solution* 1	*Calibration solution* 2
Tris(hydroxymethyl)aminomethane, mM	10	10
Nitrilotriacetic acid, mM	3	3
Potassium chloride, µM	130	130
Calcium chloride dihydrate, mM	1	1
Sodium bicarbonate, mM	5	5
Sodium nitrate, µM	100	10
Ammonium chloride, µM	10	1
pH *	8.5	7.6

* pH value indicated in Table 2.1.1 has been adjusted using hydroxide/sulfuric acid and is approximate. The actual value may vary for different portions of the same calibration solution (prepared on different days) maximum by 0.3 pH units.

2.1.3.3.4 Automated analysis procedure

The automated analysis procedure consisted of two methods: Experiment Method (procedure for the time window when the water sample from chosen depth is being pumped in the channels) and Calibration Method (procedure for ISE calibration using two calibration solutions).

Both Calibration and Experiment Methods were automated using GalvaPot v2. The detailed description of corresponding methods is given in Appendix 1. Calibration solutions were pumped through the system continuously, excluding the time window taken by Experiment Method. Starting Experiment Method caused the end of the running Calibration Method. Upon finishing Experiment Method Calibration Method was resumed. The limited internal memory of the GalvaPot v2 did not provide for an automatic saving of every data point read by the device, so the reading of the potential values was performed over specified time windows, averaged and then stored in internal memory. Every single reading was obtained by averaging the signal on each electrode over 6 s with a 12 Hz data acquisition frequency. 8-10 averaged readings were saved when running Experiment Method and 8-10 readings for each calibration solution for the time window of calibration right before the trigger and immediately after the end of the Experiment Method. As a consequence of the limited internal memory the collected data was transferred to external memory once a day.

2.1.3.3.5 Calibration solution preparation

A 2-point calibration was automatically performed before and after each profiling using calibration solutions 1 and 2. To ensure monitoring reliability, a single point calibration was carried out after every measurement at a chosen depth. The latter allowed one to correct for occasionally occurring electrode drifts if necessary.

The composition of calibration solutions is indicated in Table 2.1.1. Carbonate (CO_3^{2-}) and ammonium (NH_4^+) concentrations were recalculated for every particular calibration solution depending on its precise pH value determined using conventional pH meter and standard buffer solutions, in laboratory conditions. pH, nitrate, ammonium and carbonate concentrations chosen for preparing calibration solutions correspond to the relevant concentration ranges in lake Greifensee. The anticipated level of analytes in lake water was determined during preliminary trials of the described setup in the field.

The calcium concentration in the calibration solutions had to be chosen in a lower range than the one expected for calcium levels in lake water. The latter accounts for the fact that the addition of millimolar levels of calcium to a solution containing millimolar levels of total carbonate would cause precipitation of both calcium and carbonate, resulting in an uncertainty of the calibration solution composition affected by temperature changes as well as precipitation kinetics. Therefore, the concentration of calcium in the calibration solutions was buffered using NTA that left approximately 0.5 wt % of total calcium in the uncomplexed form. The free calcium fraction is sensitive to NTA concentration and is highly affected by pH changes. For this reason, an additional calibration of the installed ISEs was performed a few times a week using two calibration solutions containing just 10^{-3} and 10^{-2} M calcium chloride.

2.1.3.4 Field measurements

Field measurements of nutrients and chemical species related to the carbon cycle were performed at the end of August (18-22.08.2014) on the lake Greifensee, a small eutrophic lake (surface area 8.45 km^2, water volume 0.148 km^3) located in the canton of Zurich, Switzerland. The automated analysis setup described above was synchronized with the Eawag automated monitoring platform by allowing the GalvaPot v2 to accept an electric signal from the system's controller module (Idronaut Controller Module operating also with a CTD probe with traditional sensors for profiling)[2] as a trigger to start potentiometric measurements of the samples taken at different depths: 1, 2.5, 4, 5.5, 7 and 8.5 m.

The Eawag platform is equipped with a system to retrieve water from selected depths. Water was brought to the acrylic sampling chamber (volume 250 mL) through an antimicrobial, silver-nanoparticle coated and shaded flexible polyethylene tubing.[2] The trigger signal activates the external pump (boat water system pump, Jabsco PAR-Max 1) that flushes the chamber with water sample from the selected depth for 3 min at a flow rate of 4.2 L min^{-1}. After flushing the chamber Experiment Method started automatically. The sample collected in the chamber and delivered to the cells using Pump 3 was used for potentiometric measurements. A new profiling started every 4 h: at 00:00, 04:00, 08:00, 12:00, 16:00 and 20:00. The total time for potentiometric measurements at one depth was limited to about 16 min due to the Eawag automated monitoring cycle, with the entire cycle taking around 1 h 40 min.

2.1.3.5 Field data validation

2.1.3.5.1 Laboratory measurements of calcium and nitrate concentrations

To evaluate the reliability of the approach, calcium and nitrate concentrations in water were complementarily measured in filtered collected samples using flame atomic adsorption spectroscopy (AAS; Varian SpectrAA 240 FC) and ion chromatography (IC; Metrohm model 761), respectively. Water samples were collected at the same depths as described above within the time window of the ISE measurement cycle using an in-house 12V battery powered peristaltic pump with acid pre-cleaned Tygon tubing. Filtration was performed in-line on site using 0.2 µm pore size nitrocellulose membranes (Whatman) incorporated into an in-house flow-through acrylic filtration device. Sampling polypropylene tubes (volume 50 mL) were pre-cleaned for 24 h in 0.1 M HNO_3 suprapur grade (Merck), 2 times for 24 h in 0.01 M HNO_3 suprapur; followed by dipping in Milli-Q water for 12 h after each acid washing step. Samples for calcium measurements were acidified to pH 1.3 with HCl suprapur grade (Merck) within few hours after sampling. All samples were immediately stored in a cold box, then in the field laboratory at 4°C, in the dark, prior to analysis.

2.1.3.5.2 In-situ conductivity and pH measurement

Conductivity and complementary pH measurements were performed using OCEAN SEVEN 316Plus CTD multiparameter probe (Idronaut, Brugherio, Italy).[2] The automatic monitoring program with the multiparameter probe ran every 1-2 h, before and after profiling with the ISE sensing array.

2.1.4 Results and Discussion

2.1.4.1 Preliminary laboratory experiments

2.1.4.1.1 Ion-selective electrodes

Aiming at field measurements in freshwater, the choice of the potentiometric sensors was dictated by the anticipated concentration range of the ions to be detected. Freshwater compositions vary significantly depending on the country, climate, the season, the type and depth of the lake as well as anthropogenic factors.[13-16] The average freshwater concentrations of the analytes in question are normally found at about 10^{-3} M of calcium, 10^{-5}-10^{-4} M of nitrate, 10^{-6}-10^{-8} M of ammonium, 10^{-3} M of total carbonate.[17] The pH of freshwater typically ranges from 7 to 9. The indicated values represent average levels and preliminary experiments on the lake Greifensee were needed to confirm the applicability of the chosen sensors.

Considering the high calcium concentration in the lake, the choice of a sensor for calcium determination was straightforward. A PVC-based membrane doped with calcium ionophore IV was used for this purpose. The selectivity, stability and detection limits of this type of membrane have been thoroughly studied [18,19] and confirm its applicability at pH 7-9 at the millimolar concentration range for freshwater analysis.

A tridodecylamine-doped membrane was chosen for preparing the pH electrode. Membranes of this type have been subject of considerable research and have already been used in a number of applications.[20,21] A calibration curve for a PVC-based pH electrode is presented in Figure 2.1.3. Despite the applicability of the PVC-based pH sensor for water samples analysis a commercial glass electrode (half-cell, Mettler Toledo) was also implemented to ensure reliable pH detection. The latter is very important since carbonate speciation is highly affected by pH changes, and providing reliable pH data is vital for the analysis of carbonate and CO_2 levels.

Previous studies have shown PVC-based ISEs doped with carbonate ionophore VII to be reliable sensors for carbonate detection with exceptionally high selectivity over the key interfering ions, giving detection limit lower than 10^{-6} M at pH 8.0.[22] A strategy has recently been explored that allows one to directly measure CO_2 levels by measuring pH electrode against a carbonate electrode without using a traditional reference electrode.[23] Since the flow setup described above includes a reference electrode at all times, both pH and carbonate electrodes were measured against the reference electrode while CO_2 levels

may be inferred by subtraction of the two potentials values based on carbonate species equilibria.[23]

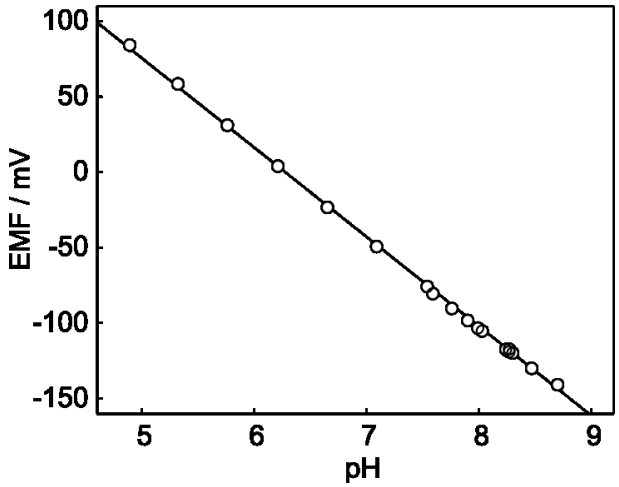

Figure 2.1.3. Calibration curve for the pH electrode with PVC-based membrane doped with tridodecylamine (TDDA). Calibration was performed in a beaker in stirring conditions.

Nitrate and ammonium levels in freshwater are quite low. Insufficient detection limits of nitrate[24] and ammonium-selective[25,26] PVC-based sensors as well as less attractive selectivity might be a limiting factor when implementing these sensors for environmental analysis. Considering the low detection limit of $\log a_{NO_3^-}^{LDL} = -4.7$ (Figure 2.1.4) and a rather low nitrate levels in freshwater (10^{-5}-10^{-4} M), monitoring data analysis needed to be performed by a nonlinear regression of the curve given in Figure 2.1.4 with an adjustment of the intercept on the EMF axis according to the experimentally obtained value.

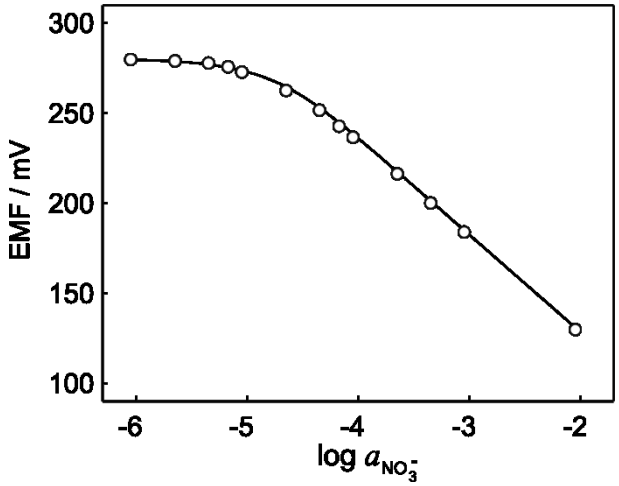

Figure 2.1.4. Calibration curve for nitrate ISE obtained using flow cell presented in Figure 1. Flow rate 0.28 mL min^{-1}, background solution composition (in total concentrations): Tris 10 mM, NTA 3 mM, KCl 130 µM, $CaCl_2 \cdot 2H_2O$ 1 mM, $NaHCO_3$ 5 mM at pH 7.8.

When choosing the composition of the membrane for ammonia sensing we aimed at preparing a membrane with the lowest possible detection limit. Considering the results of preliminary studies (Figure 2.1.5), membranes containing nonactin without additional ion-exchanger were prepared. The detection limit for the ammonium-selective electrode with a 100 µM potassium background corresponds to $\log a_{NH_4^+}^{LDL} = -5$, which is not sufficiently low for the chosen application as suggested from the average ammonium level indicated above. However, the actual ammonium concentrations may vary significantly from 10^{-8} M in the surface layer to few hundred µM in freshwater sediments.[5] Therefore, the ammonium sensor was also implemented into the flow analysis setup to allow for an estimation of ammonium level changes when profiling at larger depths.

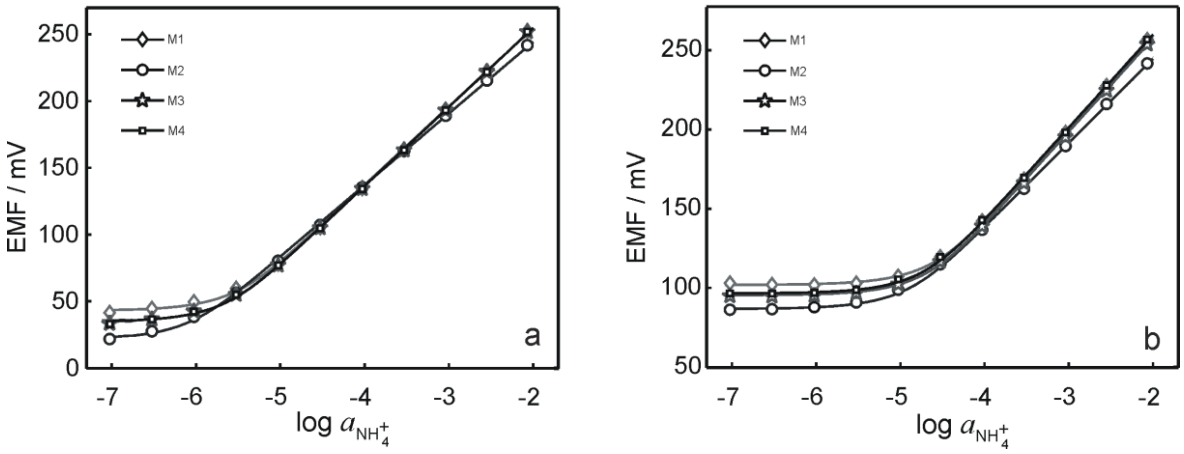

Figure 2.1.5. Calibration curves for ammonium electrodes with PVC-based membranes of the following composition: (M1) nonactin 40 mmol kg^{-1}, KTClPB 10 mmol kg^{-1}, PVC 64 mg, o-NPOE 127 mg; (M2) nonactin 3 mmol kg^{-1}, PVC 64 mg, o-NPOE 141 mg, no additional ion-exchanger; (M3) nonactin 14 mmol kg^{-1}, KTClPB 3.5 mmol kg^{-1}, PVC 67 mg, o-NPOE 130 mg; (M4) nonactin 20 mmol kg^{-1}, KTClPB 7 mmol kg^{-1}, PVC 65 mg, o-NPOE 132 mg. Calibration was performed in a beaker in stirring conditions (a) at pH 8; (b) in background solution containing 100 µM KCl (pH~6).

2.1.4.1.2 Automated analysis

The ion-selective electrode was fitted with an acrylic wall jet cap (Figure 2.1.1). The conical design of the flow cell defines a small gap between the curved ion-selective membrane and the bottom part of the cell, which defines the measurement compartment (volume ca. 100 µL). Positive pressure was always applied to the cap to minimize cross contamination and dilution effects between sample and background electrolyte. The key advantages of this design include i) a common reference electrode placed outside each flow cell at equal distance so that the potential value does not depend on the position of the ISE in the outer cell, ii) a facile membrane cleaning process between measurements of

sample and calibration solution, iii) the possibility of simple extensions to any number of ISEs using the same reference electrode with multiple wall jet caps.

Bracketed calibrations using the proposed flow analysis setup are shown in Figure 2.1.6 with the following observed electrode slopes in mV: 31.4 ± 1 for calcium, 58.3 ± 1 for pH (PVC-based electrode), 58.7 ± 1 for pH glass electrode, 31.5 ± 1 for carbonate, 37.3 ± 3 for nitrate and 7.6 ± 2 for ammonium. Single ion activities a_i were calculated based on the concentration values indicated in Table 2.1.1 according to the common relationship:

$$a_i = \gamma_i \cdot c_i \qquad \text{(eq. 2.1.1)}$$

where γ_i is the single ion activity coefficient and c_i the molar concentration of ion *i*. The pH measured by the commercial glass electrode was used to correct the carbonate and ammonium concentrations for pH dependent speciation equilibria.

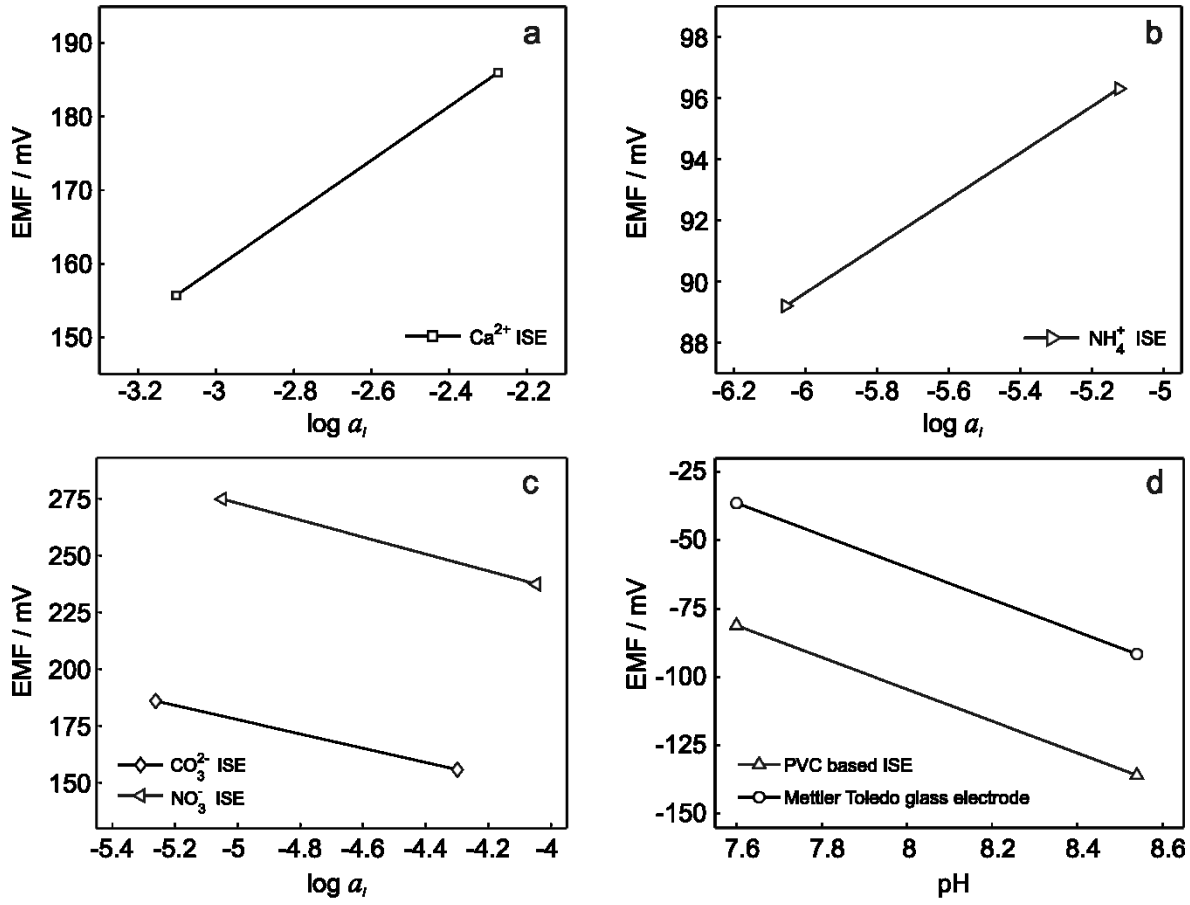

Figure 2.1.6. Bracket calibrations for ISEs integrated into field monitoring: (a) calcium PVC-based electrode; (b) ammonium PVC-based electrode; (c) carbonate and nitrate PVC-based electrodes; (d) pH PVC-based and commercial glass electrodes. Calibrations were obtained in the field in flow conditions before starting field monitoring.

As discussed above, a near Nernstian response slope was obtained for calcium, carbonate and pH electrodes, suggesting that they are adequate for quantitative analysis. In contrast, a sub-Nernstian slope for nitrate necessitated the use of a nonlinear calibration curve based on the Nicolskii equation for calculating the nitrate activity in water samples. Indeed, the deviation between linear and non-linear calibrations was important for this ion (5 to 25 % RSD depending on sample activity). The relatively high concentration of potassium deteriorates the limit of detection for the ammonium-selective membrane and explains the relatively low slope (Figure 2.1.5). Nonetheless, this electrode was maintained for comparative estimation of ammonium levels in water samples.

We note that a multivariate approach could also be efficiently applied for data analysis when observing nonlinear calibration curves, as these techniques are useful when determining concentrations close to the detection limit.[27] In this early work, it was initially preferred to apply an analytical approach based on Nicolskii equation for a rational discussion of the data.

2.1.4.2 Field measurements

Measurements on lake Greifensee were performed during a period of 90 h, starting on August 18, 2014 and finishing on August 22, 2014. Figure 2.1.7a shows the obtained potentiometric time trace between Thursday afternoon (12 pm) and Friday morning (10 am) for the five analysed ions. As discussed above, the experimental arrangement allowed for the measurement of up to eight ISEs. In this experiment the following ISEs were installed: one carbonate electrode, one glass pH electrode, two nitrate electrodes, two ammonium electrodes and two calcium electrodes. For simplicity and to avoid overlap of the graphs, just five traces, one for each type of ISE, are presented in Figure 2.1.7a,b. Every cycle consisted of two 2-point-calibrations performed both at the beginning and at the end of the cycle (four calibration points), six measurements corresponding to six water samples taken from different depths and 6 measurements corresponding to the 1-point calibration between water sample measurements. One of the cycles is separately shown in Figure 2.1.7b. Every cycle (including calibrations) took approximately 2 h to be completed and a new cycle started every 4 h. The time when a particular solution reached the surface of ion-selective membrane is indicated with vertical lines in Figure 2.1.7b: water sample measurements are highlighted with solid lines and measurements corresponding to calibration solutions 1 and 2 are indicated with dashed and dotted lines respectively.

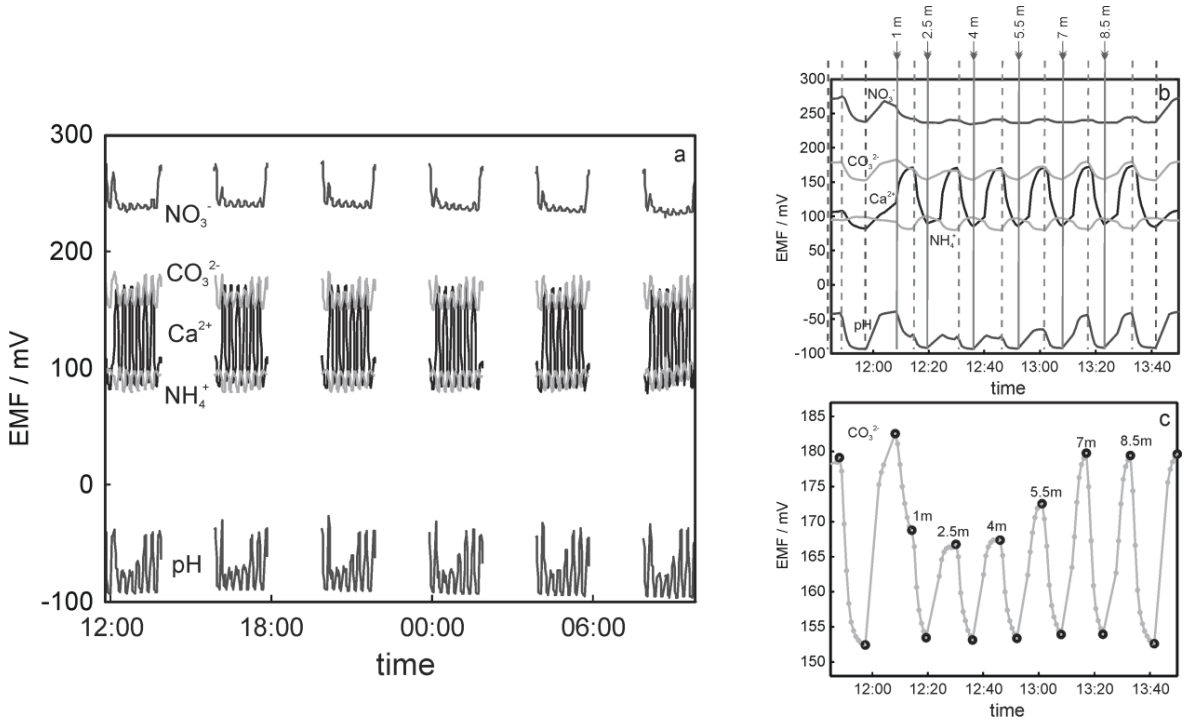

Figure 2.1.7. Potentiometric data obtained during filed measurements using proposed automated analysis arrangement (replicates not shown in the figure). (a) Experimental curves obtained during the experiment performed on 21-22.08.2014. (b) Zoom for the first cycle shown in Figure 2.1.7a. Vertical lines indicate the time when corresponding new solution reached the surface of the ISE membrane: calibration solution 1 (dashed line), calibration solution 2 (dotted line) or lake water from the depth specified in the figure (solid line). (c) Zoom for the cycle presented in Figure 2.1.7b for carbonate ISE: grey markers represent the single data points acquired by GalvaPot during field measurements, black circles correspond to the EMF value corresponding to relevant sample/calibration solution.

The collected data points are shown in Figure 2.1.7c. A confirmation of calibration reproducibility within 2 h of measurements is obtained with the injection of a standard solution immediately after measuring each lake sample. The long-term stability of sensor calibration is illustrated in Figure 2.1.8. The drift of the calibration observed during 90 h of measurements was in the range of 5-15 mV depending on the sensor and confirms the advantage of chosen approach using continuous calibration between the profiles. Considerable changes of pH and carbonate activities were observed as a function of depth. Nitrate levels did not significantly change for the first few meters, but a notable reduction of nitrate activity started to be observed at 8.5 m (see also *2.1.4.3*). The ammonium level was found to be lower than the detection limit of the electrode (ca. 10 µM with potassium background 100 µM). The ammonium concentration is an indicative parameter of the anoxic region in the lake, which is often present at larger depths [9,10] than the ones explored here. The low observed ammonium activity was therefore expected for the conditions used here.

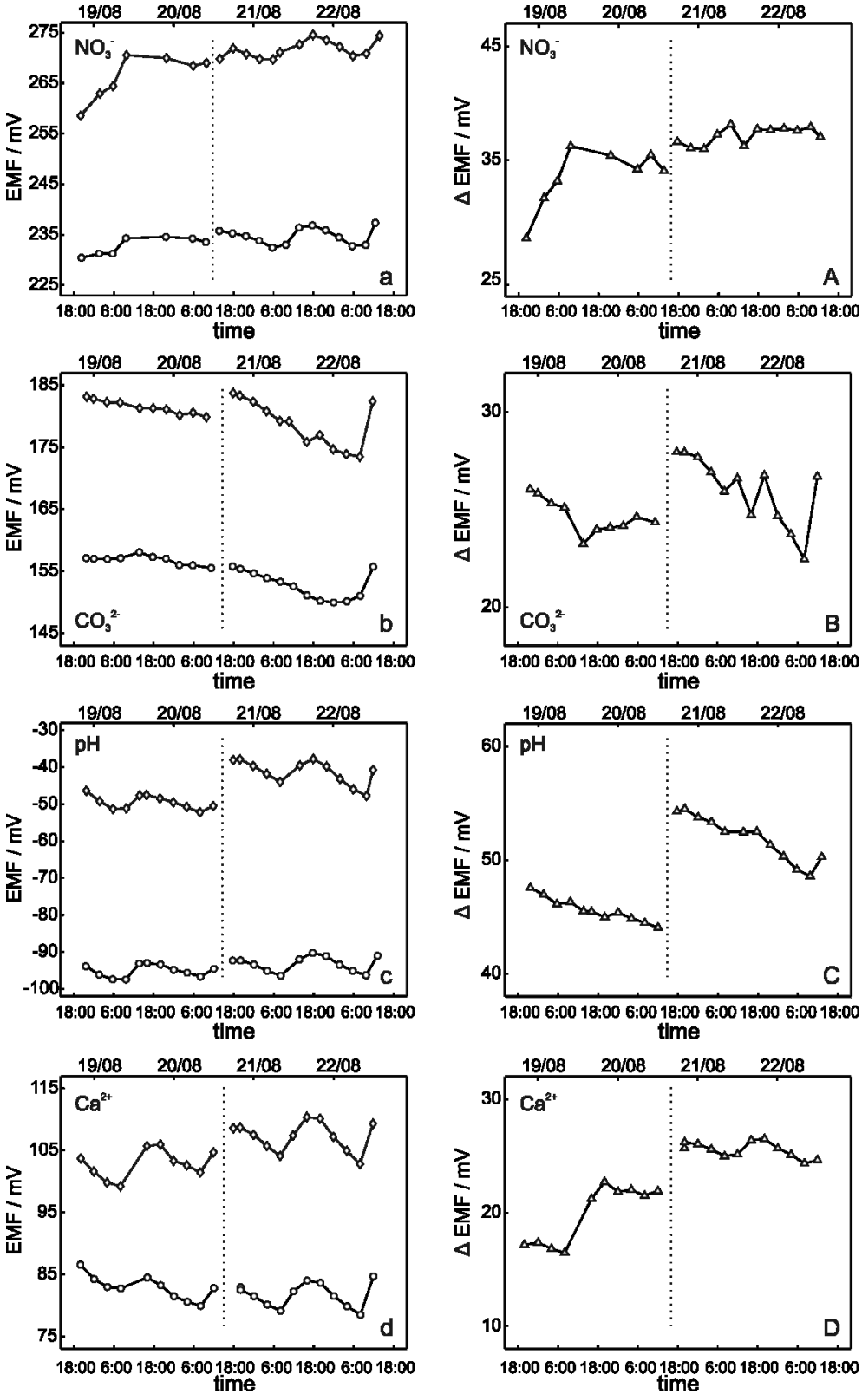

Figure 2.1.8. Stability of calibration during 90 hours of field measurements for nitrate (a,A), carbonate (b,B), pH (c,C) and calcium (d,D) ISEs. (a,b,c,d) EMF values (mV) for calibration solutions 1 (circles) and 2 (diamonds). (A,B,C,D) EMF difference (mV) between calibration solution 2 and calibration solution 1. The vertical dotted lines indicate the time when the calibration solution bottle was replaced with a new portion of calibration solution having slightly different pH.

Calcium activity is used as an example of the capability of the established sensing platform. Since the obtained activity is a function of depth and time (*f = c(depth, time)*), the data are visualized with a 2D surface plot as shown in Figure 2.1.9 and show an increase of calcium activity in the lake with depth and its decrease during the night.

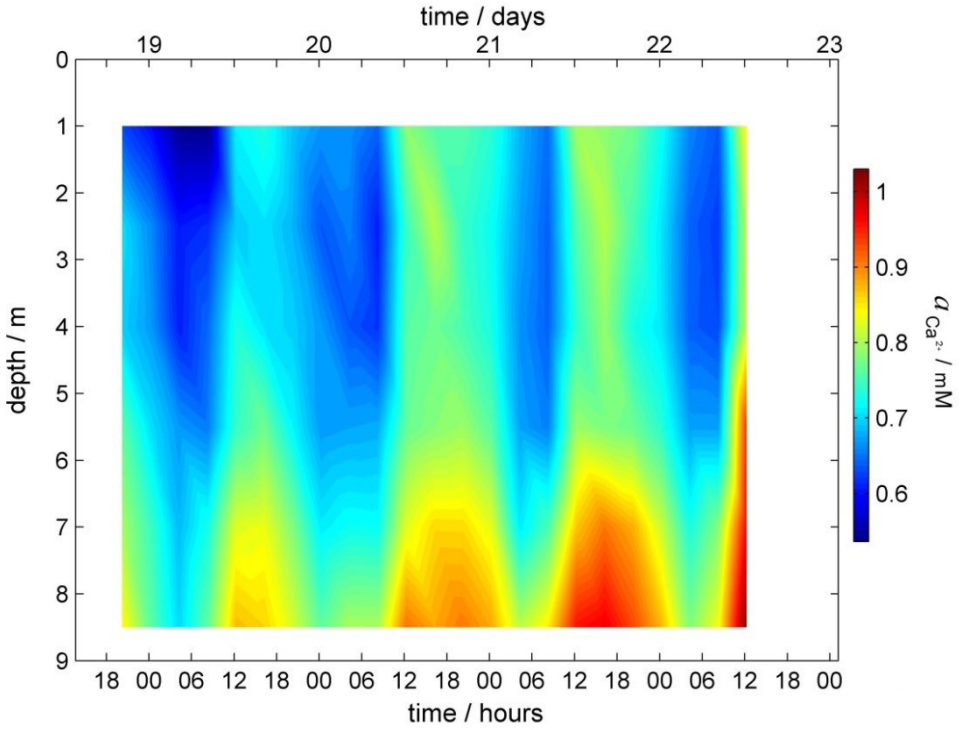

Figure 2.1.9. Surface plot for calcium profile obtained during field monitoring on the lake Greifensee (Switzerland) 18-22.08.2014.

2.1.4.3 Data validation

To validate the consistency of the approach, laboratory measurements of calcium and nitrate concentrations in lake water were performed. Figure 2.1.10 shows the correlation between ion activities determined by potentiometry in the field and the concentrations obtained with laboratory analysis of water samples taken at corresponding depths. A linear correlation is assumed based on the linear relationship between activity and concentration (equation 2.1.1). The slope of the linear regression corresponds to an apparent single ion activity coefficient γ_i^* that was estimated as the mean value of experimentally determined single ion activity coefficients $\gamma_i^{\exp} = \frac{a_i^{\exp}}{c_i^{\exp}}$, where $a_i^{\exp}$ is the single ion activity determined by ISE in the field, $c_i^{\exp}$ is the molar concentration of the ion *i* obtained by laboratory analysis. The obtained mean values γ_i^* were found as $\gamma^*_{Ca^{2+}} = 0.55$ and $\gamma^*_{NO_3^-} = 0.75$.

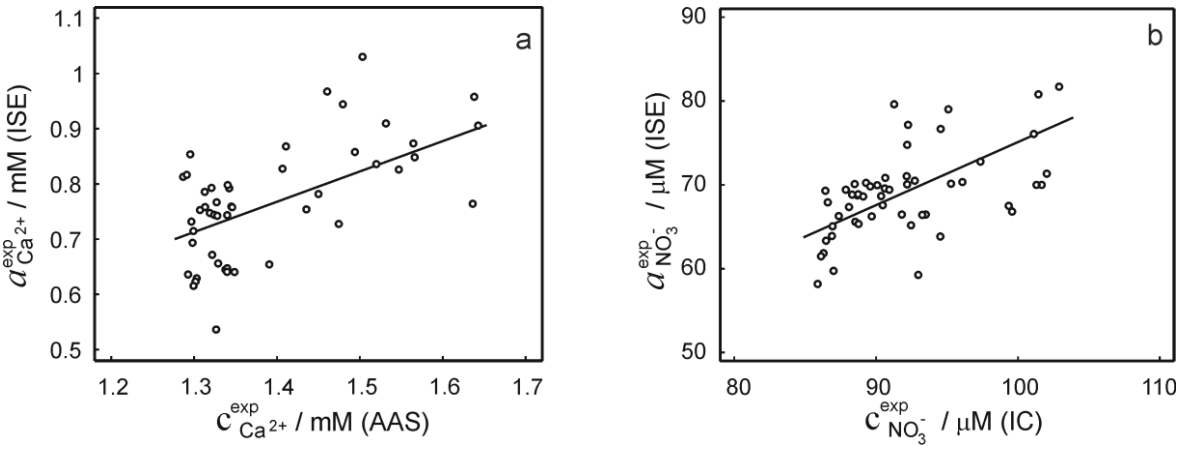

Figure 2.1.10. Correlation between activities measured in the field by ISEs and concentrations obtained within laboratory analysis using atomic absorption spectroscopy (a, calcium) and ion chromatography (b, nitrate). The slopes of linear regressions correspond to apparent single ion activity coefficients being $\gamma^*_{Ca^{2+}} = 0.55$ ($SD = 0.1$ mM) and $\gamma^*_{Ca^{2+}} = 0.75$ ($SD = 4.7$ µM).

Note that the γ_i^* value includes not only the thermodynamic contribution from the ion activity coefficients due to the ionic strength of the lake, but also any matrix effects of the natural water sample as well as systematic errors of both field and laboratory measurements. The thermodynamic contribution to the experimental γ_i^* value was estimated with the single ion activity coefficient γ_i calculated with the first approximation of the Debye-Hückel theory (bicarbonate and calcium ions were considered as relevant counter ions as these are the major species in the sample, see Appendix 1).

The value of the ionic strength was estimated based on conductivity measurements. Electrical conductivity κ is given by the following equation:

$$\kappa = \sum_i \lambda_i c_i \qquad \text{(eq. 2.1.2)}$$

where λ_i is limiting single ionic conductivity defining the contribution of individual ions (tabulated value). Ionic strength ($I = 0.5\sum_i z_i^2 c_i$) was calculated assuming calcium bicarbonate as the major contributor to conductivity and ionic strength ($\lambda_{Ca^{2+}} = 11.894\ \text{mS}\cdot\text{m}^2\cdot\text{mol}^{-1}$, $\lambda_{HCO_3^-} = 4.45\ \text{mS}\cdot\text{m}^2\cdot\text{mol}^{-1}$). [28] The conductivity of the water samples increased with depth and was found to be in the range 380 - 470 µS/cm, giving an ionic strength in the range 5.5 - 6.8 mM. Based on the simplified Debye-Hückel theory (see Appendix 1) single ion activity coefficients were found as 0.68 – 0.71 for $\gamma_{Ca^{2+}}$ and 0.91 – 0.92 for $\gamma_{NO_3^-}$ considering bicarbonate and calcium as the counter ions accordingly.

A comparison of theoretically estimated single ion activity coefficients γ_i ($\gamma_{Ca^{2+}} = 0.68 - 0.71$, $\gamma_{NO_3^-} = 0.91 - 0.92$) with apparent single ion activity coefficients γ_i^* obtained experimentally ($\gamma^*_{Ca^{2+}} = 0.55$, $\gamma^*_{NO_3^-} = 0.75$) shows γ_i^* to be somewhat lower than the estimated γ_i. It should be considered that the procedure for γ_i calculation presented above allows only a rough estimation of $\gamma_{Ca^{2+}}$ and $\gamma_{NO_3^-}$ since the complexity of the natural sample media along with relatively high ionic strength goes beyond the first approximation of the Debye-Hückel theory. To a certain extent the difference between estimated (γ_i) and experimental (γ_i^*) values may originate from systematic experimental errors deriving from calibration inaccuracy of field measurements and/or differences in sampling procedures. In particular, the samples for laboratory analysis of calcium were acidified, which may result in the release of complexed or adsorbed calcium that is not detected with ISEs.

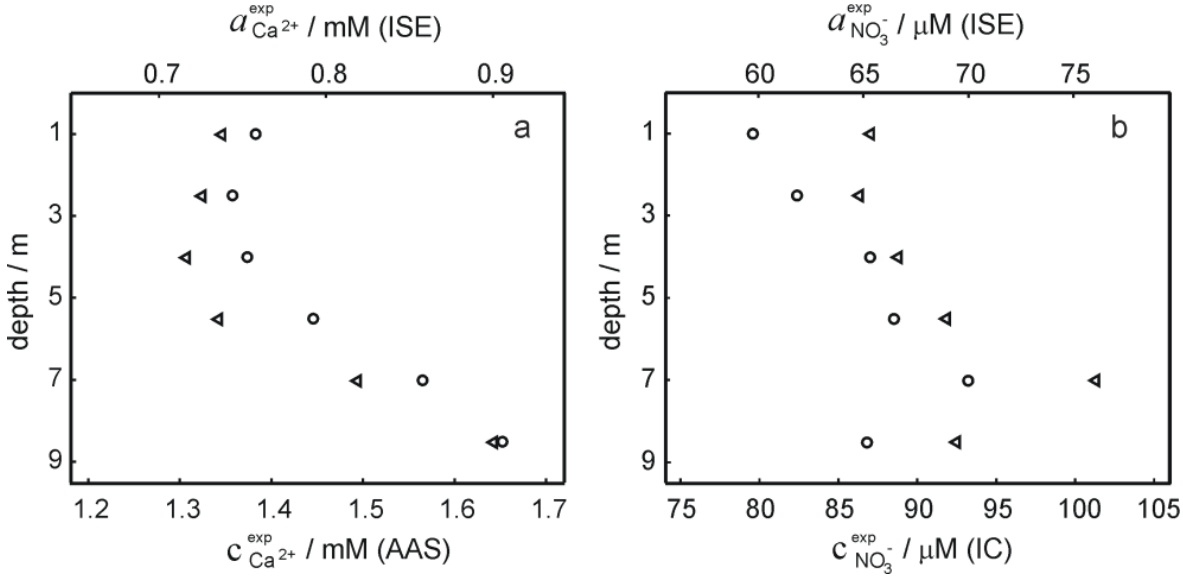

Figure 2.1.11. Field data *vs* laboratory analysis. (a) Calcium activity (circles) measured by ISE in the field and calcium concentration (triangles) measured by AAS depending on the depth. (b) Nitrate activity (circles) measured by ISE in the field and nitrate concentration (triangles) measured by IC depending on the depth. The scales of activity and concentration axes are defined by the relationship $a_i^{exp} = \gamma_i^* \cdot c_i^{exp}$ where γ_i^* is apparent single ion activity coefficient ($\gamma^*_{Ca^{2+}} = 0.55$, $\gamma^*_{NO_3^-} = 0.75$).

Activity and concentration profiles (for field and laboratory data, respectively) are presented in Figure 2.1.11. The scales of the concentration and activity axes correspond to the relationship $a_i^{exp} = \gamma_i^* \cdot c_i^{exp}$ where apparent single ion activity coefficients γ_i^* are equal to 0.55 for calcium and 0.75 for nitrate as discussed above. The profiles suggest good correlation between field and laboratory measurements. When comparing field and

laboratory results it must be taken into account that owing to the monitoring system arrangement, a manual sampling for laboratory analysis was performed with slightly different time resolution and not exactly at the same location. The latter may result in some discrepancy between field and laboratory measurements, so the data points in Figure 2.1.11 are not expected to match perfectly. Importantly, despite the relatively small changes of the parameters, the tendency of relative changes of calcium and nitrate activities agrees with the relevant concentration changes. Figure 2.1.12 shows the correlation between pH values measured using commercial pH glass electrode in the proposed flow arrangement and those obtained by EAWAG using the CTD probe that ran immediately before the ISE profiling. A good correlation between the results obtained using the two different methods confirms that the observed pH data are adequate and applicable in the presented sensing array.

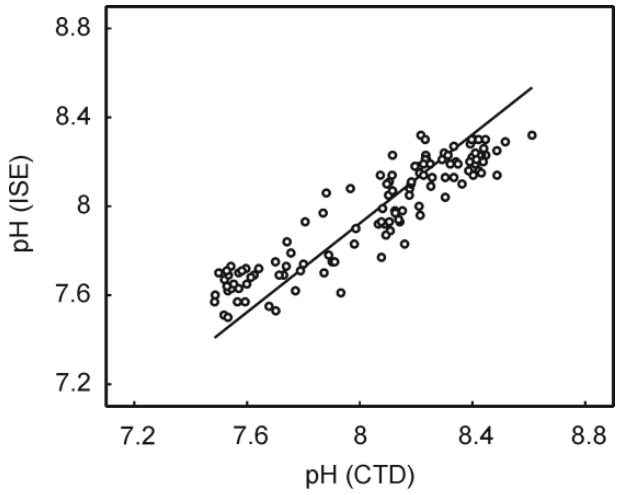

Figure 2.1.12. Correlation between pH measurements with glass electrode implemented in the proposed flow setup and alternative *in-situ* pH measurements performed by EAWAG using CTD probe ($SD = 0.2\,\mathrm{pH}$).

2.1.5 Conclusions

The potentiometric sensing array for the detection of nutrients and species relevant to the carbon cycle was successfully deployed for continuous monitoring of pH, calcium, nitrate and carbonate levels at the EAWAG monitoring platform on the lake Greifensee (Switzerland), in parallel with scanning flow cytometer measurements. The proposed setup suggests continuous calibration of potentiometric sensors between the measurements of water samples thus providing more reliable data compared to ISE arrays using relatively infrequent calibration in field conditions. Comparison of field and laboratory measurements confirms the consistency of the setup for field analysis. We believe that the

potentiometric sensing array described here may serve as a promising tool for ecological monitoring aimed at tracking and understanding environmental changes in aquatic ecosystems.

2.1.6 Acknowledgements

The author acknowledges financial support by the Swiss National Science Foundation (FNS Sinergia CRSII2-147654).

2.1.7 References

(1) Adrian, R.; O'Reilly, C. M.; Zagarese, H.; Baines, S. B.; Hessen, D. O.; Keller, W.; Livingstone, D. M.; Sommaruga, R.; Straile, D.; Van Donk, E.; Weyhenmeyer, G. A.; Winder, M. *Limnol. Oceanogr.* **2009**, 2283–2297.

(2) Pomati, F.; Jokela, J.; Simona, M.; Veronesi, M.; Ibelings, B. W. *Environ. Sci. Technol.* **2011**, *45*, 9658-9665.

(3) Yoshiyama, K.; Mellard, J. P.; Litchman, E.; Klausmeier, C. A. *Am. Nat.* **2009**, *174*, 190-203.

(4) Jacobsen, H. S.; Jensen, A. L. In *Monitoring of Water Quality: The Contribution of Advanced Technologies*; Elsevier: Aarhus, The Netherlands, 1998, pp 89-102.

(5) Maerki, M.; Muller, B.; Dinkel, C.; Wehrli, B. *Limnol. Oceanogr.* **2009**, *54*, 428-438.

(6) Odermatt, D.; Pomati, F.; Pitarch, J.; Carpenter, J.; Kawka, M.; Schaepman, M.; Wüest, A. *Remote Sens. Environ.* **2012**, *126*, 232-239.

(7) Zielinski, O.; Busch, J. A.; Cembella, A. D.; Daly, K. L.; Engelbrektsson, J.; Hannides, A. K.; Schmidt, H. *Ocean. Sci.* **2009**, *5*, 329-349.

(8) Bakker, E.; Pretsch, E. *Angew. Chem., Int. Ed.* **2007**, *46*, 5660-5668.

(9) de Beer, D.; Bissett, A.; de Wit, R.; Jonkers, H.; Koehler-Rink, S.; Nam, H.; Kim, B. H.; Eickert, G.; Grinstain, M. *Limnol. Oceanogr.: Methods* **2008**, *6*, 532-541.

(10) Muller, B.; Buis, K.; Stierli, R.; Wehrli, B. *Limnol. Oceanogr.* **1998**, *43*, 1728-1733.

(11) Bell-Vlasov, A. K.; Zajda, J.; Eldourghamy, A.; Malinowska, E.; Meyerhoff, M. E. *Anal. Chem.* **2014**, *86*, 4041-4046.

(12) Jeanneret, S.; Crespo, G. A.; Ghahraman Afshar, M.; Bakker, E. *Sens. Actuators, B* **2015**, *207*, 631-639.

(13) Heini, A.; Puustinen, I.; Tikka, M.; Jokiniemi, A.; Lepparanta, M.; Arvola, L. *Hydrobiologia* **2014**, *731*, 139-150.

(14) Sobczynski, T.; Joniak, T. *Pol. J. Environ. Stud.* **2013**, *22*, 227-237.

(15) Farhadian, O.; Kolivand, S.; Mahmoudi, K. M.; Ebrahimi, D. E.; Mahboobii, S. N. *Iran. J. Fish. Sci.* **2013**, *12*, 301-319.

(16) Goransson, E. Variation in lake water chemistry and spatial scale: analysis of the Swedish national lake monitoring programme. Ph.D. Thesis, Swedish University of Agricultural Sciences 2003.

(17) Hollocher, K.; Quintin, L.; Ruscitto, D. In *New York State Geological Association Field Trip Guidebook, 74th annual meeting: Lake George*, McClelland, J., and Karabinos, P., eds, Ed.: New York, 2002, pp C11.1- C11.15.

(18) Pretsch, E. *Chimia* **2001**, *55*, 875-878.

(19) Ceresa, A.; Bakker, E.; Hattendorf, B.; Guenther, D.; Pretsch, E. *Anal. Chem.* **2001**, *73*, 343-351.

(20) Ma, S. C.; Meyerhoff, M. E. *Mikrochim. Acta* **1990**, *1*, 197-208.

(21) Espadas-Torre, C.; Bakker, E.; Barker, S.; Meyerhoff, M. E. *Anal. Chem.* **1996**, *68*, 1623-31.

(22) Choi, Y. S.; Lvova, L.; Shin, J. H.; Oh, S. H.; Lee, C. S.; Kim, B. H.; Cha, G. S.; Nam, H. *Anal. Chem.* **2002**, *74*, 2435-2440.

(23) Xie, X.; Bakker, E. *Anal. Chem.* **2013**, *85*, 1332-1336.

(24) Arada Pérez, M. A.; Marín, L. P.; Quintana, J. C.; Yazdani-Pedram, M. *Sens. Actuators, B* **2003**, *89*, 262-268.

(25) Ghauri, M. S.; Thomas, J. D. *Analyst* **1994**, *119*, 2323-6.

(26) Davies, O. G.; Moody, G. J.; Thomas, J. D. R. *Analyst* **1988**, *113*, 497-500.

(27) Gallardo, J.; Alegret, S.; del Valle, M. *Sens. Actuators, B* **2004**, *101*, 72-80.

(28) Lide, D. R. *Handbook of Chemistry and Physics, 72th Edition*; CRC Press: Boca Raton, 1991, p 2407.

2.2 *In-situ* Detection of Species Relevant to the Carbon Cycle in Seawater with Submersible Potentiometric Probes

The work described below has been published in: Cuartero, M.; Pankratova, N.; Cherubini, T.; Crespo, G. A.; Massa, F.; Confalonieri, F.; Bakker, E. In-situ Detection of Species Relevant to the Carbon Cycle in Seawater with Submersible Potentiometric Probes. *Environ. Sci. & Technol. Lett.* **2017**, *4*, 410-415.

The aim of this work has been the development of a submersible potentiometric sensing array for monitoring of carbonate, calcium and pH in seawater and its subsequent integration for *in-situ* measurements in field conditions (Genoa Harbor, Arcachon Bay), followed by the validation of performed measurements. The successful completion of this research work accounts to a greater extent for the efforts of Dr. Maria Cuartero, however it has been nevertheless included in this doctoral thesis due to considerable input of the author into presented project.

2.2.1 Abstract

We report on the development of a submersible probe for the simultaneous potentiometric detection of carbonate, calcium and pH in seawater. All-solid-state electrodes incorporating nanomaterials provide adequate response time (< 10 s), stability (drifts < 0.9 mV h^{-1}), reproducibility (calibration parameters deviation < 0.7%) and accuracy (deviation < 8% compared to reference techniques) for real time monitoring of seawater using a flow system. The functioning of the deployable prototype was checked in an outdoor mesocosm and during a long-term monitoring in Genoa Harbor. The electrodes were working properly during three weeks and the system demonstrated capability to autonomously operate with routines for repetitive measurements, data storage and management. *In-situ* profiles observed in Genoa Harbor and Arcachon Bay were validated using on-site and *ex-situ* techniques. The validation of *in-situ* detected carbonate is a challenge since both re-equilibration of the sample with atmospheric CO_2 and the use of apparent thermodynamic constants for speciation calculations lead to some differences (deviation < 20%). The submersible probe is a promising tool for obtaining rapid and trustable information about chemical levels in marine systems. Moreover, the fluidic approach allows for the integration of other ion sensors that may require sample pretreatment.

2.2.2 Introduction

The accurate measurement of the carbonate system in seawater is of urgent importance to study ocean acidification caused by the absorption of anthropogenically emitted CO_2.[1-4] Since the concentrations of the associated chemical species, CO_2, pH, HCO_3^- and CO_3^{2-}, are interconnected by thermodynamic constants, the carbonate system can in principle be described from the measurement of just any two species among the four.[5] Their choice depends on the performance of the available analytical techniques, including the possible implementation for *in-situ* monitoring in the aquatic system of interest. Additionally, the quantification of dissolved calcium is related to the carbon cycle as it is involved in carbonate precipitation/dissolution processes and its monitoring may contribute to a more complete description of the marine system.[6,7]

With pH values frequently measured in seawater using deployable glass electrodes, HCO_3^- and CO_3^{2-} are commonly calculated from total inorganic carbon or total alkalinity using pH value after sampling, and CO_2 is detected as pCO_2 by different submersible probes that often require CO_2 to be in the gas phase.[8,9] pCO_2 measurement techniques for *in-situ* observations have been reviewed recently, discussing advantages and disadvantages of the existing approaches as well as the most promising concepts.[10] Accordingly, (i) non-dispersive infrared (NDIR) spectroscopy pCO_2 sensors constitute the most used technique for *in-situ* measurements but frequent recalibrations are needed; (ii) CO_2 sensors based on Severinghaus principle exhibit reduced sensitivity, slow response time and an unstable signal at environmental pH (ca. 8.0), therefore their *in-situ* application is not advisable;[11-13] (iii) pCO_2 optodes are still in the early stages of development, exhibiting slow response times, salinity dependence and poor stability, which must be improved before implementation into submersible probes.

An *in-situ* operation of the techniques for carbonate species analysis is especially significant. They provide much higher spatial and temporal resolution compared to centralized approaches.[14] Moreover, the manipulation of the sample during sampling, transport and measuring procedures may dramatically modify its integrity by re-equilibration of the aquatic sample with an atmospheric CO_2 level that is very different from the *in-situ* value and thus providing biased results.[5,15-17] To avoid this, the samples must be kept out of air contact during manipulation and analysis, which is very difficult. Consequently, the most robust solution would involve the measurement *in situ*.

Unfortunately, not all analytical techniques and required sample pretreatment steps are suitable for this goal.

An alternative approach is the use of all-solid-state ion-selective electrodes, which offer promising characteristics for *in-situ* implementation,[18,19] for the detection of either HCO_3^- or CO_3^{2-}. While determination of HCO_3^- in marine systems is not achievable so far by direct potentiometry owing to the high hydrophilicity of the anion and the lack of selective ionophores,[20] carbonate-selective electrodes based on N,N-dioctyl-3α,12α-bis(4-trifluoroacetylbenzoyloxy)-5β-cholan-24-amide have been satisfactorily applied for carbonate detection in freshwater and buffered marine samples,[21-23] and are promising for seawater analysis. Even if *in-situ* detection is achieved, the validation of the sensor measurements is challenging. Any reference technique requires sampling and/or indirect calculation of the species concentration using the abovementioned thermodynamic constants. The latter are not universally accepted as their apparent values strongly depend on environmental factors (i.e. salinity and temperature) and are therefore a possible source of error.[24-27]

We present here a new submersible potentiometric probe for the long-term real-time detection of pH, carbonate and calcium in seawater. A potentiometric flow cell based on miniaturized all-solid-state sensors is developed for this purpose. The flow cell is incorporated into a deployable device offering autonomous operation and the compensation for the temporal effects in the electrode responses by intermittent single point calibration steps. The system was deployed in Mediterranean and Atlantic coastal waters near Genoa (Italy) and Arcachon (France), respectively. The measurements were validated with traditional sampling techniques.

2.2.3 Experimental

2.2.3.1 Materials and reagents

Poly(vinyl chloride) (PVC), 2-nitrophenyl octyl ether (o-NPOE), bis(2-ethylhexyl) adipate (DOA), tridodecylmethyl ammonium chloride (TDMACl), potassium tetrakis[3,5-bis(trifluoromethyl)phenyl]borate (KTFPB), potassium tetrakis(4-chlorophenyl)borate (KTClPB), hydrogen ionophore I, carbonate ionophore VII, calcium ionophore IV, tetrahydrofurane (THF), sodium chloride (NaCl), hydrochloric acid (1 M HCl), sodium bicarbonate and calcium chloride were purchased form Sigma Aldrich. Artificial seawater was prepared according to the recipe proposed by Kester et al. and the required reagents were acquired in Sigma Aldrich.[28]

Multi-walled carbon nanotubes (MWCNTs) with >95% wt. purity (0.5-200 μm length and 30-50 nm diameter, M4905) were purchased from HeJi, Inc. (Zengcheng City, China). MWCNTs were oxidized to produce carboxylic acidic groups followed by amide formation with octadecylamine to yield functionalized MWCNTs (f-MWCNTs).[22] A solution of f-MWCNTs in THF was prepared (1 mg mL^{-1}) to be used for the electrode preparation.

Silver wire (0.5 mm diameter and 90 mm long) was purchased from Metrohm and micro-porous ceramic junction was supplied by Idronaut. Polyether-ether-ketone (PEEK) tubings (both OD × ID = 3.18 × 1.98 mm and OD × ID = 3.18 x 1.57 mm) were supplied by Supelco, glassy carbon SIGRADUR® (D=2 mm and 25 mm length) and KCl-gel electrolyte solution by Metrohm.

Benchtop potentiometric measurements were carried out against a double-junction Ag/AgCl/3M KCl/1 M LiOAc reference electrode (model 6.0726.100, Metrohm AG, Ionenstrasse, Switzerland) using a 16-channel EMF interface (Lawson Laboratories, Inc., Malvern, PA). Commercial glassy carbon electrode was GC-electrode-tip (6.1204.300) with a diameter of 3.00±0.05 mm (length of 71 mm including the pin for the connection) sourced from Metrohm. IPC ISMATEC peristaltic pump (Model ISM935c), flangeless ferrules (1/16 Blue and 1/8 Yellow, IDEX Health & Science), male nuts (1/16 Red and 1/8 Grn, IDEX Health & Science) and PTFE tubing (length × OD × ID = 300 mm × 1/16 in × 100 μm, Supelco) were also used for the fluidic system.

An OCEAN SEVEN 316Plus CTD multiparameter probe (Idronaut) was deployed together with the developed submersible device. Bags for collecting urine (volume of 500 mL)

bought in a local pharmacy were used as container of the calibration solution (filtered seawater from the monitored place). For the seawater filter, Swinnex Filterhalter (25 mm, SX0002500) was purchased from Merck and Whatman filter papers (num. 2, D=185 mm, 1002-185) from Sigma Aldrich.

2.2.3.2 Composition of the membrane cocktails

THF membrane cocktails based on PVC polymeric matrix, plasticizer, ion-exchanger and selective ionophore were prepared for the fabrication of pH, carbonate and calcium-selective all-solid-state electrodes using amounts for these compounds already reported.[23] The cocktail for pH sensitive membrane was prepared by dissolving 1.1 mg of hydrogen ionophore I, 0.3 mg of KTClPB, 65.8 mg of o-NPOE and 32.9 mg of PVC in 1 mL of THF. For the carbonate membrane, 4.1 mg of carbonate ionophore VII, 1 mg of TDMACl, 50 µL of DOA and 30 mg of PVC were dissolved in 1 mL of THF. In the case of the calcium membrane, 1.2 mg of calcium ionophore IV, 0.6 mg of KTFPB, 65.6 mg of o-NPOE and 32.8 mg of PVC were dissolved in 1 mL of THF. Adequate drop casting of these cocktails on the electrode surface (in our case glassy carbon modified with a film of f-MWCNTs) allows to obtain an adhered plastic membrane after THF evaporation.

2.2.3.3 Fabrication of miniaturized glassy carbon electrodes (see Figure 2.2.1e)

Hand-made glassy carbon electrodes were fabricated by gluing a glassy carbon rod (ID=1.98 mm and 20 mm long) inside a PEEK tube. A length of 5 mm of the rod was kept outside the PEEK in order to make the electrical connection with a cable formed by a copper cap at one end and a pin at the other end. The surface of the carbon rod inside the PEEK was polished first with sandpaper 301D P400 until a flat surface is reached and then with alpha alumina (0.3 micron) until the glassy carbon has specular brightness. Miniaturized glassy carbon electrodes were first modified with a f-MWCNTs film and then with the selective membrane as detailed in below (Section 2.2.3.4). Finally, the electrodes were conditioned overnight (~12 hours) in a 10^{-3} M solution of HCl, $NaHCO_3$ (experimental pH=7.2, ~$0.5 \cdot 10^{-6}$ M of CO_3^{2-}) or $CaCl_2$. This is an established protocol that allows for a complete ion-exchange process in the membrane, which improves stability and operational selectivity towards the analyte.[29] While millimolar concentrations are commonly used in this procedure, in the case of carbonate-selective electrode based on ionophore VII successful analytical performance has been demonstrated using very diluted carbonate solutions (as carbonate and bicarbonate interconvert) and even in the absence of any conditioning. [21,22]

To incorporate the electrodes in the flow cell (Section 2.2.3.6, Figure 2.2.1) yellow ferrule and green nut were adjusted on the electrode (placed at the end close to the sensing part) and then the electrical connection was placed.

2.2.3.4 Preparation of membrane-based ion-selective electrodes

Commercial glassy carbon macroelectrodes (GC-electrode-tip, 6.1204.300, Metrohm) and miniaturized hand-made glassy carbon electrodes (see Section 2.2.3.6 and Figure 2.2.1e for the fabrication) were modified with functionalized multi-walled carbon nanotubes (f-MWCNTs) in analogy to earlier work.[22] Briefly, a film of the nanomaterial was deposited on top of each electrode by drop casting 8 × 20 µL (for macroelectrodes) or 5 × 5 µL (for miniaturized electrodes) of a f-MWCNTs solution in THF (1 mg mL^{-1}), allowing each layer to dry for 10 min before depositing the next layer. Then, the corresponding membrane cocktail (see Section 2.2.3.2) was drop casted on the top of the f-MWCNTs film (5 × 50 µL or 4 × 10 µL respectively), allowing each layer to dry for 20 min. Finally, the electrodes were conditioned overnight (~12 hours) as detailed in Section 2.2.3.3. Once the sensors were prepared, they were implemented into the flow cell and finally into the submersible device.

2.2.3.5 Preparation of the reference electrode

The hand-made Ag/AgCl reference electrode was prepared by gluing with epoxy the ceramic junction inside one of the ends of a PEEK tube (ID = 1.57 mm and 20 mm long). This served as a junction between the internal electrolyte and the external sample solution. Once the glue was completely dried, the PEEK tube was filled with KCl gel. The chloridized end of the silver wire was inserted in the PEEK tube. The open end of the PEEK tube was sealed with a shrinkable material. Around 15 mm of the silver wire was kept outside of the electrode body in order to establish the electrical connection. The electrode was conditioned for three months in KCl gel.

2.2.3.6 Submersible device for *in-situ* potentiometric measurements in seawater

Figure 2.2.1a shows the flow cell developed for the *in-situ* potentiometric measurements. It consists of a cubic acrylic block (25 × 25 × 25 mm) incorporating single drilled holes: two on opposite sides for the inlet and outlet, one for a reference electrode fabricated in house[30] and the other three holes for miniaturized potentiometric electrodes. In this manner, the inlet, outlet and the electrodes are concentrically placed around an inner chamber of the cell (20 µL volume) in which the sample flows (see Figure 2.2.1b). Figure 2.2.1c shows

the fluidics of the submersible device, which uses a two-position valve (supplied by Idronaut) that allows the detection either in a calibration solution (pumped in from an external bag) or in the seawater sample. This detection part is placed into a water- and pressure-proof cylindrical housing and is connected to external fluidics driven by a submersible peristaltic pump (Figures 2.2.1f,g,h).

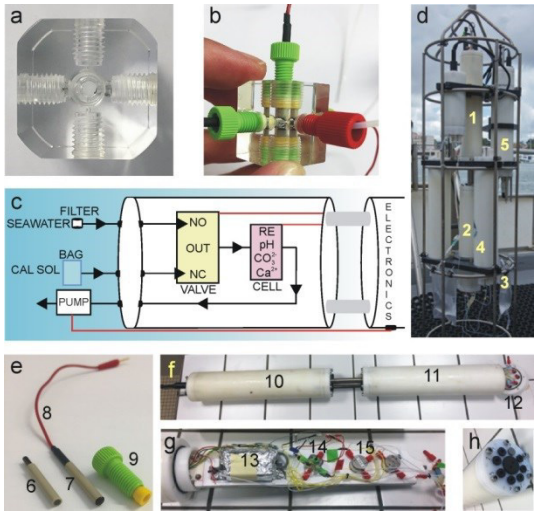

Figure 2.2.1. Images of (a) the designed potentiometric flow cell and (b) the assembled flow cell incorporating the electrodes, inlet and outlet. (c) Developed fluidics for the *in-situ* potentiometric measurements. The pump draws either filtered seawater or the calibration solution according to the valve position (NO=normally open, NC=normally close), whose outlet (OUT) is connected to the potentiometric flow cell. (d) The submersible probe is implemented into a titanium cage containing other modules as well as the pump. 1: electronics, 2: potentiometric cell, 3: bag for the calibration, 4: pump, 5: CTD multiparameter probe. (e) Picture of the electrode setup. (f) Submersible housing for electronics and the developed fluidics. (g) Experimental setup of the internal fluidics inside the submersible housing. (h) Special cap closes the submersible housing allowing the coupling between internal and external fluidics. 6: hand-made glassy carbon electrode, 7: electrode modified with the f-MWCNTs and the selective membrane, 8: electrical connection, 9: nut and ferrule for the electrode incorporation in the flow cell, 10: electronics housing, 11: housing for the potentiometric probes, 12: cap to close the housing and connected the fluidics, 13: algae module (not included in this work), 14: potentiometric flow cell, 15: valve.

When the pump starts (flow rate of 200 µL min^{-}1) with the valve in the "normally close" position (NC), the "*in-situ* calibration solution" (filtered seawater from the place where the deployment is planned) flows from the external bag to the valve and to the acrylic detection cell, and is subsequently discharged to the outside environment. In this way, the potentials of pH, carbonate and calcium electrodes are measured in flow mode in the calibration solution. If the valve is in the "normally open" position (NO), the cell is filled with filtered seawater from the aquatic system. During field deployment, the device is anchored onto a titanium cage containing the pump and other modules such as a CTD multiparameter probe (see Figure 2.2.1d). A detailed description of the measurement protocol, temperature and drift compensation as well as concentrations calculation is given

in below (see Section 2.2.3.8). Briefly, the electrodes are individually calibrated before the deployment using four standard solutions for each analyte. The slope (s) at environmental temperature (T_1) and standard potential (E^0) of each electrode is calculated. Then the potential of the three electrodes is measured in the "*in-situ* calibration solution" ($E_1^{pH}, E_1^{Carb}, E_1^{Ca}$) in order to correct for the electrodes drifts. Thereafter the device is deployed and cyclic measurements (for instance, every hour) first of the "*in-situ* calibration solution" and then of seawater from the aquatic system are accomplished. The slope of each electrode is recalculated (s') for every measurement according to the water temperature (T_2, measured by the CTD) using equation 2.2.1. The standard potential is also recalculated ($E^{0\prime}$) and therefore electrodes drifts are compensated for every measurement using the recorded potentials in the calibration solution according to equation 2.2.2.

$$s' = s\frac{T_1}{T_2} \qquad \text{(eq. 2.2.1)}$$

$$E^{0\prime} = E_2 - \left[\frac{T_2}{T_1} \cdot (E_1 - E^0)\right] \qquad \text{(eq. 2.2.2)}$$

Finally, pH, carbonate and calcium *in-situ* concentrations are calculated using the corrected calibration graphs (with s' and $E^{0\prime}$) on the basis of potentiometry using the Nernst equation:

$$E = E^{0\prime} + s' \cdot log\big(a_I(aq)\big) \qquad \text{(eq. 2.2.3)}$$

where the slope is equivalent to [2.303·RT/zF] (R=gas constant, T=temperature, z=charge of the ion and F=Faraday constant).

2.2.3.7 Description of the submersible housing

The company Idronaut (Milano, Italy) developed the submersible housing (made of acetal compolymer, Delrin),[31] which was divided into two parts (Figure 2.2.1f): one including the electronics (hardware for pump and valve control, potentiometric measurements, the adjustment of the experimental protocol, data acquisition, storage and management) and the other part to place the potentiometric probes, see Figure 2.2.1g. A special cap provides the final sealing of the module and additionally contains special nuts with water/air pressure resistance, joining the internal and external fluidics (Figure 2.2.1h). The external fluidics is based on a submersible pump to push either a calibration solution from the bag or filtered seawater from the marine system under study. The internal fluidics is based on a valve and the flow cell containing the potentiometric probes.

2.2.3.8 Experimental protocol for *in-situ* measurements and data treatment

2.2.3.8.1 Electrode calibration before deployment

After fixing the fluidic system and the potentiometric probes, closing the submersible housing and incorporating it into the titanium cage, an individual calibration graph for each electrode was performed using four standard solutions within the linear response range of each sensor covering approximately one concentration decade (i.e., four solutions in the range of 7.5-8.5 for pH, 0.08-1.00 mM for carbonate and 5.0-50 mM for calcium). Note that 600 mM NaCl background was used and the pH was additionally buffered to 8.1 for carbonate and calcium solutions (50 mM HEPES/NaOH and 50 mM Tris/H_2SO_4 buffer were used respectively). Importantly, CO_3^{2-} solutions were prepared at pH=8.1 and using increasing $NaHCO_3$ concentrations, and the final concentrations were calculated according to the constants established for H_2CO_3 in 600 mM NaCl (pK_1=5.86 and pK_2=8.95).

The standard potential (E^0) and the slope (s) were calculated for each electrode after fitting the data to the Nernst equation.[32] For the calculation of the pH, carbonate and calcium concentrations, the traditional relationship between activity and concentration was used:

$$a_i = \gamma_i \cdot c_i \qquad \text{(eq. 2.2.4)}$$

where γ_i is the single ion activity coefficient of the ion *i* calculated on the basis of the Debye-Hückel theory and considering the empirical extension of Davies applicable to seawater.[33,34] Note that liquid junction potential was neglected as previously reported for saline solutions. [35]

2.2.3.8.2 Measurement of the "in-situ calibration solution" before the deployment

Thereafter, the potential of each electrode ($E_1^{pH}, E_1^{Carb}, E_1^{Ca}$) in the "*in-situ* calibration solution" was registered in order to further correct the E^0 of each electrode. This solution has a constant pH, carbonate and calcium composition overtime as demonstrated in the laboratory for seawater samples from different locations (Costa Calida, Murcia and Genoa Harbor, Italy). For this purpose, pH, carbonate and calcium concentrations of these samples, stored in the same type of bags as the one used in the *in-situ* device, were monitored for the duration of one week by miniaturized electrodes in flow mode. Potential changes recorded for the three electrodes were in the same range of previously recorded electrodes drifts (< 1 mV h^{-1}) and therefore it can be concluded that they are not related to composition changes.

2.2.3.8.3 Programming of the submersible device

The electronics allowed one to set the following protocol for *in-situ* measurements (managed through a special software, Idronaut). 1) The pump starts (flow rate of 200 µL min^{-1}) with the valve in "normally close" position. 2) The calibration solution is flowing from the bag, passing through the potentiometric flow cell during 15 min. 3) The potential of pH, carbonate and calcium electrodes is recorded during the last 3 minutes in the flow. 4) The valve changes to "normally open" position. 6) Filtered seawater from the aquatic system under study is flowing through the system during 15 min. 5) The potential of pH, carbonate and calcium electrodes is recorded during the last 3 min in the flow. Advantageously, the electronics permits the programming of the established protocol to be repeated after certain time (i.e., every hour) for an independent *in-situ* monitoring of the aquatic system, and the results can be downloaded on a computer at any time. Notably, the multiparameter CTD was measuring *in situ*, simultaneously with the pH, carbonate and calcium potentiometric probes, so that the temperature, depth and salinity were continuously registered.

2.2.3.8.4 In-situ measurements and concentrations calculations

Once the device is deployed, repetitive measurements (for instance every hour) first in the "*in-situ* calibration solution" and then in the seawater from the aquatic system are accomplished. The slope of each electrode is recalculated (s') for every measurement according to the water temperature (measured by the CTD) using equation 2.2.1. The standard potential is also recalculated ($E^{0\prime}$) and therefore electrode drift is compensated for every measurement using the recorded potentials on the calibration solution and the equation 2.2.2.

Finally, *in-situ* concentrations of pH, carbonate and calcium are calculated using the corrected calibration graphs (with s' and $E^{0\prime}$) on the basis of potentiometry using the Nernst equation (eq. 2.2.3). The calculation procedure may be illustrated for carbonate concentration assuming fictitious potentials and temperatures, as follows: The calibration graph of the carbonate electrode before the deployment (T_1=14.90°C) is:

$$E\ (mV) = 261.7 - 28.6 \cdot log\ a_{Carb} \qquad \text{(eq. 2.2.5)}$$

The potential measured for the calibration solution before the deployment is $E_1^{Carb} = 381.11\ mV$, T_1=14.90°C). Thereafter, the device is deployed in the seawater and the calibration solution is measured ($E_2^{Carb} = 380.30\ mV,\ T_2 = 15.34°C$) and then the

seawater ($E = 376.66\,mV$) . Corrected calibration parameters are calculated using equations 2.2.1 and 2.2.2 and the corrected calibration graph is:

$$E\ (mV) = 260.8 - 28.5 \cdot log\ a_{Carb} \qquad \text{(eq. 2.2.6)}$$

Solving this equation for the potential recorded in seawater ($E = 382.50\,mV$) allows for the calculation of the carbonate activity ($a_{Carb} = 5.36 \cdot 10^{-5}$), which is converted into concentration using equation 2.2.4 and considering γ_i=0.23 (divalent ions in seawater according to Davies approach).[33,34] Finally, the calculated carbonate concentration is 0.23 mM. This procedure is repeated for every measurement in seawater.

2.2.3.9 Techniques used for validation of pH, calcium and carbonate in seawater

Flame atomic absorption spectroscopy instrument (AAS, Varian SpectrAA 240 FC) was used for the validation of calcium measurements. In the case of pH, a 877 pH lab station (Metrohm) was used. A carbon dioxide ion-selective electrode (Thermo Scientific) based on the Severinghaus principle together with its reagents kit were used for carbonate validation.

For the on-site sampling, a peristaltic pump PD5006 (Heidolph Instruments Gmbh & Co) was used and the tubing was attached to the titanium cage of the deployable system, close to the seawater inlet of the fluidics. Then, filtration was performed using 0.2 or 0.45 µm pore size PTFE syringe filters (EXAPURE). Samples for calcium detection using AAS were acidified to pH~1.3 with HCl (suprapur grade, Merck) within few hours after sampling. All collected samples were immediately stored in a cold box (when transportation was required) and finally in a fridge at 4°C until just before the validation analysis.

Regarding the measurements with the CO_2 electrode, the samples were diluted with the commercial buffer (included in the reagents kit) having a pH value of ~4.5. The concentration of total carbon dioxide (TCO_2) in the sample at this pH is calculated (considering the dilution factor) from the electrode response and then the carbonate amount is obtained at the original sample pH by using apparent equilibrium constants for the carbonic acid system calculated according to Lueker et al. using equations for specific salinity and temperature conditions: [24]

$$pK_1 = 3633.86/T - 61.2172 + 9.67770 \cdot lnT - 0.011555 \cdot S + 0.0001152 \cdot S^2 \qquad \text{(eq. 2.2.7)}$$

$$pK_2 = 471.78/T + 25.9290 - 3.16967 \cdot lnT + 0.0001122 \cdot S + 0.0001122 \cdot S^2 \qquad \text{(eq. 2.2.8)}$$

2.2.4 Results and Discussion

2.2.4.1 Characterization of all-solid-state potentiometric sensors for pH, carbonate and calcium detection in seawater

The analytical performances of potentiometric macroelectrodes for pH, carbonate and calcium were assessed in 600 mM NaCl background and at pH 8.1 (for carbonate and calcium) to mimic environmental conditions in seawater. All-solid-state ion-selective electrodes (ISEs) based on carbon nanotubes were selected since they have been already shown to provide robust detection of ions in environmental water.[22,30,36,37] Calibration graphs observed for pH, carbonate and calcium (Figure 2.2.2) followed the common Nernstian behaviour described for potentiometric sensors.[38] Importantly, the linear response ranges include the expected levels for the three species in seawater (from 7.5 to 8.5 for pH, about 10^{-4} M for carbonate and 10^{-2} M for calcium)[18], suggesting that the electrodes can be used directly for seawater analysis without any pretreatment, with a response time lower than 10 s.

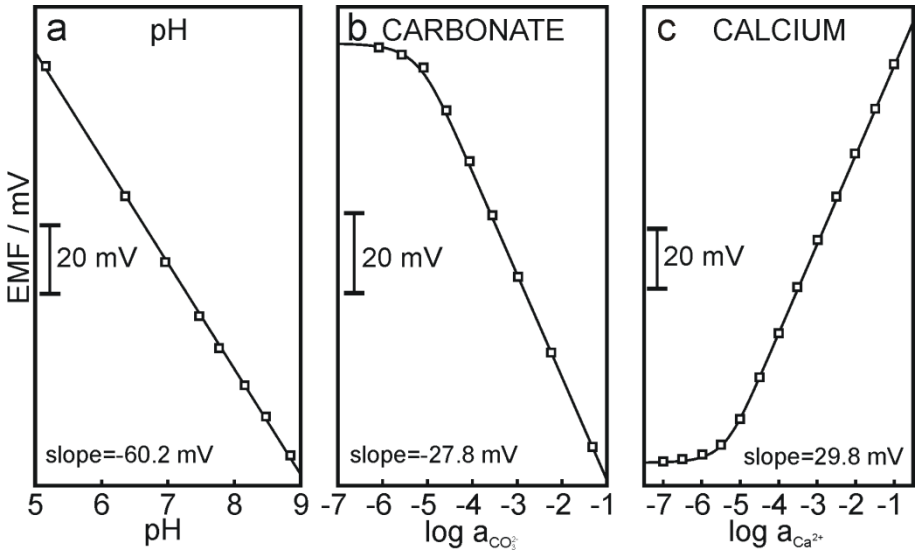

Figure 2.2.2. Potentiometric calibration graphs obtained for (a) pH, (b) carbonate and (c) calcium at 600 mM NaCl and pH=8.1 (mimicking seawater conditions).

Other response characteristics, i.e. between-day reproducibility of the calibration parameters (see Appendix 2, Table A2.1), electrode drift (see Appendix 2, Table A2.2) and selectivity (Figure 2.2.3), were additionally evaluated to assure reliability of the calculation of unknown concentrations and suitability of the sensors for long-term measurements in seawater (see Appendix 2 for more details). Although all the sensors demonstrated adequate performances in view of field measurements, even no influence of interfering ions in the potentiometric response (Figure 2.2.3), it is desired to implement simple

corrections of the calibration parameters (slope and standard potential) to compensate for temporal variations. These are expected owing to environmental factors and/or (bio)fouling, that may provide biased results when measuring *in situ*. The corrections may be performed by recalculating the electrode slopes according to observed variations of seawater temperature and repeatedly measuring the electrode potential in a calibration solution during deployment to correct the standard potential of each electrode.

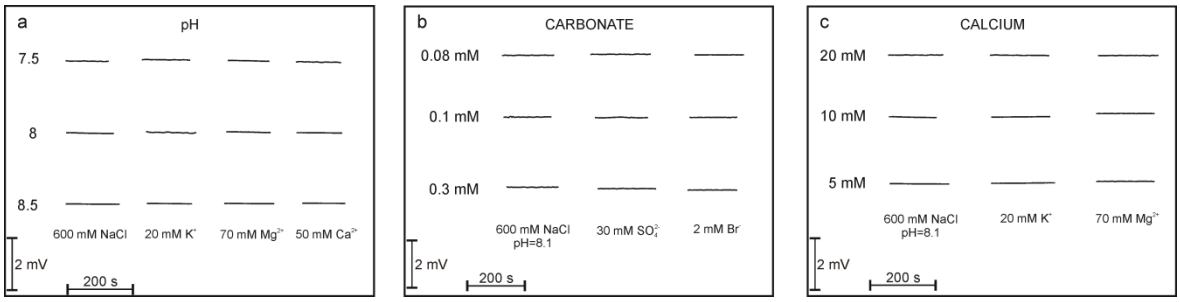

Figure 2.2.3. Selectivity study. Potentiometric responses observed for (a) pH, (b) carbonate and (c) calcium electrodes in solutions of different concentrations of the ion analytes (within the expected concentration range in seawater) and in the presence of interfering ions at concentrations slightly higher than the ones expected in seawater. (Approximate levels of the major ions in seawater: pH=7.5-8.5, CO_3^{2-} 0.1 mM, Ca^{2+} 10 mM, K^+ 10 mM, Mg^{2+} 50 mM, SO_4^{2-} 30 mM and Br^- 0.8 mM).

The analytical performances of miniaturized hand-made glassy carbon electrodes (3-fold reduced size) that are physically more suitable for the coupling to the submersible device were found to be similar to those of the macroelectrodes (see Appendix 2: Tables A2.1, A2.2). The analysis of pH, carbonate and calcium was accomplished in different seawater samples using the macroelectrodes in batch mode, the miniaturized electrodes in flow mode (using the developed flow cell) as well as reference techniques (i.e. pH-meter, CO_2 probe and atomic absorption spectroscopy respectively) in order to validate the measurements with sensors (see Appendix 2: Tables A2.3, A2.4). A good agreement was found using the different techniques (deviations < 8%), confirming the applicability of the designed potentiometric cell for seawater analysis.

2.2.4.2 Implementation and *in-situ* functioning of the submersible potentiometric probes

The next step was the physical implementation of the flow potentiometric cell into the submersible device, which is based on a fluidic system allowing the detection of either a calibration solution or seawater by the sensors (Figure 2.4.1c). The system was designed to operate automatically by controlling the fluidics (submersible pump), potentiometric outputs, data recording and managing with routines stored on board. For field deployment the module was mounted into a titanium cage together with the pump and other modules (CTD multiparameter probe), see Figure 2.2.1d.

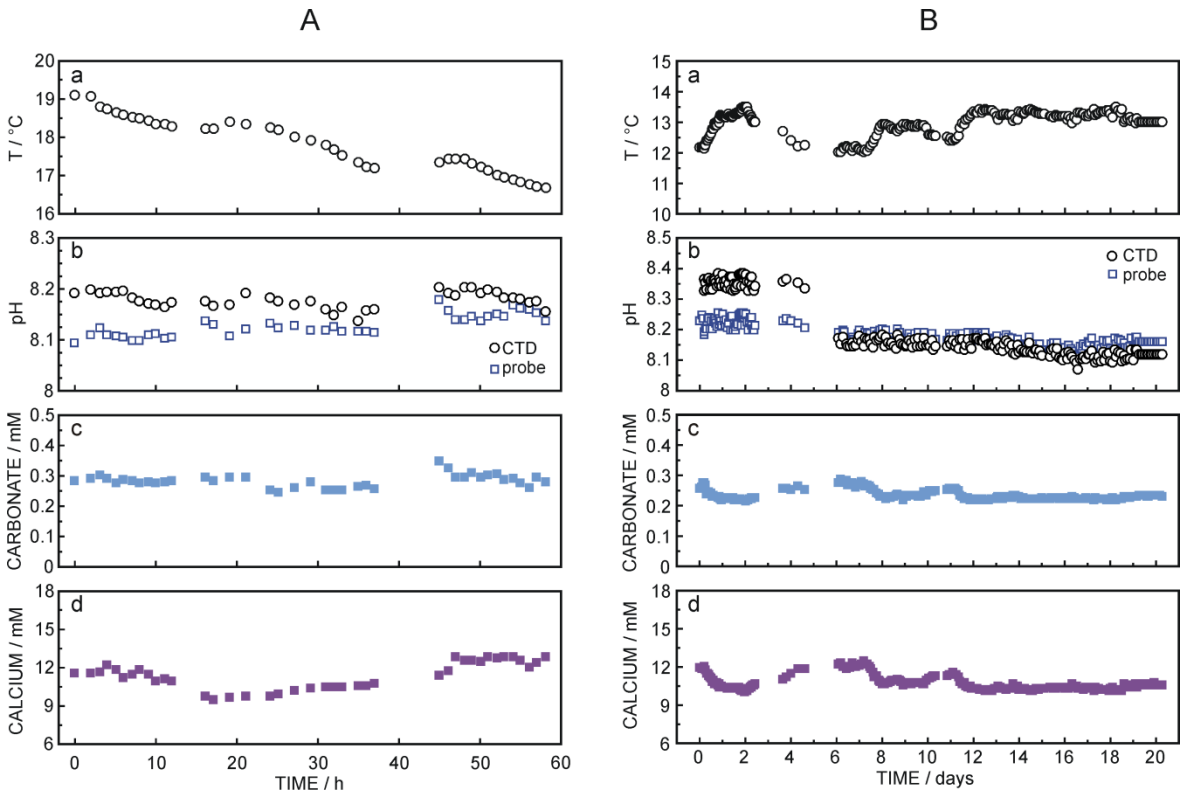

Figure 2.2.4. *In-situ* profiles obtained for (a) temperature (CTD), (b) pH (CTD and developed potentiometric probe), (c) carbonate and (d) calcium. (A) During a 58-h deployment (from June 14th, 2016 at 18:38 to June 17th, 2016 at 07:00) in an outdoor mesocosm (20000 L) placed at PiE-UPV/EHV facilities (Plentzia, Basque Country, Spain). Average salinity = 28.9 PSU. Depth of the deployment = 1.2 m. [*Note that we had bad weather during the whole deployment and this is probably the cause for the 0.15 pH units difference between the CTD and the miniaturized electrode. In addition, some points are missing because of some issues with electrical connections of the CTD probe and also system maintenance.*] (B) During a 20-days deployment (from January 18th, 2017 at 18:02 to February 6th, 2017 at 12:02) in the CNR Station at the Genoa Harbor (Italy). Average salinity = 37.93 PSU. Depth of the deployment = 4.2 m. [*Note that we realized that the CTD was not properly working during the first 6 days of the deployment and this is likely the reason for the differences found between the pH measured by the CTD and the miniaturized sensor. In addition, some points are missing because of some issues with electrical connections of the CTD probe and also system maintenance (by changing the seawater filter and refilling the calibration solution bag every week)*]

To evaluate the *in-situ* functioning of the system, the latter was deployed for 58 h in an outdoor mesocosm in Plentzia (Spain) monitoring pH, carbonate and calcium with the potentiometric probes, simultaneously with the CTD probe. The experimental protocol for *in-situ* measurements is described in the Experimental part (see Section 2.2.3.8). As shown in Figure 2.2.4A, the potentiometric probes were properly measuring during this entire time. The electrodes displayed very small drifts during the three minutes of potentiometric measurements in both the calibration solution and the seawater (< 5 μV min^{-1}). In addition, pH data were validated with the CTD measurements showing uncertainties < 0.15% in all the cases. Later, the lifetime of the sensors during real-time measurements in seawater was evaluated during a long-term experiment conducted in the Genoa Harbor (Italy) deploying

the system at 4.2 m depth from a fixed platform (CNR Station). The electrodes were working satisfactorily for three weeks (Figure 2.2.4B) displaying absolute uncertainties of $\Delta pH < 0.001$ pH units, $\Delta c_{Carb} < 0.002$ mM and $\Delta c_{Ca} < 0.02$ mM (calculated from the standard deviation of the recorded potentials). For a longer period of field work, it is currently advisable to replace the sensors to avoid biased results due to the deterioration of the membranes and reference electrodes. The pH measurements were again validated compared to the CTD data (uncertainties < 0.12% without considering the first 6 days of the monitoring).

2.2.4.3 Medium-term deployment in Genoa Harbor (Italy)

In-situ operation of the sensors was validated during the first 10 h of a 167-h monitoring period in the Genoa Harbor by sampling and measuring on site and/or *ex situ* using the same procedures as in the laboratory. Linear correlations were obtained in all the cases (Figures 2.2.5) with uncertainties lower than 0.8%, 22% and 1.6% for pH, carbonate and calcium concentrations respectively. While any possible bias could be likely associated with the sampling procedure, observed uncertainties are acceptable for pH and calcium detection although carbonate validation requires special attention. The values observed for on-site detection using macroelectrodes and the CO_2 sensor were found to be always higher than those measured *in situ* (uncertainties of 10-15% and 15-22% respectively), likely due to equilibration of the sample with atmospheric CO_2. On the other hand, the use of the CO_2 probe implies a series of calculations to obtain the carbonate concentration that are error-prone as well. This behaviour was previously also found by others who aimed to validate measurements of the carbonate system and reported deviations close to 50% due to the combination of all the mentioned factors.[15,17]

Temporal profiles observed for the whole 167-h period are shown in Figure 2.2.6, exhibiting minimum in carbonate and calcium levels that are reached during the daylight hours and coinciding with temperature maxima. These day/night cycles are in accordance with the natural fluctuations of the carbon cycle, in which the absence of light causes CO_2 production by the organisms. As natural activity in a harbour is reduced compared with the open sea[39], note that average dissolved O_2 (6.4 ± 0.3 ppm) corresponds to 83.7 ± 3.3% oxygen saturation, the carbonate increase during the night may be also related to an increase in the CO_2 levels with decreasing temperature.[40] In addition, observed increases/decreases in carbonate levels are associated with calcium concentrations following exactly the same trends.

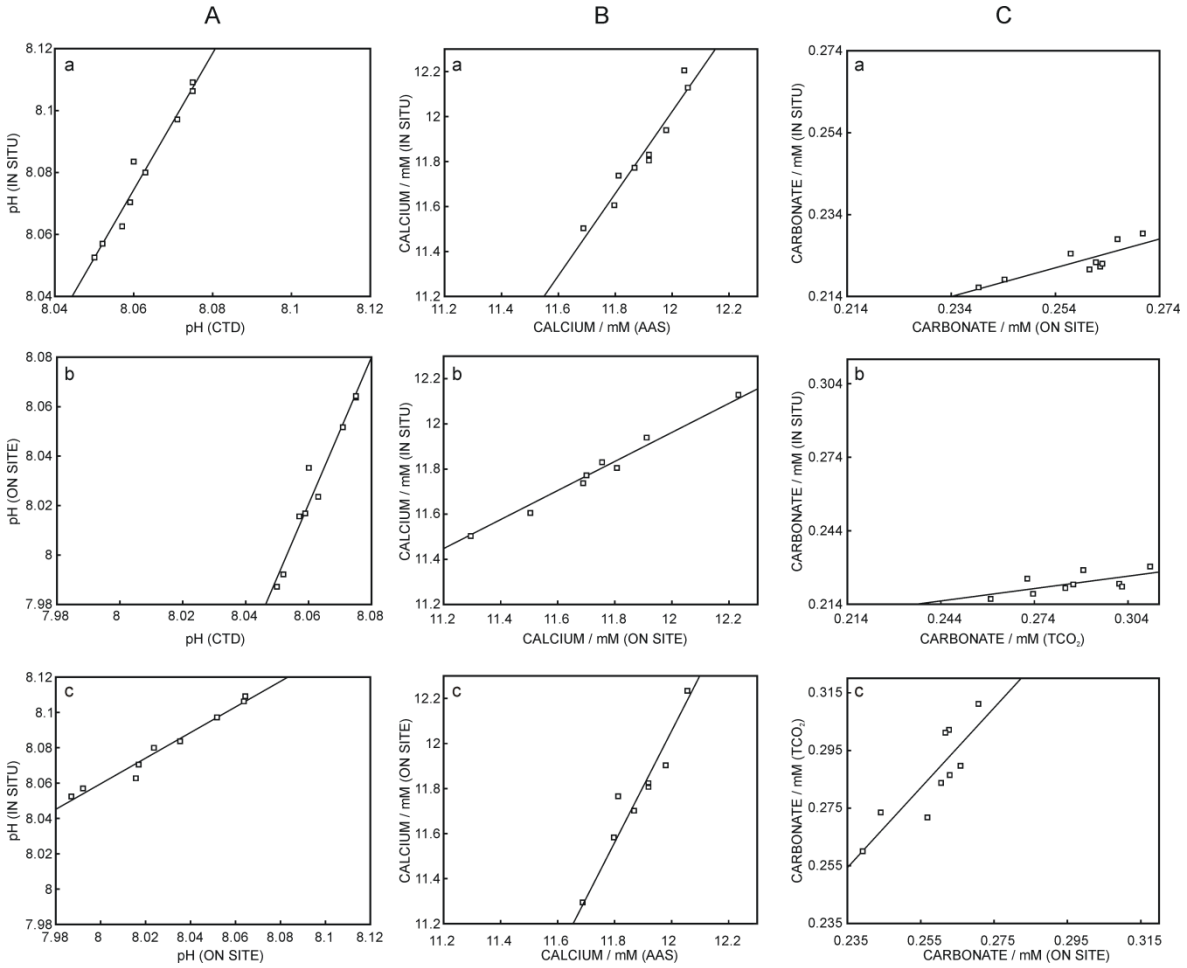

Figure 2.2.5. Validation of measurements during the first 10 hours of monitoring showed in Figure 2.2.6. (A) Validation of pH measurements: (a) correlation between CTD and *in-situ* potentiometric measurements, (b) correlation between CTD and on-site potentiometric measurements using macroelectrodes, (c) correlation between potentiometric measurements accomplished on site using macroelectrodes and *in situ*. (B) Validation of calcium measurements: (a) correlation between atomic absorption (AAS) and *in-situ* potentiometric measurements, (b) correlation between potentiometric measurements accomplished on site with macroelectrodes and *in situ*, (c) correlation between AAS and on-site potentiometric measurements with macroelectrodes. (C) Validation of carbonate measurements: (a) correlation between potentiometric measurements accomplished on site with macroelectrodes and *in situ*, (b) correlation between calculated carbonate obtained from TCO_2 using the Severinghaus sensor on site and potentiometric measurements *in situ*, (c) correlation between on-site potentiometric measurements with macroelectrodes and carbonate calculated from TCO_2 obtained by the Severinghaus sensor on-site.

Linear fits for correlations showed in Figure 2.2.5 (A): (a) $y = 2.2x - 9.66$, $R^2 = 0.99$; (b) $y = 2.97x - 15.92$, $R^2 = 0.98$; (c) $y = 0.72x + 2.26$, $R^2 = 0.99$; (B): (a) $y = 1.82x - 9.87$, $R^2 = 0.95$; (b) $y = 0.64x + 4.24$, $R^2 = 0.97$; (c) $y = 2.47x - 17.63$, $R^2 = 0.95$; (a) $y = 0.35x + 0.13$, $R^2 = 0.82$; (b) $y = 0.17x + 0.17$, $R^2 = 0.77$; (c) $y = 1.39x - 0.07$, $R^2 = 0.73$.

The average concentrations of carbonate and calcium, 0.22 ± 0.02 mmol L^{-1} and 11.82 ± 0.61 mmol L^{-1} respectively, are within the expected levels in seawater[18] and the molar percentage of carbonate with respect to calcium (~2%) coincides with the carbonate speciation at the environmental pH, as calcium is mainly associated with carbonate precipitation/dissolution processes.[41,42] The variations observed in the pH profile are within

±0.07 pH units indicating no drastic changes. A good agreement with the results from the CTD is also found.

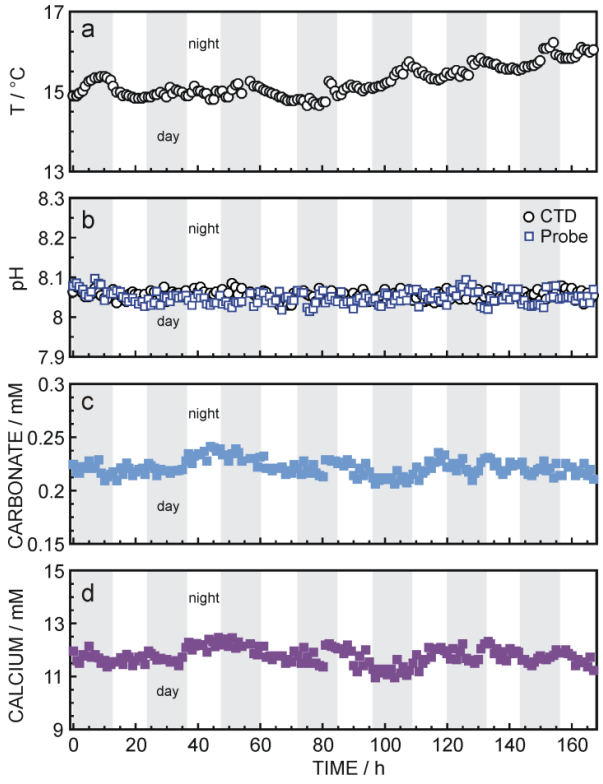

Figure 2.2.6. *In-situ* profiles obtained for (a) temperature (CTD), (b) pH (CTD and developed electrodes), (c) carbonate and (d) calcium during a 167-h deployment (from April 3th, 2017 at 07:00 to April 10th, 2017 at 12:00) in the CNR Station at the Genoa Harbor (Italy). Note that additional sampling was performed for validation during the first 10 hours. Average salinity = 37.95 PSU. Depth of the deployment = 4.2 m. Dissolved O_2 = 6.4 ± 0.3 ppm corresponding to 83.7 ± 3.3 % for oxygen saturation within the monitoring. Light hours are indicated with gray squares.[43]

2.2.4.4 *In-situ* monitoring in Arcachon Bay (France).

The submersible potentiometric probes were also tested in Arcachon Bay (France) by means of two different monitoring approaches: (i) a day/night cycle in the harbour of 14 h duration and (ii) the analysis of different locations along the freshwater effluent of the Eyre River in the bay during high tide conditions. In both cases the deployment was performed from a boat using a small crane. Importantly, the southwest corner of the bay is open to the sea, generating cycles of high and low tide thus leading to salinity cycles, which involves changes in the levels of key chemical species such as nutrients.[44] For this reason, real-time monitoring of this area is significant for understanding (bio)geochemical processes locally occurring in the bay.

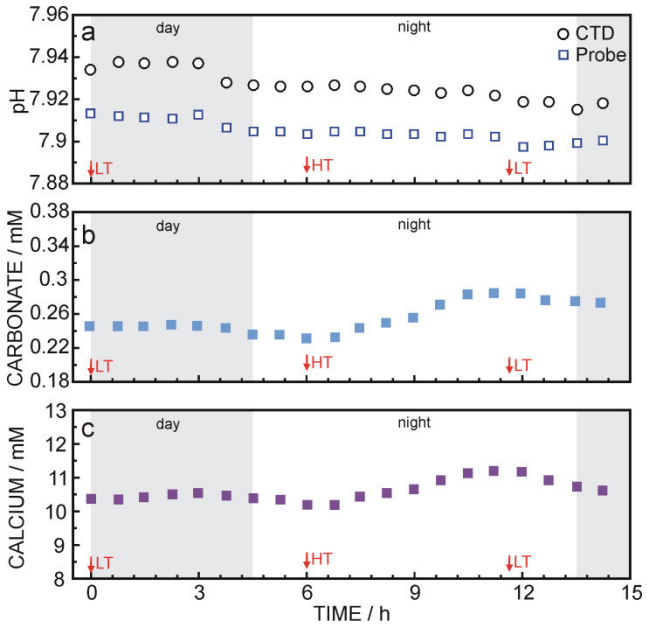

Figure 2.2.7. *In-situ* profiles obtained for (a) pH (CTD and developed electrodes), (b) carbonate and (c) calcium during a 16-h deployment (from May 17th, 2017 at 17:00 to May 18th, 2017 at 09:00) in the Arcachon Harbor. Depth of the deployment = 1.5 m. The local time for high and low tides (HT and LT) are determined according to the tidal record at Jetée d'Eyrac (44°40'N 1°10'W) and considering the temporal evolution of the seawater level in the Arcachon basin.[45,46] Light hours are indicated with gray squares.[47]

Observed profiles during the 14 h monitoring are presented in Figure 2.2.7. With regard to the pH measurements, no drastic changes were observed while, as expected, variations of carbonate and calcium levels are related to the tidal cycles. Minimal concentrations coincide with high tide conditions, while the maximum ones are found at low tides as a consequence of larger freshwater effluent loading of carbonate species, better known as "tidal flushing" effect.[48] Carbonate and calcium levels are slightly lower during the daylight hours and the carbonate-to-calcium ratio is in agreement with the speciation. Moreover, *in-situ* degree of seawater saturation with respect to calcite and aragonite may be directly calculated from calcium and carbonate concentrations according to equation 2.2.9:

$$\Omega = \frac{c_{Ca} \cdot c_{Carb}}{k_{sp}} \qquad \text{(eq. 2.4.9)}$$

where the apparent solubility product (k_{sp}) is referred to either calcite or aragonite. As observed in Figure 2.2.8, similar tidal trends were obtained and the calculated values range from 4.1 to 5.2 for calcite and from 2.8 to 3.5 for aragonite when k_{sp} values of $5.94 \cdot 10^{-7}$ and $8.76 \cdot 10^{-7}$ mol^2 L^{-2} (atmospheric pressure, T=25°C and salinity=34.5‰) are respectively used[49] (note that the calculated values may change because of temperature, pressure and salinity influence on the values of k_{sp} and, as far as we know, there are no

universal equations to calculate these values depending on the environmental conditions).[50] To the best of our knowledge, this is the first time that direct *in-situ* measurements of calcium and carbonate were accomplished in Arcachon Bay.

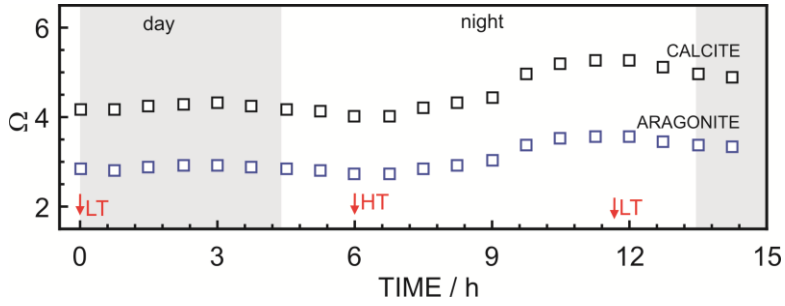

Figure 2.2.8. *In-situ* profiles for the calculated degree of seawater saturation with respect to calcite and aragonite observed during the 16-h deployment (from May 17th, 2017 at 17:00 to May 18th, 2017 at 09:00) in the Arcachon Harbor. Depth of the deployment = 1.5 m. The local time for high and low tides (HT and LT) are determined according to the tidal record at Jetée d'Eyrac (44°40'N 1°10'W) and considering the temporal evolution of the seawater level in the Arcachon basin. Light hours are indicated with gray squares.

For the second monitoring, Table 2.2.1 shows the results of a physical displacement to the west along the bay while the salinity was not drastically fluctuating. While no drastic changes were observed for pH, carbonate and calcium levels increased with westward displacement in agreement with a higher freshwater content. Validation of the observed concentrations shows uncertainties lower than 0.5%, 10% and 0.3 for pH, carbonate and calcium respectively, confirming again the suitability of the developed sensors for *in-situ* seawater analysis.

Table 2.2.1. Results obtained in different locations of Arcachon Bay (France) on May 18th, 2017 using the submersible device incorporating the multiparameter CTD (T, salinity, dissolved O_2 and pH) together with the developed potentiometric probes for pH, calcium and carbonate. Additional *ex-situ* and on-site measurements carried out for validation are included. (High tide ~11:20 am and next low tide ~17:00 pm).

Location[a]	Hour	T (°C)	PSU	DOXY[b]	pH		Ca^{2+} (mM)		CO_3^{2-} (mM)		
					CTD	*in situ*[c]	AAS	*in situ*[c]	Sev[d]	macro[e]	*in situ*[c]
AHB	9:03	17.8	32.1	6.92	7.92	7.90	10.82	10.81	0.31	0.30	0.28
PM	10:30	17.9	33.1	7.66	8.00	7.98	10.97	10.98	0.32	0.32	0.30
	10:50							11.01			0.31
LH	11:45	17.8	31.2	7.77	7.92	7.88	11.10	11.09	0.36	0.35	0.33
	12:05							11.10			0.33
CG	12:50	17.8	31.1	7.81	7.90	7.88	11.23	11.20	0.38	0.38	0.37
	13:11							11.21			0.36
	13:36							11.19			0.36

[a] AHB: Arcachon Harbor (44°39.652'N 1°09.050'W); PM: Pointe de la Matelle (44°39.708'N 1°07.711'W); LH: La Hume (44°39.750'N 1°06.709'W); CG: Chenal de Gujan (44°39.409'N 1°05.114'W).

[b] ppm

[c] In-situ measurements using the developed submersible device based on ISEs for pH, calcium and carbonate.

[d] Calculated from TCO_2 (total CO_2) obtained from on-site potentiometric measurements using a Severinghaus probe.

[e] Obtained on site by using macroelectrodes analogous to those used into the submersible probe.

2.2.5 Conclusions

We have developed submersible potentiometric probes to detect pH, carbonate and calcium in seawater in an autonomous manner with rapid data acquisition. The environmental application of the system is demonstrated in different aquatic areas of significance. The flow mode adopted for the measurements allows the correction of electrode drifts and makes it possible to integrate further inline pretreatments as needed for the potentiometric detection of other relevant ions. [30,36]

2.2.6 Acknowledgements

The author acknowledges financial support by the Swiss National Science Foundation (FNS Sinergia CRSII2-147654) and the EU Seventh Framework Program (FP7-OCEAN 2013.2 SCHeMA project - Grant Agreement 614002). We are also grateful to M. Tercier-Waeber, P. Povero, M. Castellano, C. Mirasole, J. Schafer, M. Abdou and T. Gil-Diaz for field work assistance.

2.2.7 References

(1) Martz, T. R.; Daly, K. L.; Byrne, R. H.; Stillman, J. H.; Turk, D. *Oceanography* **2015**, *28*, 40-47.

(2) Wang, Z. A.; Sonnichsen, F. N.; Bradley, A. M.; Hoering, K. A.; Lanagan, T. M.; Chu, S. N.; Hammar, T. R.; Camilli, R. *Environ. Sci. Technol.* **2015**, *49*, 4441-4449.

(3) Flecha, S.; Pérez, F. F.; García-Lafuente, J.; Sammartino, S.; Ríos, A. F.; Huertas, I. E. *Scientific reports* **2015**, *5*.

(4) Bates, N.; Best, M.; Neely, K.; Garley, R.; Dickson, A.; Johnson, R. *Biogeosciences* **2012**, *9*, 2509-2522.

(5) Choi, Y. S.; Lvova, L.; Shin, J. H.; Oh, S. H.; Lee, C. S.; Kim, B. H.; Cha, G. S.; Nam, H. *Anal. Chem.* **2002**, *74*, 2435-2440.

(6) Sun, X.; Higgins, J.; Turchyn, A. V. *Mar. Geol.* **2016**, *373*, 64-77.

(7) Jones, E. M.; Fenton, M.; Meredith, M. P.; Clargo, N. M.; Ossebaar, S.; Ducklow, H. W.; Venables, H. J.; de Baar, H. J. *Deep Sea Res.* **2017**, *139*, 181-194.

(8) Yang, D.; Guo, J.; Liu, Q.; Luo, Z.; Yan, J.; Zheng, R. *Appl. Opt.* **2016**, *55*, 7744-7748.

(9) Tamburri, M. N.; Johengen, T. H.; Atkinson, M. J.; Schar, D. W.; Robertson, C. Y.; Purcell, H.; Smith, G. J.; Pinchuk, A.; Buckley, E. N. *Mar. Technol. Soc. J.* **2011**, *45*, 43-51.

(10) Clarke, J. S.; Achterberg, E. P.; Connelly, D. P.; Schuster, U.; Mowlem, M. *Trends Anal. Chem.* **2017**, *88*, 53-61.

(11) Ishiji, T.; Chipman, D. W.; Takahashi, T.; Takahashi, K. *Sens. Actuators, B* **2001**, *76*, 265-269.

(12) Tabacco, M. B.; Uttamlal, M.; McAllister, M.; Walt, D. R. *Anal. Chem.* **1999**, *71*, 154-161.

(13) Wiegran, K.; Trapp, T.; Cammann, K. *Sens. Actuators, B* **1999**, *57*, 120-124.

(14) Nollet, L. M. L. *Handbook of Water Analysis, Second Edition*; CRC Press: Boca Raton, 2007, p 769.

(15) Martz, T. R.; Jannasch, H. W.; Johnson, K. S. *Mar. Chem.* **2009**, *115*, 145-154.

(16) Bockmon, E. E.; Dickson, A. G. *Mar. Chem.* **2015**, *171*, 36-43.

(17) Zhan, N.; Huang, Y.; Rao, Z.; Zhao, X.-L. *Chinese J. Anal. Chem.* **2016**, *44*, 355-360.

(18) Cuartero, M.; Bakker, E. *Curr. Opin. Electrochem.* **2017**, *3*, 97-105.

(19) Crespo, G. A. *Electrochim. Acta* **2017**, *245*, 1023-1034.

(20) Dabrowska, S.; Migdalski, J.; Lewenstam, A. *Electroanalysis* **2017**, *29*, 140-145.

(21) Xie, X.; Bakker, E. *Anal. Chem.* **2013**, *85*, 1332-1336.

(22) Yuan, D.; Anthis, A. H. C.; Ghahraman Afshar, M.; Pankratova, N.; Cuartero, M.; Crespo, G. A.; Bakker, E. *Anal. Chem.* **2015**, *87*, 8640-8645.

(23) Pankratova, N.; Crespo, G. A.; Afshar, M. G.; Crespi, M. C.; Jeanneret, S.; Cherubini, T.; Tercier-Waeber, M.-L.; Pomati, F.; Bakker, E. *Environ. Sci. Process. Impact* **2015**, *17*, 906-914.

(24) Lueker, T. J.; Dickson, A. G.; Keeling, C. D. *Mar. Chem.* **2000**, *70*, 105-119.

(25) Dickson, A.; Millero, F. *Deep Sea Res.* **1987**, *34*, 1733-1743.

(26) Millero, F. J.; Graham, T. B.; Huang, F.; Bustos-Serrano, H.; Pierrot, D. *Mar. Chem.* **2006**, *100*, 80-94.

(27) Lee, K.; Millero, F. J.; Campbell, D. M. *Mar. Chem.* **1996**, *55*, 233-245.

(28) Kester, D. R.; Duedall, I. W.; Connors, D. N.; Pytkowicz, R. M. *Limnol. Oceanogr.* **1967**, *12*, 176-179.

(29) Bakker, E. *J. Electrochem. Soc.* **1996**, *143*, L83-L85.

(30) Cuartero, M.; Crespo, G. A.; Bakker, E. *Anal. Chem.* **2015**, *87*, 8084-8089.

(31) Tercier, M. L.; Buffle, J.; Graziottin, F. *Electroanalysis* **1998**, *10*, 355-363.

(32) Buck, R. P.; Lindner, E. *Pure Appl. Chem.* **1994**, *66*, 2527-36.

(33) Davies, C. W. *J. Chem. Soc.* **1938**, 2093-2098.

(34) Berner, R. A. *Geochim. Cosmochim. Acta* **1965**, *29*, 947-965.

(35) Yamada, A.; Mohri, S.; Nakamura, M.; Naruse, K. *Sensors* **2015**, *15*, 7898-7912.

(36) Pankratova, N.; Cuartero, M.; Cherubini, T.; Crespo, G. A.; Bakker, E. *Anal. Chem.* **2017**, *89*, 571-575.

(37) Athavale, R.; Kokorite, I.; Dinkel, C.; Bakker, E.; Wehrli, B.; Crespo, G. A.; Brand, A. *Anal. Chem.* **2015**, *87*, 11990-11997.

(38) Bobacka, J.; Ivaska, A.; Lewenstam, A. *Chem. Rev.* **2008**, *108*, 329-351.

(39) Ruggieri, N.; Castellano, M.; Capello, M.; Maggi, S.; Povero, P. *Marine pollution bulletin* **2011**, *62*, 340-349.

(40) Weiss, R. F. *Mar. Chem.* **1974**, *2*, 203-215.

(41) Easley, R. A.; Patsavas, M. C.; Byrne, R. H.; Liu, X.; Feely, R. A.; Mathis, J. T. *Environ. Sci. Technol.* **2013**, *47*, 1468-1477.

(42) Chen, Y.; Zhang, L.; Xu, C.; Vaidyanathan, S. *Sci. Total Environ.* **2016**, *541*, 1282-1295.

(43) https://www.timeanddate.com/sun/italy/genoa?month=4&year=2017. *Time and date*, accessed August 21st, 2017.

(44) Deborde, J.; Anschutz, P.; Auby, I.; Glé, C.; Commarieu, M.-V.; Maurer, D.; Lecroart, P.; Abril, G. *Mar. Chem.* **2008**, *109*, 98-114.

(45) https://maree.info/136?d=20170517. *Annuaire des marées-France*, accessed July 3rd, 2017.

(46) https://maree.info/136?d=20170518. *Annuaire des marées-France*, accessed July 3rd, 2017.

(47) https://www.tutiempo.net/arcachon.html?datos=calendario#cal. *Mapa del tiempo*, accessed July 14th, 2017.

(48) Cook, D. O. In *Beaches and Coastal Geology*; Springer US: Boston, MA, 1982, pp 819-820.

(49) Berner, R. A. *Am. J. Sci.* **1976**, *276*.

(50) Edmond, J. M.; Gieskes, J. *Geochim. Cosmochim. Acta* **1970**, *34*, 1261-1291.

2.3 Local Acidification of Membrane Surfaces for Potentiometric Sensing of Anions in Environmental Samples

The work described below has been published in: Pankratova, N.; Ghahraman Afshar, M.; Yuan, D.; Crespo, G. A.; Bakker, E. Local Acidification of Membrane Surfaces for Potentiometric Sensing of Anions in Environmental Samples. *ACS Sens.* **2016**, *1*, 48-54.

The research described below aimed at the development of new approaches in order to overcome the pH interference for potentiometric measurements of nitrite, phosphate and other anionic species which are to be detected using ion-selective electrodes suffering from hydroxide interference.

2.3.1 Abstract

The work dramatically improves the lower detection limit of anion-selective membranes at environmental pH by using local acidification to suppress hydroxide interference at the membrane surface. Three separate localized acidification strategies are explored to achieve this, with ionophore-based membrane electrodes selective for nitrite and dihydrogen phosphate as guiding examples. In a first approach, a concentrated acetic acid solution (ca. 1 M) is placed in the inner filling solution of the PVC-based membrane electrode, forcing a significant acid gradient across the membrane. A second strategy achieves the same type of passive acidification by using an external proton source (fast diffusive doped polypropylene membrane) placed in front of a potentiometric solid contact anion-selective electrode where the thin layer gap allows one to observe spontaneous acidification at the opposing detection electrode. The third approach shares the same configuration, but protons here are released by electrochemical control from the selective proton source into the thin layer sample. All three protocols improve the limit of detection by more than two orders of magnitude at environmental pH. Nitrite and dihydrogen phosphate determinations in artificial and natural samples are demonstrated.

2.3.2 Introduction

The determination of inorganic and hydrophilic anions is essential in many areas of applied analytical chemistry, particularly for the analysis of environmental samples. This is because aquatic ecosystems are highly affected by the levels of nutrients such as phosphorus and nitrogen.[1-3] The reasonably fast response times, small dimensions, simple

operation, portability and low energy consumption of potentiometric sensors make them attractive tools for many practical applications.[4-7]

While much less progress has been achieved on the development of potentiometric anion-selective sensors in comparison to cation-selective ones, a range of anion receptors and sensors are today available.[4,6,8-10] Unfortunately, however, most reported anion receptors require a specific sample pH range, and their use above pH 7 is rarely advantageous.[8] In most cases, the strong interference from hydroxide makes them completely incompatible with the measurement of unmodified environmental samples where the natural pH normally ranges from 6.5 to 8.5.[11]

Hydroxide interference can be suppressed by acidification of the sample, but this normally requires pretreatment of the sample. It can be achieved with a cation-exchange column in its acidic form (as with a suppressor module used in ion chromatography) or a loop injector/mixing coil where the sample is mixed with acid in an adequate proportion, which can be performed in flow injection analysis.[12,13] These procedures, however, remove the sensor from direct contact with the natural sample.

Here we report on two different concepts for a localized acidification "*in situ*", without removing the sensor from the contact with the sample phase. It was found earlier that PVC-based hydrogen ion-selective membranes with a backfilling solution containing high levels of acetic acid showed unusual potentiometric response slopes even when measured in well buffered solutions.[14] It was shown that pH at the electrode surface may differ significantly from the pH in the bulk due to efficient transport of acetic acid across the polymer membrane.[14] This concept is exploited here for the first time with anion-selective polymeric membranes and subsequently modified to allow for the acidification of a thin layer by using two opposing electrodes, one to deliver the acid and the other to measure the anion of interest. An electrochemically controlled delivery of hydrogen ions, as demonstrated recently for direct alkalinity detection,[15] is applied as a third strategy to achieve instrumentally controlled thin layer acidification. Here, a hydrogen ion-selective polymer membrane acts as a proton pump for the electrochemical release of protons into the thin layer defined by the gap between the proton pump and the indicator electrode placed opposite.

2.3.3 Experimental

2.3.3.1 Materials and Chemicals

High molecular weight poly (vinyl chloride) PVC, tridodecylmethylammonium chloride (TDMACl), bis(2-ethylhexyl)adipate (DOA), 2-nitrophenyloctylether (o-NPOE), potassium tetrakis[3,5-bis(trifluoromethyl)phenyl]borate (KTFPB), potassium tetrakis(4-chlorophenyl)borate **(**KTClPB**)**, tetrakis(4-chlorophenyl)borate tetradodecylammonium salt (ETH 500), tetradodecylammonium chloride (TDDA), hydrogen ionophore I, nitrite ionophore VI, , bis(2-ethylhexyl) sebacate (DOS), chromoionophore I, tris(hydroxymethyl) aminomethane (Tris), acetic acid, hydrochloric acid (1 M), sulfuric acid, sodium hydroxide (2 M), sodium acetate, sodium chloride, sodium nitrite, potassium dihydrogen phosphate and tetrahydrofuran (THF) were purchased from Sigma–Aldrich (analytical grade). 2-Morpholinoethanesulfonic acid (MES) was purchased from AppliChem (analytical grade). Synthesis of uranyl salophene III (with t-butyl substituents) as an ionophore for dihydrogen phosphate was performed according to Rudkevich et al.[16]

Multi-walled carbon nanotubes (MWCNTs) with >95% wt. purity (outer diameters of 10-20 nm, length~50 μm) were purchased from HeJi, Inc. (Zengcheng City, China). To obtain a solution of MWCNTs in THF (1 mg mL^{-1}), a long-chain molecule octadecylamine (ODA) was grafted to the MWCNTs. Cross-linker 1,6-hexanediol diacrylate, photoinitiator 2,2-dimethoxy-2-phenylacetophenone and n-butyl acrylate monomer, all reagents in analytical and selectophore grades, were purchased from Fluka (Buchs, Switzerland).[17-19]

Porous polypropylene (PP) membranes (Celgard, 0.237 cm^2 surface area, 25 mm thickness, and kindly provided by Membrane Wuppertal, Germany) and were used as supporting material (see below).

Freshwater samples were taken from the river Arve in Geneva (Switzerland).

2.3.3.2 Membrane Preparation

2.3.3.2.1 Preparation of the indicator electrode membranes

A mixture of ionophore, ion-exchanger, plasticizer and PVC was used to prepare the cocktail for each ion-selective electrode as follows.

2.3.3.2.1.1 Nitrite-selective electrodes with inner filling solution (for Protocol A, shown in Figure 2.3.1a)

2.4 mg of nitrite ionophore VI (20 mmol kg^{-1}), 0.6 mg of ion-exchanger TDMACl (5 mmol kg^{-1}), 66 mg of PVC and 131 mg of DOS, dissolved in 2 mL of THF. The cocktail was poured into a glass ring (22 mm in diameter) placed on a glass slide and dried overnight at room temperature under a dust-free environment. After THF evaporation a membrane of 200 µm approximate thickness was obtained. Small disks (diameter ca. 8 mm) were punched from the cast films and conditioned in 1 mM $NaNO_2$ solution. The membranes were then mounted in Ostec electrode bodies with inner silver/silver chloride elements (Oesch Sensor Technology, Sargans, Switzerland).

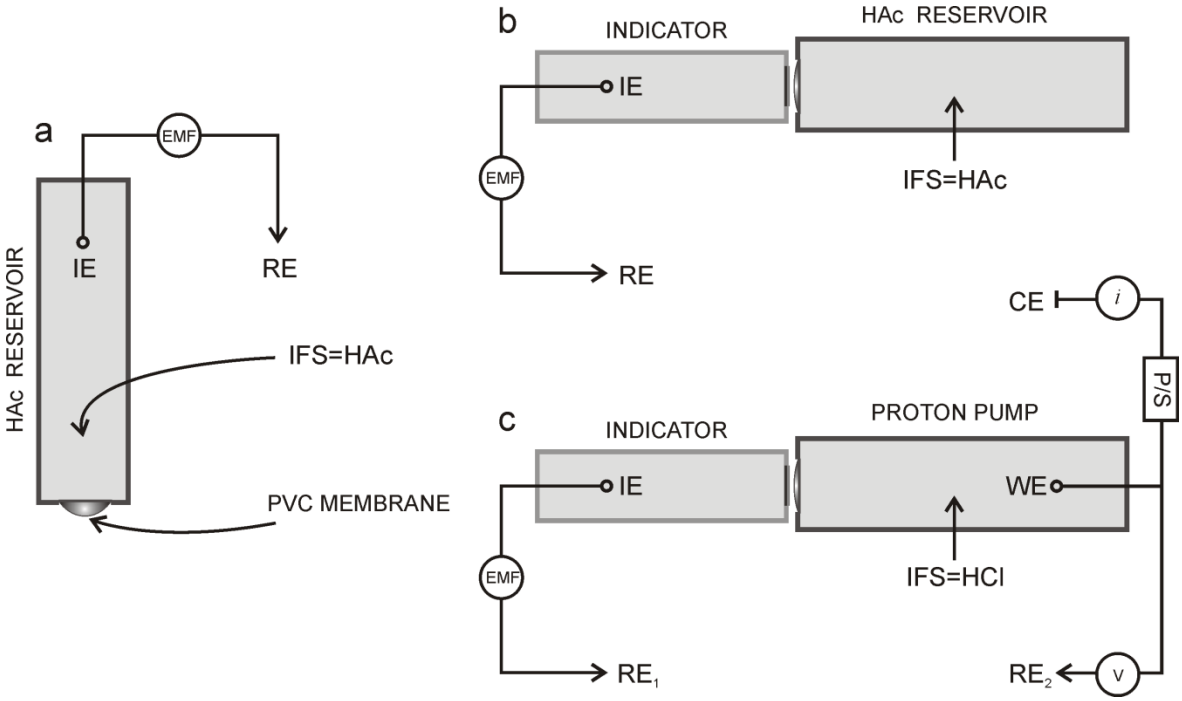

Figure 2.3.1. Explored approaches for localized acidification. IE: indicator electrode, WE: working electrode; RE, RE1 and RE2: commercial reference electrodes; CE: Pt rod counter electrode; EMF: potentiometer, V: potential reader, i: current reader, P/S: power supply; IFS: inner filling solution; GC: glassy carbon. (a) Protocol A: indicator electrode with backfilling solution containing high levels of acetic acid. (b) Protocol B: all-solid-state indicator electrode placed against acetic acid reservoir with fast diffusive membrane. (c) Protocol C: indicator electrode placed against the proton pump (WE) releasing protons when applying a constant potential.

For exploring Protocol A the inner compartment of the electrode was filled with solution containing acetic acid ~1 M and NaCl 10 mM at pH 4 (pH adjusted with NaOH). Another electrode was used for comparison (see Figure 2.3.3), filled with a conventional backfilling solution of 1 mM $NaNO_2$ + 1 mM NaCl.

2.3.3.2.1.2 All-solid-state anion-selective electrodes (for Protocols B and C, shown in Figures 2.3.1b,c)

The cocktail of functionalized multi-walled-carbon nanotubes (f-MWCNTs) was prepared by dissolving 1 mg of f-MWCNTs in 1 mL of THF. 150 µL of the cocktail (10 times 15 µL) was subsequently deposited onto the commercial glassy carbon electrode according to Yuan et al.[19] 250 µL of each PVC-based cocktail (5 times 50 µL) of the composition described below were pipetted and drop cast on the f-MWCNTs electrodes.

Composition of the PVC-based cocktails: (i) 1.2 mg nitrite ionophore VI, 0.3 mg TDMAC, 32.8 mg PVC and 65.7 mg DOS were dissolved in 1 mL THF solvent for nitrite detection. (ii) 2 mg uranyl salophene III, 0.4 mg TDDA, 32.2 mg PVC and 64.3 mg o-NPOE were dissolved in 1 mL THF solvent for dihydrogen phosphate detection. (iii) 1 mg hydrogen ionophore (I), 0.3 mg KTClPB, 32.9 mg PVC and 65.8 mg o-NPOE were dissolved in 1 mL THF solvent for pH detection. The nitrite, dihydrogen phosphate and pH electrodes were conditioned in 1 mM sodium nitrite, 10 mM sodium chloride[20] and 1 mM hydrochloric acid, respectively, for 24 h.

2.3.3.2.2 Preparation of fast diffusive membranes[15] (for Protocols B and C, shown in Figure 2.3.1b,c)

2.3.3.2.2.1 Fast diffusive proton-selective membrane (for Protocol C, shown in Figure 2.3.1c)

Porous polypropylene (PP) membranes (Celgard, 0.237 cm^2 surface area, 25 µm thickness, and kindly provided by Membrane Wuppertal, Germany) were used as supporting material. The membranes were washed with THF for 10 min to remove any possible contaminants. When the membrane was found to be completely dry (in a matter of seconds), an excess volume of 4 µL of the cocktail solution was deposited on it (see cocktail preparation below). The membrane was let in the Petri Dish for ca. 10 min to ensure a homogenous and reproducible impregnation of the pores. Afterwards, the membrane was conditioned in the solution containing 10 mM acetic acid, 10 mM sodium acetate and 10 mM sodium chloride for 40 min. Finally, the membrane was mounted in the electrode body (Oesch Sensor Technology, Sargans, Switzerland). The inner compartment was filled with 10 mM HCl.

The chemical composition of the cocktail for the deposition on the PP membrane: 120 mmol kg^{-1} of Chromoionophore I (mmol per kg of cocktail), 60 mmol kg^{-1} of KTFPB,

90 mmol kg^{-1} of ETH 500, 150 mg of o-NPOE and 1 mL of THF. THF was only used to enhance the solubility of the solid compounds into the plasticizer and was removed by evaporation before casting the membranes.

2.3.3.2.2.2 Fast diffusive membrane (for the Protocol B, shown in Figure 2.3.1b)

The fast diffusive membrane was prepared in the same way as the fast diffusive proton-selective membrane (see above). After mounting the membrane in the electrode body the inner compartment was filled with acetic acid ~1 M at pH 4 (pH adjusted with NaOH). It should be mentioned that for Protocol B the membrane does not necessarily have to be hydrogen-selective. Using nitrite-selective cocktail for the deposition of the membrane has shown similar results.

2.3.3.3 Integration of Two Electrode Bodies in the Electrochemical Cell (Protocols B, C)

To perform the measurement with the two-electrode body arrangement (see Figure 2.3.1b,c) the distance between the indicator electrode and the acetic acid reservoir (Protocol B) or the proton pump (Protocol C) was adjusted mechanically. Both electrodes were inserted into the lateral openings of the potentiometric cell and a piece of paper (100 μm) was tightly placed between them. The paper was subsequently removed from the space between the two electrodes and the cell was filled with the solution.[15] The reference and the counter (for protocol C) electrodes were immersed vertically in the same solution, outside the thin sample layer.

2.3.3.4 Instrumentation

The double-junction Ag/AgCl/3 M KCl/1 M LiOAc reference electrodes (RE_1 and RE_2, Figure 2.3.1) were purchased from Metrohm AG in Switzerland. Potentiometric measurements at zero current conditions were performed using high impedance input 16-channel EMF monitor (Lawson Laboratories, Inc., Malvern, PA). A platinum-working rod (3.2 cm^2 surface area) was used as a counter electrode for experiments with the applied potential. The applied potential was controlled by a potentiostat/galvanostat (NOVA software, Autolab). Glassy carbon electrode contained a GC-electrode-tip (6.1204.300) with a diameter of 3.00±0.05 mm and was sourced from Metrohm (Switzerland). Electrode bodies (Oesch Sensor Technology, Sargans, Switzerland) were used to mount the polymeric membranes.

2.3.3.5 Electrochemical Protocols

Illustration of the explored electrochemical Protocols is given in Figure 2.3.1. Protocol A (Figure 2.3.1a): a single indicator electrode with backfilling solution containing high levels of acetic acid (ca. 1 M HAc, pH adjusted to 4 using sodium hydroxide). Protocol B (Figure 2.3.1b): all-solid-state indicator electrode placed against acetic acid reservoir (ca. 1 M HAc, pH adjusted to 4 using sodium hydroxide). Fast diffusive polypropylene membrane (PP) allows for the passive diffusion of acetic acid into the thin sample layer. Protocol C (Figure 2.3.1c): all-solid-state indicator electrode placed against the proton pump (WE) – a fast diffusive hydrogen-selective membrane with 10 mM HCl as backfilling solution. A constant potential is applied resulting in the release of protons in the thin sample layer between the working electrode (WE) and the indicator electrode (IE). All three protocols require short sample stirring only after spiking the sample; EMF measurements with the indicator electrode were performed in nonstirring conditions.

All protocols were executed at pH 8.2-8.4 either in Tris buffer 5 mM with 1 mM sodium chloride background (pH adjusted using sodium hydroxide) or in spiked freshwater sample (without pretreatment). Calibration curves at pH 4.5 were obtained in MES buffer 10 mM with 1 mM sodium chloride background in stirring conditions.

2.3.4 Results and Discussion

The aim of this work was to establish an effective protocol for local sample acidification to improve the detection limits of potentiometric anion sensors at natural pH (6.5-8.5)[11]. Owing to the high relevance of nitrite and dihydrogen phosphate in freshwater ecosystems[21], both were selected as examples to explore and illustrate the functionality of these new concepts. The established protocols were first executed in 5 mM Tris buffer solution and subsequently in an Arve river sample. The capacity of the Tris buffer (5 mM corresponding to dn/dpH=2.8 mM at pH 8.2) was chosen higher than the buffer capacity of the Arve river sample (ca. 23 mM carbonate buffer[15] corresponding to dn/dpH=0.4 mM at pH 8.2) to illustrate the applicability of the acidification protocols for the analysis of even well buffered fresh water samples.

An anion-selective electrode based on the recently reported Co(II) salophene ionophore with aqueous inner solution was found to exhibit a Nernstian response to nitrite with a limit of detection of 10^{-6} M[22] at pH 4.5 and served as sensing electrode in approach A (Figure 2.3.1a).

For the approaches B and C, an all-solid-state nitrite and dihydrogen phosphate-selective electrode configuration (GC/f-MWCNTs/PVC membranes) was chosen. A solid-state configuration is preferable for these protocols because of the geometrically flat surface of the electrode, allowing for a better control of the distance gap between two opposing membranes (see Figure 2.3.1b,c). Moreover, it allows for a facile horizontal placement of the indicator electrode compared to one based on an aqueous inner solution, in which case trapped air bubbles can give rise to erratic responses. The obtained analytical characteristics were otherwise found to be comparable to the ones for the inner liquid configuration.[19]

Figure 2.3.2a shows calibration curves for all-solid state nitrite-selective electrodes in MES buffer at pH 4.5 (LOD = 10^{-6} M, slope -51 mV) and in Tris buffer at pH 8.3. Indeed, considering the calibration curve at pH 8.3 (slope of -12 mV) the sensor cannot be used for nitrite detection at environmental pH even at high nitrite concentration. The optimal pH range for nitrite detection is illustrated in Figure 2.3.2b (5 mM Tris buffer). Within the indicated pH range (4-6.5), the observed potential of the electrode is reasonably independent of pH, but note that the quantitative correspondence between the data in Figures 2.3.2a,b is not ideal, likely because of variations in the detection limit of the two electrodes arising from the different buffer background. At higher pH the extent of hydroxide interference becomes unacceptably large while below pH 4 the observed changes are related to nitrite speciation (nitric acid formation, pK_a = 3.4).

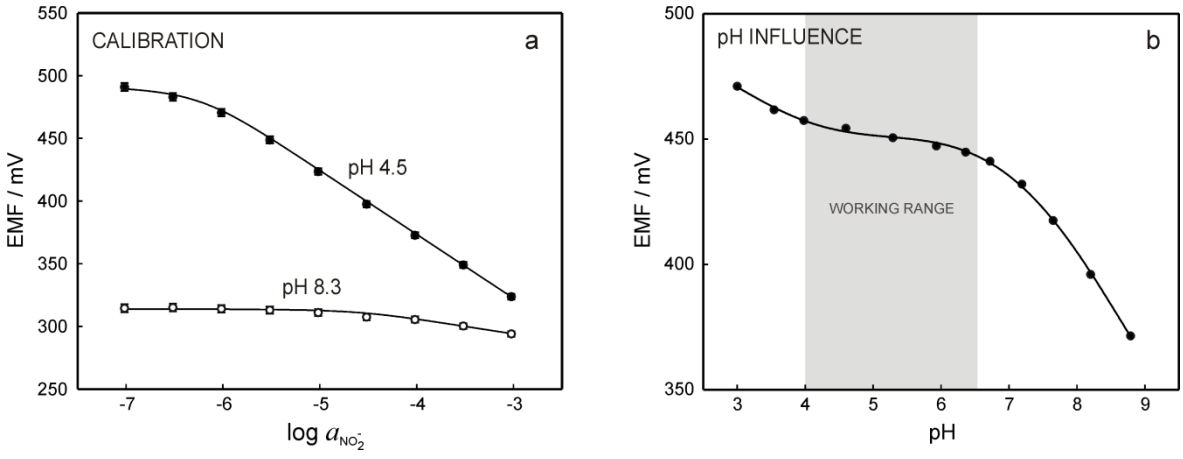

Figure 2.3.2. (a) Potentiometric calibration curves for all-solid-state nitrite-selective electrode in the beaker (stirring conditions) with 1 mM NaCl background at pH 4.5 (black markers, MES 10 mM) and 8.3 (white markers, Tris 5 mM). (b) The effect of pH on the potential of nitrite-selective electrodes in the beaker (stirring conditions) solution containing 10^{-5} M $NaNO_2$, 5 mM Tris and 1 mM NaCl background.

Techniques used for nitrite ion determination include ion chromatography, spectrophotometry, potentiometry and the use of microbial biosensors; spectrophotometric method based on the Griess reaction is the most commonly used one.[23] However, the simplicity and low cost of potentiometric techniques along with their applicability to coloured and turbid samples[23] make them a more convenient tool for *in-situ* measurements.

Although the limit of detection of the potentiometric nitrite sensor (see Figure 2.3.2), even in the appropriate pH range, is still insufficient for the detection of nitrite in unpolluted fresh waters (average nitrite concentration in fresh water ca. 10^{-8} M[24]), the proposed potentiometric sensor may be useful as an indicator of critical nitrite levels in polluted zones and aquariums. For instance, depending on the type of the fish and habitat, the toxicity of nitrite for freshwater fish may vary considerably. For example, the 96-h median lethal concentration (LC50) for rainbow trout has been reported to be less than $2 \cdot 10^{-5}$ M (1 mg L^{-1}) while largemouth bass exhibited a 96-h LC50 of ca. $1 \cdot 10^{-2}$ M (450 mg L^{-1}).[25]

The simplest concept involves a passive acetic acid release from the inner solution of the indicator electrode (Figure 2.3.1a, Protocol A). The underlying principle has been reported with PVC-based hydrogen-selective electrodes.[14] High levels of acetic acid in the backfilling solution of the ion-selective electrode give rise to a rapid acid transport through the polymer membrane, resulting in a local decrease of pH at the surface of the pH electrode (in nonstirring conditions). In that work however, it remained unclear whether efficient acid transport is also possible with membrane that contains ionophores selective for ions other than hydrogen.[14]

Indeed, we demonstrate here that the concept by Jadhav et al.[14] is applicable for the acidification of an anion-selective membrane surface, see Figure 2.3.3a. Placing a solution containing 1 M acetic acid and adjusted to pH 4 into the inner compartment of the PVC-based nitrite-selective electrode allows for the detection of nitrite down to 10^{-5} M (slope -61 mV).

This approach is conceptually elegant but may not be sufficiently mechanically robust for routine applications. Only outward bulging membranes exhibited adequate slopes and detection limits close to 10^{-5} M. This is likely due to the enhanced diffusion at the membrane edge[26] that allows for a more efficient acetic acid transport. Moreover, Protocol A requires membranes of high ion mobility, resulting in nonideal detection limits because they promote efficient transport of nitrite from the membrane to the sample as

well.[5] The concept cannot easily be applied to solid contact electrodes technology since it requires an aqueous backfilling solution.

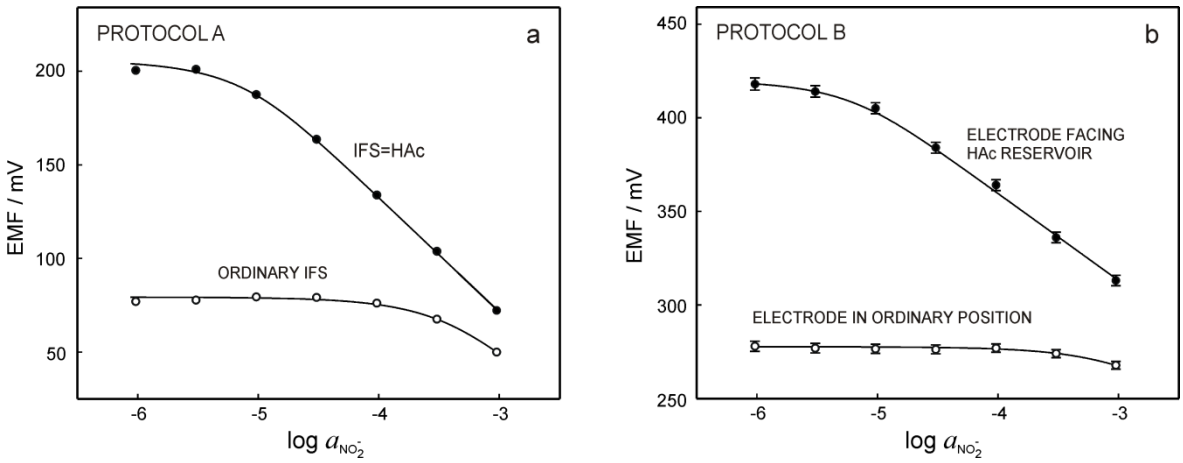

Figure 2.3.3. Protocols A and B using nitrite-selective electrode. Calibration curves in the beaker at pH 8.3 in 5 mM Tris buffer solution with 1 mM NaCl background. (a) Protocol A. Black markers: nitrite detection by applying the Protocol A (nonstirring conditions when reading the potential). White markers: nitrite detection for the electrode with "conventional" inner filling solution containing 1 mM NaNO2 and 1 mM NaCl (stirring conditions when reading the potential). IFS: inner filling solution. For the sake of convenience the data points corresponding to the white markers were shifted vertically. (b) Protocol B. Black markers: nitrite detection by applying the Protocol B (nonstirring conditions when reading the potential). White markers: nitrite detection using another all-solid-state electrode immersed vertically in the same beaker (stirring conditions when reading the potential).

The proposed approach was modified to allow for lower detection limits and the possibility of using solid contact electrodes (Figure 2.3.1b, Protocol B). The indicator electrode was placed against another electrode body filled with a reservoir consisting of 1 M acetic acid adjusted to pH 4. The polypropylene membrane provides efficient diffusion of the acid into the thin sample layer (of 40 µL volume). Figure 2.3.3b shows the calibration curves for two electrodes: one is placed in close proximity of the acetic acid reservoir and another one is immersed vertically in solution, well-spaced from the acid releasing membrane. The difference between the two calibration curves is striking, with the electrode in contact with the acid releasing membrane exhibiting a lower detection limit of 10^{-5} M (slope -47 mV).

The simplicity of experimental design is probably the main advantage of Protocols A and B. A drawback, however, is the continuity and irreversibility of the acetic acid transport that will result in a gradual contamination of the sample with acetic acid along with the depletion of the acetic acid reservoir. Based on Fick's first law of diffusion a 50% loss of acetic acid from the electrode body was estimated to occur within ca. 17 d, the acetic acid concentration at the aqueous surface of the membrane being ca. 3 mM, resulting in a flux about $4 \cdot 10^{-9}$ mol·s^{-1}·cm^{-2} (assumed inner filling solution volume of 2.2 ml, PVC membrane

diameter ca. 0.5 cm, HAc 1 M, for further details see Appendix 3). Apart from the depletion of the acetic acid reservoir, the leakage of acetic acid is undesirable since acetate is an interfering ion for some anion-selective membranes. Moreover, the sensor cannot be alternated between a pH modified and unmodified sample reading by these two methodologies.

To make the acidification process controlled and reversible, an electrochemical protocol recently explored for direct alkalinity detection (Figure 2.3.1c, Protocol C) was adapted to a controlled thin layer acidification.[15] The concept requires two independent circuits. The anion-selective indicator electrode (IE) measured at zero current is placed against a fast diffusive hydrogen-selective membrane (proton pump), as above. The proton pump now acts as a working electrode (WE) in a three-electrode cell with the respective counter (CE) and reference electrodes (RE_2) placed outside of the thin layer. The applied potential induces the reversible release of protons into the thin sample layer defined by the distance between the working electrode (WE) and the indicator electrode (IE) placed opposite each other across the sample layer. The magnitude and duration of the applied pulse depend on the pH and the buffer capacity of the sample and may be adjusted by instrumental means.

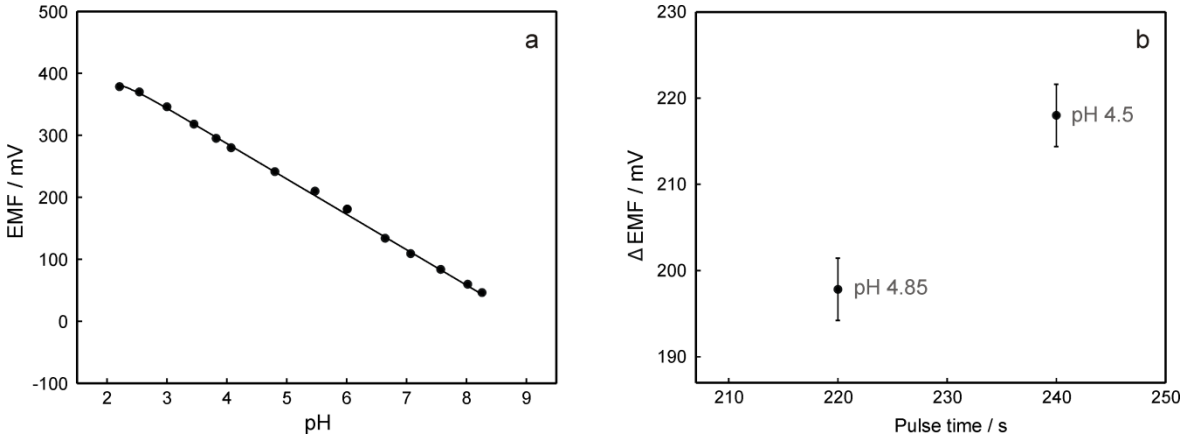

Figure 2.3.4. Protocol C using an all-solid-state hydrogen-selective electrode. Experiments in the beaker at pH 8.3 in 5 mM Tris buffer solution with 1 mM NaCl background. (a) Calibration curve in the beaker in 5 mM Tris buffer solution with 1 mM NaCl background (slope -57 mV; stirring conditions when reading the potential). (b) Illustration of the possibility of thin sample layer acidification at pH 8.3 in 5 mM Tris buffer solution with 1 mM NaCl background. Changing the pulse time at constant potential (700 mV, nonstirring conditions when reading the potential). ΔEMF: EMF difference after and before applying the pulse. The indicated pH in the thin sample layer was calculated according to the EMF changes by considering the slope of calibration curve shown above.

Figure 2.3.4 illustrates the ability of the selected protocol to acidify the thin layer sample to the desired pH (4.85 and 4.5, depending on the pulse time) by applying a potential of 700 mV (for 220 s and 240 s, respectively). To demonstrate this, a pre-calibrated all-solid-

state hydrogen ion-selective electrode was used as indicator electrode. The resulting pH in the thin sample layer was calculated based on the EMF difference before and after the pulse and considering the slope of calibration curve for the pH electrode (-57 mV, see Figure 2.3.4).

Replacing the pH sensitive electrode with an anion-selective membrane in otherwise the same setup allows one to detect anions (e.g., nitrite) in the acidified thin layer sample by eliminating hydroxide interference. To optimize the pulse parameters, a fixed potential of varying duration was applied to find the working range where the indicator electrode readings are reasonably independent of the pulse duration, as illustrated in Figure 2.3.5a. Adjustment of the pulse parameters was performed at fixed concentration of the analyte ($10^{-4.5}$ M sodium nitrite). In case a plateau is not reached when increasing the pulse time, the applied potential should be increased.

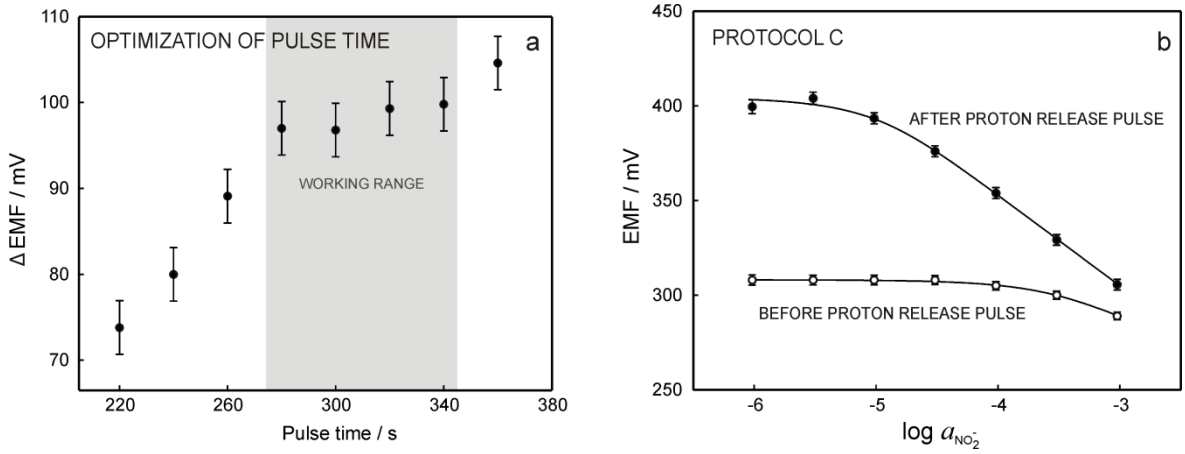

Figure 2.3.5. Protocol C using an all-solid-state nitrite-selective electrode. Experiments in the beaker at pH 8.3 in 5 mM Tris buffer solution with 1 mM NaCl background. (a) Choosing the optimum conditions for the experiment at fixed nitrite concentration ($10^{-4.5}$ M): changing the pulse time at constant potential (700 mV, nonstirring conditions when reading the potential). ΔEMF: EMF difference after and before applying the pulse. The plateau in coordinates ΔEMF-pulse time indicates the optimal working range in the given conditions. (b) Black markers: nitrite detection by applying the Protocol C (700 mV, 300 s, nonstirring conditions when reading the potential). White markers: potential readings for the same electrode before applying the pulse (nonstirring conditions when reading the potential).

As illustrated in Figure 2.3.5a, the optimum pulse duration at 700 mV was in the range of 280-340 s, hence a pulse at 700 mV during 300 s was chosen for further experiments. According to Faraday's law, the current configuration of the proton pump (inner filling solution containing 2.2 mL of 10 mM HCl) allows for ca. 850 pulses at 300 s before the total depletion of acid. It should be mentioned that the optimum pulse parameters depend on the desired pH and on the buffer capacity of the sample and thus should be adjusted for the particular experiment. Ideally, this would be achieved with the help of a thin layer-

integrated pH electrode, which may require dedicated microfabrication. The influence of the buffer concentration on the response of the nitrite-selective electrode is shown in Figure 2.3.6. Figure 2.3.5b illustrates the calibration curves of the nitrite-selective electrode before (stirring conditions) and after (nonstirring conditions) the proton release pulse in Tris buffer at pH 8.3. A significant improvement of the slope (-48 mV) and the lower detection limit (LOD = 10^{-6} M) was observed after applying the acidification pulse.

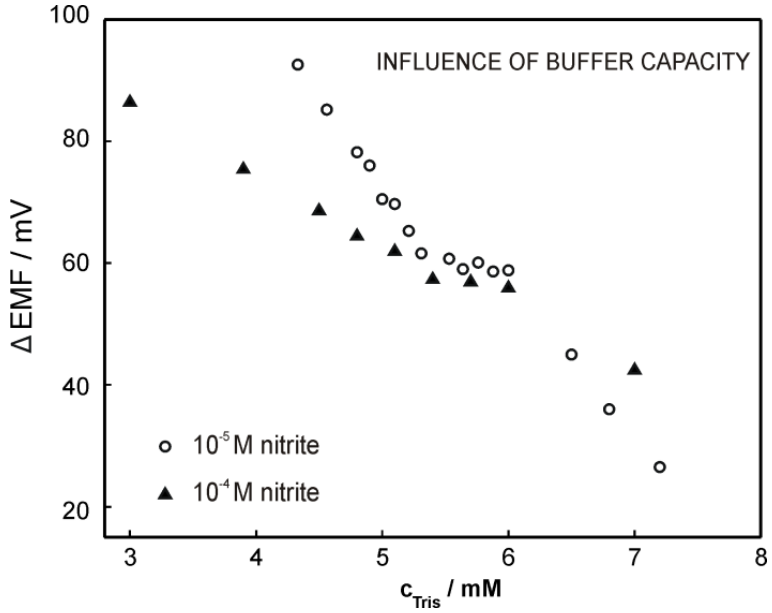

Figure 2.3.6. Influence of the buffer concentration on the response of the all-solid-state nitrite-selective electrode when applying Protocol C. Experiments performed at pH 8.2 in Tris buffer solution with 1 mM NaCl background (nonstirring conditions when reading the potential). Changing the concentration of Tris buffer in the solution with constant nitrite concentration 10^{-5} M (white circles, applied pulse: 900 mV, 500 s) and 10^{-4} M (black triangles, applied pulse: 900 mV, 380 s). ΔEMF: EMF difference after and before applying the pulse.

The same protocol was explored with dihydrogen phosphate-selective electrodes based on uranyl salophene III.[16] The calibration curves in Tris buffer at pH 8.4 are presented in Figure 2.3.7. While at pH 8.4 the electrode is not responsive to changes in phosphate concentration, the application of proton release pulses enables the detection of total phosphate down to 10^{-5} M. At slightly acidic pH most of the phosphate is in the form of dihydrogen phosphate ($pK_{a1} = 2.12$, $pK_{a2} = 7.1$). The local acidification not only minimizes hydroxide interference but helps to convert phosphate into the detectable form.

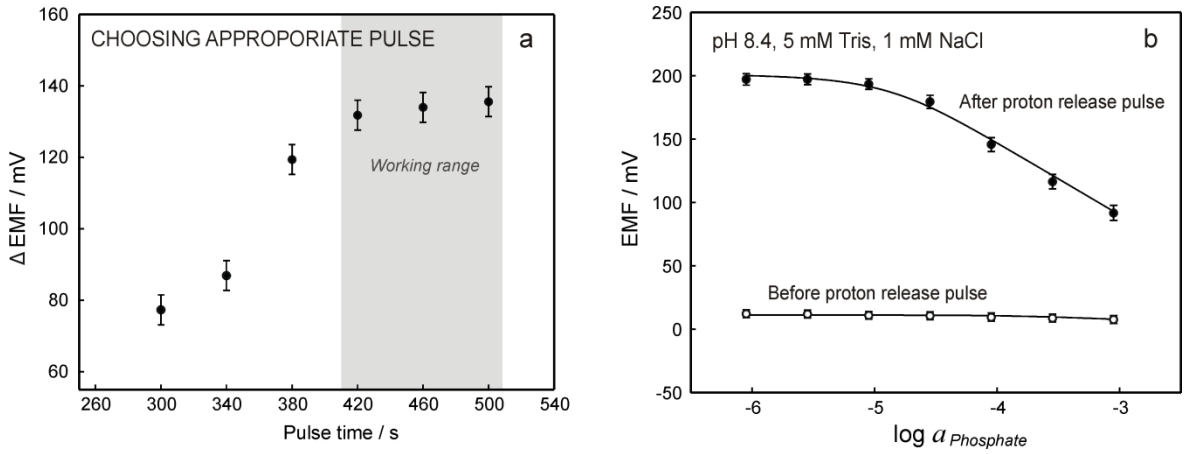

Figure 2.3.7. Protocol C using an all-solid-state dihydrogen phosphate-selective electrode. Experiments in the beaker at pH 8.4 in 5 mM Tris buffer solution with 1 mM NaCl background. (a) Choosing the optimum conditions for the experiment: changing the pulse time at constant potential (1000 mV, nonstirring conditions when reading the potential). ΔEMF: EMF difference after and before applying the pulse. The plateau in coordinates Δ*EMF-pulse time* indicates the appropriate working range in the given conditions. (b) Black markers: nitrite detection by applying the Protocol C (1000 mV, 500 s, nonstirring conditions when reading the potential). White markers: potential readings for the same electrode before applying the pulse (nonstirring conditions when reading the potential).

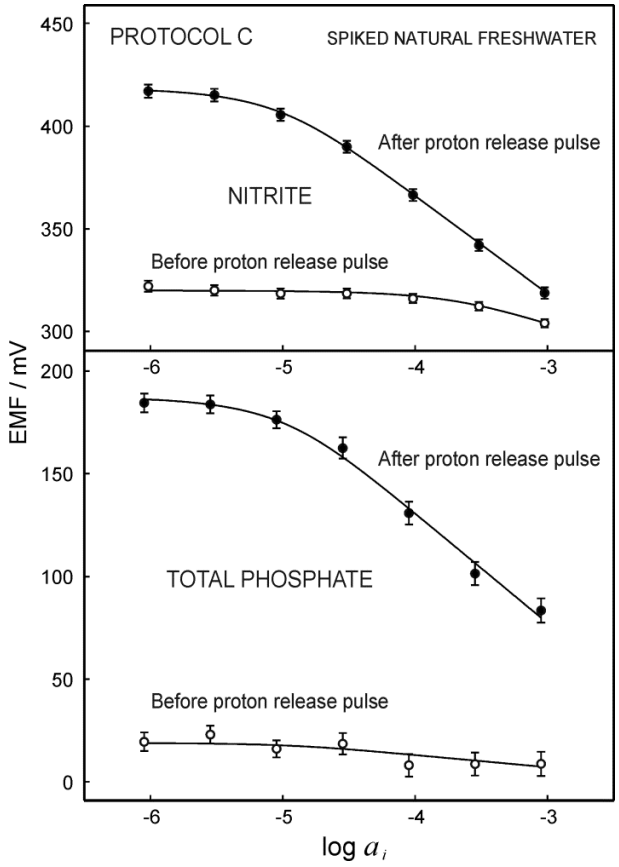

Figure 2.3.8. Protocol C using all-solid-state nitrite and dihydrogen phosphate-selective electrodes in spiked natural freshwater sample at pH 8.2. Black markers: nitrite (top)/phosphate (bottom) detection by applying the Protocol C (700 mV, 300 s for nitrite and 1000 mV, 500 s for phosphate; nonstirring conditions when reading the potential). White markers: potential readings for the same electrode before applying the pulse (nonstirring conditions when reading the potential).

Protocol C was examined in a natural sample matrix (river water). Figure 2.3.8 shows the calibration curves for nitrite and dihydrogen phosphate-selective electrodes in spiked natural freshwater (sourced from the Arve river, Switzerland). A considerable improvement of analytical figures of merit is achieved by applying the pulse sequence, with a lower detection limit of ca. 10^{-5} M for both analytes and electrode slopes of -48 mV for nitrite detection and of -54 mV for phosphate. The larger error bars observed for phosphate detection are likely caused by variations in phosphate speciation given by pH changes in the poorly buffered natural sample.

2.3.5 Conclusions

We demonstrate here the potential elegance of a local electrode surface acidification for the potentiometric detection of the anions (nitrite and dihydrogen phosphate) using ionophore-based ion-selective electrodes. Three different approaches are suggested to effectively suppress hydroxide interference by acidifying the thin sample layer adjacent to the anion-selective membrane. In the first two approaches, local acidification is accomplished by passive acetic acid release from the backfilling solution of the indicator electrode (Protocol A, simple but least robust concept) or the backfilling solution of a separate acetic acid reservoir with a fast diffusive membrane facing the indicator electrode (Protocol B, more robust but without control). The third protocol places the indicator electrode against a fast diffusive hydrogen-selective polymer membrane releasing protons when applying constant potential (Protocol C). Calibration curves for nitrite and phosphate detection obtained in spiked artificial and natural samples by applying all three protocols result in a significant improvement of the lower detection limit to ca. 10^{-5} M for both nitrite and phosphate. The advantages of Protocols A and B are their simplicity while their drawback lies in the spontaneity of the diffusion process, the gradual contamination of the sample with acetic acid and the eventual exhaustion of the acetic acid reservoir. In contrast, Protocol C is instrumentally much more complex, but also the most robust one due to its reversibility and the possibility of control: the magnitude and duration of the pulse may be tuned to increase or reduce the pH in the thin sample layer.

2.3.6 Acknowledgements

The author acknowledges financial support by the Swiss National Science Foundation (FNS Sinergia CRSII2-147654) and the EU Seventh Framework Program (FP7-OCEAN 2013.2 SCHeMA project - Grant Agreement 614002). The authors thank Thomas Cherubini for the fabrication of the potentiometric cell and Dr. Marcin Pawlak for the synthesis of the dihydrogen phosphate-selective ionophore.

2.3.7 References

(1) Margalef, R. *Oceanol. acta* **1978**, *1*, 493-509.

(2) Estrada, M.; Berdalet, E. *Sci. Mar.* **1997**, *61*, 125-140.

(3) Zielinski, O.; Busch, J. A.; Cembella, A. D.; Daly, K. L.; Engelbrektsson, J.; Hannides, A. K.; Schmidt, H. *Ocean. Sci.* **2009**, *5*, 329-349.

(4) Antonisse, M. M. G.; Reinhoudt, D. N. *Electroanalysis* **1999**, *11*, 1035-1048.

(5) Bakker, E.; Bühlmann, P.; Pretsch, E. *Chem. Rev.* **1997**, *97*, 3083-3132.

(6) Bakker, E.; Pretsch, E. *Angew. Chem.* **2007**, *46*, 5660-5668.

(7) Bobacka, J.; Ivaska, A.; Lewenstam, A. *Chem. Rev.* **2008**, *108*, 329-351.

(8) Gupta, V. K. *Arabian J. Sci. Eng., Sect. A* **2010**, *35*, 7-25.

(9) Ganjali, M. R.; Norouzi, P.; Faridbod, F. *Electrochemical Sensors*; Transworld Research Network, 2010, p 342.

(10) Sessler, J. L.; Gale, P. A.; Cho, W.-S. *Anion receptor chemistry*; Royal Society of Chemistry, 2006, p 430.

(11) Michaud, J. P. A Citizens' Guide to Understanding and Monitoring Lakes and -Streams; Washington State Department of Ecology, 1991.

(12) Howard, A. G.; Yeh, C. Y. *Anal. Chem.* **1998**, *70*, 4868-4872.

(13) Martin, G. B.; Meyerhoff, M. E. *Anal. Chim. Acta* **1986**, *186*, 71-80.

(14) Jadhav, S.; Bakker, E. *Electrochem. Solid-State Lett.* **1998**, *1*, 194-196.

(15) Afshar, M. G.; Crespo, G. A.; Bakker, E. *Angew. Chem.* **2015**, *54*, 8110-8113.

(16) Rudkevich, D. M.; Verboom, W.; Brzozka, Z.; Palys, M. J.; Stauthamer, W. P. R. V.; van Hummel, G. J.; Franken, S. M.; Harkema, S.; Engbersen, J. F. J.; Reinhoudt, D. N. *J. Am. Chem. Soc.* **1994**, *116*, 4341-51.

(17) Rius-Ruiz, F. X.; Bejarano-Nosas, D.; Blondeau, P.; Riu, J.; Rius, F. X. *Anal. Chem.* **2011**, *83*, 5783-5788.

(18) Cuartero, M.; Crespo, G. A.; Bakker, E. *Anal. Chem.* **2015**, *87*, 8084-8089.

(19) Yuan, D.; Anthis, A. H. C.; Ghahraman Afshar, M.; Pankratova, N.; Cuartero, M.; Crespo, G. A.; Bakker, E. *Anal. Chem.* **2015**, *87*, 8640-8645.

(20) Wroblewski, W.; Wojciechowski, K.; Dybko, A.; Brzozka, Z.; Egberink, R. J. M.; Snellink-Ruel, B. H. M.; Reinhoudt, D. N. *Anal. Chim. Acta* **2001**, *432*, 79-88.

(21) Yoshiyama, K.; Mellard, J. P.; Litchman, E.; Klausmeier, C. A. *Am. Nat.* **2009**, *174*, 190-203.

(22) Néel, B.; Afshar, M. G.; Crespo, G. A.; Pawlak, M.; Dorokhin, D.; Bakker, E. *Electroanalysis* **2014**, *26*.

(23) Hassan, S. S. M.; Marzouk, S. A. M.; Sayour, H. E. M. *Talanta* **2003**, *59*, 1237-1244.

(24) Hollocher, K.; Quintin, L.; Ruscitto, D. In *New York State Geological Association Field Trip Guidebook, 74th annual meeting*, McClelland, J., Karabinos, P., Ed.: Lake George, New York, 2002, pp C11.1- C11.15.

(25) Tomasso, J. R. *Aquat. Toxicol.* **1986**, *8*, 129-37.

(26) Afshar, M. G.; Crespo, G. A.; Xie, X.; Bakker, E. *Anal. Chem.* **2014**, *86*, 6461-6470.

2.4 In-line Acidification for Potentiometric Sensing of Nitrite in Natural Waters

The work described below has been published in: Pankratova, N.; Cuartero, M.; Cherubini, T.; Crespo, G. A.; Bakker, E. In-line Acidification for Potentiometric Sensing of Nitrite in Natural Waters. *Anal. Chem.* **2017**, *89*, 571-575.

The work in question intended to provide a robust, cost-effective and reagent-sparing concept for in-line acidification of the sample flow, easy-to-integrate for future *in-situ* analysis of environmental samples requiring lowering the sample pH, in particular potentiometric nitrite determination in freshwater.

2.4.1 Abstract

We report on a novel approach for in-line sample acidification that results in a significant improvement of the limit of detection of potentiometric anion-selective electrodes aiming at determining nutrients in natural waters. The working principle of the developed acidification module relies on the cation-exchange process between the sample and an ion-exchange Donnan exclusion membrane in its protonated form. The resulting in-line acidification of natural waters with millimolar sodium chloride level (freshwater, drinking water, aquarium water as well as dechloridized seawater) decreases the pH down to ~5. By using the acidification module the limit of detection of nitrite-selective electrodes significantly improves by more than 2 orders of magnitude with respect to that observed at environmental pH. The originality of the proposed flow cell lies in the possibility to adjust the pH of the sample by modifying its exposure time with the membrane by varying the volumetric flow rate. Facile coupling with a detection technique of choice, miniaturized configuration and simple implementation for long-term monitoring with submersible probes for environmental analysis are possible analytical configurations. This approach was here successfully applied for the potentiometric detection of nitrite in aquarium and dechloridized seawater samples.

2.4.2 Introduction

The importance of the reliable long-term monitoring of nutrient species (nitrites, nitrates, phosphates) in natural water lies in their significant role as indicators of anthropogenic activities that perturb aquatic ecosystems.[1-3] Currently established approaches for nutrient

detection involve sample extraction using power intensive pumps followed by analysis by expensive centralized laboratory devices while *in-situ* chemical analysers have largely been restricted to the measurements of conductivity, temperature and dissolved oxygen.[4,5] The sampling procedures are likely to result in undesired alterations of the samples and the loss of useful information. For these reasons, the concept of decentralized sensors for the *in-situ* monitoring of nutrients as well as other species has become very attractive for environmentalists.[6]

Whilst spectrophotometric techniques have been shown to be stable, sensitive and selective for nutrient detection,[3,4,7-9] potentiometric sensors have become a promising tool for the achievement of *in-situ* sensing platforms due to their simplicity, small dimensions, fast response times, portability and low energy consumption.[10-13] Unfortunately, there is still a lack of highly selective receptors for hydrophilic anions, and this initiated attempts to find alternative ways to improve the performance of anion-selective sensors using sample pretreatments involving the suppression of key interferents, i.e. hydroxide (at environmental pH between 6.5 and 9.0) and chloride (at 0.6 M in seawater).

We have recently reported a desalination approach for the potentiometric detection of nitrate in seawater by the in-line coupling of a potentiometric flow cell to an electrochemical desalination module.[14] Exhaustive electrochemical plating of chloride as silver chloride onto a silver element allows one to reduce its concentration from ca. 600 mM to ca. 3 mM, without any notable loss of other anions as confirmed by ion chromatography.[14] The potentiometric sensor based on lipophilic carbon nanotubes as ion-to-electron transducer[15,16] demonstrated adequate analytical performance for nitrate detection in dechloridized seawater down to about 0.5 μM concentration.

As for hydroxide interference, it has been shown recently that the performance of anion-selective electrodes at environmental pH can be significantly improved by using a local acidification of the membrane surface.[17] However, the proposed strategies are not easy to implement for long-term *in-situ* monitoring. We describe here a new acidification unit, with simple integration for continuous potentiometric measurements and possessing important advantages with respect to traditional acidification techniques that involve a suppressor column or a loop injector/mixing coil.[18,19]

The new acidification module works on the basis of ion-exchange and is conceptually related to a suppressor module in ion chromatography (IC). The cell comprises a cation-exchange membrane sandwiched between two rubber channels, one for the sample to be

acidified and the other for the acid solution that serves as the acid reservoir. This sort of ion-exchange Donnan exclusion membrane (i.e., FKL, FAB and Nafion) is commonly used in different electrochemical approaches.[20-23]

The proposed acidification approach is much simpler to implement into long-term monitoring instrumentation compared to classical methodologies, such as mixing with buffer solution, as it requires neither regular regeneration nor the presence of additional switching valves. In addition, the miniaturized configuration and low pressure resistance allow its simple integration for *in-situ* analysis inside a submersible probe. Finally, the proposed approach does not involve active sample modification (i.e., dilution and/or incorporation of other anions that likely deteriorate the performance of the potentiometric sensor) as in the case of a loop injector/mixing coil in flow analysis.

2.4.3 Experimental

2.4.3.1 Materials, reagents, samples and equipment

High molecular weight poly(vinylchloride) (PVC), tridodecylmethylammonium chloride (TDMACl), potassium tetrakis(4-chlorophenyl)borate (KTClPB), bis(2-ethylhexyl) sebacate (DOS), 2-nitrophenyloctylether (o-NPOE), hydrogen ionophore I, nitrite ionophore VI, sodium chloride (NaCl), sodium nitrite ($NaNO_2$), potassium chloride (KCl), calcium chloride ($CaCl_2$), hydrochloric acid solution (1.0 M, HCl), tris(hydroxymethyl) aminomethane (Tris, analytical grade) and tetrahydrofuran (THF) were purchased from Sigma. 2-Morpholinoethanesulfonic acid (MES, analytical grade) was purchased from AppliChem. Aqueous solutions were prepared in deionized water (>18 MΩ/m).

FKL cation-exchange membrane (thickness 120-130 μm) was purchased from Fumatech (FuMA-Tech GmbH, Germany). Before use, small pieces of 6×110 mm were pre-conditioned in deionized water for at least 6 h at room temperature and then at least 1 day in 1 M HNO_3 to ensure complete saturation of the membrane with hydrogen ions. The membrane was always stored in 1 M HNO_3. Micro-porous ceramic junctions were supplied by Idronaut (Brugherio, Italy). Poly(ether-ether-ketone) (PEEK) tubing (OD × ID = 3.18 × 1.57 mm) was purchased from Supelco and KCl-gel electrolyte solution from Metrohm. Silicone rubbers VMQ 50.20-01 (Angst + Pfister) were purchased from APSOparts®.

The multi-walled carbon nanotubes (MWCNTs) with >95 wt.% purity (outer diameters of 10-20 nm, length ~50 μm) were purchased from HeJi, Inc. (Zengcheng City, China). To obtain a solution of MWCNTs in THF (1 mg mL^{-1}), a long-chain molecule octadecylamine

(ODA) was grafted to the MWCNTs following the procedure described in the literature.[3,4] Cross-linker 1,6-hexanediol diacrylate, photoinitiator 2,2-dimethoxy-2-phenylacetophenone and n-butyl acrylate monomer, all reagents in analytical and selectophore grades, were purchased from Fluka (Buchs, Switzerland).

The water samples used in the present research were supplied from the following sources: Greifensee lake (Switzerland), Arve river (Geneva, Switzerland), tap water (Geneva), drinking water, aquarium sample (provided by BOGA [Bioterio de OrGanismos Aquaticos, Porto, Portugal] from a 2000-L containing 10 adult specimens of rainbow trout at 90% of dissolved oxygen, natural temperature of 13 ± 1°C and natural photoperiod) and seawater samples (1: Costa Calida (Murcia, Spain), 2: Voltri Harbor (Genoa, Italy) and 3: Portofino Bay (Genoa, Italy)).

The potentiometric measurements were carried out against a custom-made reference electrode[1] using a 16-channel EMF interface (Lawson Laboratories, Inc., Malvern, PA). Glassy carbon electrode-tip (6.1204.300) with a diameter of 3.00±0.05 mm was sourced from Metrohm (Switzerland).

A Metrohm 881 Compact IC pro chromatograph with an anion-exchange column (6.1006.520 Metrosep A Supp 5) was used for the reference method for nitrite detection in the aquarium sample. The solution containing 1 mM $NaHCO_3$ and 3.2 mM Na_2CO_3 was used as the eluent, 50 mM H_2SO_4 was used for the regeneration of the suppressor column.

IPC ISMATEC peristaltic pump (Model ISM935c, Clattbrug, Switzerland), ferrules (1/16 in, BGB Analytic AG), nuts (1/16 in, 15.7 mm long, BGB Analytic AG) and PTFE tubing (L × OD × ID = 300 mm × 1/16 × 100 μm, Supelco) were used in the flow system.

2.4.3.2 Potentiometric flow cell[14]

In order to measure the resulting pH of the acidified sample, a potentiometric flow cell containing an all-solid-state hydrogen-selective electrode was coupled to the acidification cell outlet. The prepared pH electrode was pre-calibrated in the chosen setup (acidification cell coupled to the potentiometric cell) using HCl solutions of different concentrations, then the pH of the acidified sample was measured. In some cases, the acidified sample was collected at the outlet of the acidification cell and the pH was measured with a commercial pH-meter in order to verify the results obtained with the all-solid-state electrode.

All-solid-state proton and nitrite-selective electrodes based on lipophilic multi-walled carbon nanotubes (f-MWCNTs) were prepared according to Yuan et al.[2] The cocktail for

the proton-selective membrane was prepared by dissolving 32.9 mg of PVC, 65.8 mg of o-NPOE, 0.3 mg of KTClPB and 1.1 mg of hydrogen ionophore I in 1 mL of THF. The cocktail for the nitrite-selective membrane contained 32.9 mg of PVC, 65.7 mg of DOS, 0.4 mg of TDMACl and 1.2 mg of nitrite ionophore VI in 1 mL of THF. A volume of 250 µL of the corresponding cocktail was deposited by drop casting (50 µL × 5 times) onto the surface of the glassy carbon electrode. Each layer was allowed to dry for 10 min. The hydrogen-selective electrode was conditioned in 10^{-4} M HCl overnight. The nitrite-selective electrode was conditioned for 12 hours in 0.1 M $NaNO_2$ solution and then two days in 10^{-8} M $NaNO_2$.

The potentiometric cell was comprised of a 30-angle wall-jet cell with the reference and the working electrodes placed opposite of each other. The inner volume of the cell was 13 µL. The Ag/AgCl reference electrode was prepared by gluing with epoxy the ceramic junction inside one of the ends of a PEEK tube (ID = 1.57 mm and 6 cm long). Once the glue was completely dried, the PEEK tube was filled with the KCl gel. One of the ends of the silver wire was chloridized and inserted in the PEEK tube. The open end of the PEEK tube was sealed with a shrinkable material. Around 1.5 cm of the silver wire was left outside of the electrode body in order to establish the electrical connection. The electrode was conditioned for three months in the saturated KCl gel.

2.4.3.3 Acidification cell

Figure 2.4.1 illustrates the custom-made acidification cell (open and closed). The cell consists of a piece of FKL membrane (6 × 110 × 0.120 mm) sandwiched between two rubber channels (rubber: 10 × 119 × 0.45 mm, channel: 1.7 × 100 × 0.45 mm). These elements are in turn placed between the two acrylic blocks (30 × 120 × 14 mm) tightly closing the system by screws. The ends of the channels coincide with the inlet and outlet of each block. Note that the inlets and outlets of the two blocks are placed in reverse order to provide counter flow in the two channels, namely for the sample to be acidified and for the acid solution (acid reservoir for the membrane). The pH of the sample after acidification was measured using an all-solid-state hydrogen-selective sensor in a potentiometric flow cell[14] placed after the outlet of the acidification cell. The same potentiometric flow cell was subsequently used for nitrite detection in aquarium and seawater samples, replacing the pH probe with an all-solid-state nitrite-selective electrode.

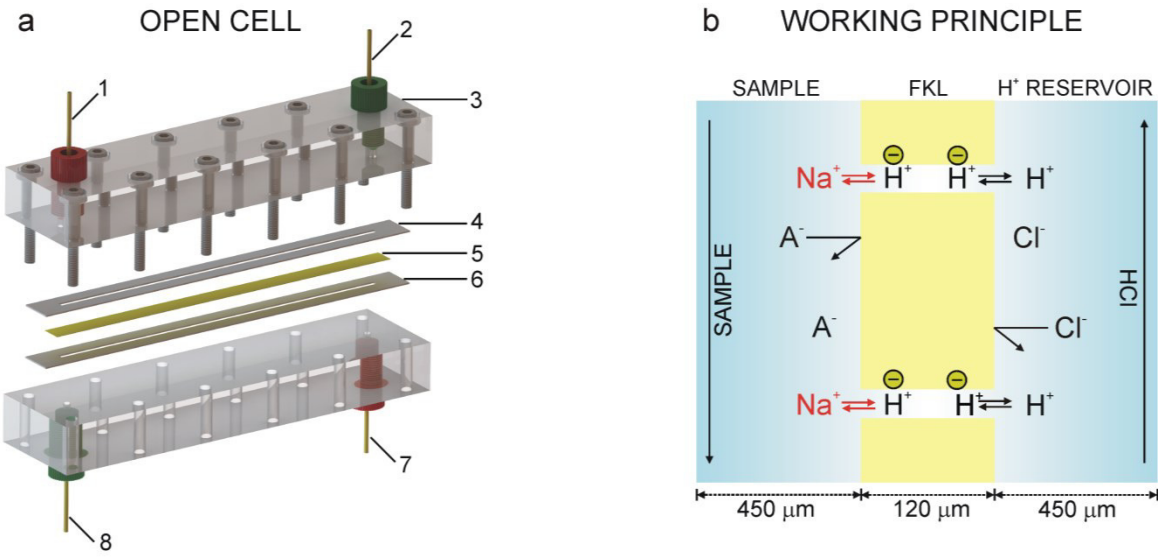

Figure 2.4.1. (a) Schematic illustration of the custom-made acidification cell: 1) inlet; 2) outlet; 3) acrylic block; 4) rubber channel; 5) FKL cation-exchange membrane; 6) rubber channel; 7) inlet; 8) outlet. (b) Working principle for the in-line acidification cell based on cation exchange between the sample and the membrane. (A^- stands for any sample anion, including nitrite and chloride). Re-conditioning of the membrane occurs by backside contact with the acid reservoir.

2.4.3.4 Desalination cell[14]

In order to reduce the chloride amount in seawater samples down to millimolar level an electrochemical desalination protocol previously established in our group was applied. The prepared desalination module was coupled in-line to the acidification unit followed by the potentiometric cell for nitrite detection in seawater.

The desalination module comprises (in the following order) the silver foil electrode, the rubber serpentine channel of 230 µm thickness for the sample, the FKL membrane, the second rubber channel of 600 µm thickness for the reference solution and finally the chlorinated silver foil. All these elements are sandwiched between two acrylic pieces (9 × 9 × 0.9 cm) that are tightly pressed by using sixteen screws. Inlets and outlets for both channels coincide with the ends of the serpentines.

The following protocol for the desalination was applied. The reference solution (0.1 M NaCl) was introduced into the cell reservoir using a peristaltic pump at 30 µL min^{-1}. Similarly, the sample was introduced into the cell through the opposite serpentine channel. Once the pump was stopped, a constant potential of 800 mV was applied for 600 s. This perturbation generates a current decay owing to the chloride electrodeposition on the working electrode (silver foil). Thereafter, the dechloridized sample was replaced by a

solution of NaCl 10^{-3} M to perform the regeneration process. The latter consisted in applying a negative potential (-900 mV) for 1200 s.

2.4.4 Results and Discussion

To evaluate the necessity of the natural water acidification for potentiometric nitrite detection, the performance of the all-solid-state nitrite-selective electrode was examined at different values of pH. Figure 2.4.2a shows the observed potentiometric calibration curves for nitrite at pH 8.2 (close to environmental pH) and 5.5 with 1 mM and 600 mM NaCl background (mimicking the chloride content in freshwater and seawater, respectively).

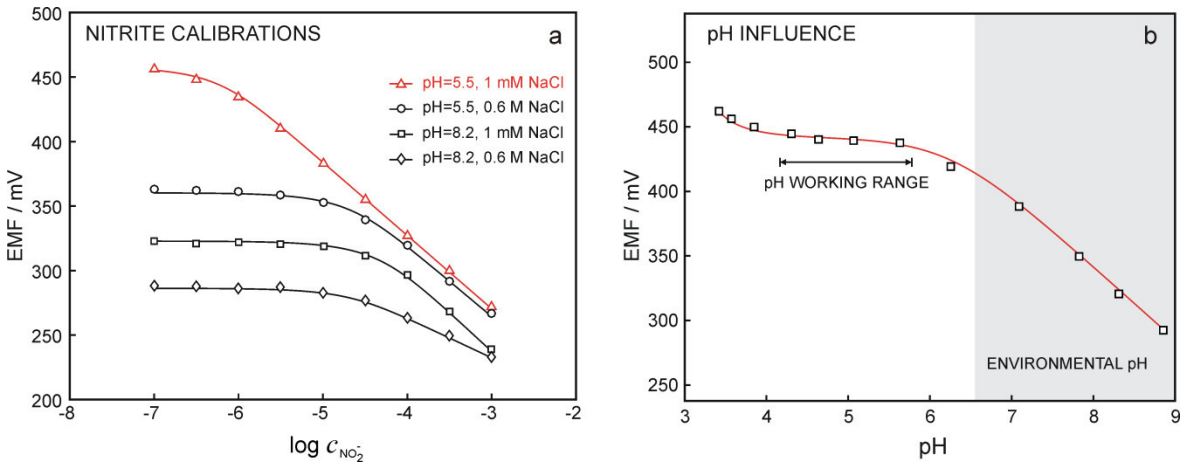

Figure 2.4.2. (a) Potentiometric calibration curves for nitrite in different media (MES buffer pH 5.5 and Tris buffer pH 8.2) in batch mode. (b) Effect of pH on the potential observed for 10-6 M NaNO2 solution in 1 mM NaCl background solution (dots for experimental data and continuous line for simulated potential). Grey box indicates the range of environmental pH.

Considering the calibrations obtained at pH 8.2 (slopes of -60.1 and -30.8 mV; LODs of 4.0×10^{-5} and 1.3×10^{-5} M, in 1 mM and 600 mM NaCl respectively) the obtained sensitivity is not suitable for nitrite detection neither in freshwater (1 mM NaCl), nor in seawater (600 mM NaCl) at environmental pH. At pH 5.5 the performance of the electrode improves significantly (slopes of -57.1 and -54.5 mV; LODs of $3.8\cdot10^{-7}$ and $1.6\cdot10^{-5}$ M, in 1 mM and 600 mM NaCl respectively). The observed LOD in 1 mM NaCl is sufficient for nitrite detection in certain natural waters (i.e., polluted freshwaters, aquarium systems and dechloridized seawater from certain locations).[24]

Figure 2.4.2b presents the influence of pH on the response of the nitrite-selective electrode in 10^{-6} M $NaNO_2$ solution. Between pH 4 to 6, the recorded potential is reasonably independent of pH. The theoretical curve describing the electrode potential considering hydroxide interference ($\log K^{pot}_{NO_2^-,OH^-} = 2$) and nitrite speciation ($pK_a = 3.4$ for HNO_2)

allows one to predict the observed pH influence (line and dots in Figure 2.4.2b respectively). For pH values above 6 the hydroxide interference becomes significant and the electrode potential decreases, while below pH 4 nitrite speciation results in the reduction of free nitrite concentration, which is accompanied with an increase in potential. The aforementioned pH range where both these processes are suppressed corresponds to the optimal working range for nitrite detection. As the pH 5.5 chosen for the calibration curves in Figure 2.4.2a was within the indicated pH range, the illustrated performance of the nitrite-selective electrode (in batch mode) corresponds to the optimal one.

Having established the required pH range for potentiometric detection of nitrite in natural waters, a new concept for in-line acidification of the target sample was proposed. To achieve this, a custom-built flow cell based on a Donnan exclusion cation-exchange membrane (FKL in H^+ form) sandwiched between two rubber channels, one for the sample and the other for the acid solution, was developed (see Figure 2.4.1a). Earlier work with such membranes for desalination already showed that they are sufficiently impermeable to the anions of interest.[14] The resulting pH of the acidified sample was measured using a potentiometric flow cell containing custom made pH probe.

The acidification of the sample flowing in one of the channels occurs through a cation-exchange process with the membrane (see Figure 2.4.1b). Considering a synthetic sample containing NaCl, Na^+ cations are rapidly exchanged by H^+ from the membrane owing to concentration gradients. The Na^+-H^+ exchange should by nearly quantitative at equilibrium and the expected pH for the sample would directly depend on the alkali metal ion concentration in the sample. For instance, a final pH of 3 is expected for the acidification of 1 mM NaCl solution in case of a complete exchange.

It has been shown that cation-exchange membranes applied for electrodialysis (e.g., FKL) exhibit a limited selectivity to different cations. The high concentration of anionic groups within the polymer structure of the membrane produces aggregations that promote the formation of a water-polymer interface where the cation-exchange occurs.[20] Therefore, the selectivity of the membrane mainly depends on coulombic interactions rather than lipophilicity as in traditional liquid membranes.[20] To further evaluate this, an examination of the pH after acidification of 10 mM samples of salts with different cations (i.e., Na^+, K^+ and Ca^{2+}) was carried out. The observed pH values at a constant flow rate (30 µL min^{-1}) were 4.3, 3.7 and 3.5 respectively, meaning that the degree of cation/proton exchange follows the order Ca^{2+}>K^+>Na^+. This sequence corresponds to the selectivity pattern

described for electrodes based on FKL membranes, as the strength of the coulombic interaction increases with ion charge while decreasing with hydrodynamic radius.[20]

One expects the rate of cation exchange to be dependent on mass transport (flow rate) and chemical composition of the two compartments. Figure 2.4.3 shows the influence of NaCl concentration, the sample flow rate and HCl concentration in the reservoir on the resulting pH. Several trends were observed: (i) The higher the sodium concentration in the sample, the lower the resulting pH; (ii) The acidification process becomes more efficient at lower flow rates, where the sample exhibits a longer residence time in the cell; (iii) The concentration of the HCl solution should at least match that of NaCl in the sample for an efficient regeneration of the membrane. Considering these results and in view of nitrite detection in water samples with a millimolar chloride level, the following parameters were chosen for further experiments: a flow rate of ca. 30 µL min^{-1} and a 0.1 M HCl concentration in the acid compartment. The performance of the acidification unit under these conditions was subsequently evaluated.

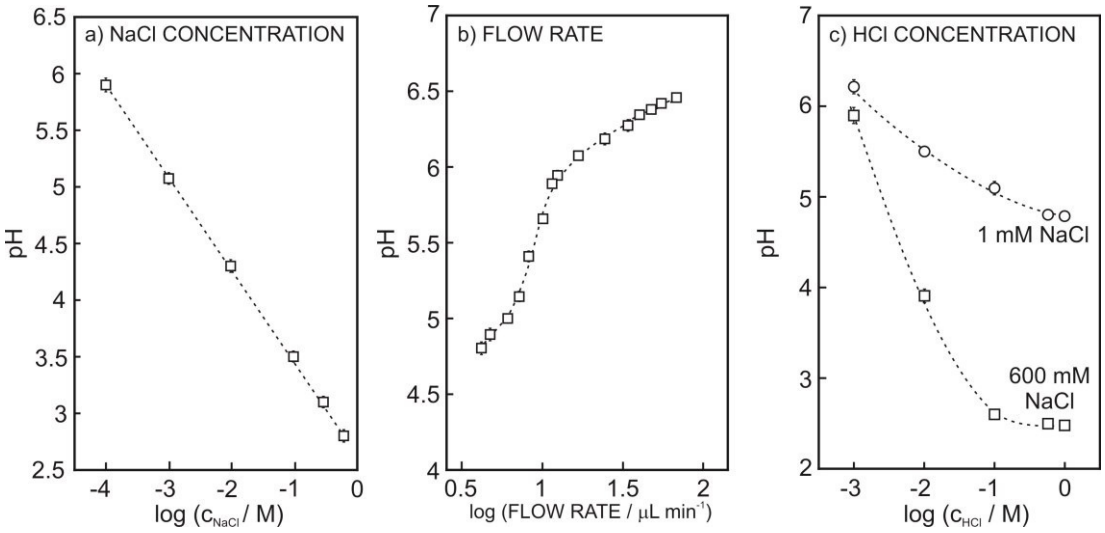

Figure 2.4.3. Influence of (a) NaCl concentration (0.1 M HCl concentration and flow rate=30 µL min^{-1}), (b) flow rate (1 mM NaCl and 0.1 M HCl) and (c) HCl concentration of the acid reservoir (flow rate=30 µL min^{-1}, squares=0.6 M NaCl and circles=1 mM NaCl) in the resulting pH after acidification. Error bars are presented for n=3 and in some occasions are smaller than the plot symbols. Dashed lines are shown to guide the eye.

The response time required to reach a steady-state of the cation-exchange process at a constant flow rate (30 µL min^{-1}) was studied by comparing the time required for the pH electrode to reach a constant potential in the same solution (1 mM NaCl) with and without acidification. The comparison of both time traces (Figure 2.4.4a) shows a similar time needed to achieve a constant potential, indicating that the acidification process is significantly faster than the response of the electrode under flow conditions (~55 s, t_{95}). In

addition, the reversibility of the ion-exchange process was evaluated by measuring the pH of acidified 1 mM NaCl solution alternating with the acidification of more concentrated solutions (10 mM and 600 mM NaCl). The resulting pH was 5.22±0.02, varying by less than 0.3 % in all cases (see Figure 2.4.4b).

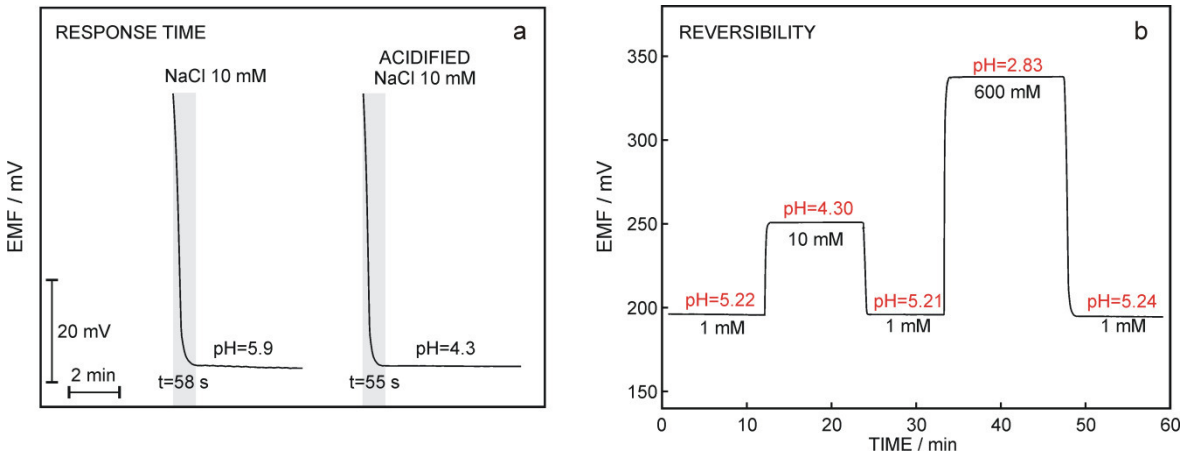

Figure 2.4.4. (a) Potentiometric time trace for all-solid-state pH electrode placed in the custom-built potentiometric flow cell: (1) 10 mM NaCl without acidification, (2) 10 mM NaCl after acidification. Note that the curves are shifted along the potential and time-axis in order to compare the response times of the electrode in both conditions. (b) Potentiometric time trace obtained for acidified samples with alternated NaCl concentrations (in the following order): 1 mM, 10 mM, 1 mM, 600 mM and 1 mM. Flow rate = 30 µl min^{-1}, 0.1 M HCl solution in the acid reservoir.

The reproducibility of the acidification process was evaluated for three weeks using the same FKL membrane as well as different FKL membranes. The same membrane was used for at least three weeks without any significant deterioration of the analytical performance (i.e. pH=5.2±0.1 for the acidified 1 mM NaCl solution, n=10) and similar pH values were obtained for the same sample using different FKL membranes (i.e. 5.2±0.2 for the acidified 1 mM NaCl solution, 2.8±0.1 for the acidified 600 mM NaCl solution).

Figure 2.4.5 shows the initial and the resulting pH values obtained for different synthetic and real-world water samples at the flow rate of 30 µL min^{-1}. Importantly, the obtained pH after acidification of lake, river, tap, drinking and aquarium water as well as dechloridized seawater is within the working range of the nitrite-selective electrode (pH 4-6). In addition, the possibility to adjust the required pH using different flow rates (i.e., changing the residence time of the sample in the cell) provides a universal platform suitable for the detection of other anions within a different pH range or for some other purpose (see Figure 2.4.3b).

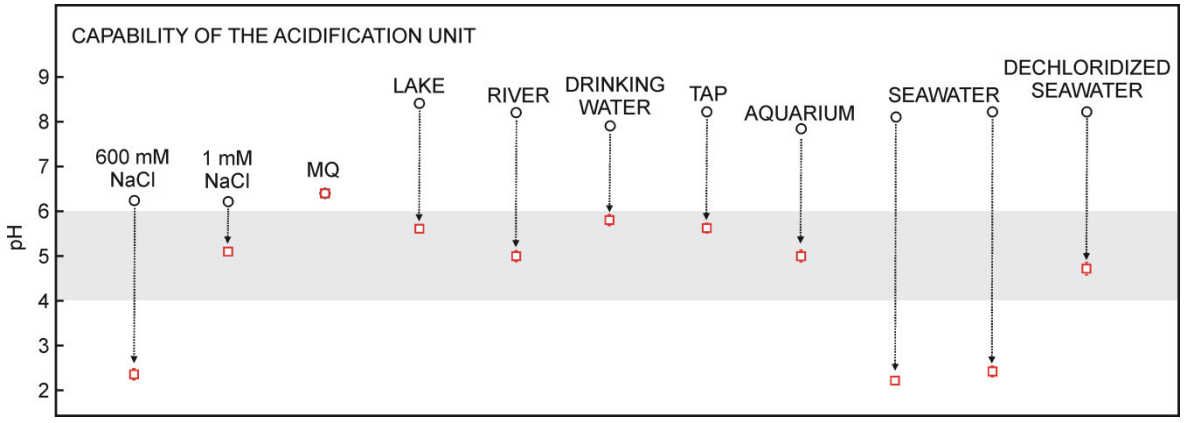

Figure 2.4.5. Initial (black circle) and modified (red square) pH after in-line acidification of different artificial and real-world samples. (0.1 M HCl and flow rate=30 µL min^{-1}). Error bars are presented for n=3 and are in some cases smaller than plot symbols. Grey box indicates the optimal pH range for potentiometric nitrite detection. Dechloridized seawater is obtained by upstream coupling of a previously described desalination unit[14] to the acidification cell.

With these operational conditions, the final coupling with potentiometric nitrite detection was accomplished and the analytical performance of the tandem system was evaluated. For this purpose, the acidification cell outlet was coupled to a potentiometric cell fitted with a nitrite-selective electrode. The electrode exhibits a Nernstian slope (-55.3 ± 1.0 mV dec^{-1}) with LOD of $(5.5 \pm 0.9)\times10^{-7}$ M, a response time faster than 1 min in the concentration range of 10^{-7}–10^{-4} M and an acceptable drift of 0.8 mV h^{-1} over 20 hours. The small differences in performance in comparison to batch mode are likely related to the higher surface-to-volume ratio in the given configuration of the flow cell and the use of a custom-made reference electrode.

The selectivity coefficients of the nitrite-selective membranes over the other major anions present in natural waters were determined using the separate solutions method[25] ($\log K^{pot}_{NO_2^-,Cl^-} = -3.7$, $\log K^{pot}_{NO_2^-,NO_3^-} = -3.3$, $\log K^{pot}_{NO_2^-,SO_4^{2-}} = -3.9$, $\log K^{pot}_{NO_2^-,H_2PO_4^-} = -4.0$, $\log K^{pot}_{NO_2^-,OH^-} = 2$). After the suppression of hydroxide and chloride interference, the detection of nitrite should be possible even in severely contaminated water samples (with increased amount of nitrite and phosphate). However, potentiometric detection of nitrite levels lower than 0.5 µM does not appear to be practical in the current configuration and requires further improvement of the sensitivity and selectivity of nitrite-selective membranes.

Finally, the detection of nitrite was performed in an aquarium sample, from a tank containing adult specimens of rainbow trout, and two dechloridized seawater samples (from the harbour and the bay in Genoa, Italy). For nitrite detection in the aquarium sample, the potentiometric cell containing the all-solid-state nitrite-selective electrode was coupled to the outlet of the acidification cell. For the analysis of seawater samples, the

desalination unit[14] was coupled upstream of the acidification cell, followed by the potentiometric cell. Nitrite concentrations of (9.7±1.0), (0.8±0.1) and (0.9±0.1) µmol L^{-1} were detected in the aquarium and the two seawater samples respectively (see Table 2.4.1). The concentration of nitrite in the aquarium sample was also determined by ion chromatography (IC) as a reference method; an adequate correlation between chromatographic and potentiometric detection was observed.

Table 2.4.1. Nitrite analysis in aquarium and dechloridized seawater samples (n=3)

Sample	Initial pH	Final pH	NO_2^- Sensor (µmol L^{-1})	NO_2^- IC (µmol L^{-1})
Aquarium	7.8	5.3	9.7±1.0	10.3±0.7
Dechloridized Seawater 2	8.0	5.1	0.81±0.08	ND
Dechloridized Seawater 3	8.0	5.0	0.90±0.05	ND

ND=not detectable volume for IC

Note that the seawater samples were not analysed by the chosen reference method (Ion chromatography, IC) since the volume of the dechloridized plug is not sufficient for the detection using the IC instrument

2.4.5 Conclusions

The practical need for the developed acidification unit was driven by the desire to eliminate the hydroxide interference for nitrite potentiometric sensors. For this purpose, a platform for the in-line pH modulation in natural waters was developed. The custom-built acidification cell allows one to improve the limit of detection of all-solid-state nitrite-selective electrode by more than two orders of magnitude compared to the detection at environmental pH. The cell was miniaturized, thereby allowing for its easy implementation for *in-situ* analysis inside a submersible probe. The resulting pH can be tuned by varying the sample flow rate (residence time in the cell). The applicability of the concept was demonstrated for nitrite analysis in aquarium and dechloridized seawater samples by coupling the acidification unit to a potentiometric flow cell. This concept can be certainly applied to other types of samples and take advantage of the coupling to any other suitable detector.

2.4.6 Acknowledgements

The author acknowledges financial support by the Swiss National Science Foundation (FNS Sinergia CRSII2-147654) and the EU Seventh Framework Program (FP7-OCEAN 2013.2 SCHeMA project - Grant Agreement 614002).

2.4.7 References

(1) Heisler, J.; Glibert, P. M.; Burkholder, J. M.; Anderson, D. M.; Cochlan, W.; Dennison, W. C.; Dortch, Q.; Gobler, C. J.; Heil, C. A.; Humphries, E.; Lewitus, A.; Magnien, R.; Marshall, H. G.; Sellner, K.; Stockwell, D. A.; Stoecker, D. K.; Suddleson, M. *Harmful Algae* **2008**, *8*, 3-13.

(2) Zielinski, O.; Busch, J. A.; Cembella, A. D.; Daly, K. L.; Engelbrektsson, J.; Hannides, A. K.; Schmidt, H. *Ocean. Sci.* **2009**, *5*, 329-349.

(3) Thouron, D.; Vuillemin, R.; Philippon, X.; Lourenco, A.; Provost, C.; Cruzado, A.; Garcon, V. *Anal. Chem.* **2003**, *75*, 2601-2609.

(4) Beaton, A. D.; Cardwell, C. L.; Thomas, R. S.; Sieben, V. J.; Legiret, F.-E.; Waugh, E. M.; Statham, P. J.; Mowlem, M. C.; Morgan, H. *Environ. Sci. Technol.* **2012**, *46*, 9548-9556.

(5) Bakker, E.; Tercier-Waeber, M.-L.; Cherubini, T.; Crespo, G.; Cuartero, M.; Crespi, M. C.; Afshar, M. G.; Jarolimova, Z.; Jeanneret, S.; Mongin, S.; Néel, B.; Pankratova, N.; Touilloux, R.; Xie, X.; Zhai, J. *Chimia* **2014**, *68*, 772-777.

(6) Athavale, R.; Kokorite, I.; Dinkel, C.; Bakker, E.; Wehrli, B.; Crespo, G. A.; Brand, A. *Anal. Chem.* **2015**, *87*, 11990-11997.

(7) Chen, G.; Yuan, D.; Huang, Y.; Zhang, M.; Bergman, M. *Anal. Chim. Acta* **2008**, *620*, 82-88.

(8) Johnson, K. S.; Petty, R. L. *Limnol. Oceanogr.* **1983**, *28*, 1260-1266.

(9) Daniel, A.; Birot, D.; Blain, S.; Treguer, P.; Leielde, B.; Menut, E. *Mar. Chem.* **1995**, *51*, 67-77.

(10) Antonisse, M. M. G.; Reinhoudt, D. N. *Electroanalysis* **1999**, *11*, 1035-1048.

(11) Bakker, E.; Bühlmann, P.; Pretsch, E. *Chem. Rev.* **1997**, *97*, 3083-3132.

(12) Bakker, E.; Pretsch, E. *Angew. Chem.* **2007**, *46*, 5660-5668.

(13) Muller, B.; Buis, K.; Stierli, R.; Wehrli, B. *Limnol. Oceanogr.* **1998**, *43*, 1728-1733.

(14) Cuartero, M.; Crespo, G. A.; Bakker, E. *Anal. Chem.* **2015**, *87*, 8084-8089.

(15) Crespo, G. A.; Macho, S.; Rius, F. X. *Anal. Chem.* **2008**, *80*, 1316-22.

(16) Yuan, D.; Anthis, A. H. C.; Ghahraman Afshar, M.; Pankratova, N.; Cuartero, M.; Crespo, G. A.; Bakker, E. *Anal. Chem.* **2015**, *87*, 8640-8645.

(17) Pankratova, N.; Ghahraman Afshar, M.; Yuan, D.; Crespo, G. A.; Bakker, E. *ACS Sens.* **2016**, *1*, 48-54.

(18) Howard, A. G.; Yeh, C. Y. *Anal. Chem.* **1998**, *70*, 4868-4872.

(19) Martin, G. B.; Meyerhoff, M. E. *Anal. Chim. Acta* **1986**, *186*, 71-80.

(20) Grygolowicz-Pawlak, E.; Crespo, G. A.; Afshar, M. G.; Mistlberger, G.; Bakker, E. *Anal. Chem.* **2013**, *85*, 6208-6212.

(21) Ogawara, S.; Carey, J. L.; Zou, X. U.; Buhlmann, P. *ACS Sens.* **2016**, *1*, 95-101.

(22) Ghahraman Afshar, M.; Crespo, G. A.; Bakker, E. *Biosens. Bioelectron.* **2014**, *61*, 64-69.

(23) Jonca, J.; Giraud, W.; Barus, C.; Comtat, M.; Striebig, N.; Thouron, D.; Garcon, V. *Electrochim. Acta* **2013**, *88*, 165-169.

(24) Patey, M. D.; Rijkenberg, M. J. A.; Statham, P. J.; Stinchcombe, M. C.; Achterberg, E. P.; Mowlem, M. *Trends Anal. Chem.* **2008**, *27*, 169-182.

(25) Bakker, E. *Anal. Chem.* **1997**, *69*, 1061-1069.

2.5 Fluorinated Tripodal Receptors for Potentiometric Chloride Detection in Biological Fluids

The work described below has accepted to publication and released online and will be soon published in: Pankratova, N.; Cuartero, M.; Jowett, L. A.; Howe, E. N.; Gale, P. A.; Bakker, E.; Crespo, G. A. Fluorinated Tripodal Receptors for Potentiometric Chloride Detection in Biological Fluids. *Biosens. Bioelectron.* **2018**, *99*, 70-76.

The initial intention of this work has been the search for new phophate receptors with increased sensitivity and selectivity, for potentiometric phosphate detection. The potentiometric response of PVC-based membranes doped with urea and thiourea-based fluorinated tripodal receptors described below, as well as with diindole and urea-based diindoles (results not reported here), towards various inorganic anions, has been investigated. None of the compounds explored have been proved to be practically applicable for phosphate detection in environmental samples, due insufficient detection limits and poor selectivity. However, few of the fluorinated tripodal receptors turned out to exhibit good selectivity towards chloride and have been shown to demonstrate adequate performance and sufficient higher detection limits for chloride detection in biological samples. The results of relevant studies are described below.

2.5.1 Abstract

Fluorinated tripodal compounds were recently reported to be efficient transmembrane transporters for a series of inorganic anions. In particular, this class of receptors has been shown to be suitable for the effective complexation of chloride, nitrate, bicarbonate and sulfate anions via hydrogen bonding. The potentiometric properties of urea and thiourea-based fluorinated tripodal receptors are explored here for the first time, in light of the need for reliable sensors for chloride monitoring in undiluted biological fluids. The ion-selective electrode (ISE) membranes with tren-based tris-urea bis(CF_3) tripodal compound (ionophore I) were found to exhibit the best selectivity for chloride over major lipophilic anions such as salicylate ($\log K^{pot}_{Cl^-/Sal^-} = +1.0$) and thiocyanate ($\log K^{pot}_{Cl^-/SCN^-} = +0.1$). Ionophore I-based ISEs were successfully applied for chloride determination in undiluted human serum as well as artificial serum sample, the slope of the linear calibration at the relevant background of interfering ions being close to Nernstian (49.8±1.7 mV). The results of potentiometric measurements were confirmed by argentometric titration. Moreover, the

ionophore I-based ISE membrane was shown to exhibit a very good long-term stability of potentiometric performance over the period of 10 weeks. Nuclear magnetic resonance (NMR) titrations, potentiometric sandwich membrane experiments and density functional theory (DFT) computational studies were performed to determine the binding constants and suggest 1:1 complexation stoichiometry for the ionophore I with chloride as well as salicylate.

2.5.2 Introduction

Chloride is one of the most critical targets in biological fluids as its concentration, along with that of some other ions such as sodium, potassium, calcium, magnesium and lithium, is used for rapid patient care decisions.[1] Accordingly, approaches to monitor these critical care species require development of sensors and devices for real-time monitoring with very high precision and accuracy.

Few methodologies are used in clinical laboratories for chloride determination, such as for example colorimetric, coulometric-amperometric and potentiometric procedures for serum analysis.[2,3] Undeniably, potentiometric sensors offer one of the most convenient non-destructive way of determining ionic species due to their low cost, simple fabrication and miniaturization and low-energy consumption.[4,5]

There exist two main types of anion-selective membranes for the potentiometric detection with ion-selective electrodes (ISEs). The first type, historically the most explored one, is the ISE membrane based on crystalline materials such as the AgCl-based solid-state electrode. However, the latter is not suitable for the analysis of biological samples since it suffers from protein adsorption to the AgCl surface.[6,7] The second type of membranes is based on polymeric matrices doped with ionophore and/or ion-exchanger. The ISEs based on polymeric membranes have recently become an attractive tool for the direct monitoring of chloride in clinical analysis[3,8-10], however only few of the receptors reported so far possess adequate performance for practical application owing to challenges arising when analysing biological fluids.

There are several issues in the development of the receptors adequate for the analysis of biological samples: i) leaching of active membrane components; ii) low biocompatibility of the membrane material with the sample and adsorption of proteins; iii) low selectivity of most receptors over interfering lipophilic anions such as salicylate, thiocyanate and bicarbonate commonly present in biological fluids.[7]

Certainly, salicylate is often the main interfering ion due to its lipophilicity, relatively high concentration and variable content in biological samples. For this reason, the determination of chloride in serum using ISEs often provides biased results owing to increased levels of salicylate in the samples from the patients who take aspirin.[9] Another challenge in potentiometric chloride detection concerns the upper detection limit of the ISEs since the high chloride concentration in clinical samples (ca. 100 mM in blood and serum) often causes strong complexation in the sensing phase, resulting in Donnan exclusion failure.[11]

While most chloride-selective ionophores reported in the past are organometallic compounds, some active membrane components reported recently are based on chloride complexation by hydrogen bonds.[12-14] Commonly used chloride-selective receptors with a metal center such as mercury, manganese or indium[11,15-17] often exhibit stability and/or toxicity issues.[13]

It is noted that most proposed receptors, both neutral and charged carriers, do not provide better selectivity and stability of chloride detection for clinical applications than traditional ion-exchanger based membrane (tridodecylmethylammonium chloride [TDMACl]).[7] Consequently, the selectivity pattern of ISEs based on lipophilic quaternary ammonium salts (such as TDMACl) is fixed and follows the Hofmeister series since the selectivity of ion-exchanger is mainly defined by the lipophilicity of the ion. The application of this type of chloride ISE is therefore limited to samples without significant concentrations of anions more lipophilic than chloride, and it would not be recommended for samples that contain salicylate or thiocyanate as in case of blood or serum samples. Nevertheless, ISEs based on quaternary ammonium salts as active membrane component are still used commercially for chloride determination in biological samples despite the aforementioned limitations, owing to the lack of selective chloride receptors.[10] To the best of our knowledge, only few studies published in the last two decades have reported on receptors with sufficiently improved potentiometric characteristics, close to those required for chloride detection in biological samples.[12-14,18] However, even fewer studies demonstrated successful application of the investigated compounds for potentiometric chloride detection in undiluted non-spiked physiological samples.[13] Thus, further efforts are required to develop chloride-selective ISEs with better selectivity, and adequate analytical performance and compatibility with biological fluids.

The tren-based fluorinated tripodal compounds were recently shown to be efficient transmembrane transporters for chloride, nitrate, bicarbonate and sulfate anions in 1-palmitoyl-2-oleoyl-*sn*-glycero-3-phosphocholine (POPC) liposomal based assays.[19,20] It

was demonstrated that fluorinated transporters are more active anion transporters than their non-fluorinated analogs.[20] To the best of our knowledge, the potentiometric properties of fluorinated tripodal compounds have not been reported in the past. This work therefore aims to examine a series of fluorinated tripodal compounds, both tris-ureas and tris-thioureas,[19] as potential candidates for chloride analysis in biological samples.

2.5.3 Experimental

2.5.3.1 Reagents, Material and Equipment

Dodecyl 2-nitrophenyl ether (DNPE), tridodecylmethylammonium chloride (TDMACl), high molecular weight poly(vinyl chloride) (PVC), tetrahydrofuran (THF), sodium chloride, sodium bicarbonate, sodium salicylate, sodium nitrate, sodium nitrite, sodium fluoride, sodium acetate trihydrate, sodium citrate, sodium bromide, potassium dihydrogen phosphate, sodium thiocyanate, sodium iodide, sodium perchlorate, potassium sulfate, magnesium chloride hexahydrate, sodium hydroxide standard solution 2 M, hydrochloric acid standard solution 1 M, tris(hydroxymethyl)aminomethane (Tris), 2-morpholinoethanesulfonic acid (MES), 4-(2-hydroxyethyl)piperazine-1-ethanesulfonic acid (HEPES) and D-(+)-glucose were purchased from Sigma−Aldrich. Urea Molecular biology grade was purchased from PanReac AppliChem. Tetrabutylammonium salicylate was derivatized from salicylic acid and tetrabutylammonium hydroxide. Tetrabutylammonium chloride, tetrabutylammonium hydroxide (in methanol, 1 M) and salicylic acid were purchased from Sigma Aldrich. DMSO-d_6 was purchased from Cambridge Isotope Laboratories. Aqueous solutions were prepared by dissolving the appropriate salts in Milli-Q water (18.2 MΩ·cm).

Ionophores I, II, III and IV were synthesized according to Busschaert et al. procedure.[19]

The artificial serum sample consisted of 111 mM NaCl, 29 mM $NaHCO_3$, 2.2 mM K_2HPO_4, 0.8 mM $MgCl_2{\cdot}6H_2O$, 2.5 mM urea and 4.7 mM glucose. [21] The human serum samples were provided by Hôpitaux Universitaires de Genève (HUG).

A commercial pH meter equipped with a pH glass electrode (827 pH lab), and a double-junction Ag| AgCl | 3 M KCl |1 M LiOAc reference electrode were purchased from Metrohm AG (Model 6.0726.100). Potentiometric measurements–at zero current conditions–were performed using high impedance input 16-channel EMF monitor (Lawson Laboratories, Inc., Malvern, PA).

2.5.3.2 Electrodes and Membrane Preparation

The membrane-based electrodes for potentiometric experiments were prepared according to well-established procedure.[22,23] The amounts of synthesized receptors I-IV (see Figure 2.5.1 for structures) taken for the preparation of ca. 200 mg of corresponding PVC-based membranes were as follows: 2.7 mg (15 mmol per kg of membrane) or 3.7 mg (20 mmol kg^{-1}) of ionophore I, 2.3 mg (15 mmol kg^{-1}) of ionophore II, 2.9 mg (15 mmol kg^{-1}) of ionophore III and 2.5 mg (15 mmol kg^{-1}) of ionophore IV. The above-indicated amount of the corresponding ionophore was mixed with 0.6 mg of ion-exchanger TDMACl (5 mmol kg^{-1}), 66 mg of poly(vinyl chloride) (PVC) and 132 mg of dodecyl 2-nitrophenyl ether (DNPE) (PVC:DNPE [1:2]) and dissolved in 2 mL of tetrahydrofuran (THF). A blank membrane (in absence of ionophore) contained 5 mmol $kg^{-1}$of TDMACl, 66 mg of PVC and 132 mg of DNPE. The prepared cocktail was poured into a glass ring (22 mm in diameter), placed on a glass slide and dried overnight at room temperature under a dust-free environment. After complete THF evaporation, a membrane of approximately 200 µm thickness was obtained. Small disks (diameter ca. 8 mm) were punched from the cast films. The obtained membranes were conditioned for two days in 1 mM KH_2PO_4 (pH~5) for selectivity screening and in 100 mM NaCl (pH~5.5) for all other experiments. After that, the membranes were mounted in Ostec electrode bodies that contain inner silver-silver chloride elements (Oesch Sensor Technology, Sargans, Switzerland). The inner compartment of the electrode was always filled with a solution containing 1 mM NaCl. The electrodes for human serum analysis were typically pre-conditioned for 1-2 days in 100 mM NaCl; long-term conditioning (for the stability experiment during 10 weeks) was performed in 1 mM NaCl in order to avoid super-Nernstian slopes.

2.5.3.3 Reference method for chloride detection

Argentometric titration with silver nitrate solution (0.1 M) and potassium chromate as indicator (so-called Mohr's method) was selected as the reference method for the determination of chloride in the human serum sample.

Preliminary deproteinization was accomplished to facilitate the endpoint visualization using acetonitrile-NaOH treatment.[24] The restrictions regarding the acceptable protein concentration for accurate direct titration of biological fluids using chromate as indicator were emphasized in the past[25] and account for the interaction between the protein and the indicator. The acetonitrile-NaOH treatment[24] consisted of adding 200 µL of NaOH

(2 mol L^{-1}) and 600 µL of deionized water to 2 mL of the serum sample and shaking it for few seconds, then adding 4 mL of acetonitrile and vortex mixing of the obtained solution for one minute using IKA Vortex Genius 3 (IKA Werke, Staufen, Germany). The resulting mixture was centrifuged for 10 min at 755×g using a Hettich Universal D-7200 (Tuttlingen, Germany). The obtained supernatant solution exhibited much less yellow coloration than the initial human serum sample suggesting in principle a significant degree of deproteinization that remarkably facilitated the visualization of the endpoint. However, the obtained degree of deproteinization was not sufficient for the application of other analytical techniques such as ion chromatography. The supernatant solution was acidified with sulfuric acid prior to titration to obtain the pH~7 which is in the range required for Mohr's method.

The ^{1}H NMR titration binding studies DFT computational studies were carried out by Laura A. Jowett, Ethan N.W. Howe and Philip A. Gale at the School of Chemistry (F11), The University of Sydney, NSW 2006, Australia. The detailed description is given in Appendix 4.

2.5.4 Results and Discussion

In this work, four different fluorinated tripodal receptors were examined as potential anion ionophores. Figure 2.5.1 presents the chemical structures of these receptors (named as ionophores I, II, III and IV) and the density functional theory based structures of 1:1 complexes formed by ionophore I with anions such as chloride and salicylate.

In a first screening, the potential response of plasticized ionophore-based membranes (15 mmol kg^{-1} ionophore) together with the blank membrane (no ionophore) towards 1 mM concentration of common inorganic anions (chloride, salicylate (Sal^{-}), bicarbonate, thiocyanate, bromide, sulfate, acetate (AcO^{-}), dihydrogen phosphate, nitrate, nitrite, fluoride, citrate ($Citr^{3-}$), perchlorate, and iodide) was evaluated. Figure 2.5.2a shows the normalized electromotive force values in 1 mM solutions of different anions (EMF'_{A}^{-}) calculated by subtracting the readout potential value in 1mM chloride solution (EMF_{Cl}^{-}) from the EMF measured in the solution of the corresponding anion (EMF_{A}^{-}) as follows: $EMF'_{A}^{-} = EMF_{A}^{-} - EMF_{Cl}^{-}$.

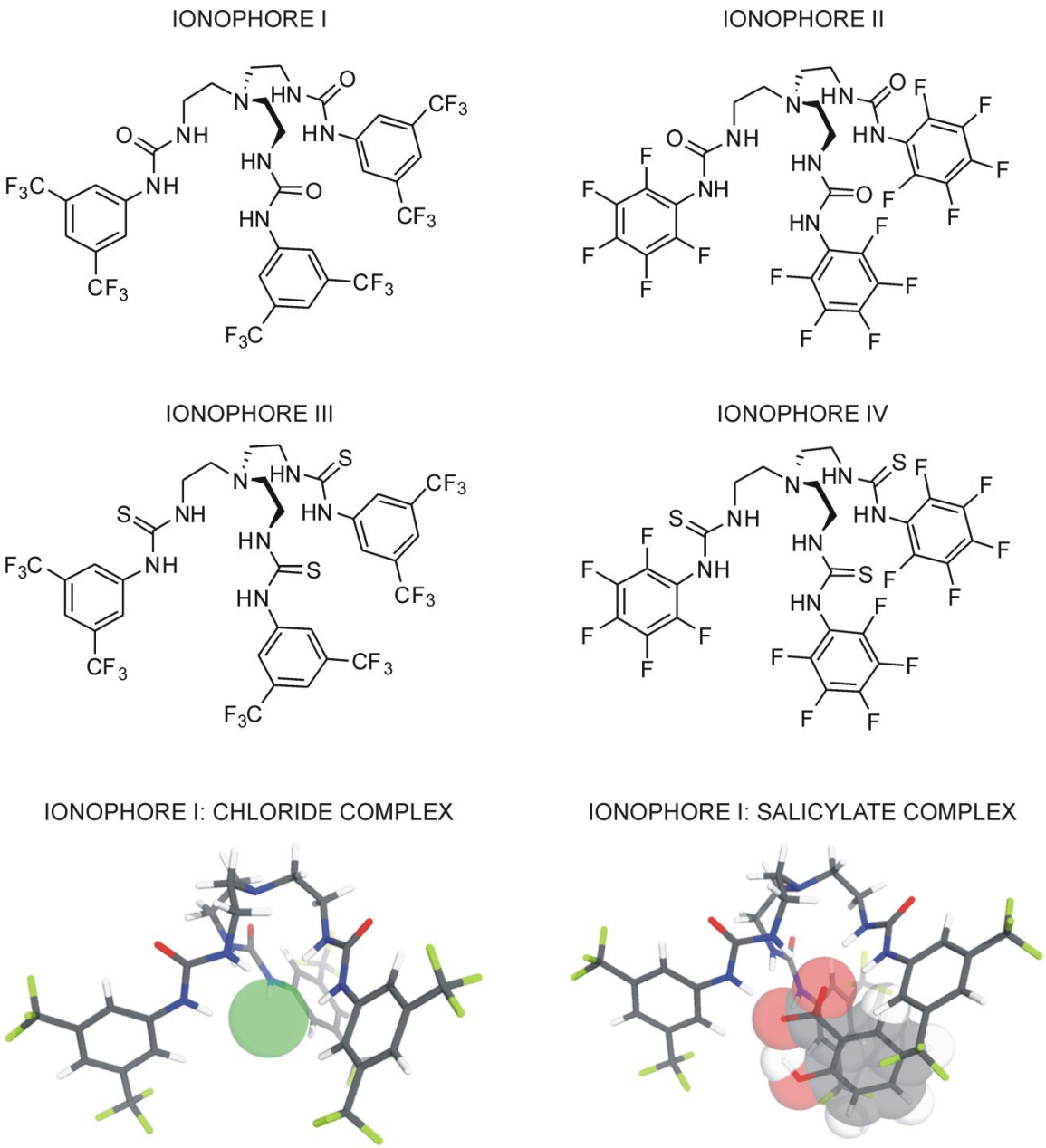

Figure 2.5.1. (Top) Structures of the ionophores I-IV: (I) Tren tris-urea bis(CF_3) [$C_{33}H_{27}F_{18}N_7O_3$]; (II) Tren tris-urea pentafluoro [$C_{27}H_{18}F_{15}N_7O_3$]; (III) Tren tris-thiourea bis(CF_3) [$C_{33}H_{27}F_{18}N_7S_3$]; (IV) Tren tris-thiourea pentafluoro [$C_{27}H_{18}F_{15}N_7S_3$]. (Bottom) DFT (M06-2X/6-31+G(d)) optimized structures of the chloride and salicylate complexes of ionophore I without counter cation in vacuum; C (gray), H (white), N (blue), O (red), F (yellow-green), Cl (green).

From the EMF' values presented in Figure 2.5.2a, the selectivity coefficients for chloride over other anions were estimated by applying the separate solutions method and schematically illustrated in Figure 2.5.2b.[26] Positive values in Figure 2.5.2a indicate a less interfering effect than chloride (i.e., for the blank membrane, EMF_F^- is +43 mV) whereas a positive value in selectivity coefficient plots means the opposite (i.e., for the blank membrane, the selectivity coefficient for chloride over perchlorate is +5.5 indicating that perchlorate is ~300.000 times more interfering over chloride at the same concentration).

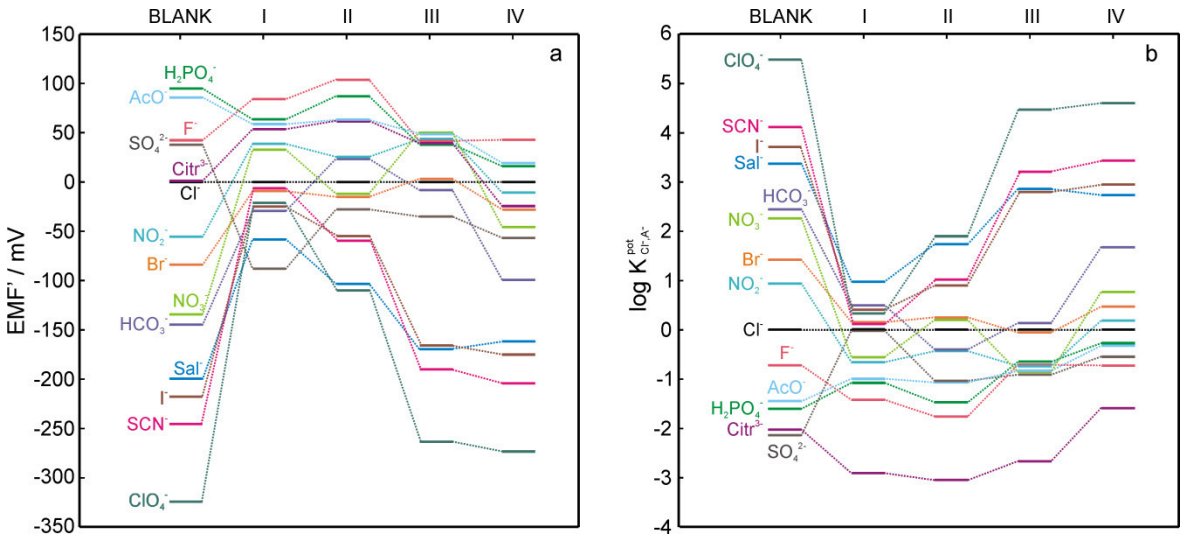

Figure 2.5.2. Selectivity screening of ISEs based on the ionophores I-IV and a blank membrane (same composition but no ionophore). (a) Potential observed in 1 mM solution of corresponding sodium/potassium salt (EMF' is the potential corrected to EMF in 1 mM NaCl). (b) Potentiometric selectivity coefficients for chloride over different anions (A^-) at 1 mM concentration. Sal^-, AcO^- and $Citr^{3-}$ stand for salicylate, acetate and citrate anions respectively.

While the blank membrane behavior follows the typical Hofmeister selectivity pattern (ClO_4^->I^->NO_3^->Br^->Cl^->F^->$H_2PO_4^-$>SO_4^{2-}), the ionophores I-IV exhibit, in general, a suppressed selectivity for chloride over sulfate ($\log K^{pot}_{Cl^-/SO_4^{2-}}$ from -1 to 0 *vs* $\log K^{pot}_{Cl^-/SO_4^{2-}} = -2.1$ for the blank membrane) and to a lesser extent over phosphate and acetate ($\log K^{pot}_{Cl^-/H_2PO_4^-}$ and $\log K^{pot}_{Cl^-/AcO^-}$ both from -1.1 to -0.3 *vs* $\log K^{pot}_{Cl^-/H_2PO_4^-} = -1.6$ and $\log K^{pot}_{Cl^-/AcO^-} = -1.5$ for the blank membrane). In contrast, the selectivity for chloride over the majority of other inorganic anions increases remarkably, including highly lipophilic anions such as perchlorate, thiocyanate, salicylate, bicarbonate and nitrate. The significantly improved selectivity for chloride over most lipophilic anions in comparison to the blank membrane is especially pronounced for ionophore I. For example, the values of $\log K^{pot}_{Cl^-/ClO_4^-}$, $\log K^{pot}_{Cl^-/SCN^-}$, $\log K^{pot}_{Cl^-/Sal^-}$, $\log K^{pot}_{Cl^-/HCO_3^-}$ decrease from +5.5 to +0.4, from +4.1 to +0.1, from +3.4 to +1.0 and from +2.4 to +0.5, respectively.

Accordingly, it has been demonstrated (see Figure 2.5.2) that ionophore I may be plausible for the detection of chloride in the presence of lipophilic anions, which is in fact highly desirable for the analysis of biological fluids since some of the anions mentioned, such as salicylate, thiocyanate and bicarbonate, are often present at significant concentrations and may therefore interfere with chloride determination. The concentration ranges for major anions in human serum are listed in Table 2.5.1. For instance, the concentration of salicylate is relatively high and variable, from a few μM to the millimolar level[27-30], which

makes it extremely difficult to calibrate the sensor by adjusting the background concentration of standard solutions as it would require additional knowledge of salicylate concentration in every particular sample prior to chloride analysis. Hence, to enable chloride determination it is essential to provide a receptor with a suppressed response towards salicylate.

Table 2.5.1. Reference range values of major anions present in human serum for healthy people

Anion (A^-)	Concentration, mM
Chloride	98-107 [28]
Bicarbonate	22-29 [28]
Salicylate [1]	0.5 [29]; 0.2-0.7 [30]; 1.09-2.17 [28]
Phosphate	0.87-1.45; 1.45-1.78 [2] [28]
Sulfate	0.2-0.5 [31]
Thiocyanate	0.017-0.069; 0.052-0.206 [3] [28]

[1] therapeutic level; [2] for children; [3] for smokers

In this context, a more careful study of ionophore I selectivity for chloride over salicylate was performed by recording a complete set of calibrations for chloride and salicylate anions. As observed in Figure 2.5.3, ionophore I exhibits the best selectivity for chloride over salicylate compared to ionophores II, III and IV. The selectivity coefficients calculated from the full calibration curves are similar to those obtained in the preliminary screening (see Figure 2.5.2b). The $\log K^{pot}_{Cl^-/Sal^-}$ equals to +3.7 for the blank membrane and +1.0, +1.9, +3.0 and +3.1 for ionophores I, II, III and IV respectively, suggesting that ionophore I may so far be the most promising candidate for chloride detection. Note that a value of +1.0 indicates that the same ISE, in two different solutions containing the same concentration level of either Cl^- or Sal^-, gives a larger response for Sal^- compared to Cl^- (by approximately –60 mV). As chloride in serum samples is at least 100-fold more concentrated than salicylate (see Table 2.5.1), chloride detection using ISEs based on ionophore I should be possible.

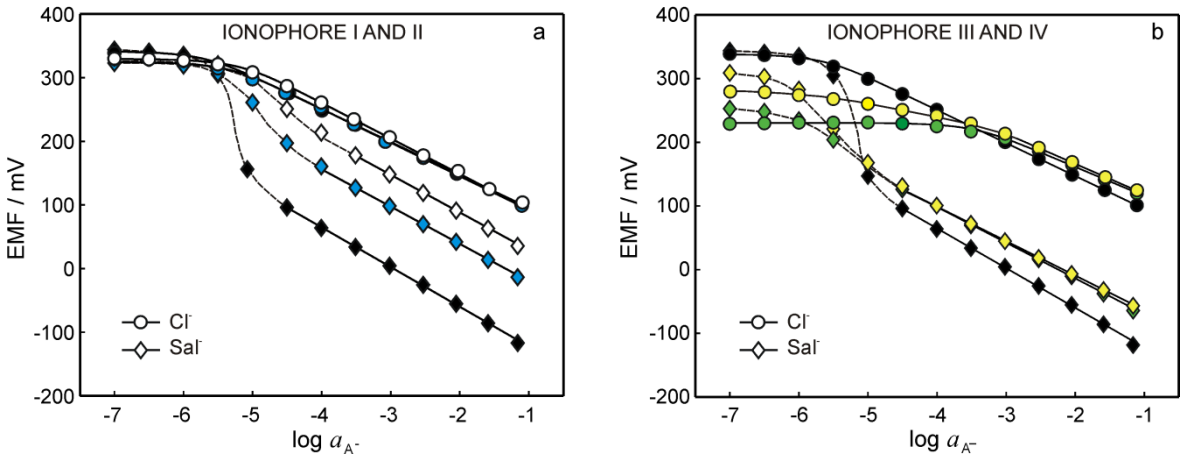

Figure 2.5.3. Calibration curves for chloride (circles) and salicylate (diamonds) for ISEs based on different receptors. (a) Ionophore I (white), ionophore II (blue), blank membrane (black), (b) ionophore III (yellow), ionophore IV (green), blank membrane (black).

The results of molecular modelling using density functional theory (DFT) calculations (M06-2X/6-31+G(d)) (Zhao et al., 2008) for the chloride and salicylate complexes with ionophore I demonstrated the optimized 1:1 host:guest geometry. The structures of the corresponding complexes obtained from the DFT calculation are presented in Figure 2.5.1. The 1:1 complexation stoichiometry is consistent with previously reported crystal structures of receptors I, III and IV with various anions (chloride, sulfate, nitrate and carbonate) [19]. The NMR titration data with TBA-chloride (in DMSO-d_6/0.5% H_2O mixture) fit best to the additive 1:2 binding model (see Appendix 4, Figures A4.1-8), thenceforth deriving the stepwise association constants (K_1 and K_2) [32]. The derived association constants of binding to chloride for receptors I-IV ($\log K_1$ & $\log K_2$) are 4.1 & 0.8, 3.4 & 0.9, 4.3 & 0.9, and 3.5 & 1.0 respectively, the weak K_2 for all receptors indicating that the formation of 1:2 host:guest complex at the working concentration of the sensor is negligible. Generally, the thiourea analogues bind chloride stronger than the urea equivalents (receptors I c.f. III and II c.f. IV) due to the more acidic NH hydrogen bond donors of thiourea.[33] Interestingly, a remarkable difference was found for bis(CF_3) and pentafluoro functionalities which resulted in significantly larger association constants for the bis(CF_3) substituent for both urea and thiourea analogues.

The derived association constants ($\log K_a$) from fitting the NMR titration data with TBA-salicylate to the 1:1 binding model for salicylate complexation for receptors I-IV were found to be 1.8, 1.4, 1.9 and 1.7 respectively. While following the same trend as observed for chloride complexation (receptor III > I > IV > II), these values are lower than those calculated above for chloride. In addition, NMR titration studies with TBA-perchlorate indicate no binding (see Appendix 4, Figures A4.9-12). The logarithmic binding constants

estimated from selectivity coefficients[34] for the receptors I, II, III and IV were found to be respectively 5.8, 4.3, 1.7 and 1.6 for chloride complex and 3.4, 2.7, 1.2 and 1.0 for salicylate complex, assuming no substantial binding of the ionophores with the perchlorate ion confirmed by the "sandwich membrane experiment" [35] (see Appendix 4 for calculation details). Therefore, similarly to NMR-based binding constants, the complex formation constants obtained by potentiometry suggest stronger binding of the receptors with salicylate. However, significant discrepancy between the absolute values is observed and the trend is different in comparison with NMR-studies (potentiometry-based trend: receptor I > II > III > IV). The latter accounts for the difference in hydration energy of the anions[36] along with the difference in organic solvent environments employed in two independent studies (from DMSO-d_6 to plasticized PVC media).

Having determined that ionophore I is the most selective one for chloride over salicylate, the composition of ionophore I-based anion-selective membrane was optimized and a membrane containing 20 mmol kg^{-1} of ionophore I and 5 mmol kg^{-1} of ion-exchanger (to give a higher slope at high concentrations of chloride with salicylate background) was chosen for further experiments.

To evaluate the suitability of the ionophore I for chloride detection in biological fluids, calibrations of the relevant ISE were performed in solution with salicylate background. The choice of the salicylate background concentration was determined by the salicylate levels in human serum which relies heavily on the diet and drug consumption since salicylic acid is a common component of anti-inflammatory drugs. A typical range of few μM or lower has been reported for serum samples of the patients not taking aspirin[27] while the values reported for the patients taking drugs containing salicylic acid vary significantly for different studies (see Table 2.5.1). Normal therapeutic salicylate level for analgesic purpose is found to be about 0.2-0.7 mM.[30] However, in severe cases of salicylate poisoning salicylate serum levels may reach the concentration of several mM; the salicylate levels higher than 2 mM lead to salicylate poisoning and require appropriate treatment[27,30,37-39] Considering the aforesaid, the calibration curves for chloride analyte (Figure 2.5.4a) were recorded at two salicylate levels: 0.5 mM (normal therapeutic level of patients taking aspirin)[30] and 2 mM (highest limit of asymptomatic patients or patients with mild salicylate poisoning) [40].

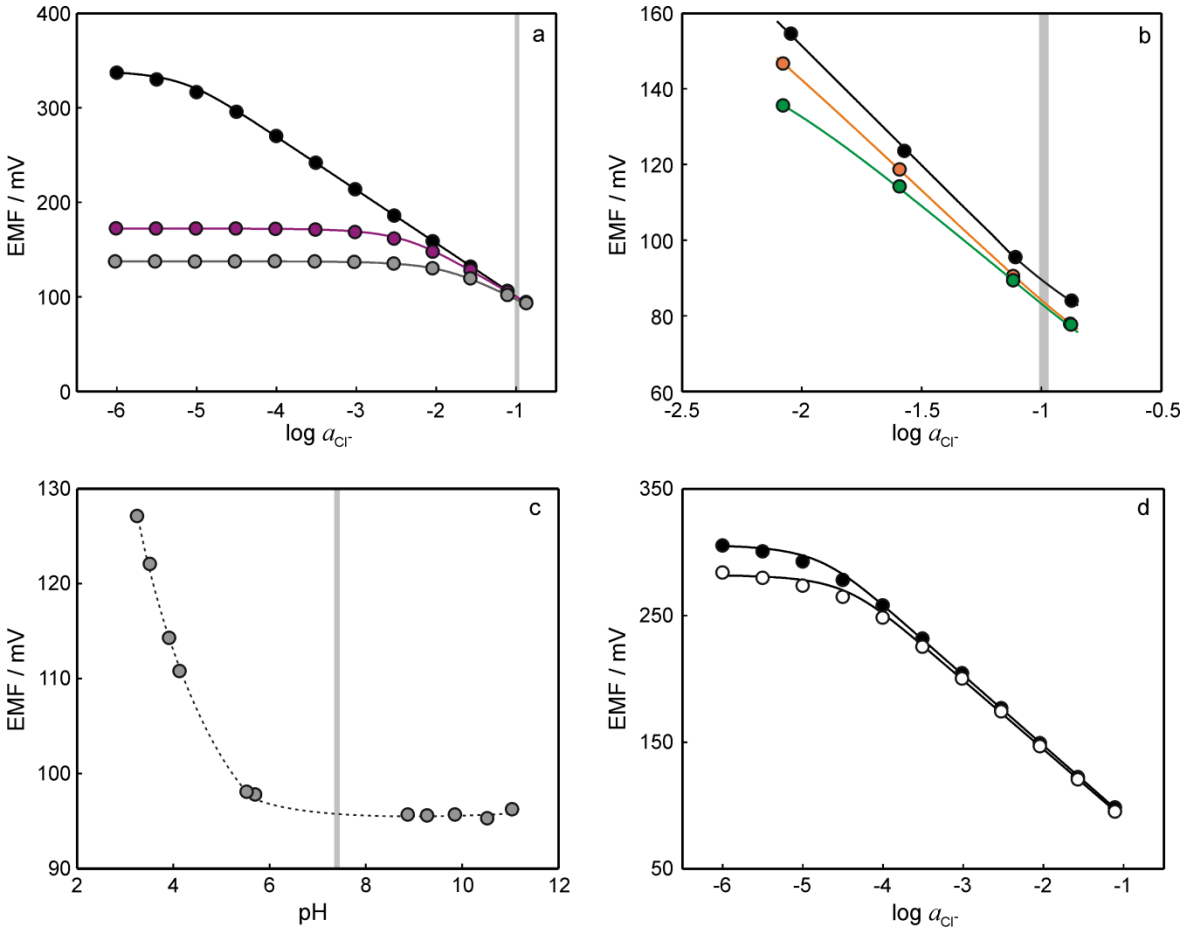

Figure 2.5.4. Influence of the background and pH on the performance of the ISE based on ionophore I. (a) Calibration curves for chloride with different salicylate backgrounds: no salicylate (black), 0.5 mM NaSal (purple) and 2 mM NaSal (gray). (b) Calibration curves for chloride with different backgrounds: no background (black), 30 mM $NaHCO_3$ acidified to pH 7.6 (orange), 30 mM $NaHCO_3$ and 0.5 mM NaSal acidified to pH 7.5 (green). (c) Potential changes upon addition of sodium hydroxide to the solution of NaCl 100 mM acidified with HCl. Dashed line is shown to guide the eye. (d) Calibration curves in water at pH 5.5 (black) and 10 (white). The grey window in the figures indicates the reference chloride range in human serum for healthy people.

As expected, the calibration curve without background electrolyte results in a Nernstian slope of 57.3±1.8 mV (n=12) with a lower detection limit (LDL) of ~10 μM. Deterioration of the electrode performance is observed both at 0.5 mM and 2 mM salicylate background resulting in slopes of 46.7±1.8 mV and 35.8±4.3 mV (n=12 and 6 respectively) accompanied with an increment of the lower detection limits up to 3 and 10 mM respectively, yet satisfactory for the measurement of chloride in the required range (approx. 100 mM).

Due to the fact that pH of blood and serum normally ranges from 7.35 to 7.45[28], it was important to characterize the influence of pH on the performance of the electrode. Figure 2.5.4c illustrates the potential changes (EMF) of the ionophore I-based ISE upon increasing the pH by successive additions of 2 M NaOH to NaCl solution preliminary

acidified with HCl to pH~3.3 (total chloride concentration 100 mM). A well-defined plateau (96.3±1.3 mV) is observed above pH~5.5 until pH~11.5 (higher pH values were not accomplished within the experiment) meaning that the performance of the ISE is nearly pH-independent in the given pH range at 100 mM chloride concentration. The EMF increase below pH~5.5 might possibly account for protonation of the tertiary amine of the tren motif resulting in the decrease of ionophore I partitioning within the PVC-based membrane. Interestingly, this observation correlates with the transmembrane anion transport activity of tren-based receptors, which were completely inactive in POPC liposomes at acidic pH.[41] To confirm the applicability of the membrane at higher pH values, the calibration in water at pH 5.5 was compared to the calibration curve obtained at increased pH (Figure 2.5.4d). A pH of 10 was chosen, as it was difficult to achieve a constant pH of 7.4 without buffering the sample. It must be noted that the experiments described here were performed in non-buffered aqueous solutions (unless specified, in the case of bicarbonate as background electrolyte). This is due to the fact that the presence of organic buffers (calibrations in Tris, MES and HEPES were performed, results not shown) significantly deteriorates the electrode performance (lower limit of detection and the slope of the calibration curve). The latter has been already reported in the past for different types of chloride sensors[7,12] based on ionophores with hydrogen bond donor groups and accounts for the complexation between the highly lipophilic buffer anions and the receptor.[12] By comparing both calibration curves, it can be seen that the increase of pH from 5.5 to 10 deteriorates the lower detection limit of the electrode only to a very modest extent ($\log a_{LDL}$ = -4.8 and -4.5 respectively), and more importantly, it does not influence the electrode performance in the concentration range required for the analysis of undiluted biological fluids.

As it follows from the selectivity coefficients presented in Figure 2.5.2 and the reference range values given in Table 2.5.1, apart from the salicylate interference, the bicarbonate interference should also be considered for the analysis of serum samples. Therefore, a calibration at 30 mM bicarbonate background was performed, along with the calibration in the solution containing both 0.5 mM salicylate and 30 mM bicarbonate (Figure 2.5.4b). The initial chloride concentration for the calibration with bicarbonate background was much higher than in Figure 2.5.4a (ca. 10 mM chloride) due to the necessity to acidify the bicarbonate solution to pH ca. 7.5 which was accomplished by spiking with hydrochloric acid. The latter was performed to achieve the required pH without introducing extraneous anions (such as sulfate etc.) that might deteriorate the electrode response. Importantly, as

can be observed in Figure 2.5.4b, the presence of bicarbonate in the solution does affect the electrode performance resulting in the slope 51.9±2.4 mV (n=6) and a shift of the intercept (E°) of ca. 7 mV. The addition of 0.5 mM salicylate to the bicarbonate at pH 7.5 affects the performance only to a small extent resulting in the slope of 49.8±1.7 mV (n=12). Thus, a very small difference in the electrode performance is observed with bicarbonate background only and the bicarbonate with the additional amount of 0.5 mM salicylate suggesting the adequacy of analysing the samples both with no salicylate and therapeutic level of salicylate using the same external calibration.

Hereafter, the chloride detection in human serum sample was accomplished using external calibration in the solution containing 0.5 mM salicylate and 30 mM sodium bicarbonate (Figure 2.5.5). For simplicity, the calibration curve in Figure 2.5.5b is shown in concentration scale (instead of activity) where the slope corresponds to 46.7±1.6 mV in log*c*-scale (n=12). The method was first validated by analysing the artificial serum sample containing 112.6 mM chloride level. An acceptable recovery of 98.8±4.3% was accomplished resulting in a chloride concentration of 110.8±4.7 mM (n=7). The potentiometric chloride detection in the human serum sample was performed multiple times at different days, every time with a set of 2 to 4 electrodes, pre-conditioned in the 100 mM NaCl solution for at least 1 day. The chloride concentration was found to be 98.6±3.8 mM (n=10).

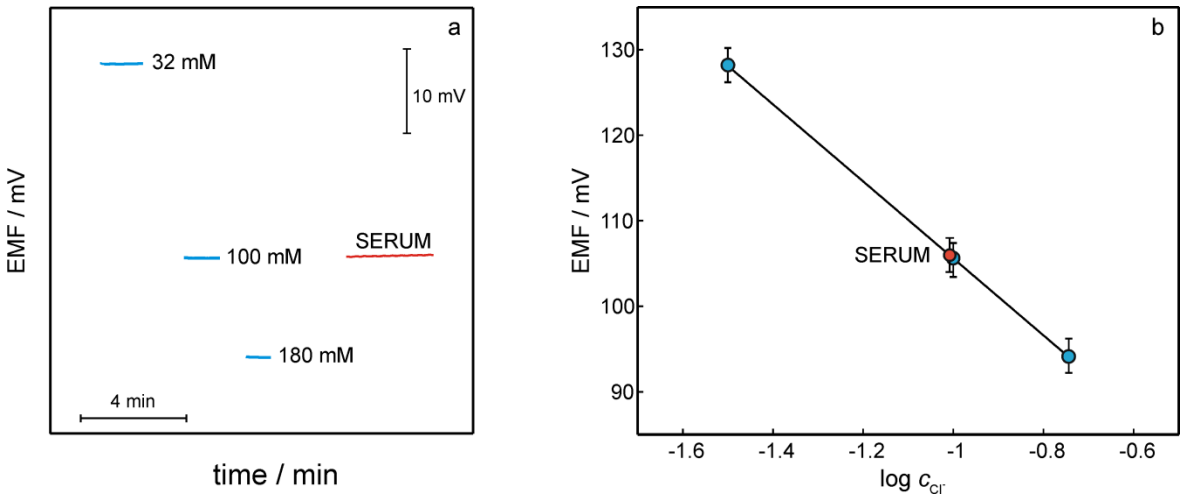

Figure 2.5.5. Chloride detection in human serum sample. (a) Potential readings for three calibration solutions with 0.5 mM salicylate background and the serum sample. Concentration of chloride in the calibration solutions is indicated in the figure. (b) Calibration curve corresponding to the results presented in Figure 2.5.5a.

To confirm the reliability of the potentiometric results, argentometric titration was chosen as a reference method for chloride detection in the sample.[25] The chloride concentration in

the artificial serum sample (112.6 mM chloride) was found to be 111.1±4.0 mM (n=8) whereas the chloride concentration in the human serum sample after deproteinization was found to be 109.3±5.9 mM (n=6). Even though the deproteinization leads to better endpoint visualization, it was observed that the titration endpoint in the real sample even after deproteinization was much less pronounced compared to the artificial sample, thus the slightly elevated (in comparison to potentiometric measurements) value obtained titrimetrically accounts most probably for the difficulties of analysing the colored serum sample with a complex matrix. The results obtained using both potentiometric and volumetric titration methods were compared by applying the F-test at NC=95% and the t-test at NC=99%. The calculated F and t values (F=2.41 and t=3.98) did not exceed the theoretical values (F =6.68; t =4.03), indicating that there are no significant differences in accuracy or precision between the two methods at the considered confidence level.

Finally, the long-term stability of ionophore I-based ion-selective membrane electrode was evaluated over a period of 10 weeks (see Figure 2.5.6). No change in electrode performance within 3 weeks of different experiments (including multiple calibrations and exposure to real serum samples) and a moderate deterioration of the electrode slope over the period of 10 weeks were observed (long-term conditioning was performed in 1 mM NaCl to avoid super-Nerstian slopes). It should be mentioned that such excellent long-term stability is rarely achievable with anion-selective receptors.

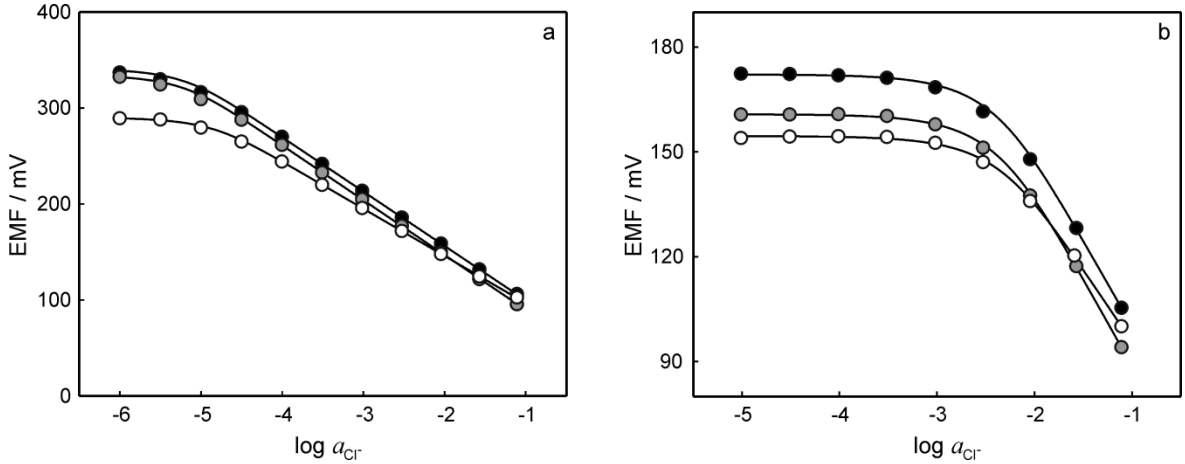

Figure 2.5.6. Stability of performance of the ISE based on Ionophore I. Calibration curves of ISE based on Ionophore I for chloride 1 week (black), 3.5 weeks (gray) and 10 weeks (white) after the first immersion of the membrane in the solution. (a) Calibration curves in water. (b) Calibration curves with 0.5 mM salicylate background.

2.5.5 Conclusions

The investigation of potentiometric properties of ion-selective electrodes (ISEs) based on fluorinated tren-based tripodal compounds, previously reported as efficient transmembrane transporters for chloride, nitrate, bicarbonate and sulfate anions facilitated by hydrogen bonding complexation, showed this new class of receptors to be promising for potentiometric anion sensing. ISEs based on tren-based tris-urea bis(CF_3) tripodal compound (ionophore I) were found to exhibit significantly improved selectivity for chloride over major lipophilic anions (such as salicylate, thiocyanate, bicarbonate and nitrate) compared to the blank ISE (without ionophore) as well as to the majority of chloride-selective receptors reported so far. The results of DFT computational studies showed the binding geometry of ionophore I complex with chloride as well as with the main interfering anion salicylate to exhibit 1:1 stoichiometry. Sufficient selectivity over salicylate and bicarbonate along with high upper limit of detection enable direct analysis of chloride in undiluted human serum. The chloride detection in human serum as well as artificial serum sample was accomplished using a poly(vinyl chloride)-based ISE, the results of potentiometric measurements were confirmed using argentometric titration. Remarkably, ionophore I was shown to exhibit a good long-term stability of potentiometric performance over the period of 10 weeks of application which is a rare success for solvent polymeric ionophore-based anion-selective membrane electrodes.

2.5.6 Acknowledgements

The author acknowledges financial support by the Swiss National Science Foundation (FNS Sinergia CRSII2-147654) and thanks Laura A. Jowett, Ethan N.W. Howe and Philip A. Gale (School of Chemistry (F11), The University of Sydney, NSW 2006, Australia) for successful collaboration and PAG for funding their research.

2.5.7 References

(1) Dimeski, G.; Badrick, T.; St. John, A. *Clin. Chim. Acta* **2010**, *411*, 309-317.
(2) Panteghini, M.; Bonora, R.; Malchiodi, A.; Calarco, M. *Clin. Biochem.* **1986**, *19*, 20-25.
(3) Frost, M. C.; Meyerhoff, M. E. *Annu. Rev. Anal. Chem.* **2015**, *8*, 171-192.
(4) Bobacka, J.; Ivaska, A.; Lewenstam, A. *Chem. Rev.* **2008**, *108*, 329-351.
(5) Bakker, E.; Telting-Diaz, M. *Anal. Chem.* **2002**, *74*, 2781-2800.
(6) Hulanicki, A.; Michalska, A. *Electroanalysis* **1995**, *7*, 692-3.
(7) Bratov, A.; Abramova, N.; Dominguez, C. *Anal. Chim. Acta* **2004**, *514*, 99-106.
(8) Oesch, U.; Ammann, D.; Simon, W. *Clin. Chem.* **1986**, *32*, 1448-59.
(9) Yoon, I. J.; Shin, J. H.; Paeng, I. R.; Nam, H.; Cha, G. S.; Paeng, K.-J. *Anal. Chim. Acta* **1998**, *367*, 175-181.

(10) Burtis, C. A.; Bruns, D. E. *Tietz fundamentals of clinical chemistry and molecular diagnostics, 7th Edition*; Elsevier Health Sciences: St. Louis, 2014, p 1075.

(11) Radu, A.; Bakker, E. *Chem. Anal.* **2005**, *50*, 71-83.

(12) Xiao, K. P.; Buehlmann, P.; Nishizawa, S.; Amemiya, S.; Umezawa, Y. *Anal. Chem.* **1997**, *69*, 1038-1044.

(13) Sabek, J.; Adriaenssens, L.; Guinovart, T.; Parra, E. J.; Rius, F. X.; Ballester, P.; Blondeau, P. *Chem. Eur. J.* **2015**, *21*, 448-454.

(14) Zahran, E. M.; Hua, Y.; Li, Y.; Flood, A. H.; Bachas, L. G. *Anal. Chem.* **2010**, *82*, 368-375.

(15) Rothmaier, M.; Schaller, U.; Morfb, W. E.; Pretsch, E. *Anal. Chim. Acta* **1996**, *327*, 17-28.

(16) Kondo, Y.; Buehrer, T.; Seiler, K.; Froemter, E.; Simon, W. *Pfluegers Arch.* **1989**, *414*, 663-8.

(17) Park, S. B.; Matuszewski, W.; Meyerhoff, M. E.; Liu, Y. H.; Kadish, K. M. *Electroanalysis* **1991**, *3*, 909-16.

(18) Gupta, V. K.; Goyal, R. N.; Sharma, R. A. *Electrochim. Acta* **2009**, *54*, 4216-4222.

(19) Busschaert, N.; Wenzel, M.; Light, M. E.; Iglesias-Hernandez, P.; Perez-Tomas, R.; Gale, P. A. *J. Am. Chem. Soc.* **2011**, *133*, 14136-48.

(20) Busschaert, N.; Karagiannidis, L. E.; Wenzel, M.; Haynes, C. J. E.; Wells, N. J.; Young, P. G.; Makuc, D.; Plavec, J.; Jolliffe, K. A.; Gale, P. A. *Chem. Sci.* **2014**, *5*, 1118-1127.

(21) Novell, M.; Guinovart, T.; Blondeau, P.; Rius, F. X.; Andrade, F. J. *Lab Chip* **2014**, *14*, 1308-1314.

(22) Craggs, A.; Moody, G.; Thomas, J. *J. Chem. Educ.* **1974**, *51*, 541.

(23) Bakker, E.; Bühlmann, P.; Pretsch, E. *Chem. Rev.* **1997**, *97*, 3083-3132.

(24) Benzo, Z.; Escalona, A.; Salas, J.; Gomez, C.; Quintal, M.; Marcano, E.; Ruiz, F.; Garaboto, A.; Bartoli, F. *J. Chromatogr. Sci.* **2002**, *40*, 101-106.

(25) Rose, C. F. M. *Biochem. J.* **1936**, *30*, 1140.

(26) Umezawa, Y.; Bühlmann, P.; Umezawa, K.; Tohda, K.; Amemiya, S. *Pure Appl. Chem.* **2000**, *72*, 1851-2082.

(27) Blacklock, C.; Lawrence, J.; Wiles, D.; Malcolm, E.; Gibson, I.; Kelly, C.; Paterson, J. *J. Clin. Pathol.* **2001**, *54*, 553-555.

(28) Duh, S.; Cook, J., Laboratory reference range values; MD, USA: University of Maryland School of Medicine. APP17 2005.

(29) Borthwick, G. M.; Johnson, A. S.; Partington, M.; Burn, J.; Wilson, R.; Arthur, H. M. *FASEB J.* **2006**, *20*, 2009-2016.

(30) Wong, A.; Mac, K.; Aneman, A.; Wong, J.; Chan, B. S. *J. Med. Toxicol.* **2016**, *12*, 130-133.

(31) Blinn, C. M.; Dibbs, E. R.; Hronowski, L. J. J.; Vokonas, P. S.; Silbert, J. E. *Arthritis Rheum.* **2005**, *52*, 2808-2813.

(32) Howe, E. N. W.; Bhadbhade, M.; Thordarson, P. *J. Am. Chem. Soc.* **2014**, *136*, 7505-7516.

(33) Gomez, D. E.; Fabbrizzi, L.; Licchelli, M.; Monzani, E. *Org. Biomol. Chem.* **2005**, *3*, 1495-1500.

(34) Ceresa, A.; Pretsch, E. *Anal. Chim. Acta* **1999**, *395*, 41-52.

(35) Mi, Y.; Bakker, E. *Anal. Chem.* **1999**, *71*, 5279-5287.

(36) Morf, W. E. *The Principles of Ion-Selective Electrodes and of Membrane Transport*; Elsevier: New York, 1981; Vol. 2, p 432.

(37) Cotty, V.; Zurzola, F.; Beezley, T.; Rodgers, A. *J. Pharm. Sci.* **1965**, *54*, 868-70.

(38) Wrathall, G.; Sinclair, R.; Moore, A.; Pogson, D. *Hum. Exp. Toxicol.* **2001**, *20*, 491-495.

(39) Goto, Y.; Makino, K.; Kataoka, Y.; Shuto, H.; Oishi, R. *J. Chromatogr. B Biomed. Sci. Appl.* **1998**, *706*, 329-335.

(40) Dargan, P. I.; Wallace, C. I.; Jones, A. L. *Emerg. Med. J.* **2002**, *19*, 206-9.

(41) Wu, X.; Judd, L. W.; Howe, E. N.; Withecombe, A. M.; Soto-Cerrato, V.; Li, H.; Busschaert, N.; Valkenier, H.; Pérez-Tomás, R.; Sheppard, D. N. *Chem* **2016**, *1*, 127-146.

2.6 Toward *in-situ* Electrochemical Phosphate Determination in Seawater

This work aimed to provide an approach for phosphate detection in seawater samples. The potentiometric sensors based on phosphate receptors reported so far are known to exhibit inadequate performance (lower detections limits, selectivity) for successful phosphate detection in environmental samples. Thus, an attempt has been made within the framework of this research to implement square wave voltammetric detection into flow analysis, using a specially developed in-line configuration allowing for the formation of electrochemically active phosphomolybdate complex. The discussion below presents a detailed description of the proposed in-line configuration and the corresponding electrochemical protocol. The results of the research described in this section have not been published yet. For any further use of the described concepts and data please acknowledge Prof. Eric Bakker* and Dr. Maria Cuartero, as well as the author of this manuscript.

2.6.1 Abstract

We report here on a novel approach for electrochemical phosphate determination in a microfluidic flow system where the reagents, necessary for the formation of electroactive phosphomolybdate complex (molybdate anions, hydrogen ions), are delivered in-line into a thin layer sample through ion-exchange membranes. The recently reported approach for in-line sample acidification based on the cation-exchange process between the sample and a cation-exchange Donnan exclusion membrane was adapted here to achieve highly acidic conditions (pH~1) necessary for successful phosphate determination. The possibility of molybdate anion transport through an ion-exchange membrane was demonstrated using different types of commercial anion-exchange membranes. A microfluidic in-line flow configuration, comprising molybdate-releasing and acidification modules coupled together, was developed, allowing for the delivery of both hydrogen and molybdate ions into the sample in order to form the electroactive complex. The proposed arrangement was first tested colorimetrically and subsequently coupled with electrochemical detection using square wave voltammetry. The ability of the approach to resolve submicromolar phosphate concentrations both in sodium chloride 0.6 M and in seawater matrix has been demonstrated.

2.6.2 Introduction

Phosphate is one of the most crucial species of all organisms as it is absolutely necessary for the growth of plants and animals.[1,2] The detailed discussion of vital importance of phosphate monitoring in aquatic systems along with the main techniques used for phosphate detection have been already outlined in the Introduction Chapter (see Chapter 1, Section 1.1.1.2) and thus will be omitted here. The current methodologies for *in-situ* phosphate monitoring are generally based on the traditional approach where molybdate and phosphate are mixed in an adequate proportion in acidic media to form the phosphomolybdate complex, which is subsequently detected colorimetrically after the reduction with ascorbic acid, in the presence of antimony.[3,4] The analysers based on the afore-mentioned methodology possess adequate accuracy and sensitivity for some field measurements but have significant disadvantages in view of field monitoring, such as large dimensions and weight, high energy consumption and costs, as well as necessity of reagent storage and addition.[5] Therefore, the development of systems for *in-situ* phosphate determination is a vital direction for the advances in environmental science and conservation.[6,7]

Potentiometric detection using ion-selective electrodes, coupled with flow injection analysis (FIA), has been used for both direct and indirect detection of phosphates.[8,9] Despite of numerous studies reported on potentiometric phosphate determination, as of today, to the best of our knowledge, there exist no phosphate receptors with sufficient sensitivity and selectivity to allow for potentiometric determination of submicromolar phosphate concentrations. The potentiometric approaches suggested so far would be satisfactory for phosphate detection only in wastewater or significantly polluted/eutrophic water, as even in moderately polluted natural water and especially in pristine waters (<0.03 μM of P) very low levels of phosphate are observed.[1,10] This is why an effort was made within this research to develop an approach based on dynamic electrochemical detection, as no potentiometric sensor with a desired performance could be found or proposed.

Phosphate as such is not an electrochemically active species, therefore, to enable the electrochemical detection, the conditions should be achieved for phosphate to form the electrochemically active complex that can be subsequently detected by means of one of non-zero current techniques, such as voltammetry, differential pulse or square wave

voltammetry or amperometry.[5,7,11,12] The following reaction of Keggin anion formation typically lies at the bases of all mentioned techniques:[13]

$$PO_4^{3-} + 12MoO_4^{2-} + 27H^+ \rightarrow H_3PMo_{12}O_{40} + 12H_2O \qquad \text{(eq. 2.6.1)}$$

The electrochemically active complex is formed in acidic conditions (pH~1) by the reaction with molybdate anions (e.g. sodium molybdate).[13] It has been shown in the past that the ratio between acid and molybdate is essential for the kinetics of complex formation as well as for overcoming the cross interferences in real sample matrix, such as for example silicate ions in seawater forming the silicomolybdate complex under similar conditions.[4,5,13] Most of the electrochemical protocols reported for phosphate detection suggest the optimum molybdate concentration to be in the millimolar range.[5,7]

Thus, the generation of two reagents in the sample is necessary for the formation of the electroactive phosphomolybdate complex: hydrogen ions and molybdate anions. There are only few in-line approaches for molybdate generation reported so far. The most common methods are flow injection analysis (FIA) or sequential injection analysis (SIA, allowing for multiple reagent injections).[14] The flow injection-based methods generally involve either direct injection of reagents into the sample flow or the injection of the sample into a flowing carrier stream, followed by reagent addition by injection or confluence; the latter results in merging of the sample and reagent zones.[14,15] There exist numerous FIA and SIA variations for the spectrophotometric phosphate determination.[14] A new approach for simultaneous generation of both molybdate and protons into the sample has been recently suggested by V. Garçon et al. for electrochemical phosphate detection.[5,11] In this approach protons are pushed electrochemically through a cation-exchange membrane (fumatech GmbH, fumapem® F-930) into the sample compartment/flow, by oxidizing the molybdenum electrode in the compartment behind the cation-exchange membrane.[5,11] The molybdate species are in turn delivered into the sample by oxidizing the secondary molybdenum electrode in the sample compartment (during shorter times, to achieve the excess of protons over molybdate).[5]

Here we describe a new thin-layer approach for releasing both hydrogen ions and molybdate species into the seawater sample flow, by coupling the previously described acidification cell[16] to the module of similar design but adapted for anion exchange, with subsequent electrochemical detection in the same flow using square wave voltammetry. Unlike in the experimental configuration proposed by V. Garçon et al.[5,11], in this approach both hydrogen and molybdate ions are being delivered to the thin sample flow passively,

via ion exchange, which makes the approach less complex and easier to accomplish. Importantly, the newly proposed configuration does not require time for diffusion of molybdate reagent which is the case for electrochemically generated molybdate at the molybdate electrode[5,11]. The proposed setup is based on an in-line configuration and is easy to integrate for subsequent *in-situ* determination in a submersible module with fluidic system and flow parameters similar to the ones previously described in Section 2.2 for the submersible probes.

2.6.3 Experimental

2.6.3.1 Materials, reagents, samples and equipment

Sodium chloride, sodium phosphate monobasic, potassium chloride, ammonium molybdate tetrahydrate, sodium molybdate dehydrate, L-ascorbic acid, potassium antimonyl-tartrate trihydrate, concentrated hydrochloric acid (HCl, 32%), hydrochloric acid solution (HCl, 1.0 M), concentrated sulfuric acid (H_2SO_4, 96%) were purchased from Sigma. Aqueous solutions were prepared in deionized water (>18 MΩ/m). The seawater samples used in the present research were supplied from Arcachon Bay (France).

Silicone rubbers (for the channels) VMQ 50.20-01 (Angst + Pfister) were purchased from APSOparts®.

Cation-exchange membrane FKL-PK-130 (thickness 110-140 µm) and anion-exchange membranes FAB-PK-130, FAS-PET-130, FAD-PET-75 and FAPQ-375-PP (thicknesses 110-130, 110-130, 70-80 and 70-80 µm respectively) were purchased from Fumatech® (FuMA-Tech GmbH, Germany). The membranes were cut in pieces of either 6×110 mm (for the acidification/molybdate module) or 15 × 30 mm (for the paper-based cell) and pre-conditioned according to pretreatment procedure indicated by the supplier. The FKL membranes were pre-conditioned in deionized water for at least 6 h at room temperature and then at least 1 day in 1 M HNO_3 to ensure complete saturation of the membrane with hydrogen ions. Pre-conditioning procedure of the anion-exchange membranes was accomplished overnight in the conditions indicated in Table 2.6.1.

2.6.3.2 Acidification and molybdate-releasing modules

The design of the acidification and molybdate-releasing modules is identical to the one reported earlier for the acidification cell[16] (Section 2.3.3) and is illustrated in Figure 2.6.1. The cell consists of a piece of cation- or anion-exchange membrane (6 × 110 mm)

sandwiched between two rubber channels (rubber: 10 × 119 × 0.45 mm, channel: 1.7 × 100 × 0.45 mm). These elements are in turn placed between two acrylic blocks (30 × 120 × 14 mm) tightly closing the system by screws. The ends of the channels coincide with the inlet and outlet of each block, the inlets and outlets of the two blocks of the same module are placed in reverse order to provide counter flow in the two channels. As concentrated acid is to be used in the acidification module (see Section 2.6.4), for long-term exploitation the silicon rubber channel material can be replaced by a more chemically stable one, e.g. FKM 10.1009.1550 (Angst + Pfister), however the silicon rubber channels were proved to serve as fine during the period of more than 2 months.

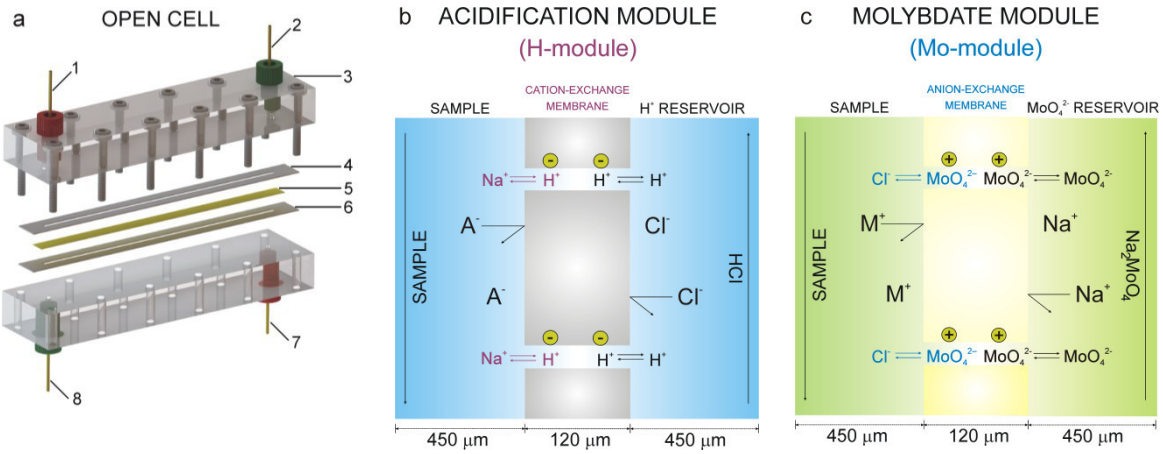

Figure 2.6.1. (a) Schematic illustration of the custom-made acidification and molybdate modules: 1) inlet; 2) outlet; 3) acrylic block; 4) rubber channel; 5) cation-/anion-exchanger membrane; 6) rubber channel; 7) inlet; 8) outlet. (b, c) Working principles for the in-line acidification module based on cation exchange (b, H-module) and in-line molybdate module based on anion exchange (c, Mo-module) between the sample and the membrane. (A^- and M^+ stand for any sample anion or cation respectively).

2.6.3.3 Colorimetric detection

The spectrophotometric detection was based on molybdenum blue (MB) reaction and the method described by J.D.H. Strickland and T.R. Parsons[3]. First, mixed reagent components were prepared separately. The ammonium molybdate solution ($S_{molybdate}$) was obtained by dissolving 15 g of ammonium molybdate tetrahydrate in 500 mL of water. The sulfuric acid solution (S_{acid}) was prepared by adding 140 mL of concentrated sulfuric acid (96%) in 900 mL of water. Ascorbic acid solution (S_{ascorb}) was prepared by dissolving 27 g of L-ascorbic acid in 500 mL of water and stored in the freezer overnight and whenever not in use. Potassium antimony tartrate solution ($S_{antimony}$) was obtained by dissolving 0.34 g of potassium antimonyl-tartrate trihydrate in 250 mL of water. Finally, the fresh mixed reagent for phosphate detection ($Reagent^{(P)}$) was prepared, the same day as the colorimetric analysis to be performed, by mixing the solutions described above in the following

volumetric ratio: $S_{molybdate}:S_{acid}:S_{ascorb}:S_{antimony}$ = 2:5:2:1. The mixed reagent was added to the sample to be analysed in the volumetric ratio 1:10 (reagent:sample). The composition of the mixed solution has been modified for the detection of phosphate in the samples passed through proton- or/and molybdate-generating modules by substituting the corresponding component (acid or/and molybdate) with equivalent aliquot of water.

The spectrophotometric detection of molybdate was accomplished using the mixed reagent with the composition identical to Reagent$^{(P)}$, by substituting the molybdate component with sodium phosphate monobasic (Reagent$^{(Mo)}$ with $S_{phosphate}$). Phosphate (total) concentration in the mixed reagent Reagent$^{(Mo)}$ was 0.01 M due to millimolar range of molybdate concentrations in the samples to be analysed. In analogy to Reagent$^{(P)}$ modifications, the composition of the mixed solution Reagent$^{(Mo)}$ has been modified for the detection of molybdate in the samples passed through proton- generating module by substituting sulfuric acid and phosphate solutions with equivalent aliquot of water.

The spectrophotometric detection of both phosphate and molybdate was accomplished using UV/VIS spectrophotometer Lambda 35 (Perkin Elmer, USA) in a flow-through quartz cell with the light path of 10 mm and 30 µL volume (Perkin Elmer, USA, part N B0631090), at the wavelength 660 nm.

2.6.3.4 Electrochemical detection

All electrochemical measurements (cyclic voltammetry, square wave voltammetry) were performed in a faradaic cage using potentiostat/galvanostat PGSTAT 128N (Metrohm Autolab, Utrecht, The Netherlands) controlled by Nova 1.11 software.

2.6.3.4.1 Bulk measurements: phosphate detection

Electrochemical experiments in the bulk solution were accomplished in a voltammetric cell made of glass, using commercial reference electrode (6.0726.100, Metrohm) with double junction (Ag | AgCl | KCl, 3 M | LiOAc, 1 M) and a platinum-working rod (3.2 cm^2 surface area) as a counter electrode. Glassy carbon (GC) electrodes (or gold electrodes, for preliminary comparative experiments) sourced from Metrohm were used as working electrodes and contained a GC-electrode-tip (6.1204.300) (or Au-electrode tip, 6.1204.320) with a diameter of 3.00±0.05 mm.

The detection phosphate was accomplished in a 5-6 mL sample volume by spiking sulfuric acid solution (S_{acid}, to achieve pH~1) and ammonium molybdate solutions ($S_{molybdate}$) in the same reagent-to-sample ratio as for colorimetric measurements (see above, Section

2.6.3.3). As the reduction of the phosphomolybdate complex was achieved electrochemically, no potassium antimonyl-tartrate and ascorbic acid reagents were needed, unlike in colorimetric approach. The square wave voltammetric detection in the bulk was performed at 250 Hz with the preceding conditioning/preconcentration step at 0 V during 60 s, both detection and conditioning without stirring. Stirring was applied between the SWV experiments, prior to every conditioning step.

2.6.3.4.2 Paper-based cell: choosing the anion-exchange membrane for anion transport

The preparation of the paper-based electrochemical flow cell was accomplished according to Cuartero et al.[17] by replacing the cation-exchange membrane used originally by the anion-exchange membrane (for the paper-cell image see inset in Figure 2.6.3). The silver foil (working electrode), one filter paper, the membrane, the second filter paper, and the silver/silver chloride foil (reference/counter electrode) were placed in the indicated order between two tightly squeezed acrylic blocks.[17] The ends of both paper-channels were dipped into two separate beakers with aqueous solutions (Solutions 1 and 2) containing either 100 mM NaCl or 100 mM Na_2MoO_4, thus obtaining the following cell: Ag|AgCl|Solution 1|membrane| Solution 2|Ag. Two special tape masks were added to the system on both sides of the membrane in order to ensure that the two filter papers do not come in contact with each other. The anion-exchange membranes were pre-conditioned according to the protocol indicated by the supplier (see Table 2.6.1).

2.6.3.4.3 Electrochemical flow cell: phosphate detection

The electrochemical flow cell with radial cross-flow was purchased from BASi® Analytical Instruments and is described in Figure 2.6.2. A glassy carbon electrode (b) of 3 mm diameter was used as working electrode, the stainless steel block (d, e) - as counter electrode and a single-junction Ag/AgCl electrode was used as reference electrode and placed vertically in the reference electrode chamber of the auxiliary block (Figure 2.6.2a, 3). The solution supplied from the inlet placed in the centre of the auxiliary block (Figure 2.6.2a, 1) is flowing from the central hole, filling the central groove of the auxiliary block, and reaches the small hole in the groove placed right at the top of the groove (arrow 4). Thereafter the solution is filling the reference electrode chamber (3) by passing through the hole in the grove (arrow 5) and finally reaches the outlet port by flowing across the reference electrode chamber (arrow 6).

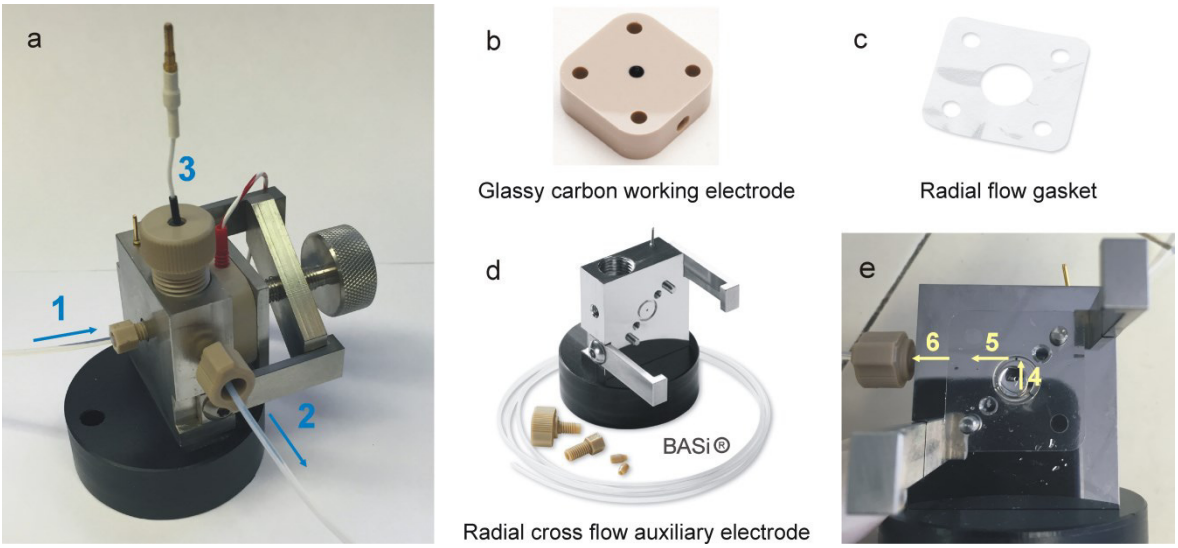

Figure 2.6.2. The design of the electrochemical flow cell purchased from BASi®. (a) Assembled cell with the glassy carbon electrode (b) as working electrode, single junction Ag/AgCl electrode (3) as a reference electrode, stainless auxiliary block (d) as a counter electrode and a flow gasket (c) as a spacer (ca. 13 µL). (1) Inlet port to centre hole of auxiliary block, (2) outlet port from the reference electrode chamber, (3) reference electrode inserted in the reference electrode chamber, (4) central hole of the auxiliary block to hole in the groove of the auxiliary block, (5) hole in the groove of the auxiliary block to the reference electrode chamber, (6) flow path from the reference electrode chamber to the outlet port.

2.6.3.5 In-line configuration for electrochemical detection in the flow cell

The general schematic diagram of the experimental arrangement proposed for electrochemical phosphate detection in the flow (flow rate ca. 40 µL min^{-1}) is shown in Figure 2.6.3. The solution delivery was achieved using two four-head ISMATEC peristaltic pump (Model ISM935c, Clattbrug, Switzerland) equipped with ISMATEC tygon tubings (inner diameter 0.76 mm), each pump allowing for the delivery of 4 flows at the same flow rate. The solutions were pumped through at 5 different positions indicated as "PUMP" in Figure 2.6.3. Therefore, 2 pumps were needed in order to place 5 single ISMATEC cassettes, each for a separate flow/tubing. First pump was used at four different positions; second pump was used at one position delivering HCl in the acidification module. Importantly, the two tubings delivering the sample/background flow should be placed on the same pump in order to achieve exactly the same flow rate and thus avoid the formation of the bubbles in the channel. The precise control of HCl flow is not critical, thus it has been placed on a separate pump to have the possibility to decrease the flow rate or to loop the flow in order to spare the reagent. The tygon tubings installed on the pumps were connected to the flow path composed of PTFE Tubings (ID 0.8 mm, BOLA). The two-position selector/switching valves (model EHMA) were purchased from VICI® (Valco Instruments Company Inc.). Valve 1 has been installed before the pump, in order to select

one of the two flows (sample/calibrant or background). Valve 2 has been installed after the pumps delivering the flow to the detection cell, in order to switch between analyte and washing solutions, without stopping the analyte flow. The latter is important in order to provide constant flow conditions in the detection cell and, more importantly, constant flow rate/residence time of the analyte plug both in acidification and molybdate modules. Both valves were equipped with the two-position actuator control modules operated by the PC. The used reagents (hydrochloric acid, sodium molybdate) and the redirected flow from Valve 2 were sampled in a waste bottle. Valve 2 has been only used for one particular experiment comprising the "washing-step" (see Section 2.6.4.2) and has been eliminated from the system for other experiments.

The development and the evolution of the reported in-line configuration as well as relevant parameters of the proposed setup (concentrations of reagents, sequence of modules etc.) present the core of this work and are discussed in detail in Section 2.6.4.

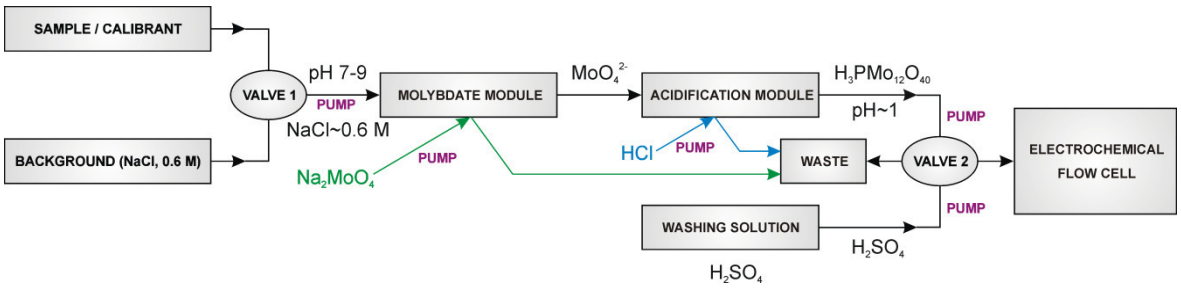

Figure 2.6.3. Schematic diagram of electrochemical detection arrangement.

In order to obtain the calibration traces, solutions with different phosphate concentrations and 0.6 M NaCl background were passed through the in-line configuration presented in Figure 2.6.3 towards the square wave voltammetric detection. The sample solutions at the inlet of the system were changed every 20 (or 10) minutes (as indicated in the main text) by switching between the calibrant and the baseline (0.6 M NaCl) using a switching valve (Valve 1). Baseline solution was flushed through the system for 20 (or 10) min after every phosphate-containing solution in order to account for the baseline drift.

2.6.4 Results and Discussion

2.6.4.1 Acidification and molybdate-releasing modules

As mentioned previously in the Introduction Section (see Section 2.6.2), generation of two reagents into the sample flow is necessary for the formation of the electroactive

phosphomolybdate complex: hydrogen ions, to provide the acidic conditions, and molybdate anions, to form the complex.

2.6.4.1.1 Acidification module (H-module)

For the generation of protons into the sample we have adapted the approach developed previously (see as well Figure 2.6.1a,b, Section 2.6.3.2) based on cation-exchange process between the sample and an ion-exchange Donnan exclusion FKL membrane in its protonated form.[16] Here it must be emphasized that the in-line approach developed within the framework of this study refers to phosphate detection in seawater, i.e. in samples containing high concentration of sodium chloride (ca. 0.6 M). The latter allows us to reach the required pH<1 as there is a sufficient amount of sodium ions (which are to be exchanged with protons from the membrane) present in the sample. The preliminary experiments have shown the flow rate of 90 µL min^{-1} and 5M HCl solution in the acid reservoir behind the FKL membrane to be sufficient to achieve pH 0.5-1 (determined using pH test strips).

2.6.4.1.2 Molybdate-releasing module (Mo-module)

2.6.4.1.2.1 Choosing the anion-exchange membrane

The next step was to enable the release of molybdate anions into the sample flow. The latter was achieved by adapting the same in-line configuration as used in the acidification module, this time for anion exchange (see Figure 2.6.1a,c). To accomplish the desired in-line configuration providing molybdate release into the sample, the right membrane material had to be chosen to allow for the efficient anion transport through the membrane into the sample compartment. Four different types of anion-exchange membranes were purchased from fumatech® GmbH: FAB-PK-130, FAS-PET-130, FAD-PET-75, and FAPQ-375-PP. The physical and chemical properties of the purchased membranes are given in Table 2.6.1.

In order to compare the anion transfer through these four membranes, a voltammetric experiment was performed using a paper-based cell of a design similar to the previously reported by Cuartero et al.[17], except for the fact that the anion-exchange membrane was used instead of the cation-exchange one (see the figure inset in Figure 2.6.4 for the paper-based cell image and Section 2.6.3.4.2 for the details). The ends of both paper-channels were dipped in two beakers with 100 mM NaCl solution obtaining the following cell: Ag|AgCl|NaCl 100 mM|membrane|NaCl 100 mM|Ag.

Table 2.6.1. Physical and chemical properties of anion-exchange membranes (fumasep®)

Physical/chemical properties	FAB-PK-130	FAS-PET-130	FAD-PET-75	FAPQ-375-PP
Reinforcement	PK	PET	PET	PP
Thickness (dry), μm	110-130	110-130	70-80	70-80
Weight per unit area, mg/cm^2	10-13	10.5-12	n/a	7.0-8.5
Ion exchange capacity, meq/g (in chloride form)	0.7-1.0	1.0-1.3	1.66	1.3-1.5
Specific conductivity, mS/cm (in chloride form)	1.0-2.5	4-6	n/a	3.5-6.0
Area resistance, Ω/cm (in chloride form)	6.0-11.0	1.7-3.0	n/a	1.0-2.0
Uptake in water, wt % (25^{O}C)	5-15	13-23	34	30-45
pH stability range	0-14	0-8	n/a	0-10
Pre-conditioning	NaCl 0.1 M	NaCl 0.1 M	NaCl 0.1 M	Dry/MQ water

Figure 2.6.4 shows a comparison between cyclic voltammograms obtained with different anion-exchange membranes as well as with no membrane at all (two paper channels adjacent to each other, placed between two acrylic blocks but dipped in two separate beakers with sodium chloride). An anodic potential scan induces the oxidation of the silver foil, resulting in a current reflecting the plating of silver chloride on the silver electrode. When an anion-exchange membrane is placed between two paper-channels, as chloride is being removed from the sample adjacent to the silver electrode (Compartment 1), the chloride anions from the other compartment adjacent to silver/silver chloride electrode (Compartment 2) must be transported across the anion-exchange membrane to maintain charge neutrality in each compartment (as chloride is the only species in the system that can cross the solution-membrane interface). This process is accompanied by the additional release of chloride ions into Compartment 2 due to reduction of the silver/silver chloride element. The backward potential sweep allows for the regeneration of the two electrodes and chloride transport back to Compartment 2.

As can be observed in Figure 2.6.4, the smallest separation between the anodic and cathodic peak potentials is observed for the FAPQ membrane. In fact the peak position for FAPQ corresponds to the peak potential in the system without the membrane, however with lower current density which suggests to some extent less efficient ion transport. The peak separation increases slightly when changing from FAPQ membrane to FAD and FAS which might account for both increase in the area resistance (see Table 2.6.1) and possible

changes in ion transport kinetics. However, no clear cathodic or anodic peaks are observed for the FAB membrane suggesting that insufficient ion transport takes place when FAB is used a separator in the paper-based cell.

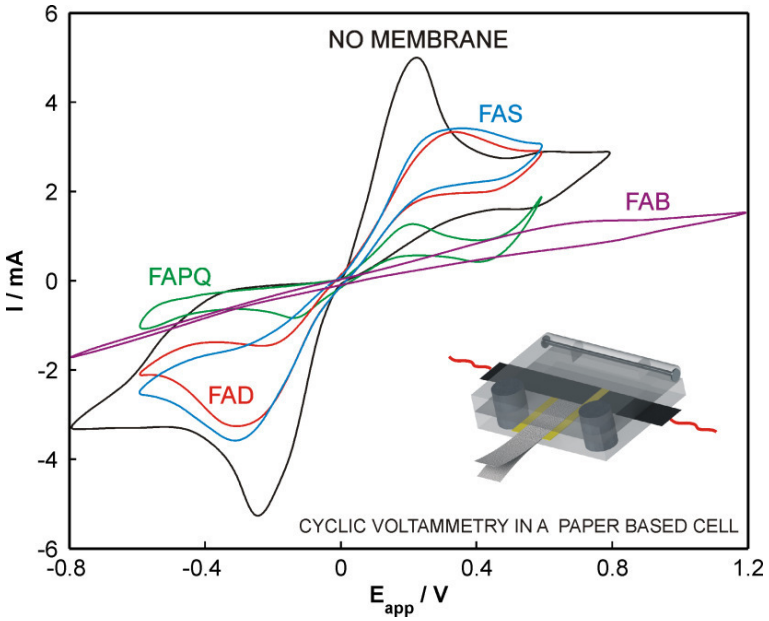

Figure 2.6.4. Cyclic voltammograms obtained at 5 mV/s scan rate* in a paper-based cell[17] with or without (black) anion-exchange membrane: Ag|AgCl|NaCl 100 mM|membrane|NaCl 100 mM|Ag. membrane = FAB-PK-130 (purple), FAS-PET-130 (blue), FAD-PET-75 (red), FAPQ-375-PP (green).

* The CV for the FAB membrane presented here refers (exceptionally) to the scan rate 10 mV/s.

Therefore, the choice has to be made between FAS, FAD and FAPQ. Despite the higher current density in the voltammograms with FAS and FAD compared to FAPQ (which is clear from a visual comparison of the areas of the cathodic/anodic peaks) suggesting less efficient transport for FAPQ, the latter was chosen for the transport experiments. The choice of the FAPQ membrane was dictated as well by the other physico-chemical properties indicated in Table 2.6.1. In particular, the FAS membrane pH stability range (from 0 to 8) is not sufficient for environmental application as pH of open-sea seawater normally ranges between 7.5 and 8.4.[18] The pH stability range for the FAD membrane has not been reported, however it was not chosen due to mechanical reasons: the initially flat and relatively thin FAD membrane (75 μm) distorts and twists upon conditioning which makes it very difficult to be integrated between two acrylic modules of the Mo-module (see Figure 2.6.1). On the contrary, as follows from the Table 2.6.1, the FAPQ membrane does not require pre-conditioning which makes it much more applicable practically, as a dry membrane is very easy to integrate in the Mo-module. Importantly, the pH stability range (0-10) is also sufficient for the desired application.

To confirm the possibility of passive molybdate release through FAPQ membrane the paper-based cell was newly assembled but this time NaCl in the second compartment (Compartment 2, adjacent to Ag/AgCl element) was substituted by 100 mM sodium molybdate solution, thus obtaining the following paper-based cell: Ag|AgCl|Na_2MoO_4 100 mM|membrane|NaCl 100 mM|Ag. The cell was dismounted after ca. 30 min (to ensure that there was enough time given for the liquid to reach the top of the filter paper and for the expected anion exchange to happen) and a few drops of the colorimetric reagent containing ascorbic acid, antimonyl tartrate, 10 mM phosphate, at pH~1 (see Experimental part, Section 2.6.3.3 for more details) were deposited on top of both papers. The intensive blue coloration of both papers from both compartments of the cell was detected visually, confirming the efficient transport of molybdate anions through the FAPQ membrane. The same experiment was repeated with a newly assembled cell by placing the FAB membrane between the paper channels, instead of FAPQ. No coloration was observed after dropping the reagent on the paper-channel dipped into sodium chloride solution. Thus, the FAB membrane was once again shown not to be applicable for the anion transport in the chosen system.

2.6.4.1.2.2 Implementing the FAPQ anion-exchange membrane into molybdate-releasing module. Preliminary colorimetric experiments: optimization of molybdate concentration in the Mo-module, execution of the module combination (Mo-module + H-module).

After having compared the membranes in the paper-based setup we implemented the FAPQ membrane as well as the FAB membrane (for the comparison) into two modules of in-line configuration presented in Figure 2.6.1a,c. It must be mentioned that, unlike in the paper-based cell setup where the small size of the FAPQ membrane (ca. 30 × 15 mm) allows for the use of the pre-conditioned membrane, here it is extremely difficult to implement a relatively long piece of the FAPQ membrane (ca. 6 × 110 mm), twisted after conditioning in water, into the Mo-module. On the contrary, no difficulties were faced in case of FAB membrane pre-conditioned in 0.1 M NaCl, probably to its more robust structure and larger thickness (see Table 2.6.1). A preliminary test was performed with both assembled Mo-modules (one with FAPQ and another one with FAB membrane) by passing NaCl 0.6 M in the sample solution and Na_2MoO_4 100 mM in the molybdate-reservoir with a low flow rate (ca. 90 µL min^{-1}), followed by subsequent addition of the colorimetric reagent to the small portion of liquid (ca. 1 mL) sampled at the outlet of the sample channel. In accordance with the previously reported experiments in the paper-based cell, no coloration has been observed for the sample coming out from the FAB-based Mo-

module, while very strong blue coloration has been noted for the sample plug from at the outlet of the FAPQ-based Mo-module. Therefore, the FAPQ-membrane was confirmed to be a promising candidate for the further experiments.

Thereafter, the molybdate transport through the FAPQ membrane of the Mo-module into the sample containing 0.6M NaCl (mimicking chloride concentration in seawater) was quantitatively characterized using colorimetric detection in a small volume UV/VIS flow cell (30 µL) installed inside the spectrophotometer at 660 nm. The flow rate of ca. 90 µL min^{-1} was chosen for all the modules/cells involved. Despite of the fact that the Mo and H-modules were not directly coupled to the spectrophotometric cell as the reagent had to be spiked into the sample before detection, the flow cell offers an important advantage of continuous absorbance readout which is important in order to adequately estimate the stability of the signal and the time intervals necessary for optimal detection.

Figure 2.6.5 illustrates a typical colorimetric response in calibration solutions containing different molybdate concentration with 0.6 M NaCl background, after addition of $Reagent^{(Mo)}$ (see Experimental part for details, Section 2.6.3.3) and passing through the cell 20 min thereafter. The 20 min time step was chosen as an optimal time from preliminary experiments. One must as well take into account that the flowing path from the sample to the detection cell takes ca. 13 min within the chosen flow setup (flow rate, inlet tubing dimensions), thus the resulting detection is being accomplished ca. 33 min after mixing the sample and the reagent. The relatively long time interval required after addition of the reagent in order to obtain the relatively stable absorbance signal accounts most probably for high temperatures of the experiment due to a very hot summer (room temperature ca. 30-35^{O}C) as well as high NaCl background. The latter results in the visible sample coloration upon addition of the $Reagent^{(Mo)}$/$Reagent^{(P)}$ even without any molybdate/phosphate (respectively) in the sample. Figure 2.6.5 confirms the adequate stability of the sample absorbance in chosen conditions. The chosen millimolar range of calibrant concentrations accounts for the optimal molybdenum background required for applying electrochemical protocols for phosphate detection, according to previously reported protocols.[5,7]

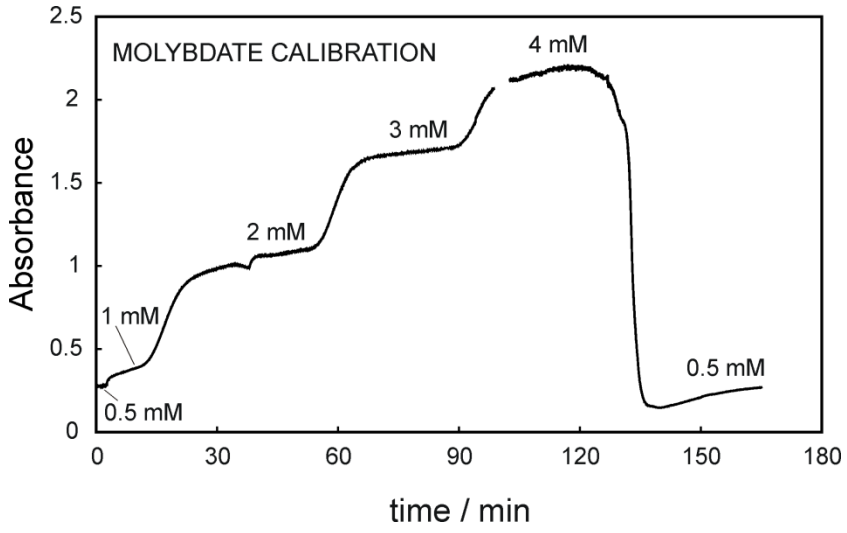

Figure 2.6.5. Colorimetric response at 660 nm in the UV flow cell (flow rate ca. 90 μL min^{-1}) in solutions containing different molybdate concentration and 0.6 M NaCl background, spiked with $Reagent^{(Mo)}$ ca. 33 min prior to detection (see text and Experimental part for the details).

The molybdenum calibration obtained from the data shown in Figure 2.6.5 is presented in Figure 2.6.6a (white circles) and was used for further experiments. To evaluate the efficiency of molybdate transport through FAPQ membrane, samples with different amount of molybdate and 0.6 M NaCl background were passed through the Mo-module and subsequently analysed in the spectrophotometric cell after spiking the $Reagent^{(Mo)}$. (Please note that here and everywhere below the time intervals between spiking the reagent and the analysis were kept constant and identical to the ones described above for molybdenum calibration.) The resulting molybdenum concentration in the sample at the outlet of the Mo-module *vs* its concentration in the feeding solution is shown in Figure 2.6.6b and suggests a linear character of this correlation with the molybdate "recovery" close to 70-75 % (apart from the first calibration point where the recovery approaches 40 %). The resulting molybdate concentration of 2 mM was chosen for further experiments in accordance with the recently described protocols for phosphate detection.[5,7] Thus, the 3 mM Na_2MoO_4 reagent was used for the feeding molybdate-reservoir of the Mo-module. Nevertheless it was kept in mind that, once the electrochemical detection is achieved and all the parameters of the complex in-line system are adjusted, the molybdate concentration in the Mo-module can be re-optimized as needed.

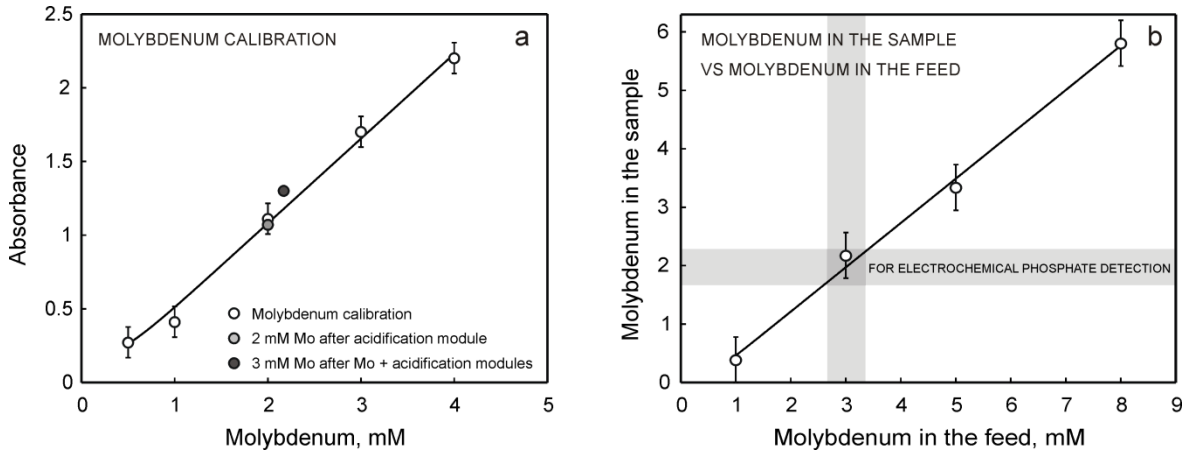

Figure 2.6.6. Molybdenum detection at 660 nm in the UV flow cell (flow rate ca. 90 µL min^{-1}). (a, white circles) Calibration line obtained from the colorimetric trace shown in Figure 2.6.5, by passing molybdate calibration solutions with 0.6 M NaCl background, spiked with Reagent$^{(P)}$, directly to UV detection (avoiding additional modules). (a, gray circle) Absorbance signal after passing the solution containing 2 mM molybdate and 0.6 M NaCl background through the H-module and subsequent spiking with Reagent$^{(Mo)}$ (but containing no sulfuric acid) prior to the detection. (a, black circle) Absorbance signal after passing the solution containing 3 mM molybdate through the Mo-module, then H-module and subsequent spiking with Reagent$^{(Mo)}$ (but containing no sulfuric acid and molybdate) prior to the detection. (b) Molybdenum concentration detected colorimetrically (using calibration line shown in Figure 2.6.6.a) at the outlet of the molybdate module *vs* initial molybdate concentration in the solution with 0.6 M NaCl background.

To make sure that no molybdate losses occur while passing the sample through the H-module the following two experiments were performed. Firstly, a sample containing 2 mM Na_2MoO_4 and 0.6 M NaCl background was passed through the H-module. The liquid sampled at the outlet of the sample compartment was spiked with the Reagent$^{(Mo)}$ containing all components but sulfuric acid (as the sample has been sufficiently acidified while passing through the H-module) and was analysed colorimetrically. Secondly, the same manipulations were performed with the sample containing 3 mM Na_2MoO_4 and 0.6 M NaCl background, after having passed it first through the Mo-module and then through the H-module. The results of the described two experiments are shown as gray and black circles in Figure 2.6.6a and confirm no visible losses of molybdenum due to coupling to the H-module: the resulting molybdate concentrations are close to the expected 2 mM value. The slightly elevated concentration (compared to the reported above) obtained for the sample having passed through both Mo- and H-modules accounts most probably for the slightly different pH of calibration solutions and analysed sample. Indeed, in this case no sulfuric acid has been added and the acidification of the sample happened passively by passing through the H-module which may have resulted in slightly different acidity.

It must be mentioned here that several attempts have been made to couple the modules in a reverse order (H-module first, then Mo-module) as it seemed more logical first to provide

the right pH conditions and then to proceed with the formation of the complex by releasing molybdate into the sample flow. However, the preliminary visual colorimetric experiments with both modules coupled in reverse order have shown that no coloration of the sample plug is observed after spiking the reagent, even if the concentration of molybdate in the molybdenum reservoir is significantly increased (up to 0.1 M Na_2MoO_4). The latter might account for the fact that molybdenum species formed in acidic media cannot cross the FAPQ membrane phase due to different charge or/and bulky dimensions. Indeed, the latter is probable since the underlying chemistry of MB reaction is in fact very complex due to the wide variety of molybdate speciation and protonation states.[19]

Given an anion-exchange membrane is used in the Mo-module, it was necessary to demonstrate whether phosphate loss occurs due to phosphate transport through the FAPQ-membrane from the sample into the molybdate-compartment. A preliminary colorimetric experiment was carried out in order to estimate possible phosphate loss, using different combinations of modules: H-module only, Mo-module only, and both modules together (Mo-module, then H-module). First, a mixed phosphate-reagent $Reagent^{(P)}$ containing ascorbic acid, potassium antimony tartrate, sulfuric acid (pH~1) and 2 mM molybdate (see Experimental part for the details, Section 2.6.3.3) was added to the calibration solutions with 0.6 M NaCl background, in order to obtain the calibration plot presented in Figure 2.6.7a. Then, solutions with different phosphate concentration and 0.6 M NaCl background were passed through the cell and subsequently analysed colorimetrically after spiking appropriate reagent. The mixed reagent for phosphate determination at the outlet of each particular module/module combination contained the same components (in the same reagent-to-sample ration) as $Reagent^{(P)}$, except from the component generated by the executed module/modules. Thus, when analysing the solution sampled at the H-module outlet, no sulfuric acid was added; when sampling at the Mo-module outlet, no molybdate was added; finally, only ascorbic acid and potassium antimony tartrate were used in case both modules were coupled together. The results of the colorimetric experiments described above are shown in Figure 2.6.7b.

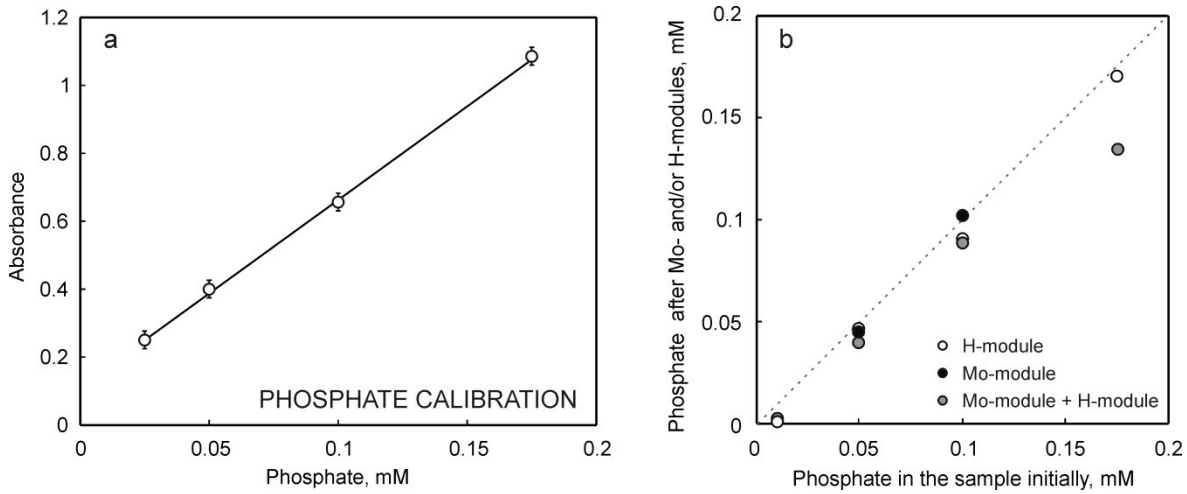

Figure 2.6.7. (a) Phosphate calibration obtained colorimetrically at 660 nm in the UV flow cell (flow rate ca. 90 µL min^{-1}) by passing phosphate calibration solutions with 0.6 M NaCl background, spiked with Reagent$^{(P)}$, directly to UV detection (avoiding additional modules). (b) Estimation of phosphate loss in the developed in-line Mo-module and/or H-module (flow rate ca. 90 µL min^{-1}), based on the calibration presented in Figure 2.6.7a. (b, white circles) Absorbance measured at 660 nm after passing phosphate solutions with 0.6 M NaCl background through the H-module and subsequent spiking with Reagent$^{(P)}$ (but containing no sulfuric acid) prior to the detection. (b, black circles) Absorbance measured at 660 nm after passing the phosphate solutions with 0.6 M NaCl background through the Mo-module and subsequent spiking with Reagent$^{(P)}$ (but containing no molybdate) prior to the detection.(b, gray circles) Absorbance measured at 660 nm after passing the phosphate solutions with 0.6 M NaCl background through the Mo-module, then H-module and subsequent spiking with Reagent$^{(P)}$ (but containing no sulfuric acid, neither molybdate) prior to the detection.

One must take into consideration that the obtained results can be only used as preliminary and semi-qualitative due to the reagent preparation procedure described above. Indeed, no perfect similarity must be expected between the samples spiked with acid and/or molybdate in a known sample-to-reagent ratio (as in case of calibration solutions) and the equivalent samples where protons and/or molybdate are being generated in the H-module and/or Mo-module. This is indeed the possible source of large losses observed at lower phosphate concentrations in Figure 2.6.7b which in fact account as well for big error due to the mentioned difference in reagent addition procedure for the sample and the calibrants. Moreover, every time the newly assembled module might have a slightly different geometry resulting in slightly different amount of protons/molybdate released in the sample. Yet the Figure 2.6.7b confirms that in the concentration range from 0.05 to 0.2 mM phosphate no dramatic loss of phosphate occurs. However, the results of this preliminary experiment suggest that the calibration and the analysis in the final configuration must be performed using the same in-line setup, always using the same modules. A more accurate estimation of phosphate loss effect (if any), especially at micromolar concentrations and lower, is only possible once a more sensitive method of detection is implemented.

2.6.4.2 Electrochemical detection in the developed in-line configuration

Electrochemical method of detection was chosen to allow for better limits of detection and at the same time for simpler potential integration of the approach for *in-situ* analysis. Following the above (Section 2.6.4.1), the final in-line configuration was chosen as simplistically presented in Figure 2.6.8. The more detailed scheme of the electrochemical detection arrangement (with relevant valves, pumps etc.) is given in the Experimental section (see Section 2.6.3.5, Figure 2.6.3)

Figure 2.6.8. Simplified schematic diagram of electrochemical detection arrangement (see Figure 2.6.3 for the detailed scheme).

Square wave voltammetry (SWV) was chosen for phosphate detection as it has been reported previously to be one of the most sensitive methods for electrochemical detection of phosphomolybdate complex in the flow as it allows for significant reduction of charging current effects.[11]

The electrochemical detection was achieved in a radial cross-flow cell described in the Experimental section (see Section 2.6.3.4.3, Figure 2.6.2). The radial flow cell gasket was chosen to provide the compartment volume of 13 µL. Unlike in the studies reported by V. Garçon et al.[11], where square wave voltammetry was accomplished on gold electrode, here a glassy carbon electrode was used as working electrode. It must be mentioned that preliminary studies have been performed with both types of electrodes (gold and glassy carbon), both in the bulk solution and in the flow cell. The results have shown that gold needs special care and regeneration of the surface after exposure to moderate concentrations of phosphomolybdate complex (even as low as 10^{-5} M), which did not seem to be easily achieved. Even polishing did not always result in satisfactory response. Gold being more capricious and the same time resulting in a very similar sensitivity, glassy carbon was chosen as a more suitable material that is easier-to-treat.

The electrochemical flow cell was coupled to the in-line setup described above, after the H-module (see Figure 2.6.8). The flow rate had to be decreased compared to the previous studies and was chosen ca. 40 µL min^{-1}. The latter is due to the very small volume of the radial cross-flow cell (13 µL) which does not allow for faster flow (leaking was noted at higher flow rates). The imposed decrease of the flow rate might cause a slight but not

critical increase in efficiency of molybdate and proton transport into the sample due to longer residence time of the sample plug in the Mo-module and H-module, respectively.

Unlike in the case of spectrophotometric measurements, here the electrochemical cell was directly coupled to the flow system. The SWVs were registered approximately every 47 sec, at two different frequencies (f = 50, 250 Hz), the amplitude (E_{SW}) has been fixed at 25 mV and the step potential (E_{step}) of 1 mV was chosen.[11] Figure 2.6.9a presents the square wave voltammograms obtained in the flow cell by passing solutions containing different amount of phosphate and 0.6 M NaCl background through the whole in-line configuration illustrated in Figure 2.6.8. In the potential window from 0 (starting potential) to 0.6 V (final potential) two peaks are observed, around 0.2 V and a bit higher than 0.3 V. The peaks correspond to the reduction of the phosphomolydate complex.

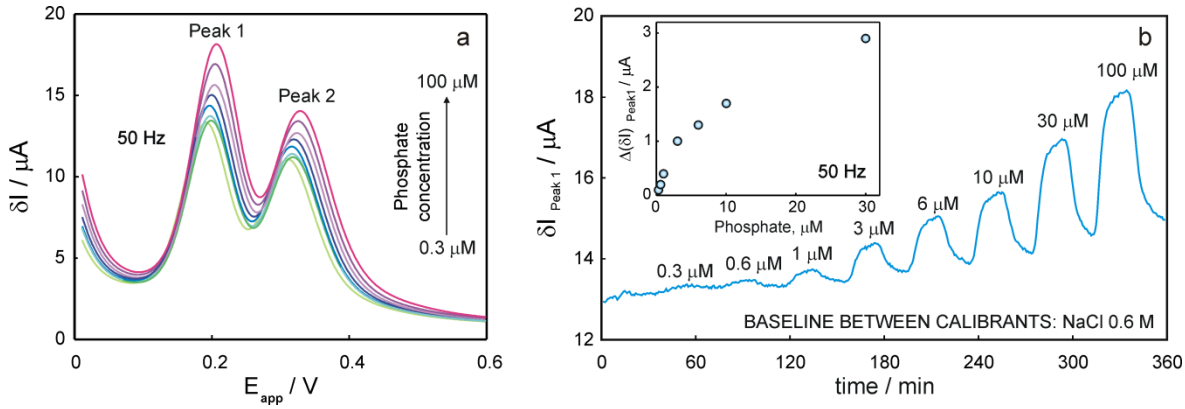

Figure 2.6.9. Square wave voltammetric detection in the developed in-line configuration (see Figure 2.6.8, flow rate ca. 40 μL min^{-1}). E_{SW} = 25 mV, E_{step} = 1 mV, f = 50 Hz. (a) Square wave voltammograms obtained for solutions containing different phosphate concentrations and 0.6 M NaCl background. (b) The peak current changes for the reduction peak at ~0.2 V (Peak 1) with time, upon changing phosphate concentration in the sample with 0.6 NaCl background. Phosphate concentrations are indicated in the figure (in μM). The signal recorded between the phosphate-containing samples corresponds to the baseline peak current (0.6 M NaCl passed through the in-line configuration). Figure inset presents the phosphate calibration curve corrected to the baseline drift: $\Delta(\delta I) = \delta I(\text{calibration solution}) - \delta I$ (preceding baseline solution).

The nature of the two reduction peaks does not find a uniform description in the literature. Most authors avoid specifying the exact reduction processes occurring at the indicated potentials. Some authors refer these two peaks to electrochemical reduction of Mo(VI) to Mo(IV) and Mo(IV) to Mo(II) respectively.[7] Others interpret the observed two peaks by the Mo(VI) reduction to two complexes comprising two different ratios of mixed oxidation states Mo(V)/Mo(VI).[11,12]

For instance, V. Garçon et al.[11] describe the two reduction peaks by the two following reactions with 2 and 3 electron-transfer:

$$\left[PMo_{12}^{(VI)}O_{40}\right]^{3-} + 2H^{+} + 2e^{-} \overset{E\approx 0.3V}{\leftrightarrow} \left[H_2PMo_2^{(V)}Mo_{10}^{(VI)}O_{40}\right]^{3-} \qquad \text{(eq. 2.6.2)}$$

$$\left[H_2PMo_2^{(V)}Mo_{10}^{(VI)}O_{40}\right]^{3-} + 3H^{+} + 3e^{-} \overset{E\approx 0.2V}{\leftrightarrow} \left[H_5PMo_5^{(V)}Mo_7^{(VI)}O_{40}\right]^{3-} \qquad \text{(eq. 2.6.3)}$$

The peak at E~0.2V (indicated as Peak 1 in Figure 2.6.9a) was chosen for further calibrations due to higher currents. However, it must be mentioned that, unlike within the studies reported by V. Garçon et al.[11] who observed the signal decrease for the reduction peak current at 0.3 V at higher concentrations, here the Peak 2 demonstrates very similar behaviour compared to Peak 1, just with slightly lower current amplitudes. Thus, Peak 2 could be potentially used instead. The latter might be relevant in case some interference is observed at 0.2 V but not at 0.3 V.

The peak current for the reduction peak at E~0.2V (Peak 1) is plotted *vs* time in Figure 2.6.9b, upon increasing phosphate concentration in solutions passed through in-line configuration presented in Figure 2.6.8 (0.6 M NaCl background, see Section 2.6.3.4.3 for details). Baseline solution (0.6 M NaCl), flushed through the system after every phosphate-containing solution, allowed for the baseline drift correction (here solutions were changed every 20 min). Thus, a calibration curve may be obtained by plotting the peak current corrected to the baseline (see inset in Figure 2.6.9b). The corrected peak current $\Delta(\delta \mathrm{I})$ for every phosphate concentration was obtained by extracting the baseline current recorded prior to passing the phosphate solution from the peak current obtained for the latter: $\Delta(\delta \mathrm{I}) = \delta \mathrm{I}(\text{calibration solution}) - \delta I(\text{preceding baseline solution})$.

An analogous trace has been obtained at the frequency 250 Hz, as presented in Figure 2.6.10a (note that the time-trace at 250 Hz is shifted down by ca. 15-20 μA in order to facilitate the comparison). However, a larger baseline drift is observed at higher frequency. Comparable results were obtained in a similar experiment with different time intervals between new solution plugs presented in Figure 2.6.10b. Here the solutions at the inlet of the system were changed every 10 min and the same solution was injected in the system three times in order check the drift both for the baseline and the phosphate-containing solution. Indeed, as can be seen in Figure 2.6.10b, a notable signal drift is observed in both cases.

The concentration of molybdate in the Mo-module was varied in order to study the influence of the latter on the performance of the system. The reagent compartment of Mo-module for the experiment presented in Figure 2.6.10c has been thoroughly washed with water for 30 min and then flushed with the molybdate solution 0.8 mM for at least 1 hour in order to ensure the complete exchange of the old solution. For the same reason, after completing the experiment, before starting the experiment shown in Figure 2.6.10d, a 8 mM molybdate solution was flushed through the Mo-module for at least 1 hour.

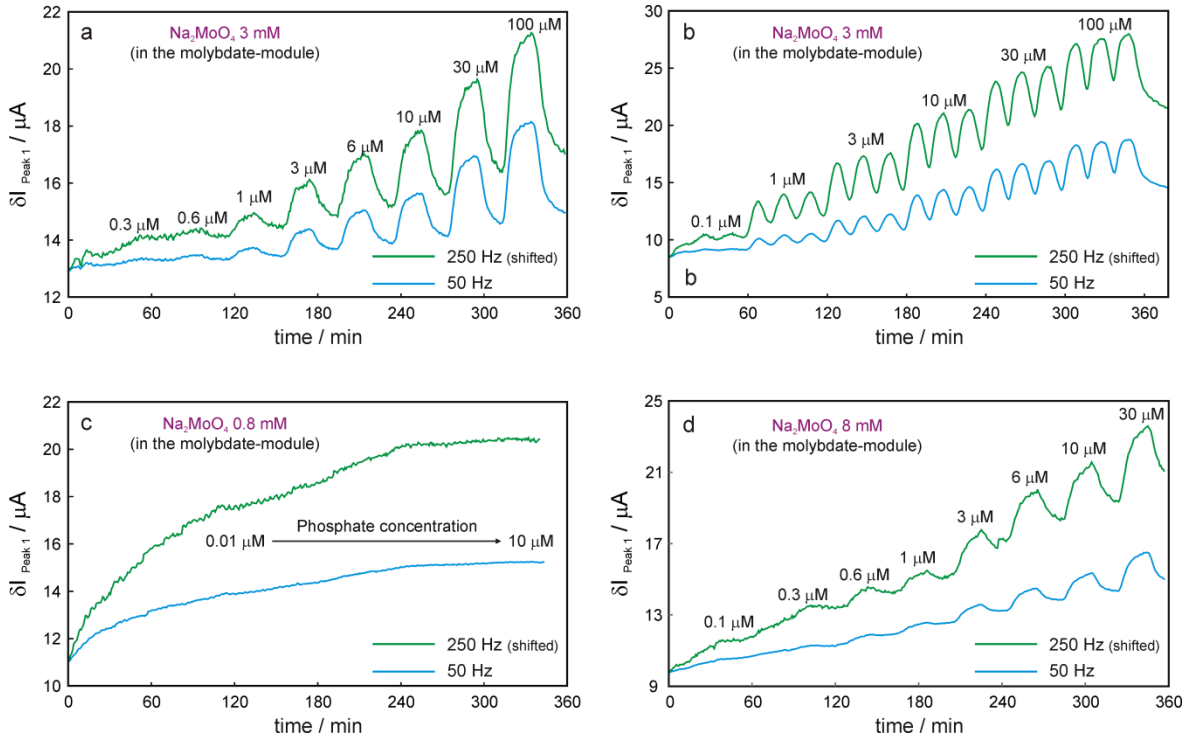

Figure 2.6.10. Comparison of phosphate calibration traces obtained by square wave voltammetric detection in the developed in-line configuration (see Figure 2.6.8, flow rate ca. 40 µL min^{-1}), using different concentration of molybdate in the Mo-module. The curves present the peak current changes (Peak 1, at ~0.2 V) with time upon changing phosphate concentration in the sample with 0.6 NaCl background. Phosphate concentrations are indicated in the figure (in µM). E_{SW} = 25 mV, E_{step} = 1 mV, f = 50 Hz (blue line), 250 Hz (green line). The green lines are shifted down by 15-20 µA in order to facilitate the comparison of the two traces. The signal recorded between the phosphate-containing samples corresponds to the baseline peak current (0.6 M NaCl passed through the in-line configuration).

The results presented in Figures 2.6.10c suggest that 0.8 mM molybdate concentration in the Mo-module is too low to resolve the desired phosphate concentrations. At the same time increasing the molybdate concentration in the module up to 8 mM results in similar response (as compared to 3 mM), however a significantly larger signal drift is observed along with a lower difference $\Delta(\delta I)$ between the baseline and the calibrant signal. Therefore, we have confirmed that the 3mM molybdate reagent concentration, chosen

based on preliminary colorimetric experiments (see Section 2.6.4.1.2.2) and previously reported electrochemical protocols,[5,7] is close to the optimum one.

Few attempts were made in order to eliminate or reduce the baseline drift. Firstly, a conditioning step (preconcentration step) was introduced at 0 V during 60 s before the SWV experiment, since the latter approach has resulted in good reproducibility in the preliminary experiments in the bulk solution. Figure 2.6.11 presents the results obtained for the bulk experiment (Figure 2.6.11a) compared to the experiment in the electrochemical flow cell (Figure 2.6.11b). The parameters of the electrochemical detection in both setups are identical (f = 250 Hz, E_{SW} = 25 mV, E_{step} = 1 mV), the conditioning/preconcentration step (0 V, 60 s) was introduced in both procedures. The bulk experiment demonstrates gradual increase of the peak potential with increasing phosphate concentration in the sample (Figure 2.6.11a), while no clear correlation between peak current and phosphate concentration is observed for the flow experiment with the conditioning step. Similar results are obtained at lower frequency (50 Hz) in the flow cell, as can be seen in Figures 2.6.12b. As follows from the peak current trace shown in Figures 2.6.12b, the erratic changes in peak current upon increasing phosphate concentration, observed in Figure 2.6.11b and Figure 2.6.12b, account for the drastic and irregular drift/decrease of the signal with time, both for the samples and the baseline. The registered drift completely conceals the phosphate response of the system.

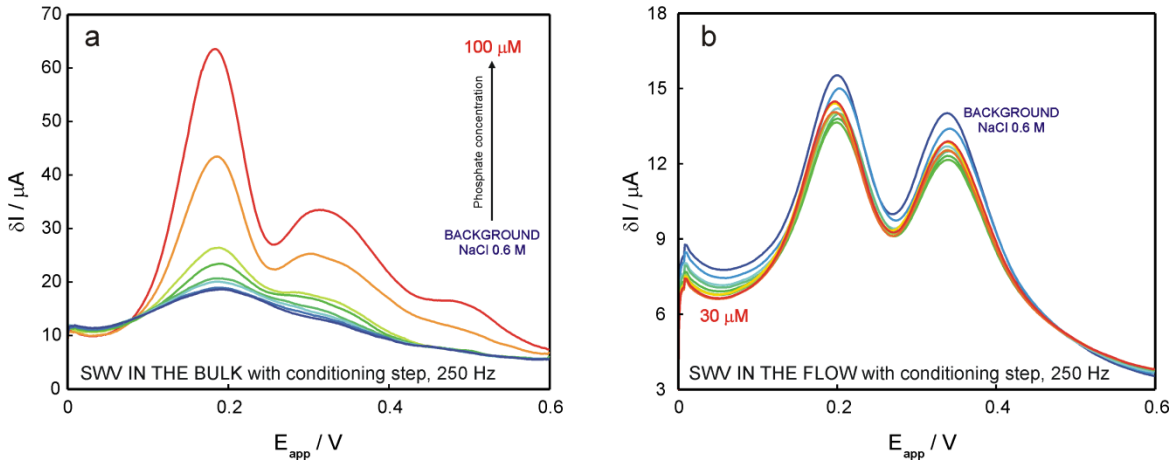

Figure 2.6.11. Comparison of square wave voltammetric detection in the bulk (a) and in the developed in-line configuration (b, see Figure 2.6.8, flow rate ca. 40 µL min^{-1}), both with a conditioning/preconcentration step at 0 V during 60 s prior to detection. E_{SW} = 25 mV, E_{step} = 1 mV, f = 250 Hz. The SWV detection in the bulk (a) and the preceding conditioning step were carried out without stirring, stirring between the experiments before every new conditioning step.

Another attempt was made to reduce the baseline drift by introducing a "washing-step" between measurements in different solutions, by cyclic voltammetry in sulfuric acid ~0.2 M for about 20 min. This method was chosen due to the fact that cyclic voltammetry

has been shown to "clean" the electrode surface in the preliminary experiments both in the bulk and in the flow. Indeed, after finishing one calibration experiment and reaching moderately high molybdate concentrations (30 µM and higher), when returning into the solution containing no molybdate neither phosphate, the two peaks ("background-peaks") would still appear on the voltammogram (results not shown). The latter accounts probably for the adsorption processes at the electrode surface.

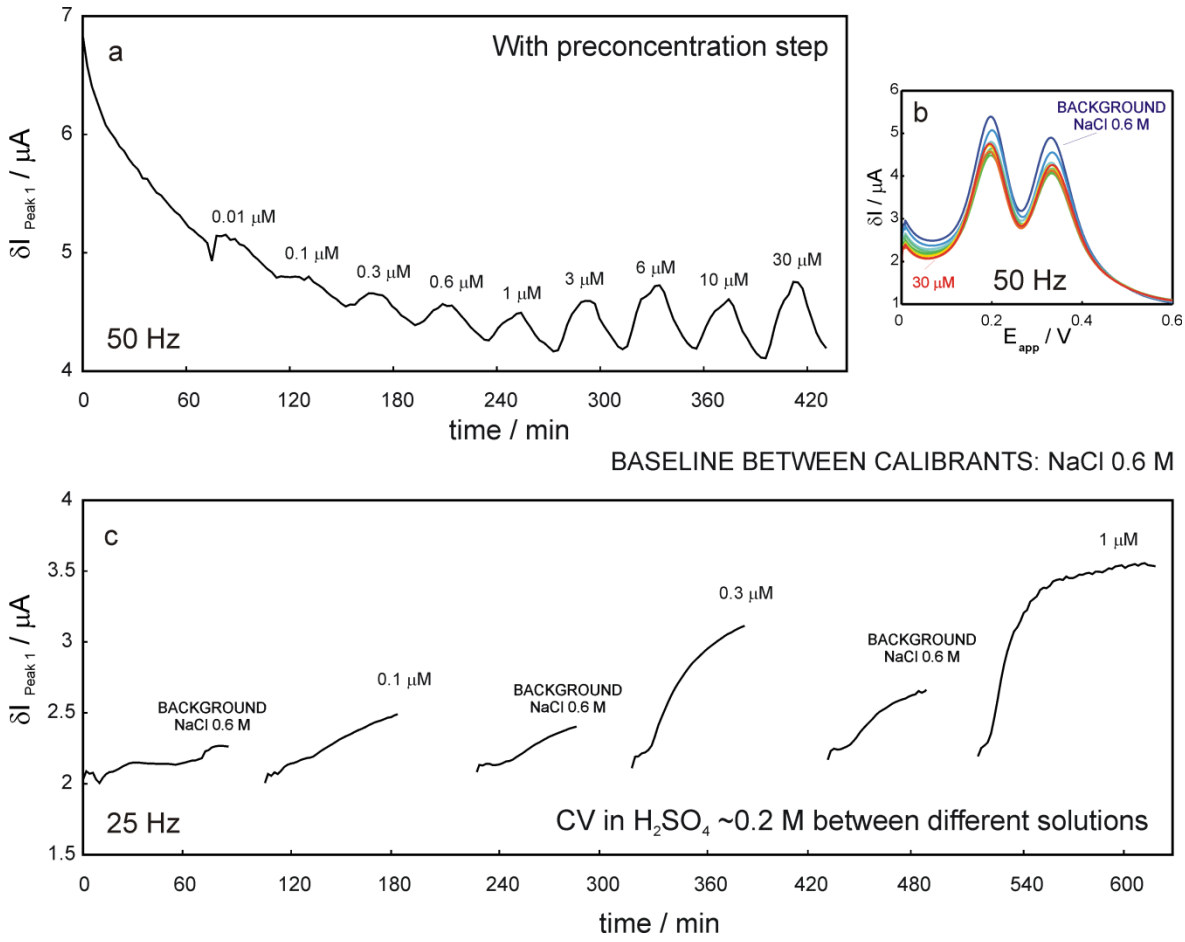

Figure 2.6.12. Exploring square wave voltammetric protocols as an attempt to reduce the baseline drift in the developed flow configuration (see Figure 2.6.8, flow rate ca. 40 µL min^{-1}). E_{SW} = 25 mV, E_{step} = 1 mV. (a, b) With a conditioning/preconcentration step at 0 V during 60 s prior to detection with stirring before the conditioning step (between different SWV experiments), f = 50 Hz. (a) The peak current changes for the reduction peak at ~0.2 V (Peak 1) with time, upon changing phosphate concentration in the sample with 0.6 NaCl background. (b) Square wave voltammograms obtained for solutions containing different phosphate concentrations and 0.6 M NaCl background. (c) With a "washing-step" by running cyclic voltammetry in sulfuric acid ~0.2 M for 20-30 min: potential window from -0.7 to 1.0 V (starting potential -0.7 V), scan rate 50 mV/s. The "washing-step" has been applied prior to SWV detection in the new sample plug (f = 50 Hz). The line illustrates the change in reduction peak current at ~0.2 V (Peak 1) with time, upon changing phosphate concentration in the sample with 0.6 NaCl background. The signal recorded between the phosphate-containing samples in (a) and (c) corresponds to the baseline peak current (0.6 M NaCl passed through the same in-line configuration). Phosphate concentrations are indicated in the figures (in µM).

It was discovered experimentally that the surface of GC working electrode could be regenerated either by polishing or by running continuous CV in a solution of sulfuric acid for ca. 20 min or less, in order to remove the "background-peaks". As polishing would have been an unacceptable procedure for the flow configuration, we have decided to implement the CV-based "cleaning" procedure in the flow by introducing another valve in the system allowing for switching between the working solution (calibrant or background) and the "washing-solution" (sulfuric acid ~0.2 M). The results of the experiment are presented in Figure 2.5.12c.

As demonstrated in Figure 2.6.12c, the introduced protocol allowed to increase the sensitivity of the method: indeed, a clear difference can be noticed already between the peak currents for the background solution and the solution containing 0.1 μM phosphate while the lower detection limit for the protocol presented above (in Figure 2.6.9) is ca. 0.6 μM. However, the integration of the "washing-step" by cyclic voltammetry does not allow for any significant reduction of the background drift: it can be clearly seen that the baseline peak current is notably increasing with time. Therefore, for the further experiments we have eliminated the "washing-step" for now, as the latter significantly increases the time of the experiment.

The last attempt to decrease the background noise was made by reversing the potential ramp direction by scanning from 0.6 V to 0 V, in contrast to the experiments shown above where the potential was changed from 0 V and 0.6 V. It must be noted that the same (reverse) potential ramp was used by V. Garçon et al.[11] for SWV phosphate detection. However, no big significance was given initially to the potential ramp direction as for a reversible redox reactions the square wave voltammograms obtained by forward and reverse scans are expected to be similar and independent of the starting potential.[20]

The calibration trace obtained for the reverse scan (see Figure 2.6.13a) is very similar to the one obtained for the forward potential ramp, however it demonstrates lower peak currents compared to the forward scan (see Figure 2.6.9 for the comparison). The latter fact hardly affects the observed lower detection limit as the peak current decreases both for the background and the calibrants to a similar extent. However, as before, a considerable drift of the baseline is observed.

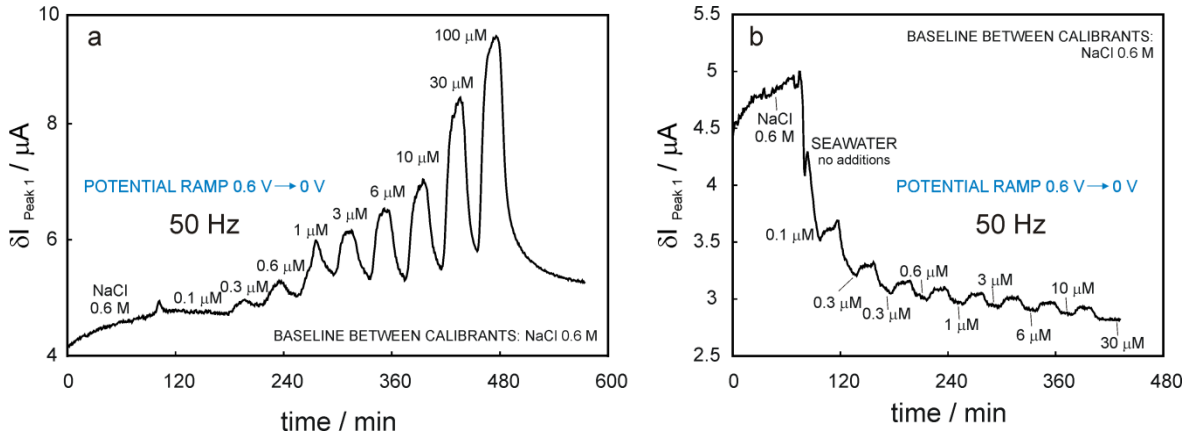

Figure 2.6.13. Phosphate calibration traces obtained by square wave voltammetric detection in the developed in-line configuration (see Figure 2.6.8, flow rate ca. 40 µL min^{-1}) using a reverse potential ramp (from 0.6 V to 0 V). E_{SW} = 25 mV, E_{step} = 1 mV, f = 50 Hz. The curves present the peak current changes (Peak 1, at ~0.2 V) with time upon increasing phosphate concentration in the sample with 0.6 NaCl (a) and seawater (b) background. Phosphate concentrations are indicated in the figure (in µM). The signal recorded between the phosphate-containing samples corresponds to the baseline peak current (0.6 M NaCl passed through the same in-line configuration).

To conclude the results of all three attempts aimed at the improvement of the baseline stability: the signal drift has not been eliminated/decreased within the framework of this work. The signal increase with time requires further thorough investigation but most probably occurs due to some surface-confined processes at the glassy carbon electrode.

Despite of the baseline drift, it was possible to demonstrate the applicability of the developed approach for phosphate detection in real seawater matrix. Figure 2.6.14a confirms the capability of the method to resolve submicromolar phosphate concentrations. However, it came as a surprise that no phosphate response is observed when reversing the potential ramp direction, as presented in Figure 2.6.13b. It can be seen that, upon reversing the potential ramp direction, a significant peak current drop occurs after introducing the seawater sample in the flow setup (see Figure 2.6.13b), both for seawater plugs spiked with phosphate and for the baseline containing neither seawater matrix nor phosphate. The baseline drift continues towards lower values, unlike in all flow experiments shown above. The latter is neither observed for the forward ramp direction in seawater sample (see Figure 2.6.14) where a notable increase of peak current is observed upon increasing phosphate concentration while a significant baseline increase occurs with time.

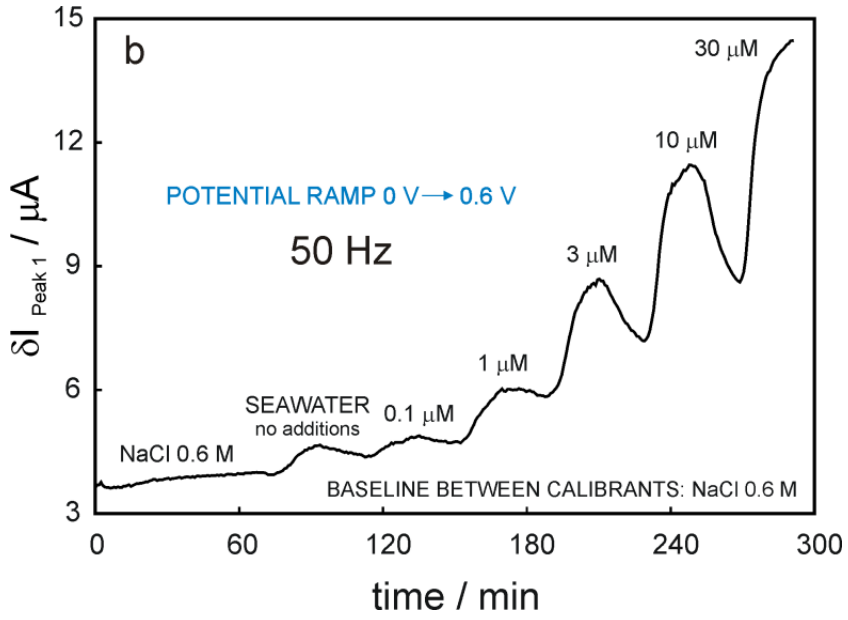

Figure 2.5.14. Phosphate calibration traces in seawater matrix obtained by square wave voltammetric detection in the developed in-line configuration (see Figure 2.6.8, flow rate ca. 40 μL min^{-1}) using a forward potential ramp (from 0 V to 0.6 V). E_{SW} = 25 mV, E_{step} = 1 mV, f = 50 Hz. The curves present the peak current changes (Peak 1, at ~0.2 V) with time upon increasing phosphate concentration in the sample with seawater background. Phosphate concentrations are indicated in the figure (in μM). The signal recorded between the phosphate-containing samples corresponds to the baseline peak current (0.6 M NaCl passed through the same in-line configuration).

The significant influence of the potential ramp direction in seawater matrix is as well reflected in the shape of the square wave voltammograms shown in Figure 2.6.15. Indeed, two distinctive reduction peaks are observed for the forward potential ramp (from 0 V to 0.6 V, Figure 2.6.15a,c) in the seawater spiked with phosphate (1 μM and 10 μM). The shape of the waves and the peak current range is very similar to those obtained earlier for SWV in phosphate solutions with 0.6 M NaCl background (shown in Figure 2.6.14), with the exception that the peak potentials are shifted towards higher values by 55-60 mV (see Figure 2.6.15e for comparison). The observed lower peak currents account most probably for slightly different experimental conditions resulting from reassembling the whole in-line setup. The latter assumption is supported by the fact that the baseline peak current (in NaCl 0.6 M, please compare Figure 2.6.9b and Figure 2.6.14) is also much lower for the second experiment. On the contrary, no peak potential shift is observed for the reversed potential ramp (from 0.6 V to 0 V, Figure 2.6.15b,d,e), however, despite of the same baseline peak current obtained in 0.6 NaCl (see Figure 2.6.13a,b for comparison), much lower currents are observed in seawater matrix compared to 0.6 NaCl background. Moreover, the two reduction peaks are much wider and merge with time.

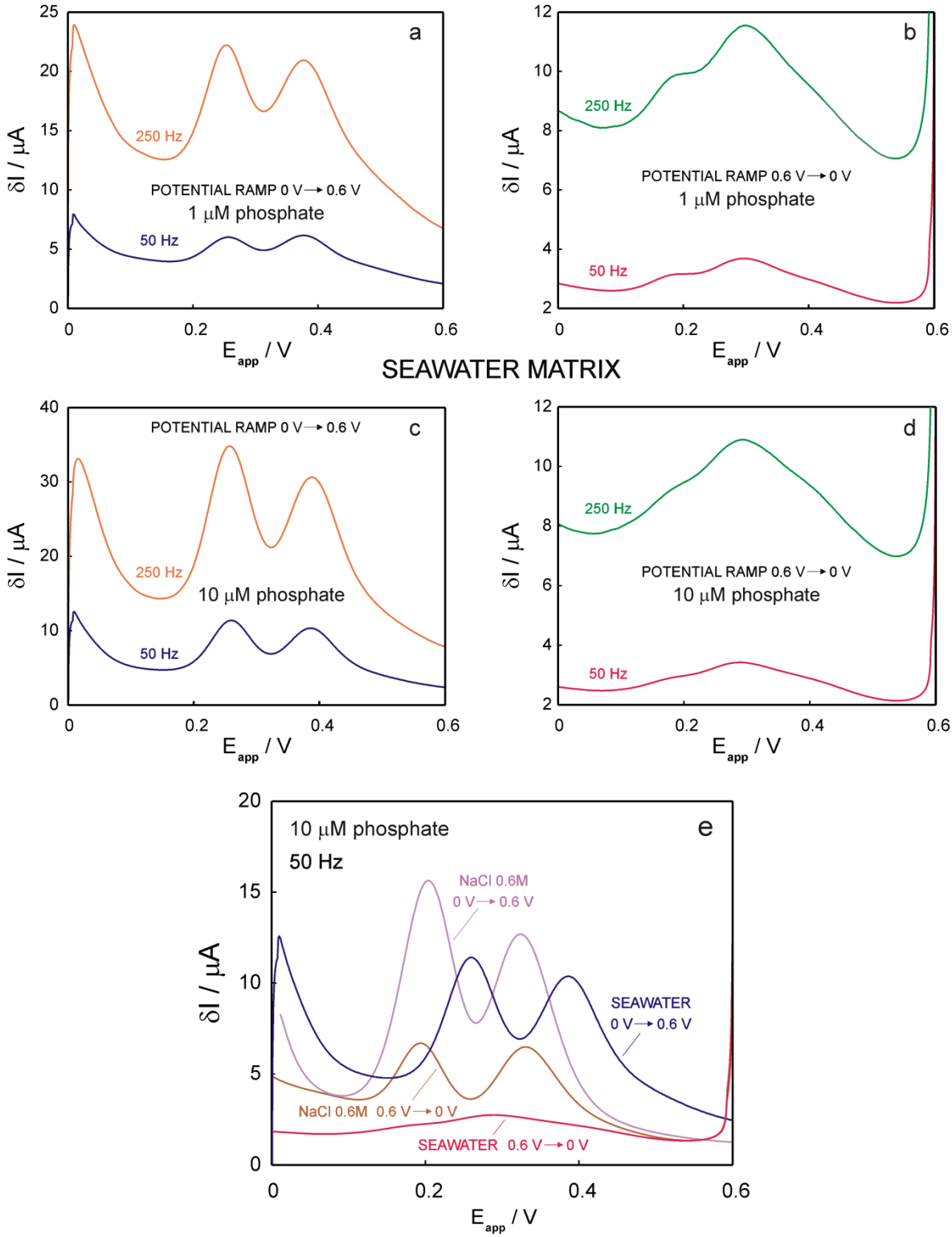

Figure 2.6.15. Comparison of square wave voltammetric detection by applying forward (from 0 V to 0.6 V) and reverse (from 0.6 V to 0 V) potential ramps in the developed in-line configuration (see Figure 2.6.8, flow rate ca. 40 μL min^{-1}). E_{SW} = 25 mV, E_{step} = 1 mV (no conditioning steps applied). (a, c) SWV by applying forward potential ramp for the solutions containing 1and 10 μM phosphate at 50 Hz (blue line) and 250 Hz (orange line) in seawater matrix. (b, d) SWV with the forward potential ramp for the solutions containing 1and 10 μM phosphate at 50 Hz (red line) and 250 Hz (green line) in seawater matrix. (e) Comparison of square wave voltammetric detection by applying forward (purple and blue lines) and reverse (brown and red lines) potential ramps at 50 Hz for the solutions containing 10 μM phosphate with 0.6 M NaCl (purple and brown lines) and seawater (blue and red lines) as background.

The observed drastic influence of the potential ramp direction in real seawater matrix may originate from interference coming from other species present in seawater and participating in redox reactions and/or surface-confined processes at the working electrode. Thus, further rigorous studies are necessary to obtain more information about the interfering processes involved as well as about the surface-confined reactions causing the baseline drift, in order to optimize the suggested protocol for real sample analysis and subsequent field monitoring.

2.6.5 Conclusions

A flow system has been developed allowing for in-line delivery of protons and molybdate anions into the sample, resulting in the formation of electroactive phosphomolybdate complex in view of subsequent phosphate detection in seawater. Concentrations of reagents were optimized in the acidification and molybdate modules, based on colorimetric experiments. The developed approach has been successfully coupled with the electrochemical phosphate detection in NaCl 0.6 M, allowing for the detection limits of ca. 0.6 µM in a simple protocol (no conditioning steps) and as low as 0.1 µM in a protocol with a "washing-step" using cyclic voltammetry in sulfuric acid between measurements.

A notable signal drift has been recorded over long-time measurements. Yet the results can be corrected for the drift by running the baseline (0.6 M NaCl) between the measurements. A drastic effect of the potential ramp direction has been observed for seawater samples. The forward potential ramp has been shown to result in adequate performance of the proposed in-line configuration for resolving submicromolar phosphate concentrations in seawater sample. However, the reverse potential ramp resulted in a gradual decrease of the peak currents, along with gradual merging of the two reduction peaks over time, and has been shown to be unable to resolve different phosphate concentrations even as high as 30 µM.

Both signal drift over time and the drastic influence of the potential ramp direction in real seawater matrix must account for some interfering surface-confined processes at the working electrode and require further studies in order to optimize the suggested protocol for real sample analysis and eliminate/decrease the baseline drift.

It should be considered that certain parameters can still be optimized within a short range of variations once the final optimal detection conditions are achieved. For example, HCl flow in the reagent compartment of the acidification module could be looped or/and HCl

concentration could be decreased in order to use less reagent or less concentrated reagent. Molybdate concentration can varied (decreased/increased within a short millimolar range) in order to achieve the best possible performance.

2.6.6 Acknowledgements

The author acknowledges financial support by the Swiss National Science Foundation (FNS Sinergia CRSII2-147654) and the EU Seventh Framework Program (FP7-OCEAN 2013.2 SCHeMA project - Grant Agreement 614002).

2.6.7 References

(1) Estela, J. M.; Cerda, V. *Talanta* **2005**, *66*, 307-331.

(2) McDowell, R. W.; Hamilton, D. P. *Mar. Freshwater Res.* **2013**, *64*, iii-vi.

(3) Strickland, J. D.; Parsons, T. R. *A practical handbook of seawater analysis*: Ottawa, 1972, p 310.

(4) Zhang, J. Z.; Fischer, C. J.; Ortner, P. B. *Talanta* **1999**, *49*, 293-304.

(5) Jonca, J.; Giraud, W.; Barus, C.; Comtat, M.; Striebig, N.; Thouron, D.; Garcon, V. *Electrochim. Acta* **2013**, *88*, 165-169.

(6) Paytan, A.; McLaughlin, K. *Chem. Rev.* **2007**, *107*, 563-576.

(7) Kolliopoulos, A. V.; Kampouris, D. K.; Banks, C. E. *Anal. Chem.* **2015**, *87*, 4269-4274.

(8) Chen, Z.; De Marco, R.; Alexander, P. W. *Anal. Commun.* **1997**, *34*, 93-95.

(9) Chen, Z.; Grierson, P.; Adams, M. A. *Anal. Chim. Acta* **1998**, *363*, 191-197.

(10) Nollet, L. M. L. *Handbook of Water Analysis, Second Edition*; CRC Press: Boca Raton, 2007, p 769.

(11) Barus, C.; Romanytsia, I.; Striebig, N.; Garçon, V. *Talanta* **2016**, *160*, 417-424.

(12) Talarico, D.; Cinti, S.; Arduini, F.; Amine, A.; Moscone, D.; Palleschi, G. *Environ. Sci. Technol.* **2015**, *49*, 7934-7939.

(13) Jonca, J.; Leon Fernandez, V.; Thouron, D.; Paulmier, A.; Graco, M.; Garcon, V. *Talanta* **2011**, *87*, 161-167.

(14) Gray, S.; Hanrahan, G.; McKelvie, I.; Tappin, A.; Tse, F.; Worsfold, P. *Environ. Chem.* **2006**, *3*, 3-18.

(15) Trojanowicz, M. *Flow injection analysis: instrumentation and applications*; World Scientific: Singapore, 2000, p 481.

(16) Pankratova, N.; Cuartero, M.; Cherubini, T.; Crespo, G. A.; Bakker, E. *Anal. Chem.* **2017**, *89*, 571-575.

(17) Cuartero, M.; Crespo, G. A.; Bakker, E. *Anal. Chem.* **2015**, *87*, 1981-1990.

(18) Chester, R.; Jickells, T. *Marine Geochemistry, 3rd edition*; John Wiley & Sons: Oxford, 2012, p 411.

(19) Nagul, E. A.; McKelvie, I. D.; Worsfold, P.; Kolev, S. D. *Anal. Chim. Acta* **2015**, *890*, 60-82.

(20) Komorsky-Lovric, S.; Lovric, M. *Int. J. Electrochem. Sci.* **2014**, *9*, 435-444.

3 CONCLUSIONS

- A newly-proposed autonomously running flow analysis setup, comprising an array of PVC-based ion-selective electrodes with liquid inner filling solution, has been successfully integrated for continuous on-site measurements in lake Greifensee (Switzerland) for potentiometric determination of calcium, nitrate, carbonate ions and pH, using an automatized continuous two-point calibration. The results of on-site field analysis have been validated by laboratory measurements. The developed sensing array may serve as a promising tool for continuous on-site monitoring of any ionic species detectable by potentiometry. (Section 2.1)

- Thereafter, another potentiometry-based array has been proposed, this time for *in-situ* monitoring. The developed array is submersible and autonomous and is composed of all-solid state potentiometric sensors sensitive to carbonate, calcium ions and pH. The submersible potentiometric probes have been successfully deployed in the sea (Genoa Harbor in Italy, Arcachon Bay in France). The significant advantage of the suggested setup, compared to the one previously executed in lake Greifensee, is its operation *in situ* requiring no pumping for the sample. The latter is critical for the detection of carbonate species since pumping must affects the carbonate equilibrium due to uncontrolled introduction of air in the sample flow by the boat water pump. The suggested flow setup provides for frequently performed automatized one-point calibration which allows for the correction of the electrode drifts. (Section 2.2)

- Further on, two new principally different concepts have been developed for the sample acidification in order to suppress hydroxide interference for potentiometric detection of anions in environmental samples. Both concepts have been explored with

ionophore-based membrane electrodes selective for the detection of nitrite or/and phosphate.

The first concept requires no flow and is based on local electrode surface acidification by proton release in the thin layer adjacent to the electrode membrane. Three different approaches were developed for the implementation of the proposed concept. All three require no pretreatment and suggest direct contact of the sensor with the natural sample. In a first approach, a concentrated acetic acid solution is placed in the inner filling solution of the PVC-based membrane electrode, forcing a significant acid gradient across the membrane. A second strategy achieves the same type of passive acidification by using an external proton source placed in front of a potentiometric solid contact anion-selective electrode where the thin layer gap allows one to observe spontaneous acidification at the opposing detection electrode. The third approach shares the same configuration, but protons are released by electrochemical control from the selective proton source into the thin layer sample. (Section 2.3).

The second concept suggests acidification of the bulk solution in a flow. The principle is based on the ion-exchange process between cations present in the sample and protons released through the preconditioned cation-exchange membrane (FKL, fumasep®) with constantly renewed hydrochloric acid reservoir behind the membrane. The acidification occurs in-line and allows for various resulting pH, depending on the flow rate, cation concentration in the sample compartment and acid concentration in the acid compartment. Moreover, the concept can be relatively easily adapted for *in-situ* measurements and provides for long-term continuous determination. No additional valves are required unlike with ion-exchange column where the latter needs to be periodically rinsed and re-conditioned. (Section 2.4)

- In the process of searching for a highly selective and sensitive phosphate receptor, instead of the latter, an ionophore has been discovered with remarkable performance for chloride detection in biological samples. The potentiometric properties of a series of fluorinated tripodal compounds have been investigated here and chloride detection in the undiluted serum samples has been accomplished, using ion-selective electrodes based on tren-based tris-urea bis(CF_3) tripodal compound (here labeled as Ionophore I), followed by successful validation using argentometric titration. It has been shown that doping the membrane with Ionophore I resulted in significantly improved potentiometric selectivity for chloride over major lipophilic anions, in comparison to traditionally used membranes

based on ion-exchanger tridodecylmethylammonium chloride (TDMACl) only. In fact, currently commercially available chloride ionophores do not provide better selectivity and stability for clinical applications than traditional TDMACl. At the same time, very few studies report on successful application of the newly-proposed compounds for potentiometric chloride detection in undiluted physiological samples. Apart from the remarkably improved performance of the ion-selective membranes doped with Ionophore I compared to TDMACl, the receptor in question has been shown to exhibit a good long-term stability of potentiometric performance over the period of 10 weeks. (Section 2.5)

- A microfluidic in-line flow configuration has been proposed for mixing of the sample with molybdate and hydrogen ions in order to form electrochemically active phosphomolybdate complex subsequently detected by square wave voltammetry. The principle of reagent (hydrogen and molybdate ions) delivery in the described in-line arrangement is based on the previously developed acidification module and accounts for the ion transport into the sample flow through cation-exchange membrane or anion-exchange, respectively. Phosphate concentrations as low as 0.1 μM could be resolved in a 0.1 M NaCl background. The proposed approach has been found to be applicable for the determination of submicromolar phosphate concentrations in seawater matrix when using square wave voltammetric detection with a forward potential ramp. Few issues, such as baseline drift and probable interferences in real sample matrix, still need to be resolved before implementing the developed setup for *in-situ* analysis of seawater. Nevertheless, the suggested approach builds a promising platform for phosphate detection in seawater by methodologies requiring formation of phosphomolybdate complex, be it electrochemical detection, as suggested here, or traditionally used colorimetric detection. The proposed setup is based on in-line configuration and is easy to integrate for subsequent *in-situ* determination in a submersible module of similar configuration as described in Section 2.2. (Section 2.6)

4 APPENDICES

APPENDIX 1. COMPLEMENTARY INFORMATION FOR CHAPTER 2.1

Table A1.1 GalvaPot method description as exemplified by the method chosen for the experiment performed on 21-22.08.2014: (a) Experiment Method and (b) Calibration Method.

a. Experiment Method		
Step N	Command	Command description
1	Pump 0003 0001 0202 0000	Start Pump 3 counterclockwise with speed 20.2 rpm
2	Pump 0002 0000 0202 0000	Stop Pump 2
3	Pump 0001 0000 0202 0000	Stop Pump 1
4	Pump 0004 0001 0024 0000	Start Pump 4 counterclockwise with speed 2.4 rpm
5	Pump 0005 0001 0024 0000	Start Pump 5 counterclockwise with speed 2.4 rpm
6	Pump 0006 0001 0202 0001	Start Pump 6 counterclockwise with speed 20.2 rpm
7	Dely 0180	Delay 180 sec
8	MesP 0008 0006	Measuring potential on eight channels averaging over 6 seconds for one channel
9	MesP 0008 0006	Measuring potential on eight channels averaging over 6 seconds for one channel
10	MesP 0008 0006	Measuring potential on eight channels averaging over 6 seconds for one channel
11	MesP 0008 0006	Measuring potential on eight channels averaging over 6 seconds for one channel
12	MesP 0008 0006	Measuring potential on eight channels averaging over 6 seconds for one channel
13	Pump 0001 0001 0202 0000	Start Pump 1 counterclockwise with speed 20.2 rpm
14	Pump 0003 0000 0202 0000	Stop Pump 3
15	Pump 0002 0000 0202 0000	Stop Pump 2
16	Pump 0004 0001 0024 0000	Start Pump 4 counterclockwise with speed 2.4 rpm
17	Pump 0005 0001 0024 0000	Start Pump 5 counterclockwise with speed 2.4 rpm
18	Pump 0006 0001 0202 0001	Start Pump 6 counterclockwise with speed 20.2 rpm
19	MesP 0008 0006	Measuring potential on eight channels averaging over 6 seconds for one channel
20	MesP 0008 0006	Measuring potential on eight channels averaging over 6 seconds for one channel
21	MesP 0008 0006	Measuring potential on eight channels averaging over 6 seconds for one channel
22	End	End of Experiment Method
b. Calibration Method		
Step N	Command	Command description
1	Pump 0001 0001 0202 0000	Start Pump 1 counterclockwise with speed 20.2 rpm
2	Pump 0002 0000 0202 0000	Stop Pump 2
3	Pump 0003 0000 0202 0000	Stop Pump 3
4	Pump 0004 0001 0024 0000	Start Pump 4 counterclockwise with speed 2.4 rpm
5	Pump 0005 0001 0024 0000	Start Pump 5 counterclockwise with speed 2.4 rpm
6	Pump 0006 0001 0202 0001	Start Pump 6 counterclockwise with speed 20.2 rpm
7	MesP 0008 0006	Measuring potential on eight channels averaging over 6 seconds for one channel
8	MesP 0008 0006	Measuring potential on eight channels averaging over 6 seconds for one channel
9	MesP 0008 0006	Measuring potential on eight channels averaging over 6 seconds for one channel

10	MesP 0008 0006	Measuring potential on eight channels averaging over 6 seconds for one channel
11	MesP 0008 0006	Measuring potential on eight channels averaging over 6 seconds for one channel
12	MesP 0008 0006	Measuring potential on eight channels averaging over 6 seconds for one channel
13	MesP 0008 0006	Measuring potential on eight channels averaging over 6 seconds for one channel
14	MesP 0008 0006	Measuring potential on eight channels averaging over 6 seconds for one channel
15	Pump 0002 0001 0202 0000	Start Pump 2 counterclockwise with speed 20.2 rpm
16	Pump 0001 0000 0202 0000	Stop Pump 1
17	Pump 0003 0000 0202 0000	Stop Pump 3
18	Pump 0004 0001 0024 0000	Start Pump 4 counterclockwise with speed 2.4 rpm
19	Pump 0005 0001 0024 0000	Start Pump 5 counterclockwise with speed 2.4 rpm
20	Pump 0006 0001 0202 0001	Start Pump 6 counterclockwise with speed 20.2 rpm
21	MesP 0008 0006	Measuring potential on eight channels averaging over 6 seconds for one channel
22	Dely 0240	Delay 240 sec
23	MesP 0008 0006	Measuring potential on eight channels averaging over 6 seconds for one channel
24	MesP 0008 0006	Measuring potential on eight channels averaging over 6 seconds for one channel
25	MesP 0008 0006	Measuring potential on eight channels averaging over 6 seconds for one channel
26	Pump 0001 0001 0202 0000	Start Pump 1 counterclockwise with speed 20.2 rpm
27	Pump 0002 0000 0202 0000	Stop Pump 2
28	Pump 0003 0000 0202 0000	Stop Pump 3
29	Pump 0004 0001 0024 0000	Start Pump 4 counterclockwise with speed 2.4 rpm
30	Pump 0005 0001 0024 0000	Start Pump 5 counterclockwise with speed 2.4 rpm
31	Pump 0006 0001 0202 0001	Start Pump 6 counterclockwise with speed 20.2 rpm
32	MesP 0008 0006	Measuring potential on eight channels averaging over 6 seconds for one channel
33	MesP 0008 0006	Measuring potential on eight channels averaging over 6 seconds for one channel
34	MesP 0008 0006	Measuring potential on eight channels averaging over 6 seconds for one channel
35	MesP 0008 0006	Measuring potential on eight channels averaging over 6 seconds for one channel
36	End	End of Calibration Method

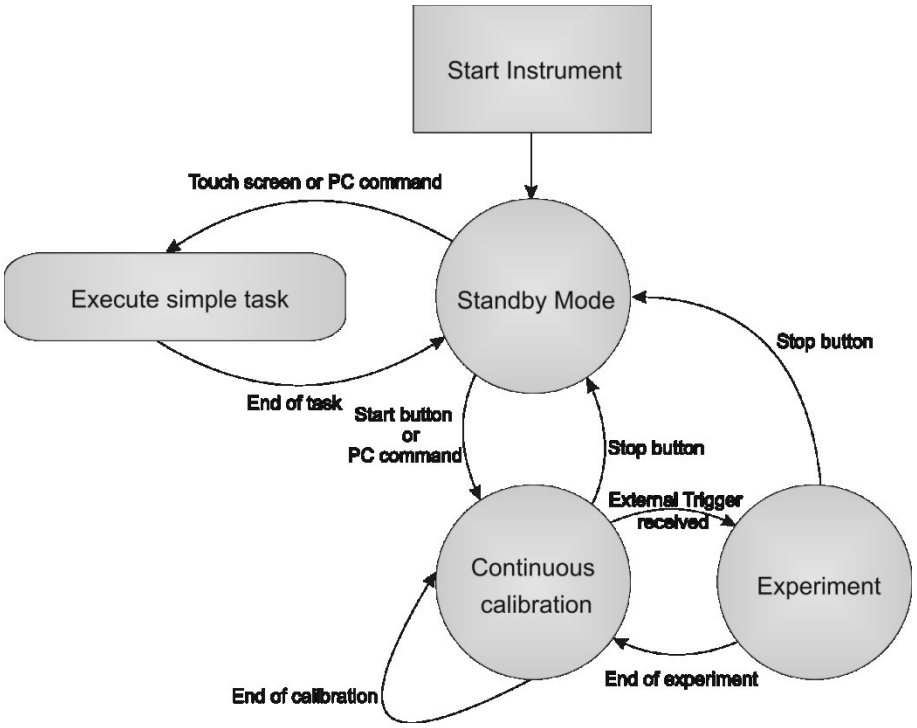

Figure A1.1. Working modes of GalvaPot v2.

Calculation of single ion activity in calibration solutions

Single ion activities a_i in calibration solutions were calculated based on concentration values indicated in Table 2.1.1 (main text) according to the conventional relationship:

$$a_i = \gamma_i \cdot c_i \qquad \text{(eq. A1.1)}$$

where γ_i is single ion activity coefficient and c_i the molar concentration of ion *i*.

γ_i was calculated in three steps:

1. The ionic strength I of the calibration solution was calculated using the following equation:

$$I = 0.5 \sum_i z_i^2 c_i \qquad \text{(eq. A1.2)}$$

2. Mean ion activity coefficients $\gamma_\pm$ for carbonate, ammonium and nitrate salts in mixed calibration solutions were calculated using the first approximation of the Debye-Hückel theory:

$$\log \gamma_{\pm} = -A|z_+ z_-|\sqrt{I} \qquad \text{(eq. A1.3)}$$

Mean ion activity coefficients $\gamma_{\pm}$ for concentrated calcium chloride solutions (1 mM and 10 mM $CaCl_2$) were calculated using the extended Debye-Hückel theory:

$$\log \gamma_{\pm} = -\frac{A|z_+ z_-|\sqrt{I}}{1 + B\sqrt{I}} + CI \qquad \text{(eq. A1.4)}$$

z_+ and z_- in equations A1.2 and A1.3 are charges of the ion *i* and corresponding counter ion; monovalent counter ions were considered since major ion species (sodium, bicarbonate, chloride) in calibration solutions are monovalent, and A is a parameter that is a function of temperature (A = 0.5108 at 25^{O}C). A is proportional to $T^{-3/2}$ (T is temperature in Kelvin) and changes inconsiderably in the range of the explored temperatures, thus for γ_i estimation we assume A to be constant. B and C are fittable parameters ($B \sim T^{-1/2}$, C with an unknown dependence on temperature) that are tabulated for most electrolytes.[1]

3. The simplified Debye-Hückel convention was used to calculate single ion activity coefficients γ_i ($\gamma_{Ca^{2+}}$, $\gamma_{NH_4^+}$, $\gamma_{NO_3^-}$ and $\gamma_{CO_3^{2-}}$) considering monovalent counter ions, as mentioned earlier:

$$\log \gamma_+ = \left|\frac{z_+}{z_-}\right| \log \gamma_{\pm} \quad (a)$$
$$\log \gamma_- = \left|\frac{z_-}{z_+}\right| \log \gamma_{\pm} \quad (b) \qquad \text{(eq. A1.5)}$$

The calculation procedure may be illustrated using carbonate activity coefficient calculation as an example. First, the ionic strength of the calibration solutions was calculated with equation A1.2 considering concentrations and charges of all the species present: K^+, Na^+ (including sodium added in the form of NaOH for adjusting the pH of calibration solution 1, NH_4^+, Ca^{2+} (free), $[Ca(NTA)]^-$, Cl^-, HCO_3^-, CO_3^{2-}, NO_3^-, $[OCH_2(HOCH_2)_2CNH_2]^-$ (dissociated TRIS), $[N(CH_2CO_2)_3]^{3-}$, $[NCH_2CO_2H(CH_2CO_2)_2]^{2-}$ (from NTA dissociation), SO_4^{2-} (for calibration solution 2 acidified with H_2SO_4). An ionic strength of 10.5 mM and 11.2 mM was obtained for calibration solutions 1 and 2, respectively. Second, mean ion activity coefficients $\gamma_{\pm}(Na_2CO_3)$ were calculated using

equation A1.3 where $z_+ = 1$, $z_- = -2$, $A = 0.5108$ resulting in $\log \gamma_{\pm}(Na_2CO_3)$ being -0.105 and -0.108 respectively. Finally, single ion activity coefficients $\gamma_{CO_3^{2-}}$ were calculated according to equation A1.5b where $z_+ = 1$, $z_- = -2$ giving $\gamma_{CO_3^{2-}} = 0.62$ for calibration solution 1 and $\gamma_{CO_3^{2-}} = 0.61$ for calibration solution 2.

To calculate single ion activities a_i according to equation A1.1, the pH measured by commercial glass electrode was used to correct carbonate and ammonium concentrations c_i for speciation using the acid dissociation constants:

$$K_{a2}(H_2CO_3) = \frac{c_{H^+} \cdot c_{CO_3^{2-}}}{c_{HCO_3^-}}, pK_{a2} = 10.32$$

$$K_a(NH_4^+) = \frac{c_{H^+} \cdot c_{NH_3}}{c_{NH_4^+}}, pK_{a2} = 9.25 \qquad \text{(eq. A1.6)}$$

References

(1) Meier, P. C. *Anal. Chim. Acta* **1982**, *136*, 363-368.

APPENDIX 2. COMPLEMENTARY INFORMATION FOR CHAPTER 2.2

Tables A2.1a,b. Between-day reproducibility of calibration parameters, slope (s) and standard potential (E^0) obtained for pH, carbonate and calcium potentiometric sensors based on (a) macroelectrodes and (b) miniaturized electrodes. A daily calibration during 5 days was accomplished for each electrode (n=2 for each species). E1-E6 labels indicate that two different electrodes were used for each analyte.

(a) Macroelectrodes:

calibration parameters	pH		CO_3^{2-}		Ca^{2+}	
	E1	E2	E3	E4	E5	E6
slope (mV)	-60.2 ± 0.1	-59.9 ± 0.1	-27.8 ± 0.2	-26.3 ± 0.1	29.8 ± 0.2	28.3 ± 0.2
E^0 (mV)	469.7 ± 2.5	475.2 ± 3.1	257.4 ± 2.2	249.5 ± 1.8	473.7 ± 2.9	480.0 ± 3.0

(b) Miniaturized electrodes:

calibration parameters	pH		CO_3^{2-}		Ca^{2+}	
	E1	E2	E3	E4	E5	E6
slope (mV)	-60.9 ± 0.2	-60.5 ± 0.1	-26.3 ± 0.2	-26.9 ± 0.2	28.8 ± 0.1	28.0 ± 0.2
E^0 (mV)	473.2 ± 1.9	492.5 ± 3.3	219.0 ± 3.1	234.0 ± 2.0	475.5 ± 1.7	469.2 ± 2.7

Tables A2.2a,b. Drifts of the electrode potentials observed in artificial seawater in the short term (during 24 h), medium term (during 50 hours) and long term (100 hours) using (a) macroelectrodes and (b) miniaturized electrodes. E1-E6 labels indicate that two different electrodes were used for each analyte.

(a) Macroelectrodes:

monitoring	pH		CO_3^{2-}		Ca^{2+}	
	E1	E2	E3	E4	E5	E6
short-term (mV h^{-1})	0.04	0.03	0.04	0.05	0.03	0.03
medium-term (mV h^{-1})	0.1	0.2	0.3	0.2	0.2	0.1
long-term (mV h^{-1})	0.4	0.6	0.7	0.8	0.5	0.4

(b) Miniaturized electrodes:

monitoring	pH		CO_3^{2-}		Ca^{2+}	
	E1	E2	E3	E4	E5	E6
short-term (mV h^{-1})	0.05	0.05	0.06	0.05	0.04	0.02
medium-term (mV h^{-1})	0.2	0.2	0.2	0.2	0.2	0.3
long-term (mV h^{-1})	0.7	0.8	1.1	1.0	0.8	1.0

Table A2.3. Results obtained for pH and calcium detection in seawater samples from Genoa coast (Italy) [Samples 1 and 2], Costa Calida (Murcia, Spain) [Samples 3 and 4] and Plentzia (Bilbao, Spain) [Sample 5]. pH was detected with (i) the potentiometric flow cell, (ii) in the beaker with macroelectrodes and (iii) with a pH-meter. Calcium was detected with (i) the potentiometric flow cell, (ii) in the beaker with macroelectrodes and (iii) with AAS.

sample	pH			Ca^{2+} (mM)		
	pH-meter	macroelectrodes[a]	flow cell[a]	AAS[a]	macroelectrodes[a]	flow cell[a]
1	8.01	7.99 ± 0.10	8.10 ± 0.10	12.25 ± 1.22	13.10 ± 0.75	12.30 ± 0.71
2	8.17	8.16 ± 0.07	8.15 ± 0.12	11.95 ± 1.10	12.03 ± 0.90	12.10 ± 1.12
3	7.98	7.92 ± 0.10	7.95 ± 0.10	12.10 ± 0.81	11.98 ± 1.11	11.95 ± 0.07
4	8.05	8.07 ± 0.08	8.00 ± 0.08	11.97 ± 0.16	11.77 ± 1.03	11.70 ± 0.52
5	8.15	8.15 ± 0.10	8.10 ± 0.05	12.41 ± 0.73	12.52 ± 0.52	12.63 ± 0.91

[a] Average ± SD (n=3)

Table A2.4. Results obtained for carbonate detection in seawater samples collected from Genoa coast (Italy) [Samples 1 and 2], Costa Calida (Murcia, Spain) [Samples 3 and 4] and Plentzia (Bilbao, Spain) [Sample 5], using three different approaches: (i) commercial CO_2 probe based on Severinghaus principle, (ii) in the beaker with macroelectrodes, (iii) with the potentiometric flow cell. Temperature, salinity and pH values are included in the table because they are needed for the calculation of carbonate concentration from the TCO_2 measured by the Severinghaus sensor.

Parameters				CO_3^{2-} (mM)[a]		
sample	T (°C)	salinity (PSU)	pH	Severinghaus	macroelectrodes	flow cell
1	22.1	37.01	8.01	0.25 ± 0.00	0.24 ± 0.01	0.23 ± 0.01
2	22.2	38.02	8.17	0.25 ± 0.00	0.24 ± 0.00	0.25 ± 0.02
3	22.2	37.52	7.98	0.20 ± 0.00	0.18 ± 0.01	0.20 ± 0.01
4	22.1	38.16	8.05	0.19 ± 0.01	0.18 ± 0.00	0.19 ± 0.01
5	22.1	37.95	8.15	0.25 ± 0.01	0.24 ± 0.01	0.24 ± 0.01

[a] Average ± SD (n=3)

Note that, all the potentiometric measurements were accomplished under identical conditions of sample handling, temperature and stirring in order to avoid errors coming from different amounts of dissolved CO_2 during sample/environment equilibration.

APPENDIX 3. COMPLEMENTARY INFORMATION FOR CHAPTER 2.3

Estimation of acetic acid loss rate from the inner filling solution of the electrode
(Protocol A, see Figure 2.3.1a).

The rate of acetic acid loss was estimated based on Fick's first law of diffusion assuming linear concentration gradient in the diffusion layer in aqueous phase:

$$J_{\mathrm{HAc}}(t) = -D^{aq}_{\mathrm{HAc}} \frac{c^{o,aq}_{\mathrm{HAc}} - c^{*,aq}_{\mathrm{HAc}}}{\delta^{aq}},$$

where $J_{\mathrm{HAc}}(t)$ is the diffusion flux, D^{aq}_{HAc} - diffusion coefficient of acetic acid in the aqueous solution, $c^{o,aq}_{\mathrm{HAc}}$ - concentration of acetic acid in the aqueous phase at the electrode membrane surface, $c^{*,aq}_{\mathrm{HAc}}$ - concentration of the acetic acid in the bulk of the aqueous phase, δ^{aq} - thickness of diffusion layer in the aqueous phase.

$$D^{aq}_{\mathrm{HAc}} = 1.2 \cdot 10^{-5}\, cm^2 \cdot s^{-1} \quad [1]$$

$c^{o,aq}_{\mathrm{HAc}}$ was estimated based on the Tris buffer capacity (5 mM Tris, pH 8.3) resulting in $c^{o,aq}_{\mathrm{HAc}} = 3.15\, mM$. The estimation is based on the assumption that the resulting proton concentration at the surface is significantly lower than millimolar level and the influence of pH at the electrode surface is negligible compared to the capacity of the buffer. The assumption is in agreement with the data presented by Jadhav at al.[2] and with our data confirming that the pH at the membrane surface is in the working range of nitrite electrode between 4 and 6.5 (see Figure 2.3.2b).

$c^{*,aq}_{\mathrm{HAc}}$ was approximated as 0 considering the large sample volume (100 mL) compared to the volume of inner filling solution (2.2 mL). δ^{aq} was assumed to be equal to 100 µm (which is thickness of the spacer used to define the thin layer).

References

(1) Leaist, D. G.; Lyons, P. A. *J. Solution Chem.* **1984**, *13*, 77-85.
(2) Jadhav, S.; Bakker, E. *Electrochem. Solid-State Lett.* **1998**, *1*, 194-196.

APPENDIX 4. COMPLEMENTARY INFORMATION FOR CHAPTER 2.5

^{1}H NMR Titration Binding Studies

^{1}H NMR titrations were conducted on a Bruker Avance AVII400 FT-NMR spectrometer, operating at a frequency of 400 MHz for ^{1}H NMR with the probe temperature maintained at 298 K as determined using a variable temperature unit (± 5 K). All anions (chloride, salicylate and perchlorate) were added as tetrabutylammonium (TBA) salts, and were dried under high vacuum (< 1.0 mmHg) for 24 h before use. Stock solutions of host (~5.0 mM) were prepared in DMSO-d_6/0.5% H_2O mixture. The stock solutions (500 μL) were transferred into air-tight screw-cap NMR sample tubes (5 mm ID), and the same host stock solutions were then used for the preparation of standard titrant solutions containing approximately 100 mM of the various TBA-anion salts, hence maintaining the concentration of host constant (~5.0 mM) throughout the entire titration experiment.

In all cases, all proton resonances were monitored to study the trends of the change in chemical shifts. Thenceforth, both NH proton resonances were recorded, providing multiple sets of data from which the association constants were determined by global fitting analysis to the 1:1 and additive 1:2 (for TBA-chloride data only) binding models using the supramolecular.org web applet.[1,2] It should be emphasized that the global analysis approach of fitting all data sets simultaneously, greatly enhances the quality of the nonlinear curve fitting analysis. The covariance of fit is calculated by dividing the (co)variance of the residual (experimental data − calculated data) with the (co)variance of the experimental data. This value is independent of the number of parameters but reflects the distributions of the residuals. It is used here as a quantitative index to assess the quality of the fit between the fitting to the 1:1 and 1:2 binding models; the lower the value of the index, the better the fit.

Titration studies with TBA-perchlorate salts did not induce the downfield shifts of both NH proton resonances for all ionophores I-IV in this study, indicative of no binding toward perchlorate anion.

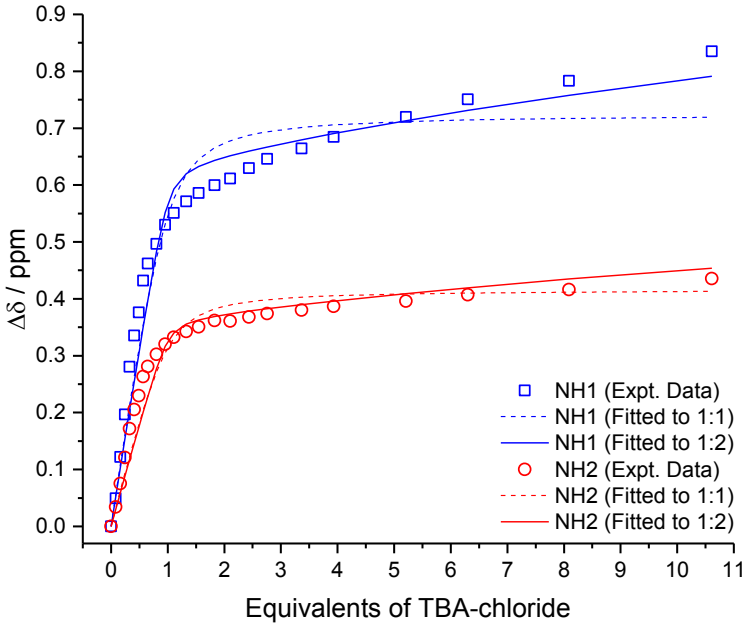

Figure A4.1. Fitted binding isotherms of ^{1}H NMR titration (400 MHz, 298 K) of ionophore I (4.9 mM) with TBA-chloride in DMSO-d_6/0.5% H_2O mixture, showing the change in chemical shifts (Δδ) for thiourea NH resonances, fitted to the 1:1 and additive 1:2 binding models. Covariance of fit: 0.041 and 0.029 for 1:1 and 1:2 respectively.

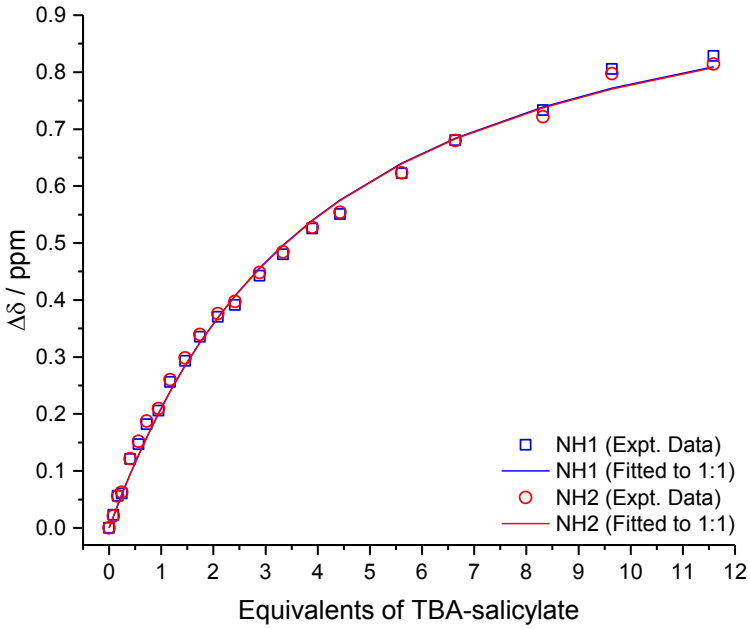

Figure A4.2. Fitted binding isotherms of ^{1}H NMR titration (400 MHz, 298 K) of ionophore I (4.9 mM) with TBA-salicylate in DMSO-d_6/0.5% H_2O mixture, showing the change in chemical shifts (Δδ) for thiourea NH resonances, fitted to the 1:1 binding model. Covariance of fit: 0.0038.

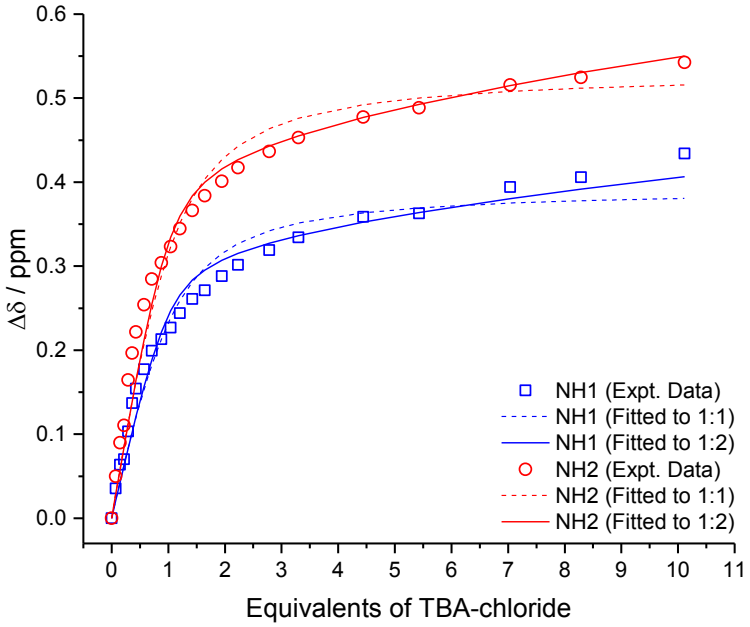

Figure A4.3. Fitted binding isotherms of ^{1}H NMR titration (400 MHz, 298 K) of ionophore II (5.2 mM) with TBA-chloride in DMSO-d_6/0.5% H_2O mixture, showing the change in chemical shifts (Δδ) for thiourea NH resonances, fitted to the 1:1 and additive 1:2 binding models. Covariance of fit: 0.030 and 0.022 for 1:1 and 1:2 respectively.

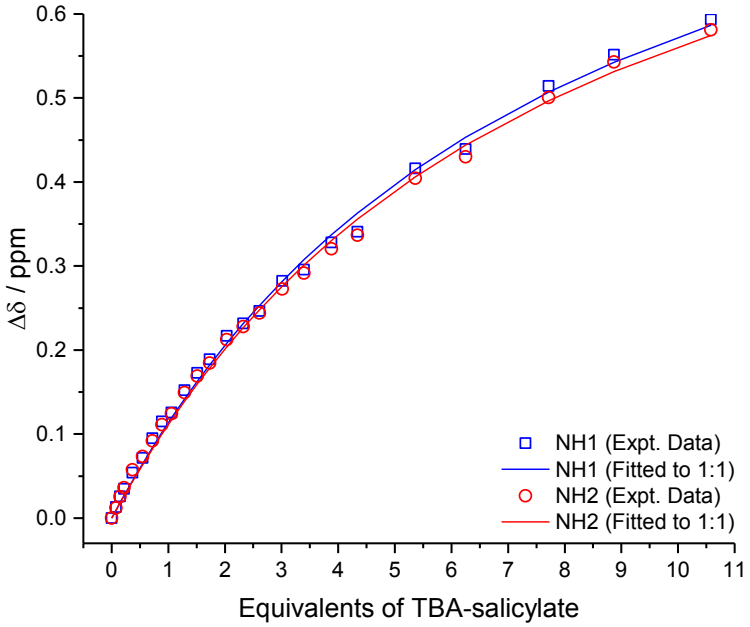

Figure A4.4. Fitted binding isotherms of ^{1}H NMR titration (400 MHz, 298 K) of ionophore II (5.2 mM) with TBA-salicylate in DMSO-d_6/0.5% H_2O mixture, showing the change in chemical shifts (Δδ) for thiourea NH resonances, fitted to the 1:1 binding model. Covariance of fit: 0.0027.

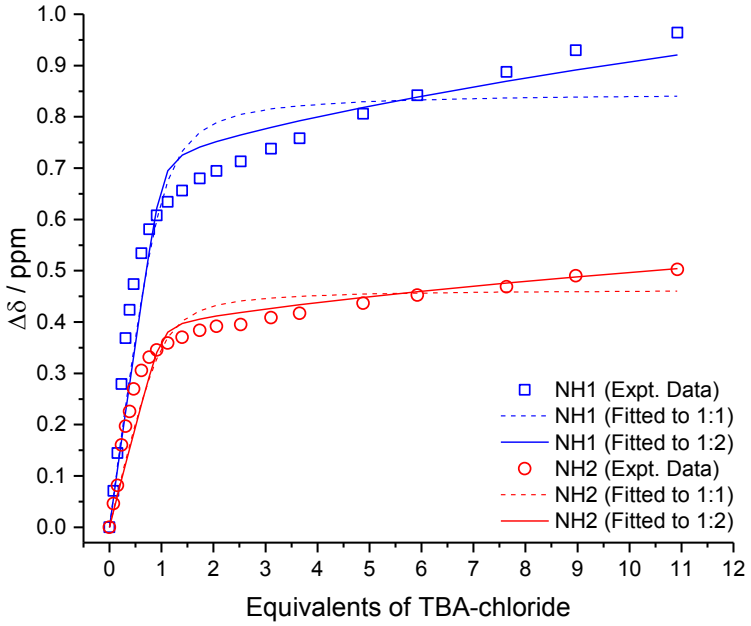

Figure A4.5. Fitted binding isotherms of ^{1}H NMR titration (400 MHz, 298 K) of ionophore III (4.9 mM) with TBA-chloride in DMSO-d_6/0.5% H_2O mixture, showing the change in chemical shifts (Δδ) for thiourea NH resonances, fitted to the 1:1 and additive 1:2 binding models. Covariance of fit: 0.062 and 0.048 for 1:1 and 1:2 respectively.

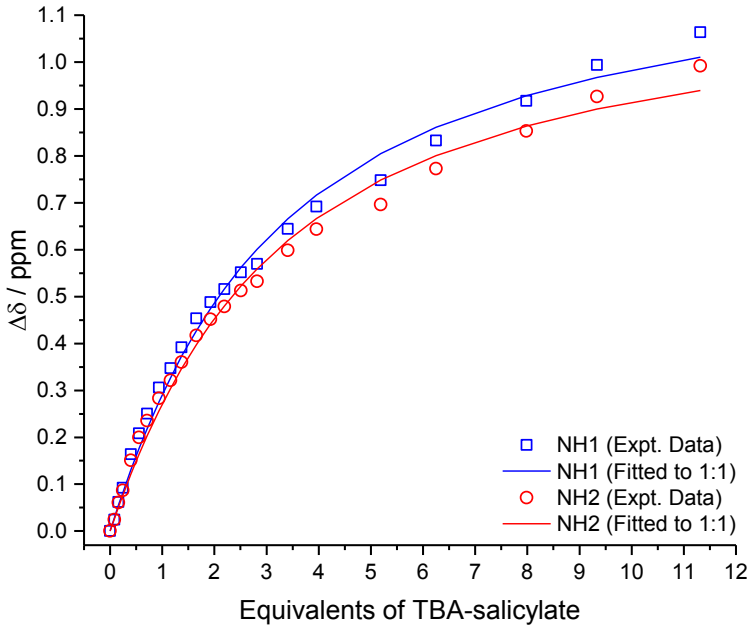

Figure A4.6. Fitted binding isotherms of ^{1}H NMR titration (400 MHz, 298 K) of ionophore III (4.9 mM) with TBA-salicylate in DMSO-d_6/0.5% H_2O mixture, showing the change in chemical shifts (Δδ) for thiourea NH resonances, fitted to the 1:1 binding model. Covariance of fit: 0.0071.

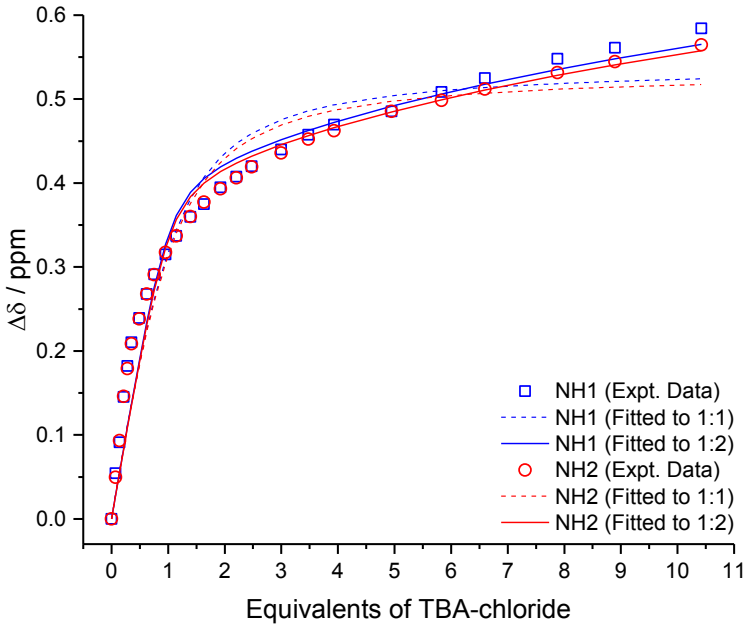

Figure A4.7. Fitted binding isotherms of ^{1}H NMR titration (400 MHz, 298 K) of ionophore IV (5.6 mM) with TBA-chloride in DMSO-d_6/0.5% H_2O mixture, showing the change in chemical shifts (Δδ) for thiourea NH resonances, fitted to the 1:1 and additive 1:2 binding models. Covariance of fit: 0.050 and 0.034 for 1:1 and 1:2 respectively.

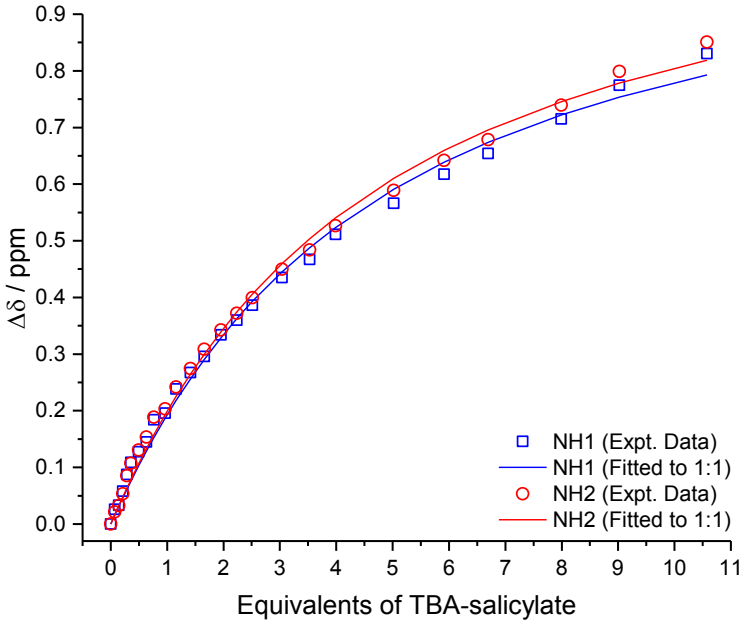

Figure A4.8. Fitted binding isotherms of ^{1}H NMR titration (400 MHz, 298 K) of ionophore IV (5.6 mM) with TBA-salicylate in DMSO-d_6/0.5% H_2O mixture, showing the change in chemical shifts (Δδ) for thiourea NH resonances, fitted to the 1:1 binding model. Covariance of fit: 0.0046.

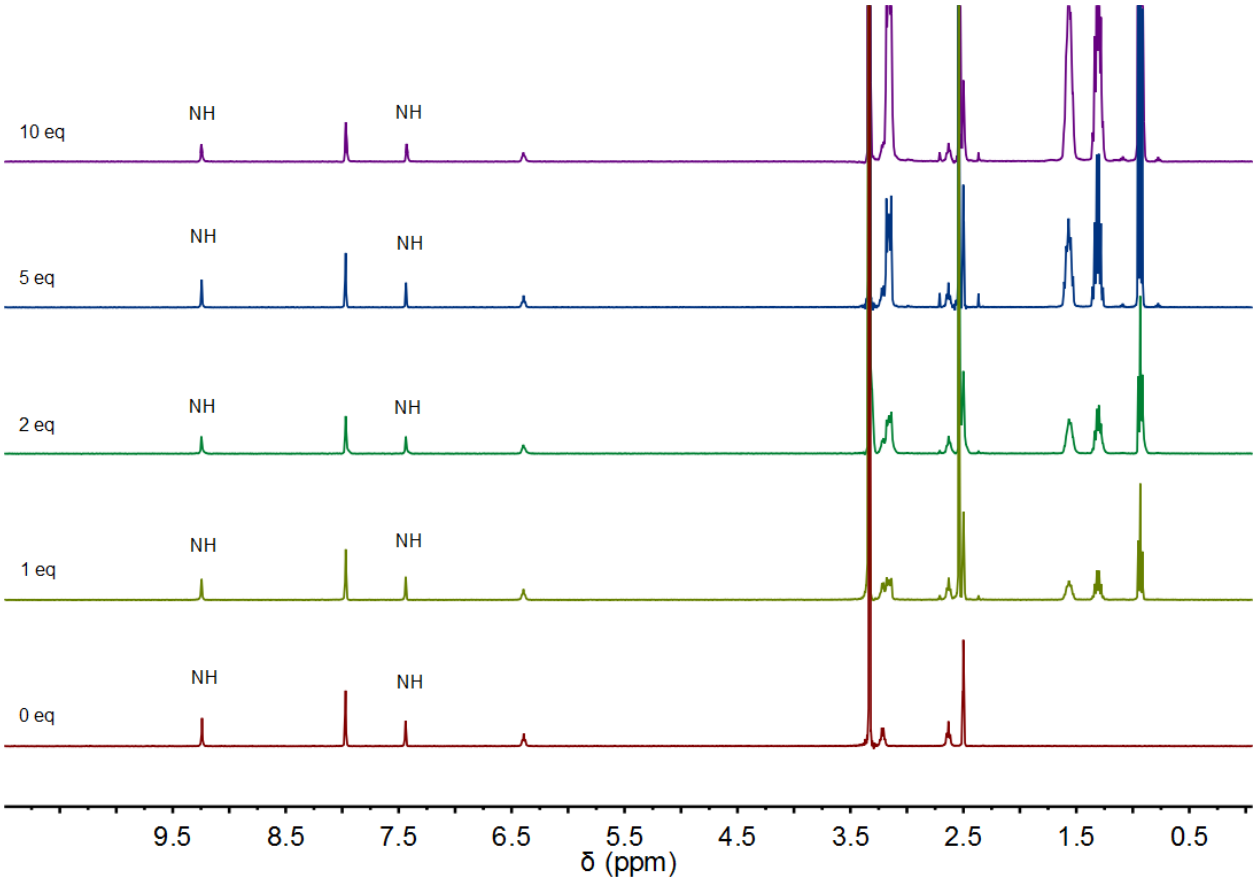

Figure A4.9. Selected partial ^{1}H NMR titration (400 MHz, 298 K) spectra of ionophore I (5.0 mM) with TBA-perchlorate in DMSO-d_6/0.5% H_2O mixture, showing no change in chemical shifts (Δδ) for both urea NH resonances up to 10 mole equivalents of guest-to-host ratio; indicative of no binding to perchlorate anion.

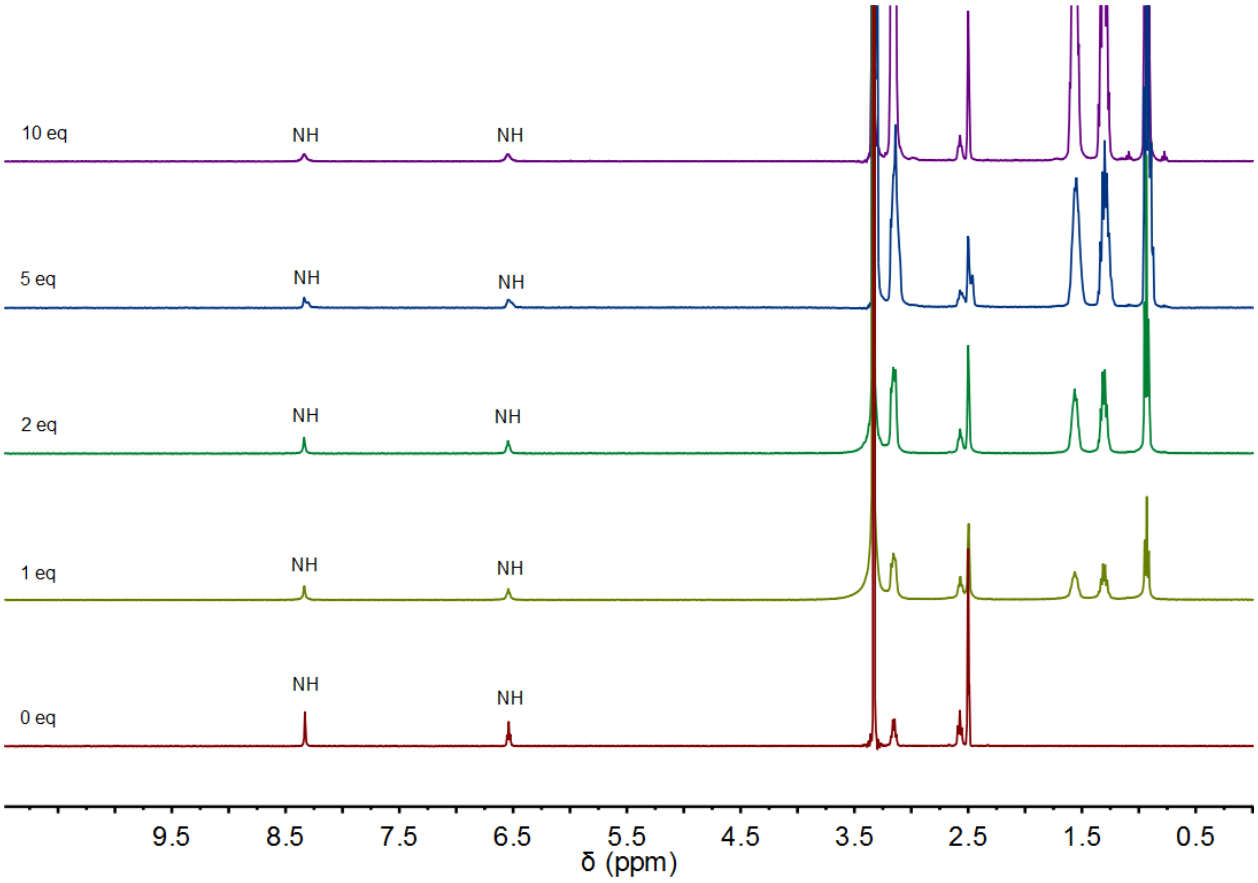

Figure A4.10. Selected partial ^{1}H NMR titration (400 MHz, 298 K) spectra of ionophore II (5.0 mM) with TBA-perchlorate in DMSO-d_6/0.5% H_2O mixture, showing no change in chemical shifts ($\Delta\delta$) for both urea NH resonances up to 10 mole equivalents of guest-to-host ratio; indicative of no binding to perchlorate anion.

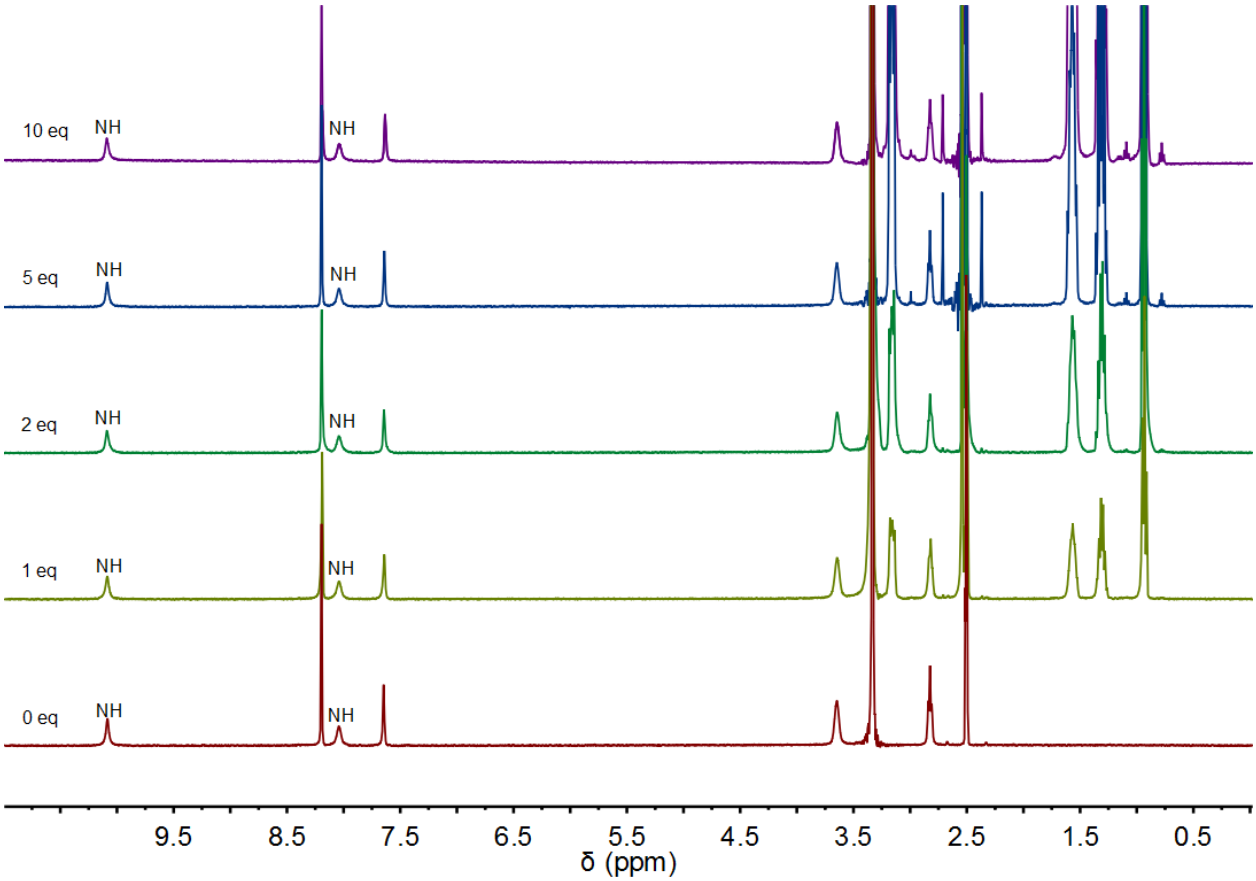

Figure A4.11. Selected partial ^{1}H NMR titration (400 MHz, 298 K) spectra of ionophore III (5.0 mM) with TBA-perchlorate in DMSO-d_6/0.5% H_2O mixture, showing no change in chemical shifts (Δδ) for both thiourea NH resonances up to 10 mole equivalents of guest-to-host ratio; indicative of no binding to perchlorate anion.

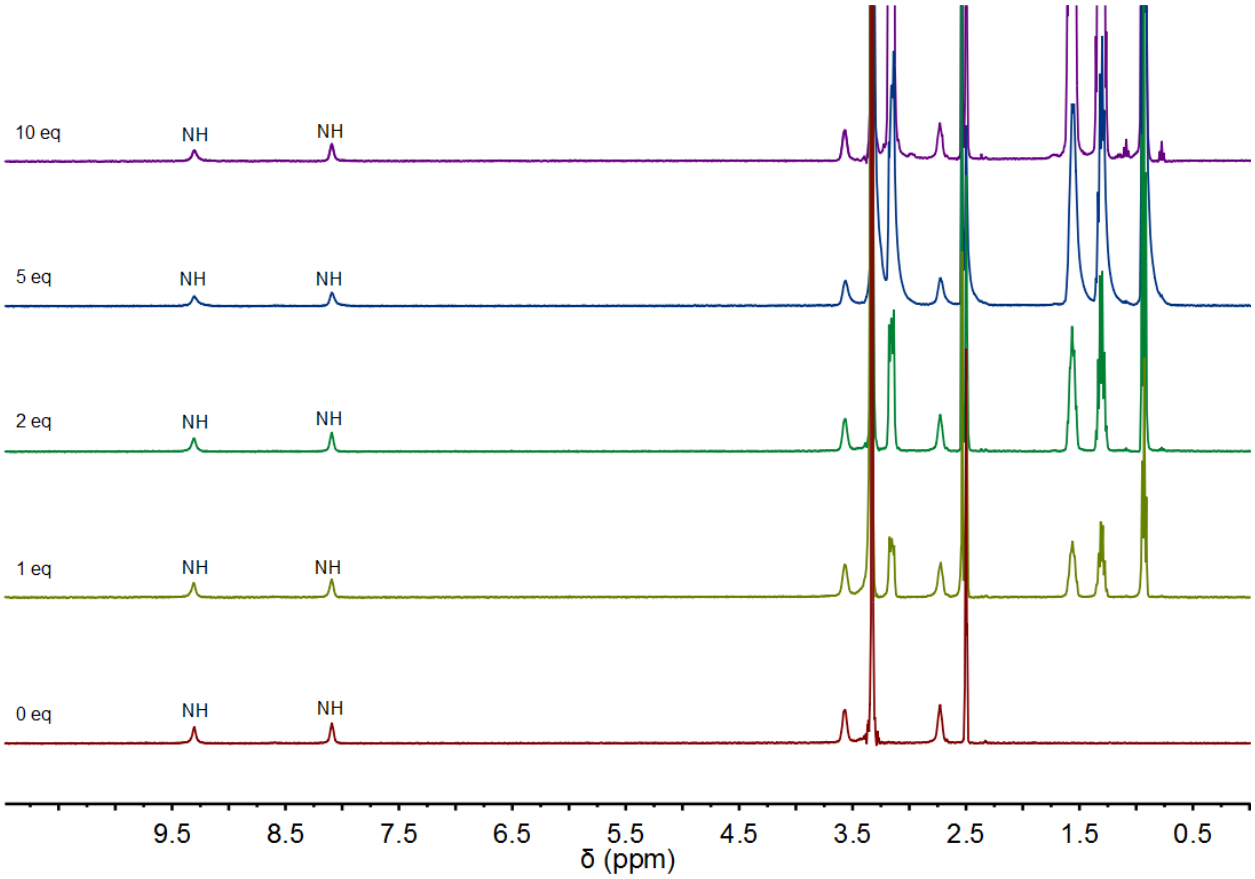

Figure A4.12. Selected partial ^{1}H NMR titration (400 MHz, 298 K) spectra of ionophore IV (5.0 mM) with TBA-perchlorate in DMSO-d_6/0.5% H_2O mixture, showing no change in chemical shifts (Δδ) for both thiourea NH resonances up to 10 mole equivalents of guest-to-host ratio; indicative of no binding to perchlorate anion.

DFT Computational Studies

DFT calculations were performed using the Gaussian 09 software package. All DFT calculations were performed using the default spin restricted closed shell wavefunctions. The geometry of the free host ionophore I, host-guest complexes of ionophore I with chloride and salicylate and the unbound salicylate were optimized at the M06-2X/6-31+G(d) level of theory in vacuum and the default "fine" integration grid implemented in the Gaussian 09 software was employed throughout. The molecular graphics were generated using the PyMOL Molecular Graphics System.

Single point energy calculations for all the fully optimized structures were performed with the larger basis set, with polarisation and diffuse functions for both hydrogen and heavy atoms at the M06-2X/6-311++G(d,p) level of theory. The approach for calculating the binding energy of host–guest complexes can be described from the series of equations (A4.1–4):

(A4.1) $\Delta E_{\text{binding}} = \Delta E_{\text{complexation}} + \Delta E_{\mathbf{H}\text{-reorganization}} + \Delta E_{\mathbf{G}\text{-reorganization}}$

(A4.2) $\Delta E_{\text{complexation}} = E_{\mathbf{HG}(\text{complex})} - E_{\mathbf{H}(\text{complex})} - E_{\mathbf{G}(\text{complex})}$

(A4.3) $\Delta E_{\mathbf{H}\text{-reorganization}} = E_{\mathbf{H}(\text{complex})} - E_{\mathbf{H}(\text{free})}$

(A4.4) $\Delta E_{\mathbf{G}\text{-reorganization}} = E_{\mathbf{G}(\text{complex})} - E_{\mathbf{G}(\text{free})}$

Here, $\Delta E_{\text{binding}}$ represents the binding energy for host-guest complexes from the overall contribution of stabilizing interactions ($\Delta E_{\text{complexation}}$), and the energy compensation (or gain) from structural reorganization of the host and guest molecules during the event of complexation. Since chloride anion is a monoatomic species, only the energy differences for structural reorganization of salicylate ($\Delta E_{\mathbf{G}\text{-reorganization}}$) and ionophore I ($\Delta E_{\mathbf{H}\text{-reorganization}}$) will be considered.

Energy calculation summary in vacuum using DFT at M06-2X/6-311++G(d,p)//M06-2X/6-31+G(d)))

$E_{\text{H(free)}}$ = -2308788.34 kcal/mol

$E_{\text{G(free salicylate)}}$ = -310841.84 kcal/mol

$E_{\text{HG(chloride complex)}}$ = -2597682.60 kcal/mol

$E_{\text{H(chloride complex)}}$ = -2308763.57 kcal/mol

$E_{\text{G(chloride complex)}}$ = -288818.59 kcal/mol

$E_{\text{HG(salicylate complex)}}$ = -2619697.45 kcal/mol

$E_{\text{H(salicylate complex)}}$ = -2308762.25 kcal/mol

$E_{\text{G(salicylate complex)}}$ = -310838.40 kcal/mol

$\Delta E_{\text{complexation(chloride)}}$ = -100.44 kcal/mol

$\Delta E_{\text{complexation(salicylate)}}$ = -96.81 kcal/mol

$\Delta E_{\text{H-reorganization(chloride)}}$ = 24.76 kcal/mol

$\Delta E_{\text{H-reorganization(salicylate)}}$ = 26.09 kcal/mol

$\Delta E_{\text{G-reorganization(chloride)}}$ = 0 kcal/mol

$\Delta E_{\text{G-reorganization(salicylate)}}$ = 3.44 kcal/mol

$\Delta E_{\text{binding(chloride)}}$ = -75.67 kcal/mol

$\Delta E_{\text{binding(salicylate)}}$ = -67.28 kcal/mol

Discussion

The DFT computed binding energies (in vacuum) for the chloride and salicylate complexes of ionophore I demonstrated stronger binding of chloride to salicylate by an energy difference ($\Delta\Delta E_{\text{binding}}$) of 8.39 kcal/mol, which corresponds to a binding constants difference (ΔK_a) of 1.43 × 10^6 M^{-1}. This corroborates the strong preferential binding of chloride over salicylate as demonstrated by the experimental binding constants from the NMR and potentiometric studies (in DMSO-d_6 and plasticized PVC media respectively).

Estimation of formal complex formation constants from potentiometric experiments.

The complex formation constants for ionophores I, II, III and IV were estimated according to Ceresa and Pretsch [3] from the selectivity coefficients for chloride and salicylate over perchlorate assuming that perchlorate does not interact with the receptors. The following formula was used to estimate the values of formal formation constants:

$$\beta_{IL_{n_I}} = \frac{K_{I,J}^{pot}(IE)}{K_{I,J}^{pot}(L)[L_T - n_I R_T / |z_I|]^{n_I}}$$

where $\beta_{IL_{n_I}}$ is the formation constant of the complex $IL_{n_I}^{z_I}$ (ionophore L with the ion I^{z_I}, z_I is the charge) having the stoichiometric factor n_I, L_T is the total concentration of the ionophore, R_T is the total concentration of lipophilic ionic sites (concentration of ion-exchanger TDMACl in this case), $K_{I,J}^{pot}(IE)$ and $K_{I,J}^{pot}(L)$ are respective potentiometric selectivity coefficients for the membrane based on ion-exchanger (IE) only and the membrane containing the same amount of ion-exchanger plus the ionophore L. ClO_4^- was taken as the ion J^{z_J} as the most lipophilic anion among the ions explored here, to meet the requirement $R_T = [J^{z_J}]$ in the membrane phase, thus assuming no substantial binding of the ionophores with the perchlorate ion.

Indeed, the results of the experiment using the sandwich membrane method[4,5] for complex formation constant estimation of ionophore I with chloride and perchlorate suggest a much weaker binding with perchlorate than with chloride (logK_a equal to 2.13±0.10 and 7.93±0.03 for perchlorate and chloride 1:1 complex respectively)*. The NMR titration studies of all receptors with TBA-perchlorate indicate no binding of the perchlorate anion to the receptors (see Figures A4.9-12).

*The membranes for the experiment using sandwich membrane method were pre-conditioned over two nights in the 10 mM solution of corresponding salt (10 mM sodium perchlorate or sodium chloride), the experiments were performed with stirring in a beaker with 50 mL of the same solution as used for conditioning.

Table A4.1. Logarithmic complex formation constants [M^{-1}] obtained using NMR studies and potentiometry for the receptors I, II, III and IV with chloride and salicylate. Only 1:1 host:guest complex formation is considered.

RECEPTOR	CHLORIDE COMPLEX		SALICYLATE COMPLEX	
	NMR titrations	Potentiometry*	NMR titrations	Potentiometry*
Ionophore I	4.1	5.8	1.8	3.4
Ionophore II	3.4	4.3	1.4	2.7
Ionophore III	4.3	1.7	1.9	1.2
Ionophore IV	3.5	1.6	1.7	1.0

*The estimation of the formation constants by potentiometry were carried out by comparison with a reference ion, perchlorate, assuming no binding to that ion. The utilization of different solvents, DMSO and DNPE for NMR and potentiometry respectively, makes unreliable the direct comparison between the obtained constant formations. On the other hand, from the sandwich data that perchlorate does bind to some extent to ionophore I, and that this may partially explain the difference in stability constants between the potentiometric data and by the sandwich membrane (see above).

References

(1) Thordarson, P. *Chem. Soc. Rev.* **2011**, *40*, 1305-1323.

(2) www.supramolecular.org. Accessed December 10th, 2016.

(3) Ceresa, A.; Pretsch, E. *Anal. Chim. Acta* **1999**, *395*, 41-52.

(4) Qin, Y.; Mi, Y.; Bakker, E. *Anal. Chim. Acta* **2000**, *421*, 207-220.

(5) Shultz, M. M.; Stefanova, O. K.; Mokrov, S. B.; Mikhelson, K. N. *Anal. Chem.* **2002**, *74*, 510-517.